# Deep-water sinuous channels:
## their development and architecture

Michal Janocko

Dissertation for the degree of Philosophiae Doctor (Ph.D.)


UNIVERSITY OF BERGEN
2011

# CONTENTS



**Papers:**

**I.** **Janocko, M., Nemec, W., Henriksen, S.** and **Warchoł, M.**
The diversity of deep-water sinuous channel belts and slope valley-fill complexes. *Mar. Petrol. Geol.* (MS in review).

**II.** **Janocko, M., Cartigny, M., Nemec, W.** and **Hansen, E.W.M.**
Turbidity current hydraulics and sediment deposition in erodible sinuous channels: laboratory experiments and numerical simulations.
*Mar. Petrol. Geol.* (MS in review).

**III.** **Janocko, M.** and **Nemec, W.**
The facies architecture and formation of deep-water point bars: an outcrop perspective. *Sedimentology* (MS in review).

# Acknowledgements

The research presented in this dissertation was carried out at the Department of Earth Science, University of Bergen, during my 3-year scholarship that commenced in March 2008. Statoil ASA kindly provided the offshore seismic dataset explored in my study and granted financial support, including expenses related to my fieldwork, participation in conferences and seismic interpretation work at the Statoil Research Centre in Trondheim. I wish to thank Statoil ASA and Dr. Sverre Henriksen in particular for offering me this research opportunity and thereby contributing to my professional career and my development as a petroleum geologist.

I wish to express my sincere gratitude to Prof. Wojciech Nemec (University of Bergen) for his designing of the project and his outstanding supervision and inspiring attitude during my whole study. He actively participated in the fieldwork, offered invaluable advice and discussions, and spent many days on improving the manuscripts of our papers. I also wish to thank him for giving me the freedom to realize my own ideas and to achieve my goals.

I am also much indebted to my co-supervisor Dr. Sverre Henriksen (Statoil ASA) for his continuous support, enthusiasm and stimulating discussions, for his practical advice and hospitality during my months spent in Trondheim, and for his constructive review of one of the manuscripts. Dr. Ernst Hansen (Complex Flow Design AS) acted as my second external co-supervisor and is kindly thanked for introducing me to the world of computational fluid mechanics, offering useful advice and following up on my research with great interest. I thank him also for kindly allowing me to stay at his house during one of my research visits to Trondheim.

The research project benefited further from the help of many geologists who kindly offered guidance in the field, technical help and valuable discussions. Therefore, I extend my gratitude to Prof. Ben Kneller, Dr. Bryan Cronin, Prof. Hasan Çelik, Prof. Ibrahim Türkmen and his students, Dr. Michał Warchoł, Dr. Mehmet Cihat Alçiçek, Ediz Kırman, Prof. Juraj Janočko, Dr. Peter King, Dr. Enrico Bonamini, Dr. Carlo Messina, Dr. Anna Pontén, Dr. Riccardo Basani, Dr. Evgeniy Tantserev, Dr. Romain Rouzairol, Dr. Anjali Fernandez and Dr. Juraj Oslanec.

Lastly, but foremost, I wish to thank my parents and Susannah Williams for their love, emotional and financial support, patience, encouragement and motivation during these three most busy years of my life. This thesis is dedicated to you.

Bergen, 30 September 2011

# Abstract

The study combines an interpretation of 3D seismic and well-core dataset with laboratory experiments, process-based 3D numerical simulations and analysis of outcrop analogues to explore the varied architecture and formative processes of submarine sinuous channels. On the basis of their seismic imagery from a sector of the West African Neogene continental slope, deep-water channel belts are divided into four main categories and their origin is explained: (1) meandering non-aggradational channel belts, which form when the turbiditic system is near its potential equilibrium profile; (2) levéed aggradational channel belts, which evolve from incipient meandering conduits perturbed by system aggradation; (3) erosional cut-and-fill channel belts, which evolve by down-cutting of either moderately sinuous levéed or highly sinuous meandering conduits; and (4) hybrid channel belts, which result from a failed or incomplete transformation instigated by either aggradation or down-cutting. The channel belts are typically stacked upon one another into fining-upwards valley-fill complexes, showing the turbiditic system's evolution from a deep incision to transient equilibrium state − with the formation of coarse-grained lag deposits and non-aggradational meandering channel belts − and further to aggradation with the formation of levéed channel belts and eventual abandonment.

On the basis of laboratory experiments and numerical CFD simulations, the diversity of sinuous channel belts is attributed to four key factors that control the spatial pattern of sediment erosion and deposition in a conduit: (1) the relationship between the flow's desired substrate equilibrium gradient and the host channel's actual slope gradient; (2) the relationship between the length scale of the flow's rotational helicoid and the channel's pre-existing curvature; (3) the relationship between the flow thickness and the channel depth; and (4) the relationship between the flow power and the channel bank strength. Channel meandering occurs uniquely when the flows are in hydraulic equilibrium with the channel slope, in phase with the channel curvature, in size or moderately undersized relative to the channel depth, and are modestly erosive with respect to the channel substrate. The diversity of channel-belt sedimentary architecture derives mainly from the formation of different intra-channel depocentres. Simulations indicate at least five different kinds of possible channel bars, including: classical point bars; bars formed in the channel-bend inflection zone at the inner- to outer-bank or outer- to inner-bank transition; and outer-bank bars formed directly upstream or downstream of the bend apex. Every bar type requires particular flow conditions, but some of them may form concurrently or alternate with one another in certain circumstance.

The study's outcrop investigations are focused on the architectural diversity of deep-water point bars, which are volumetrically most significant and hence potentially most important as reservoir elements. Point bars vary greatly in: (1) their size, depending on the channel depth and extent of its lateral migration; (2) the geometry, facies and inclination of the component beds as well as the degree of bed basal erosion, depending on the variety of turbidity currents involved; and (3) the occurrence of internal erosional truncations, depending on the point-bar planform transformation. Apart from their major differences in this respect, the deep-water point bars have a number of key features in common, from which inferences can also be drawn about the meandering process as such. Their horizontal or gently inclined erosional bases indicate that the meandering channels undergo lateral migration in quasi-equilibrium slope conditions. Sparse levées indicate bypassing spill-out flows. The cohesive encasing deposits point to the importance of bank strength, as in meandering fluvial channels. The laterally accreted beds show updip fining and tractional oblique updip transport, which indicate a rotating flow helicoid rising against the inner bank, spreading its bedload over the point-bar flank and segregating laterally sediment grain sizes. The downdip parts of beds indicate a higher sediment concentration in the flow core part passing along the channel thalweg.

The study as a whole contributes significantly to an understanding of the diversity of deep-water sinuous channel belts and their sedimentary architectures, and also shedding new light on the variability of submarine point bars and the process of channel meandering.

# Introduction

Submarine sinuous channels are major conduits through which both coarse clastic sediment and organic carbon-bearing mud suspension are transported to the deep sea (Johnson *et al.*, 2001; Wynn *et al.*, 2007). They may extend for up to a thousand kilometres along the sea floor (Bouma *et al.*, 1985; Pirmez & Imran, 2003; Nakajima, 2006) and form large sediment repositories that are important hydrocarbon reservoirs in many parts of the world (Prather, 2003). It is the significance of submarine channels as sediment conveyors and the reservoir potential of sinuous channel belts that have in recent years drawn wide interest and led to a large and ever growing body of literature on their architecture and formation.

The remarkable research efforts and increase in knowledge notwithstanding, the sedimentary and architectural diversity and formative conditions of deep-water sinuous channels are still poorly understood − due to the following main reasons: (1) nearly all available seismic datasets are from the petroleum industry, targeting deep reservoirs where internal channel-belt architecture and its elements are beyond seismic resolution; (2) modern submarine channels are inaccessible and difficult to study, and are not necessarily good analogues for all ancient sinuous channels; (3) outcrops and well cores of sinuous channel-belt deposits are relatively few, lack three-dimensionality and have seldom been studied in sufficient detail; (4) laboratory experiments on turbidity-current flow in sinuous channels have been simplistic, poorly monitored and suffering from the scaling problem; (5) process-based numerical simulations have been limited mainly to the flow of sediment-free density currents in non-erodible channels; and (6) the general lack of a coherent integrated approach combining laboratory and numerical experiments with seismic and outcrop studies has led to biased and often conflicting *ad hoc* notions about the development of deep-water sinuous channels.

In the lack of verifiable physical concepts explaining the formation and variation of turbiditic channel systems, analogies have often been drawn from fluvial systems. Indeed, the quantitative relationships between the channel sinuosity and valley gradient and between the meander wavelength, channel width and curvature radius appear to be similar in these vastly different systems (Kolla *et al.*, 2007). Detailed studies of side-scan sonar and 3D seismic-reflection imagery have also revealed a number of qualitative similarities, such as a wide range of channel sinuosities, bend cut-offs, point bars, chutes, asymmetrical channel profile, riffle-and-pool morphology of channel thalweg zone, erosional terraces, levées, crevasses and crevasse splays (Klaucke & Hesse, 1996; Peakall *et al.*, 2000; Abreu *et al.*, 2003; Kneller, 2003; Pirmez & Imran, 2003; Posamentier & Kolla, 2003; Babonneau *et al.*, 2004; Mayall *et al.*, 2006; Posamentier *et al.*, 2007; Wynn *et al.*, 2007). On the other hand, ample evidence has been given that − on a closer inspection − the morphology of sinuous submarine channels is fundamentally different from that of their fluvial counterparts. For example: the width and depth of turbiditic channels tend to decrease downslope (Flood & Damuth, 1987; Wynn *et al.*, 2007); the sinuous turbiditic channels may host outer-bank bars and nested mounds, features geometrically unlike any fluvial bars (Phillips, 1987; Timbrell, 1993; Clark & Pickering, 1996; Peakall *et al.*, 2000; Straub *et al.*, 2008; Nakajima *et al.*, 2009); turbiditic channels may decrease their sinuosity and migrate towards the centre of the channel belt by outer-bank accretion (Kane *et al.*, 2008; Nakajima *et al.*, 2009); the lateral migration of turbiditic channels may be accompanied by significant vertical aggradation (Posamentier & Kolla, 2003; Samuel *et al.*, 2003; Mayall *et al.*, 2006; Beaubouef *et al.*, 2007; Cronin *et al.*, 2007; Kolla *et al.*, 2007); turbiditic channel belts often show a ribbon-shaped geometry with prominent 'gull-wing' levées (Mayall & Stewart, 2000; Kneller, 2003; Gee & Gawthorpe, 2007); and their levées may include large sediment waves (Normark *et al.*, 1980; Nakajima *et al.*, 1998; Migeon *et al.*, 2001). It has also been suggested that the meandering turbiditic channels are much less prone to downstream translation than meandering rivers and tend to reach faster a limit of planform transformation (Peakall *et al.*, 2000). Last, but not least, there is a major difference between the sedimentary facies and heterogeneity of turbiditic and fluvial channel belts, reflecting the obvious differences between a river flow and the episodic flow of turbidity currents (e.g., Arnott *et al.*, 2007; Donselaar & Overeem, 2008; Dykstra & Kneller, 2009).

The realization of these differences and the scarcity of flow measurements from natural deep-water channels have led to a considerable number of laboratory experiments and a few numerical studies attempting to simulate the flow of turbidity currents in sinuous channels. However, laboratory experiments proved to be a formidable task and gave contradictory results, mainly because of the scaling problem. Since sediment particles in a laboratory cannot be scaled down without avoiding the effect of cohesion, most of the experiments were conducted by using saline, particle-free density currents or some very low-concentration turbidity currents scaled on the basis of the densimetric Froude number. Prefabricated sinuous channels with non-erodible banks were used, which additionally precluded a realistic representation of natural channels, where the feedback among the flow intrinsic dynamics, erosion and deposition is expected to play a crucial role.

The focus of laboratory experiments and numerical simulations was thus far on the pattern of flow velocity at channel bends, rather than the pattern of sediment deposition. Although the pattern of sedimentation in a channel may not necessarily follow spatial velocity structure, the flow velocities are relatively easy to measure in comparison to other variables, such as flow density, and are considered to be one of the main factors governing the erosion and deposition in submarine channels (e.g., Straub *et al.*, 2011). Laboratory and numerical simulation studies have shown helicoidal

rotation of density current at channel bends, but the direction of flow rotation varied from one study to another. Rotation similar as in meandering rivers, with the flow rising along the floor towards the inner bank, was reported from experiments by Kassem & Imran (2004), Imran *et al.* (2007; 2008), Islam & Imran (2008) and Islam *et al.* (2008). An opposite direction of rotation, with the flow rising along the floor against the outer bank, was shown by Corney *et al.* (2006), Keevil *et al.* (2006; 2007), Peakall *et al.* (2007), Amos *et al.* (2010) and Giorgio Serchi *et al.* (2011). This reverse pattern of flow circulation was initially postulated to be characteristic of all sinuous submarine channels, as opposed to rivers, but a consensus has now been reached that either pattern of flow rotation can be expected to occur in deep-water conduits (Giorgio Serchi *et al.*, 2011).

Laboratory experiments with sinuous channels using sediment-laden turbidity currents or a mobile sediment substrate were relatively few, showing deposition at the bend outer bank (Kane *et al.*, 2008; Straub *et al.*, 2008; 2011), downstream part of the bend inner bank (Peakall *et al.*, 2007; Kane *et al.*, 2008; Amos *et al.*, 2010; Straub *et al.*, 2011) or on the levées and in overbank area (Kane *et al.*, 2010; Straub *et al.*, 2008; 2011). Although these loci of sediment deposition and the geometry of the three types of deposits are in agreement with observations from natural channel belts, their formation remains inadequately documented and poorly understood, because of the difficulty with a continuous monitoring of sediment motion in laboratory flumes in all three dimensions. On the basis of measured 2D velocity profiles and overhead camera filming, the deposition of sediment at channel banks has been attributed to either flow separation at the bank, with the sediment dumped from turbulent suspension in a low-velocity zone (Peakall *et al.*, 2007; Amos *et al.*, 2010; Straub *et al.*, 2011), or flow run-up on the outer bank, with a loss of capacity and a rapid deposition due to increased concentration (Amos *et al.*, 2010; Straub *et al.*, 2011). A consensus now is that these two causes of localized deposition are virtually independent of the direction of flow rotation, and hence remain poorly defined in terms of the flow conditions. Similarly unclear is the formation of other deposit types, such as point bars, nested mounds and other varieties of outer-bank bars, which are yet to be produced and hydraulically analysed in laboratory and numerical experiments.

The aim of the present study was to address some of the contentious aspects of the development and sedimentary architecture of deep-water sinuous channel belts, with a special focus on meandering systems. A multidisciplinary approach has been chosen, combining insights from sedimentology, geomorphology, seismic interpretation, laboratory experiments and CFD (computational fluid dynamics) simulations. The study consisted of three independent but interrelated parts, each concerned with a different kind of insight and a different level of detail. The first part (**Paper I**), based on 3D seismic and well-core data from a continental-slope succession of West Africa, was meant to assess in qualitative and quantitative terms the diversity of submarine sinuous channel belts and their architectural elements, and to analyse their development in submarine valley-fill successions. The second part (**Paper II**) was based on laboratory experiments and numerical simulations of turbidity currents in erodible sinuous channels, with the aim to clarify the hydraulic conditions for the formation of various architectural elements − particularly channel bar types − as a main cause of channel-belt diversity. Special focus was on the identification of physical conditions in which deep-water meandering channels and their single most important element – the point bars − form. This latter topic was followed further in the third part of the study (**Paper III**), where geometrical reconstruction and facies analysis of point-bar deposits in outcrop sections were used to recognize the mechanism of submarine channel meandering. A wide range of outcrop cases, combined with a synthesis of earlier-published examples, allowed for a tentative classification of deep-water point bars and their styles of heterogeneity, which may potentially serve as a useful guide in subsurface exploration and development of reservoir models.

By combining different kinds of data and scales of observation, the present study has provided cross-verified evidence shedding vital new light on the development and sedimentary architecture of deep-water sinuous channels − from their flow conditions to stratigraphic evolution in submarine valleys.

# Summary of Papers

**Paper I**

**Janocko, M., Nemec, W., Henriksen, S.** and **Warchoł, M.** The diversity of deep-water sinuous channel belts and slope valley-fill complexes. *Mar. Petrol. Geol.* (MS in review).

This paper focuses on the architecture of deep-water sinuous channel belts and their evolution in valley-fill complexes in a West African Miocene continental-slope succession. The study combines the interpretation of 3D seismic and well-core data with observations from a range of outcrop analogues. On the basis of planform, cross-section, seismic facies and location with respect to channel bends, five main types of channel-belt elements are recognized from seismic images: lateral-accretion packages (LAPs), outer-bank mounds/bars, levées, non-turbiditic mass-transport deposits (MTDs) and last-stage channel-fills. These elements occur in various combinations, but no single channel belt combines all of them, which suggests that some elements may be mutually exclusive. On the basis of their planform,

cross-sectional geometry and range of architectural elements involved, the sinuous channel belts can be classified into four distinctive categories: meandering non-aggradational channel belts, levéed aggradational channel belts, erosional cut-and-fill channel belts and hybrid channel belts. Quantitative analysis indicates that the meandering channels form when the system is roughly at its equilibrium profile. They evolve from nearly straight to highly sinuous by increasing first the bend amplitude (transverse expansion) and then the conduit length (longitudinal expansion). The levéed channels are thought to develop from incipient meandering conduits perturbed by aggradation, whereas the erosional channels considered to evolve from either moderately sinuous levéed or highly sinuous meandering conduits, inheriting their sinuosity. Hybrid channels signify a failed or incomplete channel transformation. The four types of sinuous channel belts may occur isolated or stacked upon one another into complexes, which may be unconfined or, as is often the case, confined by the relief of submarine incised valley and its external levées.

Channel-belt complexes evolving in incised valleys typically show an upward-fining trend and a decrease in sandstone net/gross. They commonly evolve from a state of deep erosion to a transient equilibrium state with the deposition of a coarse lag or non-aggradational meandering channel belts, which are commonly succeeded by MTDs emplaced when the valley reached its maximum relief. The middle to upper part of valley-fill consists of levéed channel belts recording aggradation, with possible development of non-aggradational meandering channel belts in the uppermost part prior to the valley abandonment. Similar meandering channel belts may also occasionally occur in the middle part of a valley-fill succession. The observed variation among valley-fills can be attributed to external factors (e.g., halokinesis, slope tectonics) or to an autogenic forcing related to the evacuation of sediment from the valley, base-level change and mud accretion on the adjoining slope.

**Paper II**

**Janocko, M., Cartigny, M., Nemec, W.** and **Hansen, E.W.M.** Turbidity current hydraulics and sediment deposition in erodible sinuous channels: laboratory experiments and numerical simulations. *Mar. Petrol. Geol.* (MS in review).

The paper combines laboratory experiments and 3D numerical simulations to explain the hydraulic conditions for the formation of various channel bars as a main cause of the observed architectural diversity of deep-water sinuous channel belts On the basis of previous studies, key factors are identified that control the spatial pattern of sediment deposition in submarine sinuous channels and the process of channel meandering. A conceptual combination of various system conditions gives eighteen different scenarios, which are simulated to reveal formation of five main types of intra-channel depocentres: meander bars (point bars); bars formed in the channel-bend inflection zone at the inner- to outer-bank or outer- to inner-bank transition; and outer-bank bars formed directly upstream or downstream of the bend apex. Every bar type appears to require particular flow conditions, but some bars may form concurrently or alternate with one another in certain circumstance.

The simulations also address the controversial issue of flow rotation at the bends of submarine sinuous channels. A detailed 3D monitoring of flow velocity structure shows that the flow helicoid may rotate either inwards or outwards, or may virtually lose its structure in the case of a grossly oversized flow. If the length scale of the flow helicoid matches the channel curvature, the flow rotation at a channel bend is directed inwards irrespective of others conditions. If the flow is out of phase with the channel, the direction of the helicoid rotation depends on the flow velocity and the angle at which the flow velocity core approaches the bend's outer bank. A transient, local impact on the direction of flow rotation is exerted by the elevation of the flow velocity core above the channel floor. The study confirms and expounds on many previous laboratory observations pertaining to the flow of turbidity currents in sinuous non-meandering channels. However, the study also indicates that the meandering process may not be scale-independent and that the development of subaqueous meandering channels in small-scale laboratory or numerical experiments may be a formidable task. Inferences about channel meandering conditions based on small-scale experiments should thus be considered with much caution.

**Paper III**

**Janocko, M.** and **Nemec, W.** The facies architecture and formation of deep-water point bars: an outcrop perspective. *Sedimentology* (MS in review)

This paper describes a wide range of deep-water point-bar deposits and reviews earlier-published cases with the aim to clarify the processes by which submarine channels meander. Although all point bars are formed by a common process of lateral accretion, they may exhibit significant differences in the character of their beds. Notable differences include the point-bar size, the geometry and sedimentary facies of the point-bar beds, bedding inclination, the degree of erosion at bed bases and the occurrence of erosional truncations marking point-bar planform transformation. Six point-bar types are distinguished on a descriptive basis: (1) point bars composed of sand-mud couplets; (2) point bars composed of sand beds; (3) point bars comprising couplets of mudclast rudite and sand; (4) point bars made of gravel-sand couplets; (5) point bars composed of beds with updip-segregated gravel and sand; and (6) point bars composed of gravel beds.

Apart from their major differences, the deep-water point bars have a number of key features in common, from which inferences can be drawn about the meandering process as such. Their horizontal or gently inclined erosional bases indicate that the meandering

channels undergo lateral migration in quasi-equilibrium slope conditions. Sparse levées indicate bypassing spill-out flows. The cohesive deposits that encase point bars suggest an importance of bank strength, as in the case of meandering fluvial channels. The laterally accreted beds show updip fining and tractional oblique updip transport, which indicate a rotating flow helicoid rising against the inner bank, spreading its bedload over the point-bar flank and segregating laterally grain sizes. The downdip parts of beds indicate a significantly higher sediment concentration in the flow thalweg zone.

The observed differences among meander belts have an important bearing on their heterogeneity, but are beyond the seismic resolution and indiscernible from seismic images. However, the six main categories of point bars are readily identifiable from a well-core sample, and their detailed characteristics provided by the present study can thus serve as a useful guide for the recognition and characterization of ancient meander belts and for the development of their models as hydrocarbon reservoirs.

# Conclusions and Perspective

The present study − by combining cross-verifiable evidence from 3D seismic imagery, well cores, outcrop sections, laboratory experiments and CFD numerical simulations − has provided unprecedented new insights in the development and architectural diversity of submarine sinuous channel belts, from their internal flow conditions to stratigraphic evolution in submarine incised valleys. Some of the crucial insights include the identification of the physical conditions for deep-water channel meandering and point-bar formation, which were earlier speculated about confusingly on the basis of inadequate laboratory experiments and an analogy drawn with terrestrial rivers.

Four main categories of deep-water sinuous channel belts have been recognized and their genetic relationships inferred: meandering non-aggradational channel belts, levéed aggradational channel belts, erosional cut-and-fill channel belts and hybrid channel belts. A range of channel bars, or intra-channel depocentres, and the hydraulic conditions for their formation have been recognized as a main cause of the architectural diversity of submarine sinuous channel belts. A six-category descriptive classification of deep-water point bars has been suggested on empirical basis, highlighting their diverse styles of heterogeneity and providing a potentially useful guide for subsurface exploration and reservoir modelling of ancient meander belts.

As the resolution of 3D seismic data increases and the search for new outcrop cases continuous, it is possible that some other architectural elements of sinuous channel belts may be recognized, adding further to our understanding of their architectural diversity and improving the suggested models. CFD simulations should then be used to explain the hydraulic conditions for the formation of such newly-recognized channel bars or local depocentres. Numerical simulations and laboratory experiments should also be used to explore the hydraulics and depositional conditions at submarine channel confluences − a topic that proved to be quite fascinating with respect to alluvial rivers. After all, the channel systems on submarine slopes are known to abound in confluences (e.g., Bouma *et al.*, 1985; Nakajima, 2006)

It is highly desirable to acquire more hydraulic measurements from natural turbiditic channels, not least in order to calibrate numerical simulations. Significant progress is being made in this direction by attempts to deploy modern laboratory techniques of flow velocity measurement in submarine settings (Sumner *et al.*, 2011). So far only saline density currents have been measured in this way and the results can only serve as an analogue for turbidity currents. On the other hand, the majority of modern submarine sinuous channels does not seem to be in slope-equilibrium conditions and hence are no actively meandering today. Channel cases for instrumental measurements will thus need to be carefully selected and their state of development well-recognized in order to avoid confusing or inconclusive costly results.

Numerical CFD simulations are the least costly and most attractive method to study turbidity currents and their flow in pre-designed submarine channels, as they allow a continuous full 3D monitoring of all flow parameters and − unlike laboratory experiments − do not require downscaling of the flow and its sediment properties. The CFD software becomes ever more advanced and the computational power and speed of computers increases, offering undeniably the best analytical method if its simulation results are carefully verified on the basis of outcrop, 3D seismic and laboratory studies

In laboratory experiments, future work should focus on the flow and sedimentation pattern of turbidity currents in erodible sinuous channels, rather than prefabricated plastic- or concrete-made conduits. The flume tanks should ideally be made larger than those used at present, in order to minimize the effects of downscaling, and the measurements of velocity and sediment concentration should preferably be taken in all three dimensions to give a more reliable picture of the flow behaviour.

# References


**Abreu, V., Sullivan, M., Pirmez, C.** and **Mohrig, D.** (2003) Lateral accretion packages (LAPs): an important reservoir element in deep water sinuous channels. *Mar. Petrol. Geol.*, **20,** 631–648.

**Amos, K.J., Peakall, J., Bradbury, P.W., Roberts, M., Keevil, G.,** and **Gupta, S.** (2010) The influence of bend amplitude and planform morphology on flow and sedimentation in submarine channels. *Mar. Petrol. Geol.*, **27,** 1431–1447.

**Arnott, R.** (2007) Stratal architecture and origin of lateral accretion deposits (LADs) and conterminous inner-bank levee deposits in a base-of-slope sinuous channel, lower Isaac Formation (Neoproterozoic), east-central British Columbia, Canada. *Mar. Petrol. Geol.*, **24,** 515–528.

**Babonneau, N., Savoye, B., Cremer, M.** and **Bez, M.** (2004) Multiple terraces within the deep incised Zaire Valley (ZaïAngo Project): are they confined levees? In: *Confined Turbidite Systems* (Eds S.A., Lomas and P. Joseph), *Geol. Soc. London Spec. Publ*., **222**, 91−114.

**Beaubouef, R.T., Rossen, C.** and **Lovell, R.W.W.** (2007) The Beacon Channel: a newly recognized architectural type in the Brushy Canyon Formation, Texas, USA. In: *Atlas of Deepwater Outcrops* (Eds T.H. Nilsen, R.D. Shew, G.S. Steffens and J.R.J. Studlick), *AAPG Stud. Geol.*, **56,** 432–443.

**Bouma, A.H.**, **Normark, W.R.** and **Barnes, N.E.** (Eds) (1985) *Submarine Fans and Related Turbidite Systems* (Eds A.H. Bouma, W.R. Normark and N.E. Barnes). Springer-Verlag, New York.

**Clark, J.D.,** and **Pickering, K.T.** (1996) Architectural elements and growth patterns of submarine channels: applications to hydrocarbon exploration. *AAPG Bull.*, **80,** 194–221.

**Corney, R.K.T., Peakall, J., Parsons, D.R., Elliott, L., Amos, K.J., Best, J.L., Keevil, G.M.** and **Ingham, D.B.** (2006) The orientation of helical flow in curved channels. *Sedimentology*, **53**, 249–257.

**Cronin, B.T., Çelik, H., Hurst, A., Gul, M., Gürbüz, K., Mazzini, A.** and **Overstolz, M.** (2007). Slope-channel complex fill and overbank architecture, Tinker channel, Kırkgecit Formation, Turkey. In: *Atlas of Deepwater Outcrops* (Eds T.H. Nilsen, R.D. Shew, G.S. Steffens and J.R.J. Studlick), *AAPG Stud. Geol.*, **56,** pp. 363–367.

**Donselaar, M.E.** and **Overeem, I.** (2008) Connectivity of fluvial point-bar deposits: An example from the Miocene Huesca fluvial fan, Ebro Basin, Spain. *AAPG Bull.*, **92**, 1109−1129.

**Dykstra, M.** and **Kneller, B.** (2009) Lateral accretion in a deep-marine channel complex: implications for channelized flow processes in turbidity currents. *Sedimentology*, **56,** 1411–1432.

**Flood, R.D.** and **Damuth, J.E.** (1987) Quantitative characteristics of sinuous distributary channels on the Amazon deep-sea fan. *Geol. Soc. Am. Bull.*, **98**, 723–738.

**Gee, M.J.R.** and **Gawthorpe, R.L.** (2007) Early evolution of submarine channels offshore Angola revealed by three-dimensional seismic data. In: *Seismic Geomorphology: Applications to Hydrocarbon Exploration and Production* (Eds R.J. Davies, H.W. Posamentier, L.J. Wood and J.A. Cartwright). *Geol. Soc. London Spec. Publ.*, **277**, 223−235.

**Giorgio Serchi, F., Peakall, J., Ingham, D. B.** and **Burns, A. D.** (2011) A unifying computational fluid dynamics investigation on the river-like to river-reversed secondary circulation in submarine channel bends. *J. Geophys. Res.*, **116**, paper C06012, doi:10.1029/2010JC006361.

**Imran, J., Islam, M.A., Huang, H., Kassem, A., Dickerson, J., Pirmez, C.** and **Parker, G.** (2007) Helical flow couplets in submarine gravity underflows. *Geology*, **35**, 659−662.

**Imran, J., Islam, A. M.** and **Kassem, A.** (2008) Discussion of "The orientation of helical flow in curved channel" by Corney et al.. *Sedimentology*, **55**, 235−239.

**Islam, A. M.** and **Imran, J.** (2008) Experimental modeling of gravity underflow in a sinuous submerged channel. *J. Geophys. Res.*, **113**, C07041, doi:10.1029/2007JC004292.

**Islam, M.A., Imran, J., Pirmez, C.** and **Cantelli, A.** (2008) Flow splitting modifies the helical motion in submarine channels. *Geophys. Res. Lett.*, **35**, L22603, doi:10.1029/2008GL034995.

**Johnson, K.S., Paull, C.K., Barry, J.P.** and **Chavez, F.P.** (2001) A decadal record of underflows from a coastal river into the deep sea. *Geology*, **29**, 1019–1022.

**Kane, I.A., McCaffrey, W.D.** and **Peakall, J.** (2008) Controls on sinuosity evolution within submarine channels. *Geology*, **36,** 287–290.

**Kassem, A.** and **Imran, J.** (2004) Three-dimensional modeling of density current, II. Flow in sinuous confined and unconfined channels. *J. Hydraul. Res.*, **42**, 591−602.

**Keevil, G.M., Peakall, J., Best, J.L.** and **Amos, K.J.** (2006) Flow structure in sinuous submarine channels: velocity and turbulence structure of an experimental submarine channel. *Mar. Geol.*, **229**, 241−257.

**Keevil, G.M., Peakall, J.** and **Best, J.L.** (2007) The influence of scale, slope and channel geometry on the flow dynamics of submarine channels. *Mar. Petrol. Geol.*, **24**, 487−503.

**Klaucke, I.** and **Hesse, R.** (1996) Fluvial features in the deep-sea: new insights from the glacigenic submarine drainage system of the Northwest Atlantic Mid-Ocean Channel in the Labrador Sea. *Sed. Geol.*, **106**, 223–234.

**Kneller, B.C.** (2003) The influence of flow parameters on turbidite slope channel architecture. *Mar. Petrol. Geol.*, **20,** 901–910.

**Kolla, V., Posamentier, H.W.** and **Wood, L.J.** (2007) Deep-water and fluvial sinuous channels:

characteristics, similarities and dissimilarities, and modes of formation. *Mar. Petrol. Geol.*, **24**, 388−405.

**Mayall, M.** and **Stewart, I.** (2000) The architecture of turbidite slope channels. In: *Deep-water Reservoirs of the World* (Eds P. Weimer, R.M. Slatt, A.H. Bouma and D.T. Lawrence), pp. 578–586. Proceedings of the Gulf Coast Section SEPM Foundation 20th Annual Research Conference, Houston.

**Mayall, M., Jones, E.** and **Casey, M.** (2006) Turbidite channel reservoirs – key elements in facies prediction and effective development. *Mar. Petrol. Geol.*, **23**, 821−841.

**Migeon, S.**, **Savoye, B.**, **Zanella, E.**, **Mulder, T.**, **Faugères, J.-C.** and **Weber, O.** (2001) Detailed seismic-reflection and sedimentary study of turbidite sediment waves on the Var Sedimentary Ridge (SE France): significance for sediment transport and deposition for the mechanisms of sediment-wave construction. *Mar. Petrol. Geol.*, **18**, 179−208.

**Nakajima, T.** (2006) Hyperpycnites deposited 700 km away from river mouths in the central Japan Sea. *J. Sed. Res.*, 76, 60–73.

**Nakajima, T., Peakall, J., McCaffrey, W.D., Paton, D.A.** and **Thompson, P.J.** (2009) Outer-bank bars: a new intra-channel architectural element within sinuous submarine slope channels. *J. Sed. Res.*, **79,** 872–886.

**Nakajima, T.**, **Satoh, M.** and **Okamura, Y.** (1998) Channel-levee complexes, terminal deep-sea fans and sediment wave fields associated with the Toyama deep-sea channel system in the Japan Sea. *Mar. Geol.*, **147**, 25−41.

**Normark, W.R.**, **Hess, G.**, **Stow, D.A.V.** and **Bowen, A.J.** (1980) Sediment waves on the Monterey Fan levee: a preliminary physical interpretation. *Mar. Geol.*, **37**, 1−18.

**Peakall, J., McCaffrey, W.D.,** and **Kneller, B.C.** (2000) A process model for the evolution, morphology, and architecture of sinuous submarine channels. *J. Sed. Res.*, **70**, 434−448.

**Peakall, J., Amos, K.J., Keevil, G.M., Bradbury, P.W.** and **Gupta, S.** (2007) Flow processes and sedimentation in submarine channel bends. *Mar. Petrol. Geol.*, **24,** 470–486.

**Phillips, S.** (1987) Dipmeter interpretation of turbidite-channel reservoir sandstones, Indian Draw field, New Mexico. In: *Reservoir Sedimentology* (Eds R.W. Tillman and K.J. Weber), *Soc. Econ. Paleontol. Mineral. Spec. Publ.*, **40,** 113–128.

**Pirmez, C.** and **Imran, J.** (2003) Reconstruction of turbidity currents in Amazon Channel. Marine and Petroleum Geology, 20, 823−849.

**Posamentier, H.W.** and **Kolla, V.** (2003) Seismic geomorphology and stratigraphy of depositional elements in deep-water settings. *J. Sed. Res.*,**73,** 367–388.

**Posamentier, H. W., Davies, R. J., Cartwright, J. A.** and **Wood, L. J.** (2007) Seismic geomorphology - an overview. In: *Seismic Geomorphology: Applications to Hydrocarbon Exploration and Production* (Eds R.J. Davies, H.W. Posamentier, L.J. Wood and J.A. Cartwright). *Geol. Soc. London Spec. Publ.*, **277**, 1−14.

**Prather, B.E.** (2003) Controls on reservoir distribution, architecture and stratigraphic trapping in slope settings. *Mar. Petrol. Geol.*, **20**, 529−545.

**Samuel, A., Kneller, B.C., Ralan, S., Sharp, A.** and **Parsons, C.** (2003) Prolific deep-marine slope channels of the Nile Delta, Egypt. *AAPG Bull.*, **87**, 541−560.

**Straub, K.M., Mohrig, D., McElroy, B.** and **Buttles, J.** (2008) Interactions between turbidity currents and topography in aggrading sinuous submarine channels: a laboratory study. *Geol. Soc. Am. Bull.*, **120,** 368–385.

**Straub, K.M., Mohrig, D., Buttles, J., McElroy, B.** and **Pirmez, C.** (2011) Quantifying the influence of channel sinuosity on the depositional mechanics of channelized turbidity currents: a laboratory study, *Mar. Petrol. Geol.*, **28,** 744–760.

**Sumner, E.J., Peakall, J., Parsons, D.R., Darby, S., Wynn, R.B.** and **Dorrell, R.M.** (2011) Three-dimensional flow field evolution within a channelized density-driven current in the Black Sea. In: Internal architecture, bedforms and geometry of turbidite channels, Abstract Book (Eds M. Mayall, I.A. Kane and B. McCaffrey). *Geol. Soc. London*, London.

**Timbrell, G.** (1993) Sandstone architecture of the Balder Formation depositional system, UK quadrant 9 and adjacent areas. In: *Petroleum Geology of Northwest Europe: Proceedings of the 4th Conference* (Ed. J.R. Parker), pp. 107–121. *Geol. Soc. London*.

**Wynn, R.B., Cronin, B.T.** and **Peakall, J.** (2007) Sinuous deep-water channels: genesis, geometry and architecture. *Mar. Petrol. Geol.*, **24**, 341−387.

# I

# The diversity of deep-water sinuous channel belts and slope valley-fill complexes

Michal Janocko [a], Wojciech Nemec [a], Sverre Henriksen [b], Michał Warchoł [c]

[a] *Department of Earth Science, University of Bergen, Allégaten 41, 5007 Bergen, Norway*
[b] *Statoil Research Centre, Arkitekt Ebbels veg 10, Rotvoll, 7005 Trondheim, Norway*
[c] *Statoil Research Centre, Sandsliveien 90, Sandsli, 5020 Bergen, Norway*

Submitted to *Marine and Petroleum Geology*

**Abstract**

The study combines interpretation of 3D seismic imagery of submarine sinuous channel belts in offshore West Africa with observations from a range of outcrop analogues. Five main architectural elements of slope channel belts are recognized: lateral-accretion packages (LAPs), outer-bank mounds/bars, levées, non-turbiditic mass-transport deposits (MTDs) and last-stage channel-fills. Channel belts differ in their planform, cross-section and the range of architectural elements involved. Four types of sinuous channel belts are distinguished, formed by meandering non-aggradational channels, levéed aggradational channels, erosional cut-and-fill channels and hybrid channels. Analysis indicates that meandering channels form when system is near its potential equilibrium profile. They evolve from nearly straight to highly sinuous by increasing first the bend amplitude and then the conduit length. Levéed channels are thought to evolve from incipient meandering conduits perturbed by aggradation and erosional channels to evolve from either levéed or meandering conduits, inheriting their sinuosity. Hybrid channels signify a failed or incomplete transformation. The channel belts occur isolated or stacked into multi-storey complexes, unconfined or formed within incised valleys. Unconfined complexes, composed of levéed channel belts, are relatively uncommon. Valley-confined complexes predominate and are overlain by isolated channel belts, often confined by the valley external levées.

Valley-fill complexes are characterized by an upward fining and a general decrease in sandstone net/gross. The majority of slope valley-fills in the study area and other reported cases show a development from deep incision to a transient equilibrium state recorded by the deposition of coarse sediment lag or non-aggradational channel belts, which are commonly overlain by MTDs emplaced when the valley reached its maximum relief. The middle to upper part of valley-fill consists of levéed channel belts recording aggradation, with possible development of non-aggradational meandering channel belts in the uppermost part prior to the valley abandonment. Similar meandering channel belts may also occasionally occur in the middle part of valley-fill succession. It is suggested that the variation among valley-fills can be due to external factors, such as slope tectonics and salt movements, or to an internal forcing through the interplay of valley incision depth, base-level change, turbidite-system equilibrium profile and slope general aggradation rate.

*Keywords:* Offshore West Africa, 3D seismics, Turbidite, Meandering, Levée, Point bar, Lateral accretion package, Outer-bank mound

## 1. Introduction

The last decade saw significant advances in the sedimentological understanding of deep-water sinuous channels and their features. Detailed studies of side-scan sonar and 3D seismic-reflection imagery have revealed a range of architectural elements associated with sinuous channels, such as lateral-accretion packages (LAPs) (Abreu et al., 2003; Mayall et al., 2006; Kolla et al., 2007; Labourdette, 2007), nested mounds (Clark and Pickering, 1996; Peakall et al., 2000), outer-bank bars (Nakajima et al. 2009), non-turbiditic mass-transport deposits (Deptuck et al., 2003; Samuel et al., 2003; Heinio and Davies, 2007; Armitage et al., 2009), levées (Clemenceau et al., 2000; Skene et al., 2002; Babonneau et al., 2004; Hubbard et al., 2009), crevasse splays (Demyttenaere et al., 2000; Mayall and Stewart, 2000; Posamentier and Kolla, 2003; Cross et al., 2009) and last-stage channel-fills (Kneller, 2003; Wynn et al., 2007). Most of these elements have been recognized in outcrops as sandy to gravelly deposits (e.g., Morris and Normark, 2000; Lien et al., 2003; Dykstra and Kneller, 2009; Kane et al., 2009; Kane and Hodgson, 2011) and are considered to be important components of hydrocarbon reservoirs (Prather, 2003; Mayall et al., 2006).

However, the previous studies have also indicated that elements of one type vary as sedimentary deposits and that it is unlikely for all architectural elements to occur within a single channel belt (e.g., Abreu et al., 2003; Kane et al., 2008; Amos et al., 2010; Janocko et al., 2011). Although some elements may be genetically linked, the development of one type of element may require flow conditions that virtually preclude formation another element type. This depositional variability of channelized flows and the variability of elements as sedimentary deposits may have a direct bearing on the observed diversity of deep-water channels (Abreu et al., 2003; Kneller, 2003; Nakajima et al., 2009). Studies of architectural elements in connection with the planform and cross-sectional geometry of channels may thus shed more light on the formative processes of these highly diversified systems and help predict their reservoir properties.

## 2. The aim of the present study

The present study documents the seismic characteristics of deep-water sinuous channels in an upper- to middle-slope setting in offshore West Africa and supplements these observations with well-core data and a range of outcrop analogues. We revisit further the taxonomic concept of channel classification (cf. Mayall and Stewart, 2000; Morris and Normark, 2000; Pirmez et al., 2000; Kneller, 2003), with a special focus on intra- and extra-channel architectural elements and the temporal changes in channel development within deep-water slope valleys.

The 3D seismic dataset used in the study extends about 25 km seawards, from the West African palaeo-shelf edge to the middle zone of continental slope, and covers an area of 80×55 km (4400 km$^2$). The stratigraphic interval studied is of Miocene age. The dataset is a post-stack time-migrated volume with a bin spacing of 12.5×12.5 m and a sampling interval of 4 ms. Seismic frequency ranges from 20 to 60 Hz, with an

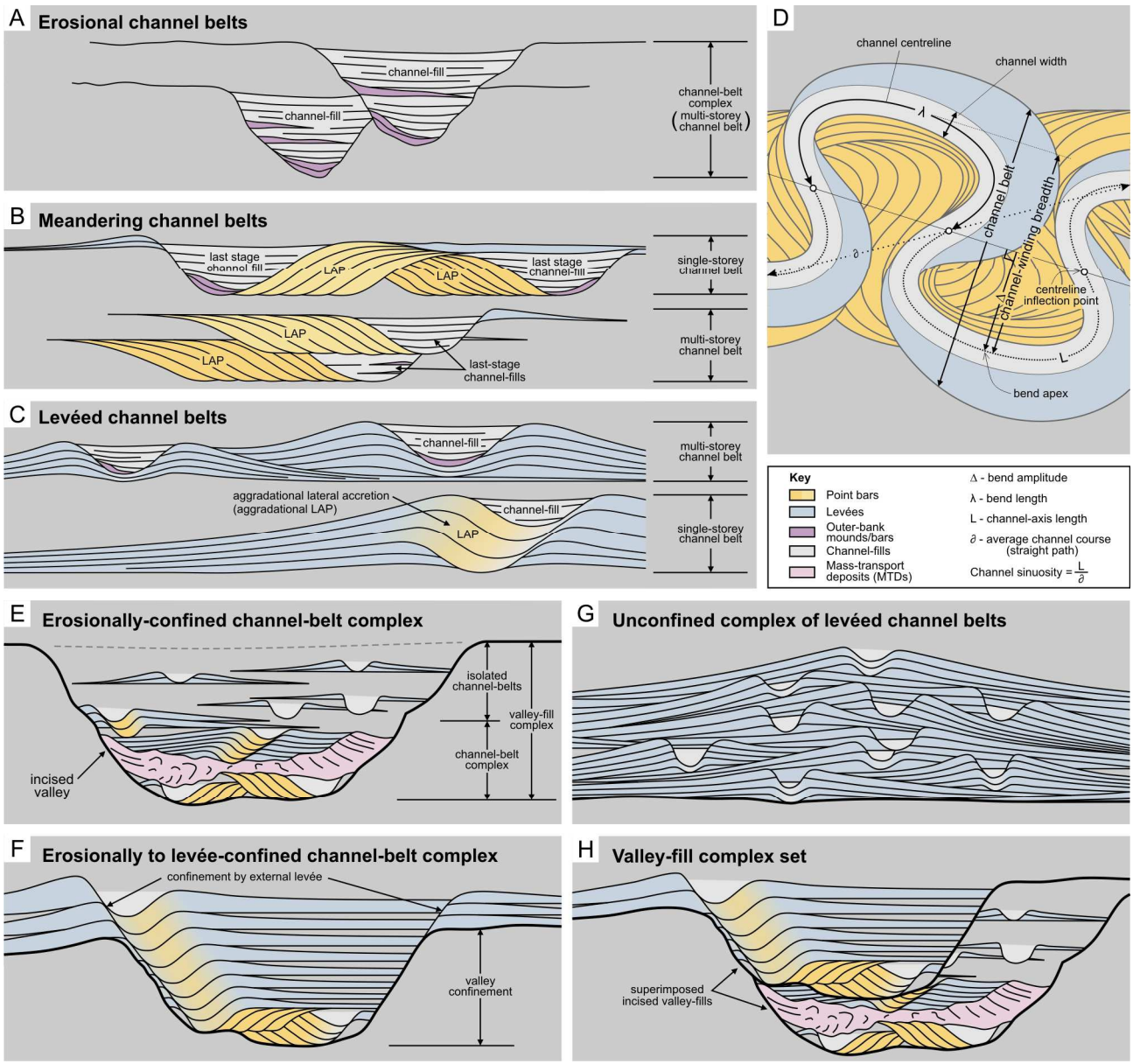


**Fig. 1.** Schematic diagrams illustrating basic terminology used in the present study. (A) Erosional channel belts. (B) Non-aggradational meandering channel belts. (C) Aggradational levéed channel belts. (D) Descriptive geometrical parameters of sinuous channel planform. (E) Erosionally confined channel-belt complex. (F) Erosionally to levée-confined valley-fill complex. (G) Unconfined complex of vertically offset-stacked levéed channel belts. (H) Valley-fill complex set. For definitions and further explanation, see text.

average of 40 Hz corresponding to a vertical resolution of ca. 10 m. The volume has been processed to zero-phase and displayed in SEG normal polarity, such that the positive amplitude (black or dark-blue hue in the display) reflects greater acoustic impedance. An average seismic velocity of 2000 m/s was used in the conversion of two-way travel time to metric depth for the purpose of calculating rock thicknesses in metres.

More than 1600 m of core samples were recovered from 29 wells in the study area. However, the samples and gamma logs from only five wells are utilized in this study, because the majority of the drilling targets are in areas with poor seismic resolution, where both seismic interpretation and well-to-seismic ties are extremely difficult. The problems with resolution are due to salt diapirism.

The quality of seismic data allows recognition of such stratigraphic features as valley-fills, palaeochannels, channel belts and their main architectural elements. The seismic recognition and interpretation of architectural elements have been bolstered by outcrop analogue studies from the Miocene Mt. Messenger Fm. of New Zealand, the Eocene Kırkgecit Fm. of Turkey, the Late Cretaceous Rosario Fm. of Mexico and the Late Carboniferous Ross Fm. of Ireland. The purpose of using outcrop analogues was to get an insight in the facies composition and depositional process of the elements from which no drilling samples were available. Cross-referring evidence from seismic imagery, outcrops and experiments is crucial to an understanding of turbiditic systems.

## 3. Terminology

Descriptive sedimentological terminology is after Harms et al. (1982) and Collinson and Thompson (1982). *Submarine channel* is defined as a conduit formed by and conveying sediment-gravity flows. Channelized flows deposit coarse sediment both inside and directly outside the conduit, which itself may migrate, and the resulting sand-prone and possibly gravel-bearing sedimentary body is referred to broadly as a *channel belt* (Bridge, 2003). Channel belts formed by simple downcutting and vertical aggradation are referred to as

*erosional channel belts* (Fig. 1A); those showing significant lateral accretion and conduit sideways migration are referred to as *meandering channel belts* (Fig. 1B); and those with seismically detectable levées are referred to as *levéed channel belts* (Fig. 1C). Some channel belts show major vertical aggradation combined with lateral accretion of sediment, which is called aggradational lateral accretion (Fig. 1C, lower part). Multi-storey channel belts, stacked vertically upon one another with or without significant offset, are referred to as *channel-belt complexes* (Fig. 1A–C).

The deepest, hydraulic axial zone of a channel is referred to as the *channel thalweg* (Bridge, 2003). It does not correspond strictly to the plan-view geometrical axis, or centreline, of the channel (Fig. 1D), which is more convenient to use in the analysis of channel-belt seismic maps. Accordingly, the sinuosity index of a channel or its particular segment is defined as the ratio of the centreline length to the corresponding straight-line distance (Bridge, 2003). Channels with a sinuosity index equal or greater than 1.1 are considered to be sinuous, non-straight. Other geometrical parameters of channel planform used in the study are (Fig. 1D):

- *channel width* – considered to be the maximum local distance between the channel banks;
- *channel depth* – measured as the vertical relief from the channel base in axial zone to the bank or levée crest;
- *channel bend amplitude* (or radius of curvature) – defined as the maximum departure of channel centreline from a straight-line path through the centreline inflection points;
- *channel bend half-wavelength* – the distance between centreline inflection points measured along the channel centreline; and
- *channel-winding breadth* – measured as the amplitude of the channel centreline bends.

A *submarine incised valley* (Carlson et al., 1982; Prather, 2003) is an underwater slope conduit incomparably deeper than the system largest channels, cut in earlier deposits by excessively erosive sediment-gravity flows. In contrast to the more permanent deep submarine conduits, such as bedrock canyons, the incised valleys are cut and filled by the channelized turbiditic system, possibly several times over during the time-span of its activity. Submarine incised valleys may not necessarily be related to sea-level changes and the fluvial incised valleys formed by forced regressions (Dalrymple et al., 1994), but they similarly result from major re-adjustments of the system morphometric profile.

Large-scale levées that flank an incised valley are referred to as *external levées*, whereas the smaller-scale levées flanking individual channels are called *internal levées* (Kane and Hodgson, 2011). Channel belts formed within the valley confinement are considered to be *erosionally confined* (Fig. 1E), whereas those constrained laterally by external levées are considered to be *levée-confined* (Fig. 1F). A submarine incised valley-fill commonly evolves from erosionally confined to levée-confined (Fig. 1F). An aggradational stack of levéed channel belts unrelated to a valley is referred to as an *unconfined channel-belt complex* (Fig. 1G).

A *valley-fill complex* may comprise a complex of multi-storey channel belts as well as isolated channel belts (Fig. 1E) or be composed mainly or entirely of mud. Mud-prone abandoned valley-fills occur in the study area, but are not considered here. Two or more valley-fill complexes stacked upon one another (Fig. 1H) are referred to as a *valley-fill complex set* (cf. Sprague et al., 2002).

## 3. Architectural elements of sinuous deep-water channels

An architectural element is a depositional body defined by its geometry, facies assemblage, scale, a particular formative process or suite of processes, and its depositional setting (Miall, 1985). In seismic interpretation of ancient deposits, the recognition of architectural elements is generally based on their geometry, scale and depositional setting, whereas facies composition and processes are inferred from other geological data (e.g., outcrop analogues, laboratory experiments, numerical modelling). The elements described here occur within sinuous channel belts and indicate sites of preferential sediment deposition by the channelized flows involved.

### *3.1. Lateral-accretion packages (LAPs)*

Lateral-accretion packages (Abreu et al., 2003) appear in attribute maps and time slices as features similar to fluvial scroll bars (Fig. 2B) or as crescent-shaped high-amplitude reflection patches (Fig. 2B). They may locally appear also as closely spaced, high-amplitude sinuous threads (Fig. 3A, C). In seismic profiles, LAPs are typified by discontinuous, offlapping shingled reflections dipping at 5–10° towards the last-stage channel thalweg (Fig. 2, sections B–B', C–C' and D–D'). In places where the LAP thickness is below the seismic tuning thickness (i.e., seismic wavelength), the inclined reflections are unrecognizable and the package appears as a single, continuous high-amplitude reflection (Fig. 2, section A–A'). The LAPs in such a case can only be inferred from attribute maps. The bases and tops of LAPs are generally flat and horizontal. The areal extent of LAPs is in the range of 40–480 $m^2$ and their thicknesses are up to 30 m.

The sedimentary facies of LAPs are inferred from drilling cores. Four separate cores from three different channel belts at the base of valley-fill complexes have been analysed (Figs. 3 and 4). On the basis of seismic sections and attribute maps, each LAP is considered to be an element of a single-storey channel belt formed by the lateral migration of a sinuous channel. The two cores from channel belt A both show an overall fining-upward trend and similar facies, as they consist of massive to planar parallel-stratified, normally-graded sandstone beds with scattered mudclasts (Fig. 4, cores A1 and A2). Sandstones are mainly coarse- to fine-grained, overall slightly coarser in core A1. Mudclasts are angular to subrounded and 0.5–20 cm in length. They occur either at the bed base, where they often show imbrication, or in the bed middle part where they are more scattered and lack preferential orientation. Core A2 shows also normally-graded beds of sand-rich mudclast conglomerate.

The core from channel belt B shows beds of sand-supported, extra- and intra-formational conglomerates in the lower part, whereas the upper part is dominated by planar parallel-stratified to ripple cross-laminated sandstone beds (Fig. 4, core B1). Extraformational lithic clasts are up to 5 cm in size, but the maximum size of mudclasts reaches 22 cm. The conglomerate beds show planar parallel stratification with clast imbrication and typically pass upwards into a massive or crudely stratified sandstone. The core from channel belt C shows only the lower part of the LAP, which differs from the others in that it consists of thick, amalgamated, massive to crudely stratified sandstone beds (Fig. 4, core C1). The bed bases are erosional, commonly strewn with imbricated mudclasts up to 8 cm in length. These thick beds are intercalated with minor thin beds of planar parallel-stratified to ripple cross-laminated sandstone capped with siltstone.

The LAPs are interpreted to represent point bars formed due to the lateral channel migration. Each shingled high-amplitude reflection dipping towards the last-stage channel in the seismic profiles corresponds to a low-impedance interval with a thickness of less than ¼ of the seismic wavelength. The shingled seismic signature of the LAPs is thus more a function of lithology than of true bedding. For example, a single sandstone bed rich in mudclasts in its lower part will produce two separate reflections of low and high amplitude, respectively.

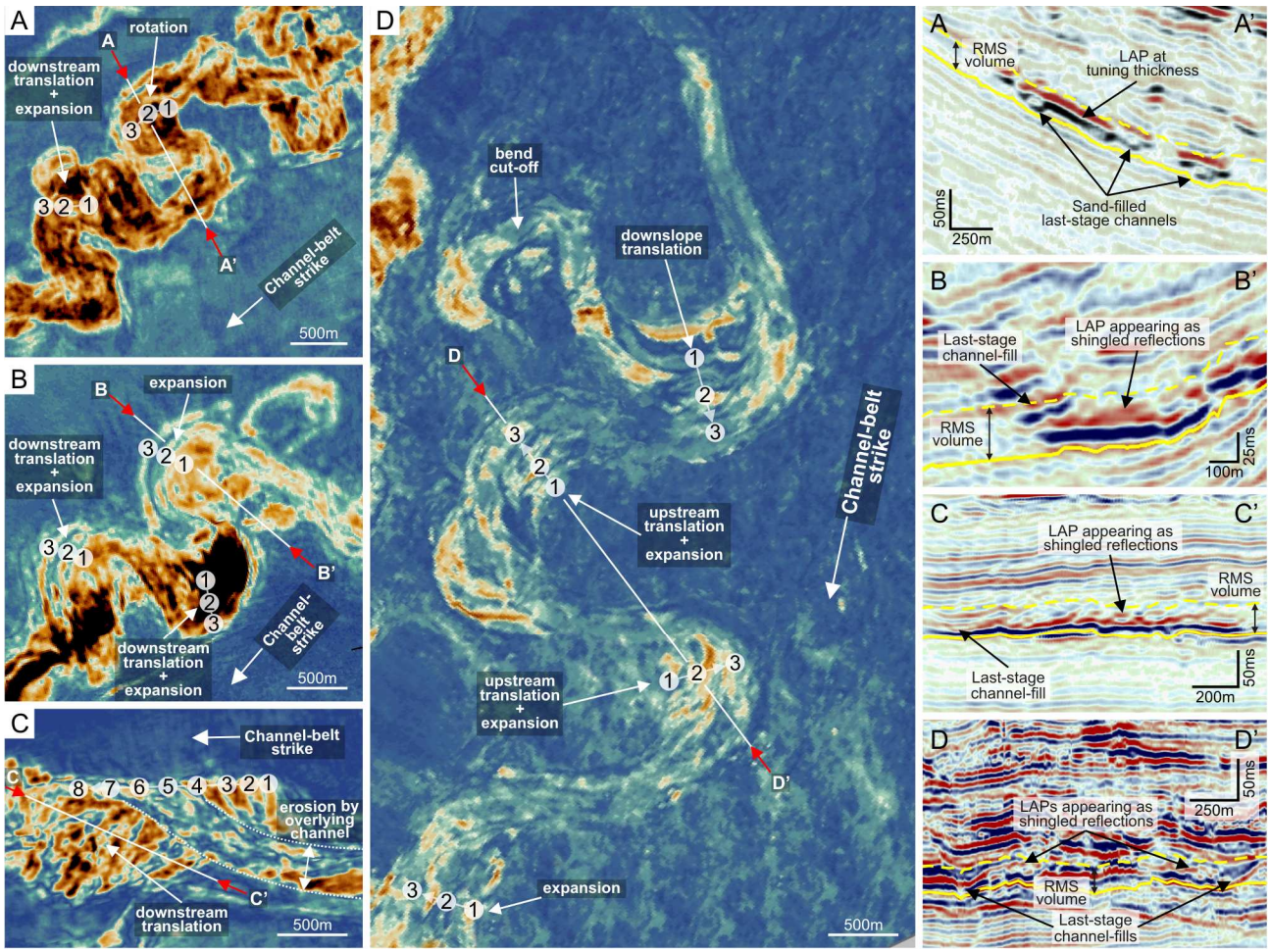


**Fig. 2.** Seismic attribute maps (A–D) and corresponding vertical sections showing the planform and cross-sectional geometry of lateral accretion packages (LAPs) in the study area. (A) Map of LAPs manifested as high-amplitude reflection threads, showing channel-loop rotation and expansion combined with downstream translation. The LAPs have a thickness at the margin of seismic resolution and appear as a single high-amplitude reflection (see cross-section A–A'). (B) Map of LAPs resembling fluvial scroll bars, with the crescent-shaped patches of high-amplitude reflections showing bend expansion followed by expansion with downstream translation. In vertical section, the LAPs show up as shingled reflections dipping towards the last-stage channel thalweg (see cross-section B–B'). (C) Map of a purely downstream-translated LAP, with high-amplitude reflection threads and with a pattern of shingled reflections in vertical section (see cross-section C–C'). (D) Map of LAPs with a scroll-like pattern showing bend expansion combined with downstream and upstream translation; cross-section D–D' shows shingled reflections. Note that the LAP bases and tops are generally flat and that the LAP planform development may vary from one bend to another.

On the basis of their planform development, the point bars in the studied channel belts can be classified as expansional, downstream or upstream translational, rotational or representing a combination of these three main modes of evolution (Fig. 2; terminology after Brice, 1974). The development of point bars appears to vary from one channel-belt segment to another and lacks any systematic spatial trend. This variability suggests that the planform evolution of point bars may depend strongly on the local seafloor gradient and substrate cohesiveness, which would in turn control the planform of channel bends and curvature of their transitions.

The lower parts of point-bar LAPs are dominated by stratified sand-supported conglomerates and massive to crudely stratified sandstones. The stratified conglomerates and sandstones represent the turbidite division $R_1$ of Lowe (1982) and division *b* of Bouma (1962), respectively, and are interpreted to be tractional upper flow-regime deposits of low-density turbidity currents (sensu Lowe, 1982). Although massive sandstones occur mainly in the lower part of LAPs, they can be found also in the middle and upper part. They represent the turbidite division $S_3$ of Lowe (1982) and indicate sand deposition by rapid dumping from a decelerated, high-density turbidity current (see also Lowe, 1988). The deceleration and abrupt basal densification of flow can be attributed to its oblique climbing on the point bar, with flowline expansion towards the inner bank and frictional loss of energy (Janocko et al., 2011). The planar parallel-stratified to ripple cross-laminated sandstone beds are classical Bouma-type turbidites T*bc*, deposited by low-density turbidity currents and occurring mainly in the upper part of point-bar LAPs.

Point-bar deposits similar to those in the West African offshore channel belts can be found elsewhere exposed on land. An analogous example is afforded by the Waikiekie South Beach cliff section of the Mount Messenger Formation in New Zealand's North Island (Janocko and Nemec, 2011). The LAP here is smaller than the seismically recognized cases, but has a similar geometry and similar facies assemblage (Fig. 5). The channel belt occurs at the base of a valley-fill complex (Fig. 5A, B), which is located in the lower part of a large valley-fill complex set (Arnot et al., 2007). The estimated channel-belt width is ~170 m, with about two-thirds of it occupied by the LAP. The LAP is 6 m thick, composed of beds with a mean inclination of 8°. The deposits are laterally-accreted couplets of massive mudclast conglomerate and planar parallel-stratified sandstone (Fig. 5C, D), with the last-stage aggradational channel-fill composed of amalgamated, massive to crudely

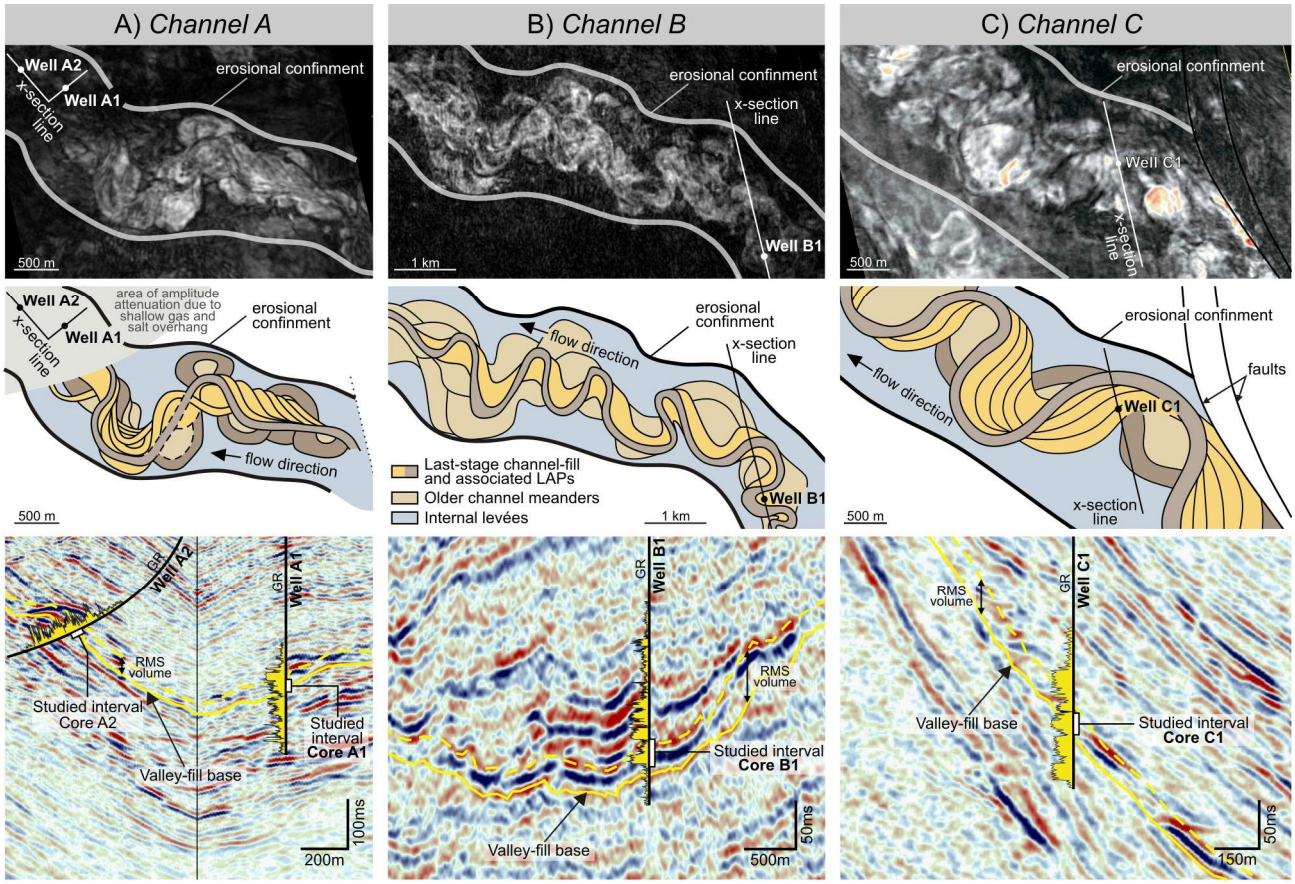


**Fig. 3.** Seismic maps (upper row), their interpretation (middle raw) and the corresponding vertical sections (lower row) of meandering channel belts at the base of valley-fill complexes in the study area. The channel belts are interpreted to be single-storey non-aggradational meander belts that evolved by bend cut-off and lateral shifting. The seismic sections include gamma-ray (GR) well logs of the meander belts, with the corresponding core logs and facies details shown in Fig. 4.

stratified sandstone beds occasionally bearing basal mudclast lags (Fig. 5A, B). The mudclast conglomerates have sandy matrix, consist of angular to subrounded clasts up to 30 cm in length and have a clast- to matrix-supported texture. Most of these conglomeratic divisions are normally graded, but some show a coarse-tail inverse grading. They are thickest in their down-dip parts and tend to thin up-dip in the LAP cross-section, where they also become finer grained and their bases less erosional. The sandstone divisions, in contrast, are lenticular in the LAP section and their down-dip parts are generally thinner, truncated by the overlying bed (Fig. 5D). The top and base surfaces of the LAP are planar, originally horizontal, although the lateral migration of channel thalweg involved uneven scouring and resulted in local morphological irregularities of the channel-belt base (Fig. 5A, B).

The successive conglomerate-sandstone couplets in the LAP are thought to be products of density-layered bipartite flows (cf. Postma et al., 1988). Mudclasts were derived from erosion of the underlying, semi-consolidated slope mud. The mudclast conglomerates were deposited by erosive turbidity currents that charged themselves at the base with cohesive material and underwent abrupt deceleration at the channel bend. Basal densification of the flow due to rapid suspension fall-out (Lowe, 1988) was then accompanied by cohesive freezing of the bedload layer. Inversely-graded conglomerates suggest a co-genetic debris flow spawned and dragged briefly along by the flow, with the size of mudclasts diminished by the stronger frictional shear near the base. The overlying sandstone division T*ab* of each couplet was deposited by flow that rid itself of the excess basal load and kept dumping sand directly from turbulent suspension before reversing to deposition from upper-stage plane-bed tractional transport (Harms et al., 1982; Lowe, 1982).

### *3.2. Outer-bank mounds/bars*

The sinuous channels in seismic-volume attribute maps commonly show longitudinal patches of high-amplitude reflections in the apical zone of channel bends (Fig. 6). These features are associated mainly with relatively sharp bends of high-sinuosity channels, levéed or non-levéed, and occur also in the last-stage channels of some meander belts. Their occurrence seems to be independent of the channel width/depth ratio. In vertical seismic sections, these features appear as high-amplitude horizontal reflections at the base of channel belt, but may be indiscernible if too thin relative to seismic resolution, though visible in attribute map. Their areal extent is in the range of 5–60 $m^2$ and thicknesses up to 30 m. No drilling cores of these deposits are available, but their laterally continuous high-amplitude seismic signature indicates coarse-grained deposits with little or no facies heterogeneity.

The high-amplitude reflection patches at channel thalweg bends are thought to represent deposits recognized elsewhere as “outer-bank bars” (Nakajima et al. 2009) or “nested mounds” (Phillips, 1987; Timbrell, 1993; Clark and Pickering, 1996). Although there seem to be significant differences in the extent and geometry of the architectural elements reported under these two labels, the high-amplitude patches in the present case cannot be differentiated due to insufficient seismic resolution. Nevertheless, the evidence that the outer-bank high-amplitude patches occur mainly at sharp channel bends, irrespectively of the channel aspect ratio and presence of levées, suggests that they represent coarse-grained deposits formed by an abrupt local deceleration of flow and are not necessarily related to the flow overspill (cf. Clark and Pickering, 1996).

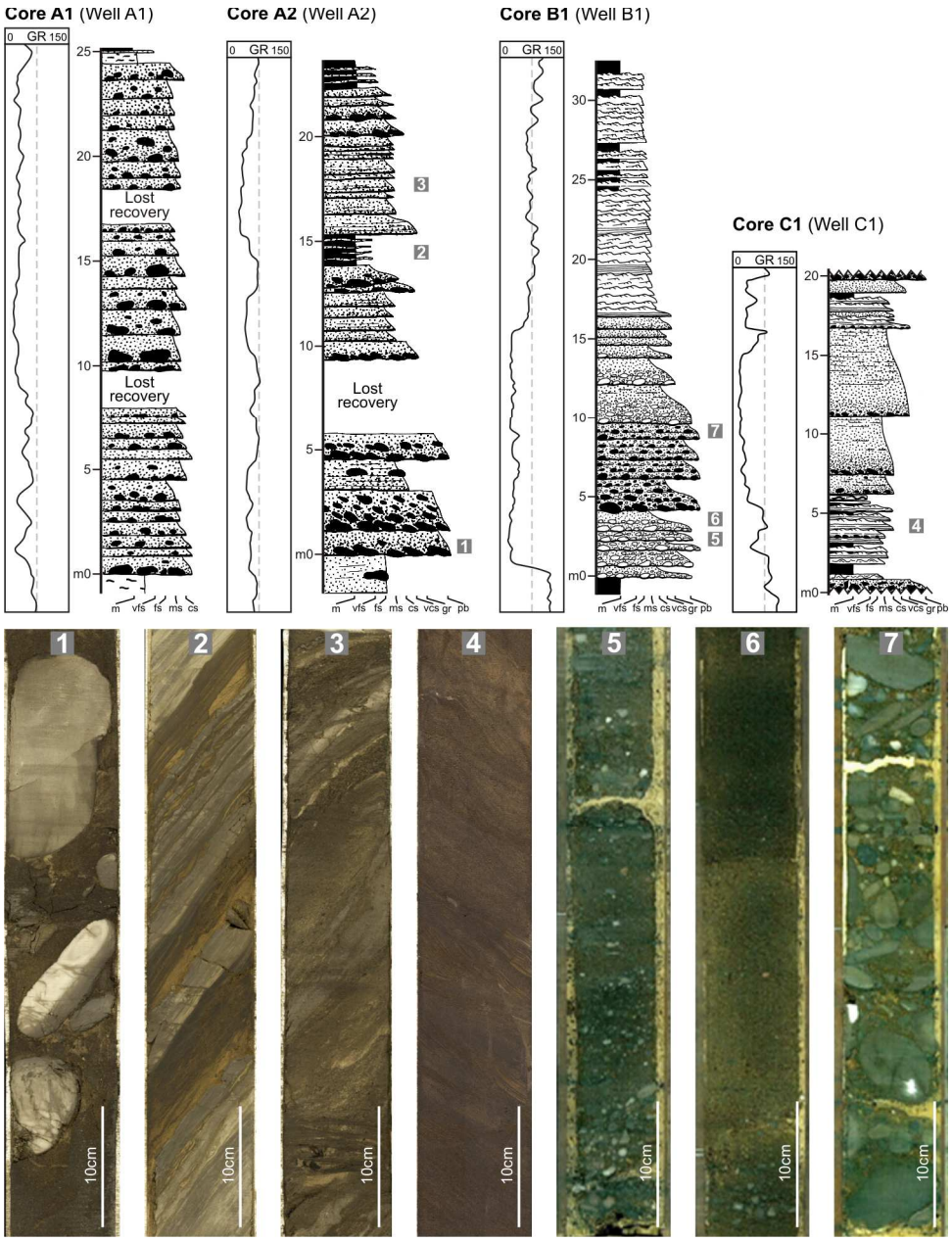


**Fig. 4.** Sedimentological well-core logs and photographic facies details of the meander belts shown in Fig. 3. Well logs A1–B1 show whole point-bar LAP successions and well log C1 shows the lower part of a point-bar LAP. Log grain-size scale: m = mud; vfs to vcs = very fine to very coarse sand; gr = granule gravel; pb = pebble gravel. GR is the well gamma-ray log.

An outcrop analogue of such deposits is afforded by the San Fernando canyon section of the Rosario Fm. in Baja California, Mexico (Fig. 7; Janocko and Nemec, 2011). The outcrop shows a meandering channel belt in the lower part of a submarine valley-fill complex. The belt LAP consists of conglomerate-sandstone couplets inclined at ~6° towards the last-stage channel and downlapping an erosional, originally horizontal base of the channel belt. The last-stage channel-fill consists of conglomerate-sandstone couplets that show aggradational lateral accretion, with the conglomerate divisions thinning and sandstone divisions thickening in the updip direction. In the lowermost couplet, the parallel-stratified conglomeratic division forms a mound with an irregular convex-upward top and with the strata changing laterally their attitude from paralleling the LAP bedding at the inner bank to gently rising against the outer bank. The conglomerate bed truncates the underlying beds, which suggests that the depositing flow had initially broadened the conduit by eroding its both banks. The overlying sandstone division has a sub-horizontal top and an uneven thickness compensating for the morphological irregularity of the conglomerate top. The conglomerate clast imbrication indicates sediment transport obliquely towards the outer bank (Janocko and Nemec, 2011), which suggests that the flow helicoid at the channel bend was rising against the outer bank. This evidence supports the hypothetical interpretation by Nakajima et al. (2009) of the origin of outer-bank bars.

The mounded conglomerate unit is considerably smaller than the host channel and hence is probably an outer-bank mound, rather than an outer-bank bar (cf. Nakajima et al., 2009). However, the attitude of its internal stratification suggests that the mound might possibly aggrade more and evolve into a thicker accretionary bar if the depositing flow had a longer duration or similar flows reoccurred (see Kneller and Branney, 1995; Vrolijk and Southard, 1997). We thus infer the features reported as outer-bank bars may simply be more pronounced accumulations of nested mounds, variously modified by

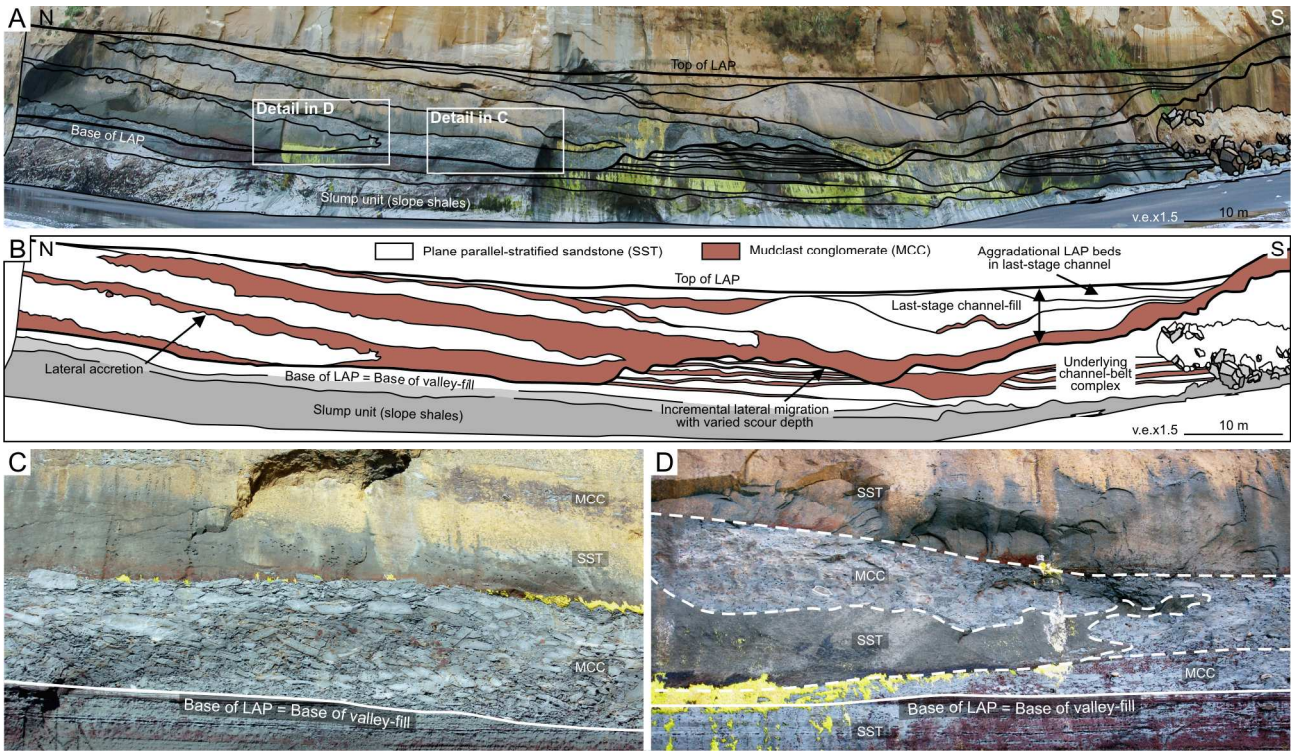


**Fig. 5.** Outcrop section of a meandering channel belt in the Mount Messenger Fm. at the Waikiekie South Beach, New Zealand's Northern Island. (A) Cliff photomosaic and (B) overlay drawing of the point-bar LAP and associated last-stage channel-fill. The close-up details show: (C) a mudclast conglomerate-sandstone couplet in the LAP and (D) a down-dip pinchout of the sandstone division. Note the hydroplastic deformation caused by sediment loading.

intervening flows, and that both these features owe their origin to channelized flows rising against the outer bank at a channel bend.

### *3.3. Mass-transport deposits (MTDs)*

Non-turbiditic mass-transport deposits, attributed to such processes as slides, slumps and debris flows, occur at various scales in submarine channels and valleys. Slide blocks from valley walls are among the largest features, with an areal extent reaching 1500 $m^2$ and thicknesses up to 120 m. In seismic attribute maps, they are recognizable as low-amplitude, elongate to crescent-shaped features associated with scallop-shaped scars at channel or valley margins (Fig. 8A). In seismic cross-sections, slide blocks show rotational bases, stepped tops and undisturbed, parallel low-amplitude internal reflections (Fig. 8B, E).

Slump deposits appear in attribute maps as circular or crescentic high-amplitude patches (Fig. 8C). In cross-sections, they typically show curved rotational bases and internal transparent pattern of low-amplitude discontinuous reflections (Fig. 8D). They are often laterally more extensive than slide blocks, with areas of up to 2000 $m^2$ and thicknesses reaching 50 m. Deposits attributed to large debris flows may or may not be associated with slump scars and are typically spread across the entire width of the channel or valley (Fig. 8F). In both plan view and cross-section, they appear as transparent to chaotic seismic facies with a sharp, often erosional base and irregular top. In the study area, the MTDs are generally recognized in valleys, rather than in channels, which may be due to the limited seismic resolution or to a natural scarcity of channel-bank collapses, as compared to the gravitational instability of steep valley walls.

MTDs have been reported from deep-water channels and valleys (e.g., Droz and Bellaiche, 1985; O'Connell et al., 1995; Morris and Normark, 2000; Deptuck et al., 2003; Samuel et al., 2003; Heinio and Davies, 2007; Armitage et al., 2009), and are considered to be an important element affecting the evolution of submarine conduits and their hydrocarbon storage potential (Prather, 2003). In the present case, the local collapses probably played a major role in the development of deep-water incised valleys from erosional channels. The emplacement of MTD may cause flow retardation and enhance deposition in the thalweg zone (Peakall et al., 2000; Nakajima et al., 2009) or may cause flow avulsions (Fig. 8C), whereas the uneven top relief of slump and slide bodies may pond turbidity currents or entrap channels (Fig. 8B; Faulkenberry, 2004).

The internal character of MTDs varies, depending upon the collapsing sediment facies of the channel or valley wall and the intensity of shear deformation involved. As end-members, slide blocks are relatively coherent and internally intact, whereas debris-flow bodies are strongly homogenized by pervasive shear. The MTDs derived from channel-bank levée collapses tend to be sand-prone (Kane and Hodgson, 2011), but for this reason also have a low preservation potential in an active channel. The more cohesive, mud-prone MTDs will provide abundant mudclasts and affect the rheological properties of subsequent currents, while possibly affecting also the physiographic development of the channel (Hodgson, 2009).

### *3.4. Levées*

Levée deposits are the largest and most extensive sand-prone architectural element of sinuous channel belts. They are thus important as an exploration target and element of reservoir characterization. They occur at various scales, and their morphology and facies help to shed light on the character of flows conveyed by the channel. Levées occurring in isolated unconfined channel belts, in unconfined and confined channel-belt complexes and at valley margins (Fig. 9) are described separately below.

In isolated unconfined channel belts, levées are typically two

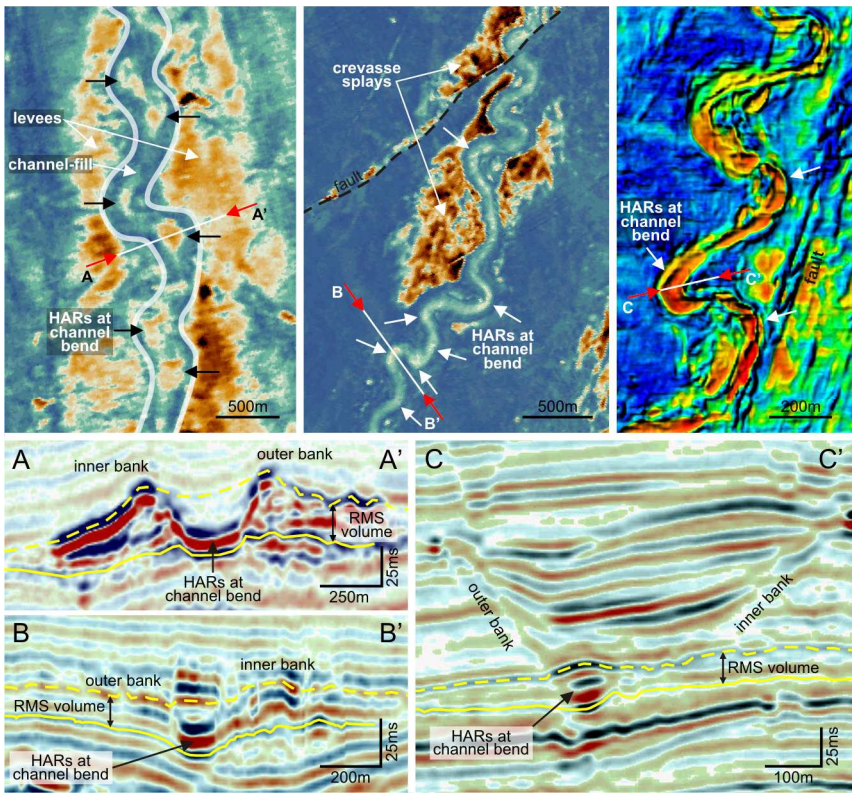


**Fig. 6.** Seismic maps of levéed aggradational channel belts (top left and middle) and an erosional channel belt (top middle) in the study area. The RMS volumes shown by the maps are indicated in the corresponding vertical sections below. The high-amplitude reflections (HARs) at channel bends are thought to represent outer-bank mounds/bars.

or more reflections thick and characterized by a gull wing-shaped cross-section (Fig. 9A). The reflections downlap the underlying deposits and range from low-amplitude discontinuous to high-amplitude continuous. In all cases, the levée reflections are of higher amplitude than the reflections of the associated channel-fill. The height of the outer-bank levées (40–60 m) generally exceeds the height of the inner-bank levées (30–50 m) along the entire studied course of a channel. The top surface of these levées is typically smooth and their thickness decreases in an exponential or hyperbolic (power-law) manner with distance from the channel (Fig. 9E). Some of the large outer-bank levées have an undulating, wavy top downstream of

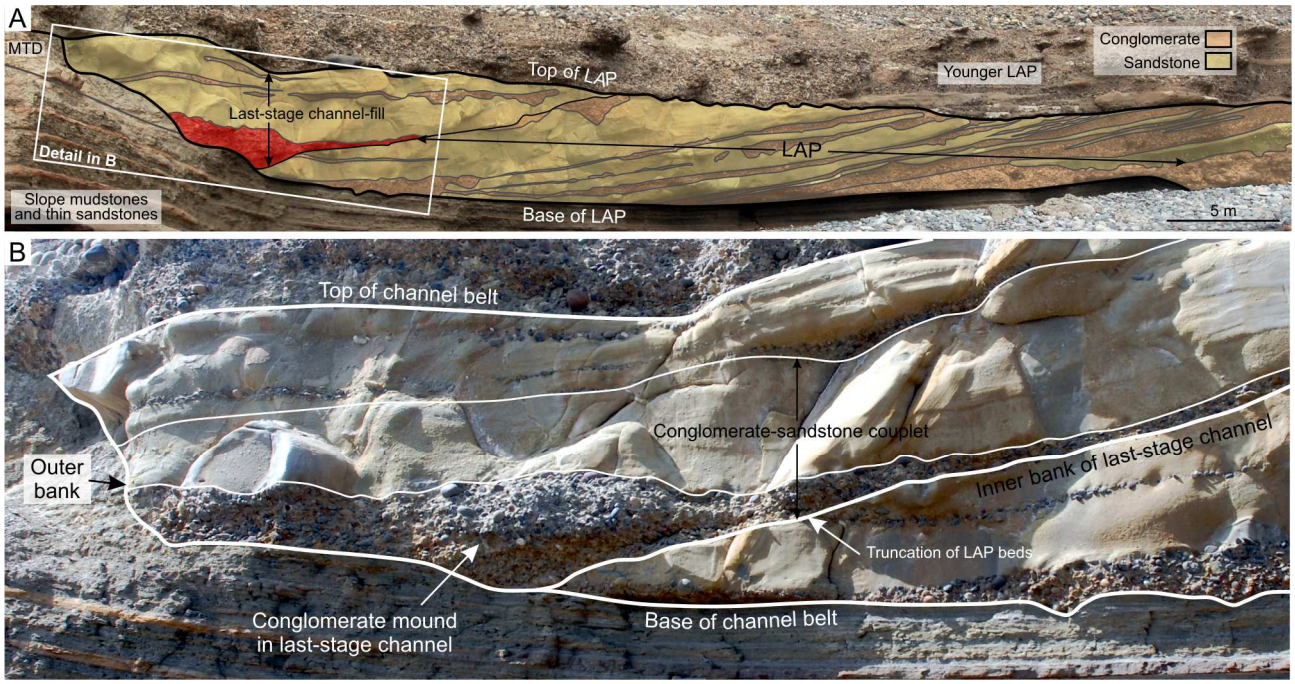


**Fig. 7.** (A) Outcrop section of a meandering channel belt in the Rosario Fm., Mexico, showing a conglomeratic outer-bank mound (indicated in red) at the base of the last-stage channel-fill. (B) Close-up view of the mound, showing how the plane-parallel stratification of the mound changes laterally its attitude from paralleling the LAP bedding on the right to sloping gently away from the outer bank on the left. Note the erosional base of the overlying conglomerate-sandstone couplet truncating the LAP beds to the right.

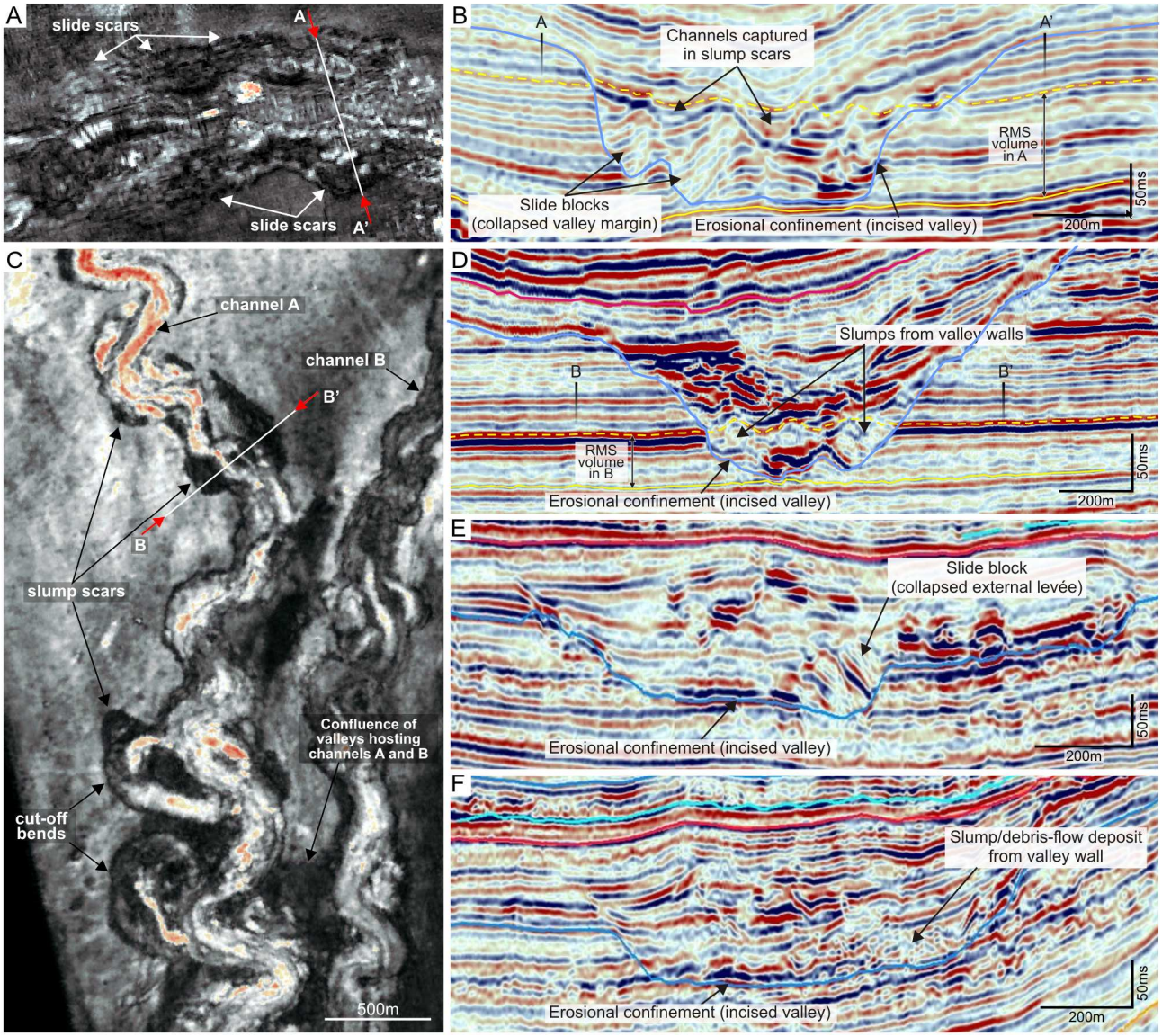


**Fig. 8.** Seismic evidence of mass-transport deposits (MTDs) in the valley-fill complexes in the study area. The seismic maps (A, C) and corresponding vertical sections (B, D) show evidence of slides and slumps. Slide, slump and possible debris-flow deposits are shown also in the two other sections (E, F).

channel bends (Fig. 9A), which is attributed to the formation of overbank sediment waves. More irregular, jagged tops may be due to synsedimentary gravitational faults dipping away from the channel. The continuity of reflections from the levée and channel-fill varies considerably, and so does probably the connectivity of these two elements. In most cases, the reflections in the upper part of levée can be traced to the last-stage channel-fill, but those in the lower part tend to terminate at the channel bank. In seismic attribute maps, the levées in unconfined solitary channel belts appear as areas of a high-amplitude signal declining away from the channel. The levée width tends to be inversely proportional to the channel-belt gradient.

In unconfined or weakly-confined channel-belt complexes, levées are typically stacked in a compensational manner and show complex geometries (Fig. 9B). In simple cases, the levées show continuous, onlapping high-amplitude reflections and an exponential decrease of thickness away from the channel (Fig. 9F). In more intricate cases, where younger levées extend over an abandoned levéed channel belt, the overlapping levée shows an irregular, concave- to convex-upward top and continuous, similarly undulated high-amplitude reflections (Fig. 9B). The levée relief varies from less than 20 m to more than 100 m. There is rarely a continuity of reflections from the levée to channel-fill, except where an abandoned channel segment was buried by levées of adjacent active channel. In seismic maps, the levées are asymmetrical and increase in areal extent with a decrease of channel-belt gradient.

In confined channel-belt complexes, levéed channel belts tend to show systematic aggradation, rather than compensational stacking (Fig. 9C). The confined mode of channel-belt development typically results in simpler levée geometry than observed in unconfined complexes. Two types of levées, internal and external, are associated with confined channel-belt complexes (Kane and Hodgson, 2011). The external levées in cross-sections are typified by downlapping, high-amplitude continuous reflections and locally show small cross-cutting crevasses (Fig. 9C). The continuity of external levée reflections to the valley-fill is poor in erosionally-confined channel-belt complexes, but good in levée-confined complexes (Fig. 9C). The thickness of proximal levée varies from 50 to 120 m, and the levée lateral tapering trend is best approximated by an exponential function (Fig. 9G). In attribute maps, the external levées are recognizably asymmetrical, with scoop-shaped indentations (collapse scars) at the inner margin. The internal levées, in turn, are gull wing-shaped and 20–50 m thick,

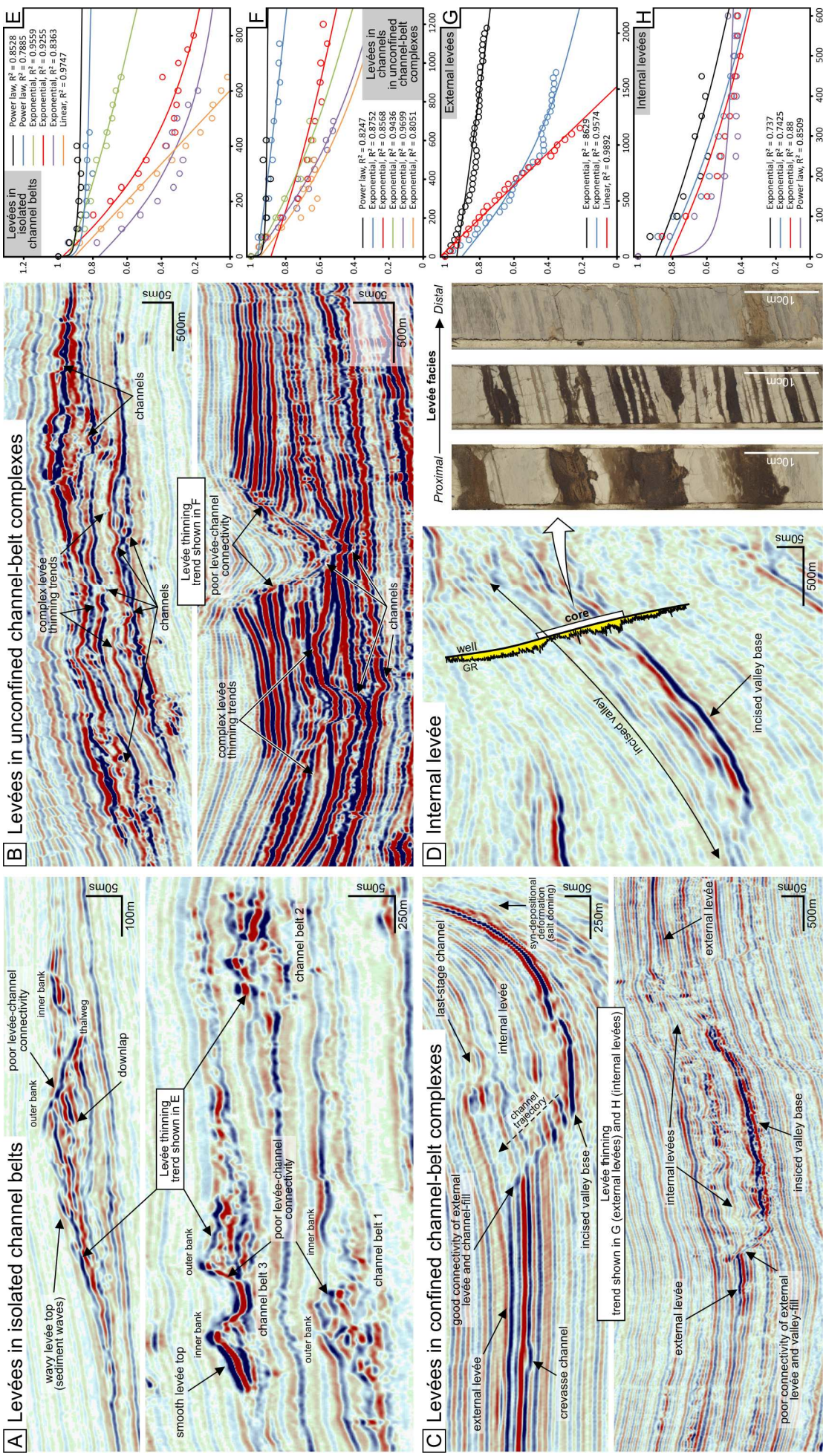


**Fig. 9.** Seismic evidence of levées in the study area. (A) Example seismic sections showing levées in unconfined isolated channel belts, where the levées downstream of sharp bends locally have wavy tops attributed to the occurrence of sediment waves. (B) Example seismic sections showing levées in unconfined multi-storey channel-belts stacked in a compensational manner. (C, D) Example seismic sections showing levées in channel belts confined by valley relief or external levées, with well-core photographs of internal levée facies. The diagrams to the right show the lateral thinning trend of levées in isolated (E) and multi-storey channel belts (F), and of the external (G) and internal levées (H) in submarine valleys in the study area.

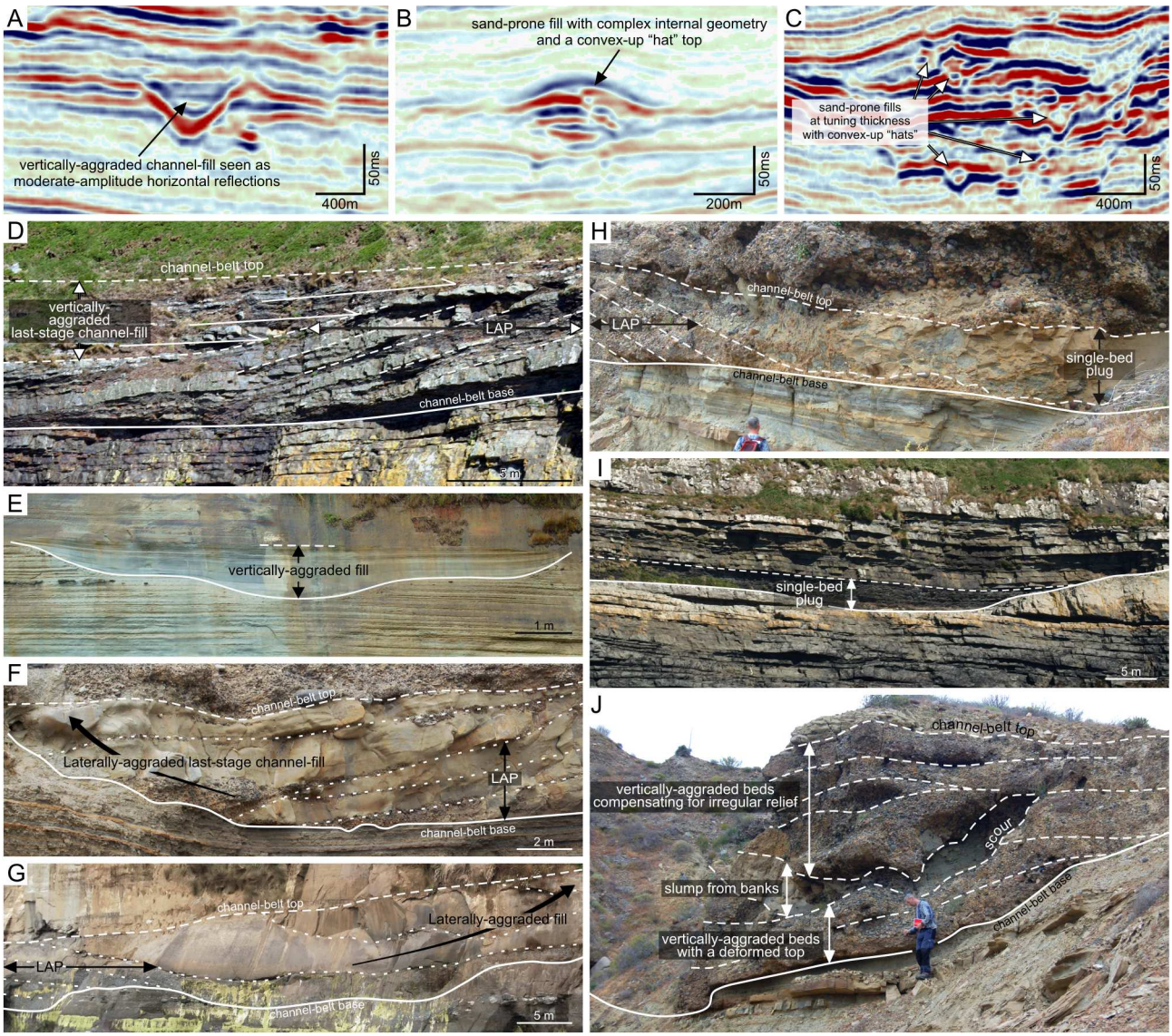


**Fig. 10.** Seismic evidence and outcrop analogues of last-stage channel-fills. (A) Aggradational fill of an erosional channel with one-side levée, seen as moderate-amplitude horizontal reflections. (B) Sand-prone fill of an erosional channel with complex internal geometry and a convex-up "hat" top due to differential compaction. (C) Sand-prone fills of levéed channels at seismic tuning thickness, showing convex-up "hat" tops. (D) Aggradational, thinly-bedded heterolithic fill of a meandering channel in the Ross Fm., Rehy Cliffs, Ireland. (E) Aggradational fill of a small erosional channel, comprising amalgamated planar parallel-stratified sandstone beds, in the Mt. Messenger Fm., Waikiekie South Beach cliff, New Zealand. (F) Laterally-aggraded fill of a meandering channel, composed of parallel-stratified conglomerate-sandstone couplets, in the Rosario Fm., Pelican Point, Mexico. (G) Laterally-aggraded fill of a meandering channel, comprising massive and parallel-stratified sandstone beds with occasional mudclast lags, in the Mt. Messenger Fm., Waikiekie South Beach, New Zealand's North Island. (H) Single-bed plug of a meandering channel, composed of sand-rich mudclast conglomerate, in the Rosario Fm., San Fernando Canyon, Mexico. (I) Single-unit plug of a small erosional channel, composed of laminated mudstone, in the Ross Fm., Kilbaha Cliffs, Ireland. (J) Composite channel-fill with a basal package of vertically-aggraded conglomerate beds thinning against outer bank, deeply re-scoured and overlain by bank-derived fine-grained slump deposit, whose uneven relief was smoothed and buried by a new aggradational package of conglomerate beds; example from the Rosario Fm., San Fernando Canyon, Mexico.

characterized by continuous to discontinuous low-amplitude reflections (Fig. 9C) downlapping the substrate and often also onlapping the confinement margin. Their lateral thinning trend is best described by an exponential function (Fig. 9H). In attribute maps, the internal levées show up as uniform or patchy low-amplitude zones paralleling the sinuous planform of the associated channel. A 50-m core sample from the internal levées in one of the channel complexes (Fig. 9D) shows a fining- and thinning-upward trend and a sandstone net/gross of 19 %. The deposits are thinly bedded (1–30 cm), planar parallel-stratified to ripple cross-laminated sandstones interlayered with mudstones.

The deposition of levées in deep-water channel belts is attributed to the overspill of turbidity currents conveyed by the channel. A turbidity current spills out of the channel because it is either volumetrically too large for the channel capacity or in a hydraulic disequilibrium with the channel geometry. The channel-forming currents are thought to be considerably thicker than the actual channel depth and hence inevitably spilling out, but also an intervening smaller current may run up on the outer bank at channel bends and spill over until the flow volume critically declines and inertia drive dissipates (Straub et al., 2008). Currents may spill out excessively in response to the local plugging of channel by MTDs and will also increasingly spill over as the last-stage channel begins to be filled with sediment prior to abandonment.

The outer-bank levée in most of the studied channel belts is higher than the inner-bank levée, which suggests that the flow superelevation and outer-bank run-up at channel bends played a significant role (Straub et al., 2008, 2011; Amos et al., 2010).

The exponential outward-thinning trend of levées is consistent with similar observations from levéed channels in many other submarine systems (Skene et al., 2002; Skene and Piper, 2005). Kane et al. (2010) have attributed the exponential trend to the spill-out of sustained (long-duration), quasi-steady high-competence flows, which is in agreement with the hydraulic conditions for the formation of overbank sediment waves found on levées (Fig. 9A; Nakajima and Satoh, 2001; Cartigny et al., 2010).

The poor connectivity of levée and channel-fill in isolated channel belts and unconfined channel-levée complexes suggests that the denser, channel-confined parts of flows were commonly bypassing the bends and eroding the outer bank, even though these sinuous channels generally show little or no lateral migration. The notion of erosional bypass is supported by the differential aggradation of the channel floor and levées.

In contrast, the connectivity of levée and channel-fill appears to be good in the aggradational channel belts of erosionally- or levée-confined channel-belt complexes. The channels in such settings were apparently conveying fully depositional flows, with the channel-floor aggradation keeping pace with the levée build-up.

The external levées are thought to form when the overbank flow from a channel inside the valley spills out beyond the valley margins (Kane et al., 2010). These levées are unlikely to be connected with the parental channel-fill because of the negligible capacity of valley walls to store sediment and the valley-margin tendency for mass wasting.

### *3.5. Last-stage channel-fills*

The last-stage channel-fills, as an element heralding channel-belt abandonment, are generally deposited by flows differing from those which formed and shaped the channel belt (Clark and Pickering, 1996; Kneller, 2003; Wynn et al., 2007) and hence are genetically unrelated to the belt's other, earlier-formed architectural elements. However, the channel-fills themselves are an important element, because they vary from sand- to mud-prone, may constitute a major part of channel belt and determine the connectivity of the channel belt's other architectural elements.

In seismic cross-sections, the last-stage channel-fills show high- to low-amplitude continuous horizontal reflections (Fig. 10A) indicative of vertical accretion. If the channel-fill is dominated by sand, its seismic signature tends to be a convex-upward "hat" (Fig. 10B, C) attributed to the differential compaction of the axial sandy fill and adjacent muddier deposits (Posamentier, 2003). The hat-form signature typifies channel-fills that are at or below the seismic tuning thickness, but may probably occur at any scale or resolution. In attribute maps, the last-stage channel-fills show up as either low- to high-amplitude continuous threads or high-amplitude discontinuous patches.

Last-stage channel-fills have been documented and categorized by several authors (e.g., May et al., 1983; Mutti and Normark, 1987; Shanmugam and Moiola, 1988; Cook et al., 1994). Factors that determine channel-fill facies include the parameters of last-stage flows, the pre-existing channel topography and the location of the channel in the submarine environment and in respect to coeval active channels. The key flow parameters are the ratio of flow thickness to channel depth and the duration and sediment load of the flows. The channel depth and sinuosity will determine the thickness and spatial distribution of the infill deposits, with possible slides and slumps related to the channel bank steepness. Some channels or their cut-off segments are abandoned abruptly and then gradually filled by spill-out flows from adjacent active channels, slope-derived minor "wild" flows and/or hemipelagic sedimentation. Such "passive" channel-fills may thus be highly heterogeneous or virtually mud-dominated and their facies are difficult to predict, as they will bear virtually no genetic relationship to the whole preceding development of the channel belt.

The sedimentary facies and internal architecture of last-stage channel-fills are generally difficult to recognize from seismic imagery due to its insufficient resolution, but can possibly be inferred on the basis of an understanding of particular channel-belt development combined with outcrop- analogue studies. Four outcrop examples (Fig. 10D–J) have been selected to illustrate variation in the last-stage fills of meandering and erosional sinuous channels, with sandstone net/gross ranging from 0 to 100 %. The examples show four different styles of channel-fill architecture: vertical aggradation, aggradational lateral accretion, single-bed plugging and a polygenic infill.

Last-stage channels filled by simple vertical aggradation (Fig. 10D, E) are found in both erosional and meandering channel belts and typically consist of margin-onlapping tabular beds with a thinning upward trend. Internal scours abound in larger channels, with the individual beds commonly thinning or pinching out towards the channel margins. The channel-fill may be sandy and possibly gravel-bearing or be heterolithic, composed of sand-mud couplets. The deposits are thus either products of bypassing "oversized" non-incising flows or products of waning flows that were considerably "undersized" with respect to the channel hydraulic geometry and fully dissipated within the channel. The demise of the channel occurs because none of these flow varieties can possibly keep the channel active, while depositing sediment in it.

Last-stage channels filled by aggradational lateral accretion are typical of meandering channel belts (Figs. 5B and 10F, G; see Wynn et al., 2007, case 3 in fig. 18; Dykstra and Kneller, 2009, fig. 12). These channel-fills may range from fully sandy and possibly gravelly to mud-rich heterolithic, but typically consist of planar parallel-stratified to ripple cross-laminated sandstone beds, some with a massive division and dewatering structures. The lateral accretion suggests that the depositional stacking pattern of turbidites was similar as during the formation and growth of the channel point bars, but the flow magnitude had apparently decreased to render the flows fully depositional, incapable of eroding the outer bank and maintaining channel migration.

Last-stage channels plugged by a single deposit are typically shallow conduits finalizing the development of some erosional and some meandering channel belts. The channel-fill deposit may be a normally-graded, massive and/or stratified sandstone or mudclast conglomerate, with its coarsest-grained part at the channel thalweg, or may be mudstone (Fig. 10H, I). The coarse-grained deposit, whether a turbidite or a deposit of debris flow spawned by turbidity current, is attributed to a flow that was grossly "oversized" with respect to the channel capacity. The flow would likely be erosive in the channel upper reaches, as indicated by the common occurrence of mudclasts (Fig. 10H), and the erosional bulking of sediment would then render it highly depositional and essentially non-erosive upon its arrival in the lower reaches. Muddy channel-plugs are rare in the middle to lower parts of submarine slopes, but may be more common in the upper parts. Their origin is attributed to the accumulation of hemipelagic mud is an abandoned channel or to an accidental emplacement of a local slope-derived mudflow.

Last-stage channels filled with polygenic deposits are some of the relatively deep conduits with low aspect ratios that typify erosional channel belts. Such channel-fills show a complex architecture and are often highly heterogeneous (Fig. 10J). Their basal sandy turbidites are commonly deformed by the emplacement of a bank-derived fine-grained slump deposit (MTD), possibly multiple, which is covered by mud-capped turbidites with uneven bases, draping and smoothing the irregular relief of the underlying slump deposit. The infilling of the channel thus apparently commenced with erosive flows, undercutting the outer bank and causing its collapses, which

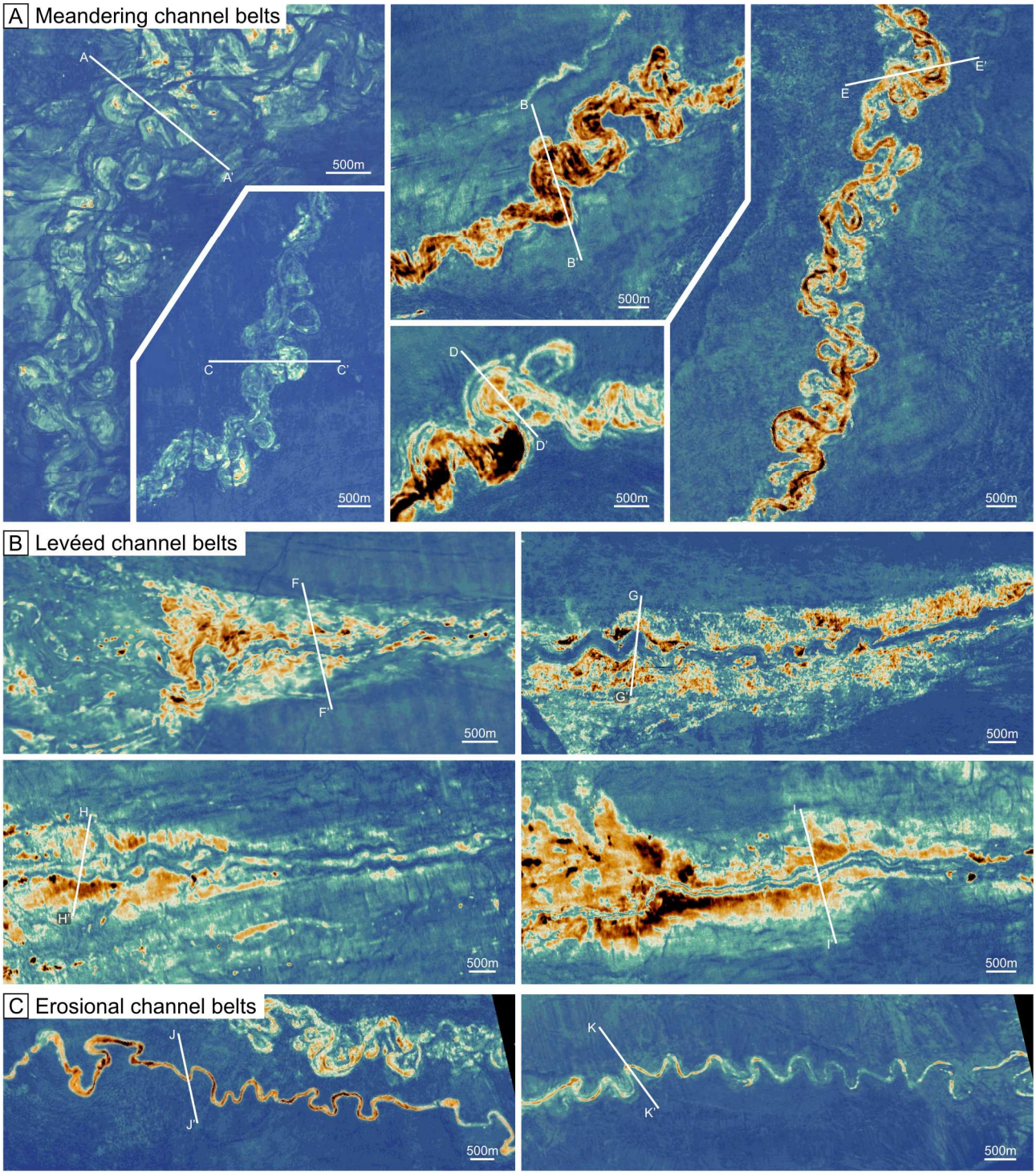


**Fig. 11.** Seismic RMS attribute maps showing planform characteristics of sinuous channel belts in the study area. (A) Meandering non-aggradational channel belts. (B) Levéed aggradational channel belts. (C) Erosional cut-and-fill channel belts. The corresponding vertical sections A–A' to K–K' are shown in Fig. 13.

were followed by smaller and fully depositional flows waning within the channel. This kind of channel-fill may be limited to single bends and its occurrences are thus difficult to predict.

## 4. Channel-belt types

On the basis of their planform, cross-sectional geometry and range of architectural elements, the deep-water sinuous channel belts in the study area have been classified into four main categories (Fig. 1A–C): (a) meandering channel belts, formed by laterally migrating non-aggradational sinuous conduits and generally lacking levées; (b) levéed channel belts, formed by aggradational sinuous conduits showing little or no lateral migration; (c) erosional channel belts, formed by the cut-and-fill of a sinuous conduit with no significant lateral migration and only minor levées; and (d) hybrid channel belts, combining features of the other three categories.

### *4.1. Meandering channel belts*

Meandering channel belts in seismic maps are characterized by a high-sinuosity (1.9–2.8) conduit, regular and smoothly-

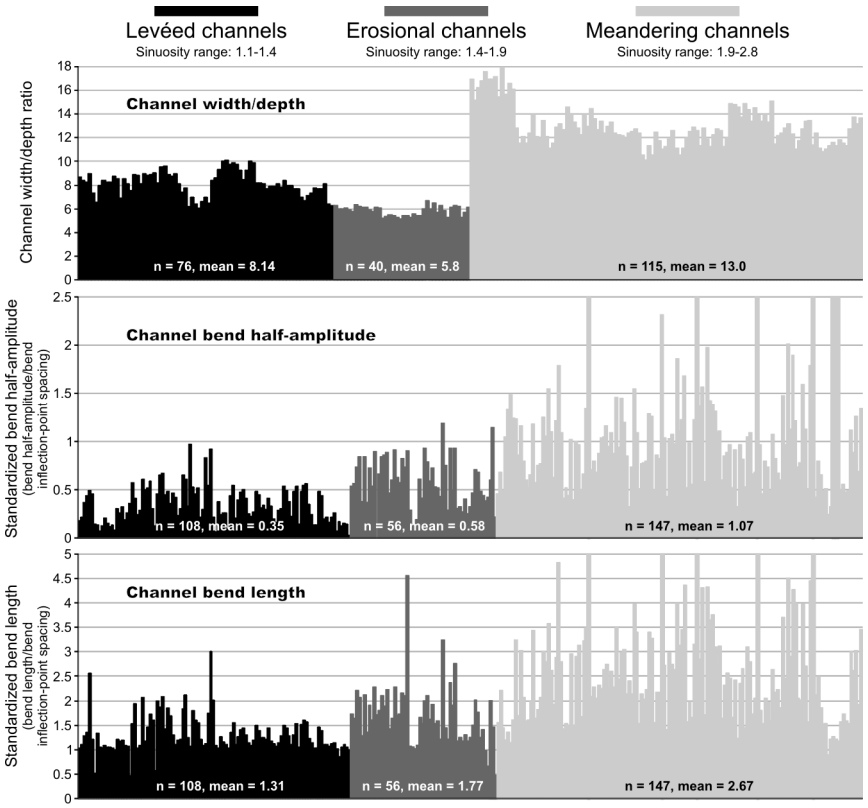


**Fig. 12.** Statistical comparison of the planform geometrical characteristics of the three main types of sinuous channels in the study area. The mean values pertain to the parameter specified on diagram vertical axis; the horizontal axis accommodates individual datasets; n = number of data. Note that the levéed channels are characterized by a moderate width/depth ratio, low sinuosity and low bend half-amplitude and length; the meandering channels are characterized by a high width/depth ratio, high sinuosity and also high bend half-amplitude and length; and the erosional channels are characterized by intermediate values of all these parameters. This evidence supports the notion that erosional channels are formed by entrenchment of either a meandering or a levéed primary conduit.

curved meander bends and evidence of bend cut-offs (Figs. 11A and 12). Characteristic feature are LAPs formed on the inner side of channel bends. The last-stage channels show up as continuous, high- to moderate-amplitude threads with high-amplitude patches at the bends representing outer-bank mounds/bars. Levées and intra-channel MTDs are lacking.

In seismic cross-sections, these channel belts are typified by LAPs that appear as shingled reflections dipping towards the last-stage thalweg (Fig. 13A, section A–A'). LAPs are not recognizable in channel-belts thinner than the seismic tuning thickness, where they instead appear as a single, laterally extensive reflection of anomalously high amplitude (Fig. 13A, section B–B'). The last-stage channels have a width/depth ratio in the range of 10–20 (Fig. 12), higher than in the other channel-belt types, and the channel-fill shows low-amplitude reflections indicating vertical aggradation or aggradational lateral accretion. Channel widths reach 325 m and depths of 25 m. The inclination of channel outer and inner banks at the bend apices is in the range of 8–14° and 5–10°, respectively. Core samples from meander belts show a fining-upward succession composed of amalgamated, crudely stratified, mudclast-bearing sandstone beds in the lower part and mainly ripple cross-laminated sandstone beds in the upper part (Fig. 4). Conglomerates may occur in the basal part.

The meandering channel belts occur typically at the base of large incised valley-fills, where they are directly overlain by aggradational levéed channel belts.

### *4.2. Levéed channel belts*

Levéed channel belts are characterized by conduits with low to moderate sinuosities (1.1–1.4) and irregular, occasionally sharp bends, and by laterally extensive levées appearing in maps as uniform to patchy high-amplitude zones on both sides of the channel (Figs. 11B and 12). The channel-fill shows lower amplitudes than the overbank deposits, although bright-amplitude patches occur, particularly at the apices of channel bends. These patches correspond to outer-bank mounds/bars. LAPs are lacking in isolated channel belts, but occur as aggradational packages in confined channel-belt complexes. No channel bend cut-offs and channel-margin collapse scars or MTDs have been recognized.

In seismic cross-sections, the levéed channel belts show a characteristic gull-wing shape with high-amplitude signature of levées and low-amplitude signature of aggradational channel-fill (Fig. 13B). The levée reflections lack continuity with those of the channel-fill, except for the last-stage deposits. The base of the channel belt is generally flat, but may be slightly uneven due to variable depth of thalweg scour. The channel width/depth ratio is in the range of 6 to 10 (Fig. 12), with the channel widths reaching 900 m and depths 100 m. Channel banks are mainly symmetrical, inclined at 11–18°.

The levéed sinuous channel belts predominate in the study area, occurring as isolated features (Fig. 9A) or as components of evolving channel-belt complexes (Fig. 9B, C).

### *4.3. Erosional channel belts*

In seismic cross-sections, the erosional sinuous channel belts are V- or U-shaped features with relatively high-amplitude reflections, inset in deposits with low-amplitude horizontal reflections (Fig. 13C). The channel-belt thicknesses are up to 300 m, generally exceeding those of the other channel-belt varieties. Channel width/depth ratio is in the range of 5–7

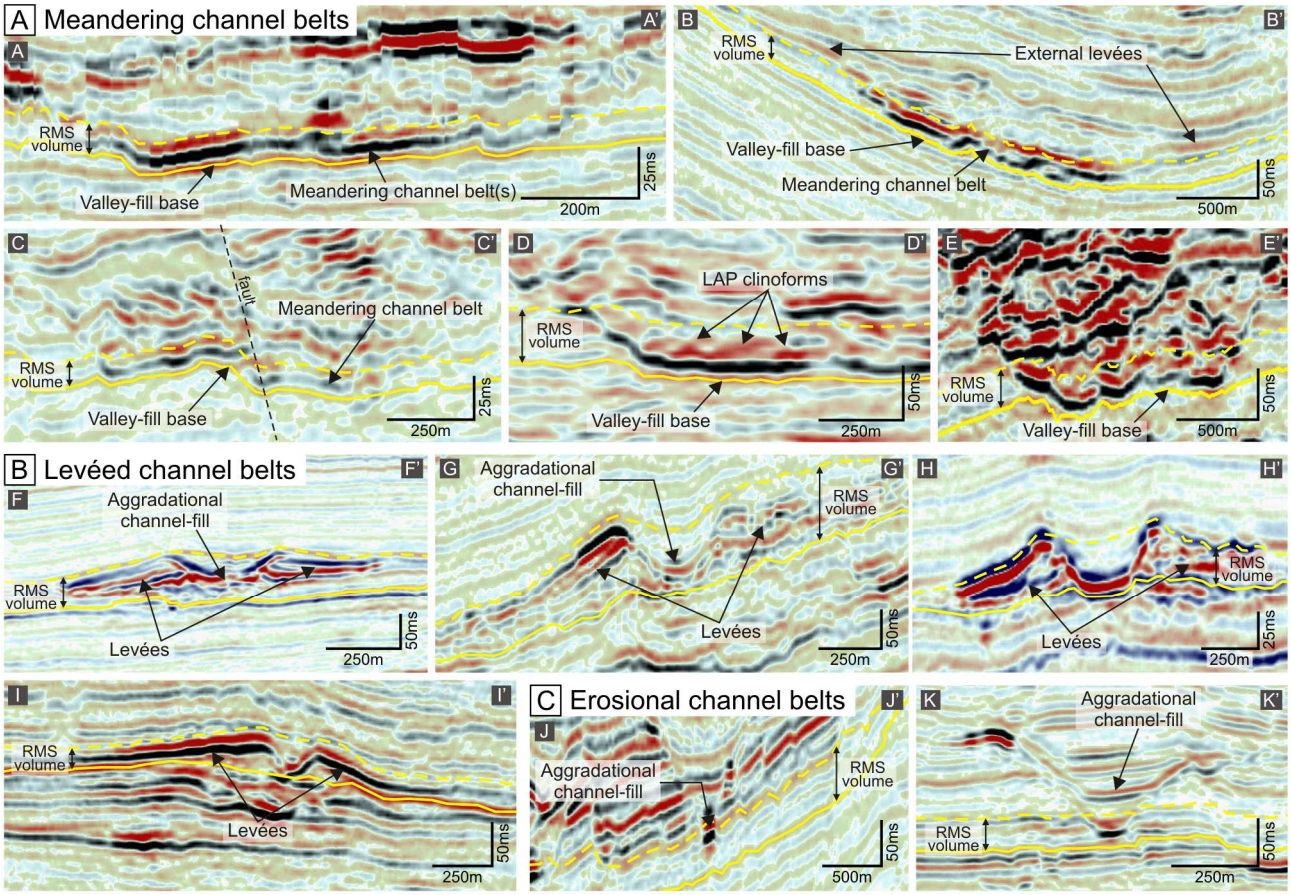


**Fig. 13.** Vertical seismic sections of meandering (A), levéed (B) and erosional channel belts (C) in the study area. The location of cross-section lines A–A' to K–K' is shown in Fig. 11. For descriptive and interpretive comments, see text.

(Fig. 12). Channel banks are mainly symmetrical, inclined at 15–18°, and the outer bank tends to be steeper in higher-sinuosity channels. The base of channel belt has a smooth V- or U-shape, but shows a stepped profile in belts with significant phases of erosional rejuvenation, indicated by intra-channel palaeotopographic terraces. The last-stage channel-fill is characterized by continuous, high-amplitude horizontal to convex-upward (hat-shaped) reflections in the basal part, up to 50 m thick, and by low-amplitude, onlapping or converging continuous reflections in the remaining higher part. LAPs are lacking and bank collapse scars or MTDs are rare. Likewise, levées are generally lacking, though may occur in smaller, less incised channel belts.

In attribute maps, the erosional channel belts appear as moderate- to high-amplitude sinuous threads with bright patches at the bends interpreted as outer-bank mounds/bars. The higher-amplitude thread is often bordered by lower-amplitude patches corresponding to the upper part of the channel-fill (Fig. 11C). Channel sinuosity is in the range of 1 to 2, and channel bends have moderate lengths and half-amplitudes (Fig. 12).

### *4.4. Hybrid channel belts*

Channel belts that show a combination of the above-described architectures and cannot readily be divided into single-type segments are considered to be hybrid varieties. The most common variety are channel belts with planform characteristics similar to those of levéed sinuous channels, but which are commonly larger, characterized by a well-incised thalweg and less extensive levées (Fig. 14A). Other hybrid belts show various combinations of LAPs, outer-bank bars/mounds and extensive levées at the individual bends (Fig. 14B-D). The hybrid channel belts are distinguishable in cross-sections, but are generally more difficult to recognize in attribute maps due to the overlapping and cross-cutting relationships of the diverse architectural elements.

## 5. The evolution of channel belts in submarine valleys

The study area affords more than twenty valley-fill complexes, with multi-storey and isolated channel belts either erosionally confined or erosionally- to levée-confined. The valley-fills vary in scale, architectural complexity and location on the submarine slope, but their vertical succession and stacking pattern of channel-belt types appear to be similar, though not without some notable departures. Three examples (Table 1) are described below to illustrate the development and observed variation of valley-fill complexes.

Valley-fill complex I (Table 1, Fig. 15) shares its internal architecture with a vast majority of valley-fills in the study area. Its basal part consists of a high-sinuosity meandering channel belt with LAPs, bend cut-offs and a high sandstone net/gross (Fig. 15, time windows 1 and 2). It is overlain by a series of aggradational, high-sinuosity levéed channel belts (Fig. 15, time window 3) which lack LAPs, decrease in sinuosity and assume disorderly directions increasingly unrelated to the direction of underlying channel belts ("disorganized" stacking sensu McHargue et al., 2011). However, the channel belts at some of their down-stream bends apparently evolved in continuity with the underlying meander-belt loops, showing aggradational lateral accretion and consistent directional trend (Fig. 15). The channel belts in the upper part of the valley-fill complex

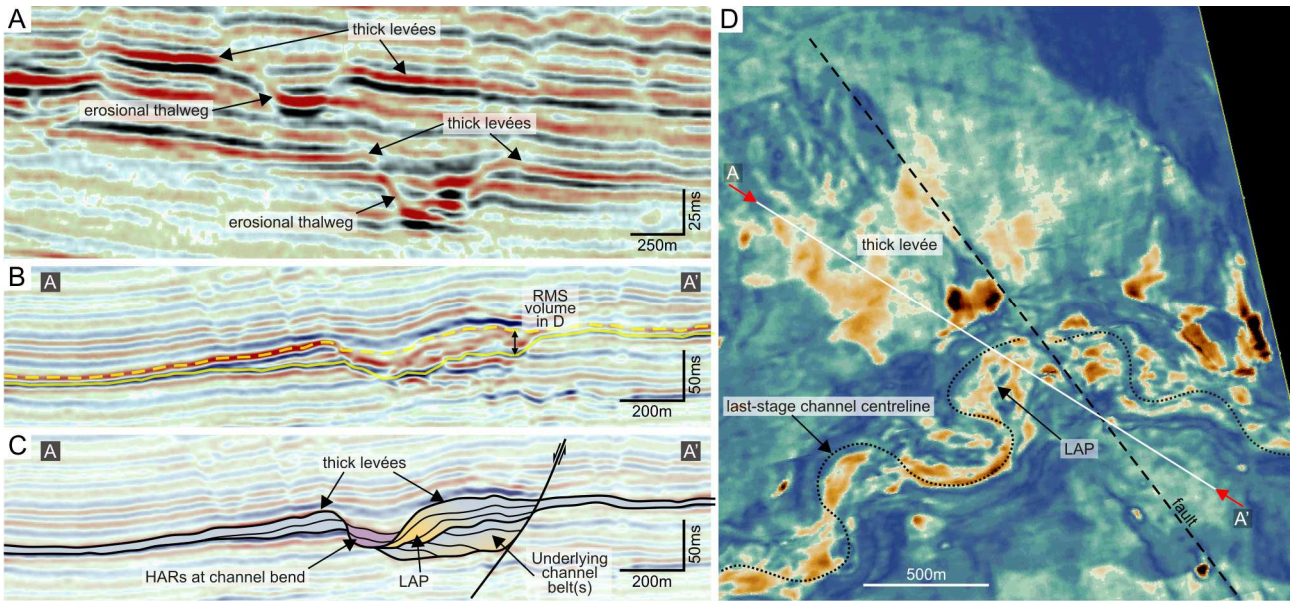


**Fig. 14.** Examples of hybrid-type channel belts from the study area. (A) The most common hybrid variety are channel belts with an erosional thalweg and thick levées. (B-D) Uncommon hybrids are channel belts showing both LAPs and thick levées.

(Fig. 15, time windows 3 and 4) are vertically offset and confined by external levées. They mimic the architectural pattern of the underlying levéed channel belts, but have wider and deeper thalweg zones, lower sinuosity and thicker gull wing-shaped levées. They show bright-amplitude spots on the inner side of some bends, which may indicate modest point bars. The topmost part of the valley-fill complex shows a belt of large, moderately sinuous, mud-plugged levéed channel with a directional trend similar to that of the underlying channel belt (Fig. 15, time window 5).

Valley-fill complexes II and III (Table 1) are examples illustrating less common stratigraphic architectures. Complex II (Fig. 16) is an incised valley-fill with an uneven, terraced base bearing some "hanging" erosional relics of meander belts. The succession commenced with an erosional channel belt of moderate sinuosity (Fig. 16, time window 1) which was covered by valley wall-derived MTDs and overlain further by a series of multi- to single-storey hybrid levéed channel belts. High-amplitude reflection wedges pinching out against valley walls represent levées and can be observed in most cross-sections of the palaeovalley (Fig. 16, time window 3). The corresponding channel-fills had been removed by incision of the overlying younger valley.

Complex III in its basal part shows a meandering channel belt with many bend cut-offs and a last-stage conduit that was slightly deepened by incision before being filled (Fig. 17, time window 1). The channel belt was buried by MTDs and overlain further by a moderately sinuous meandering channel-belt that evolved into an aggradational levéed channel belt (Fig. 17, time window 2). The overlying succession shows a double alternation of meandering and low-sinuosity levéed channel belts (time windows 3 and 4). The valley-fill as a whole is highly heterogeneous, differing from those formed by consistent, uninterrupted aggradation.

The main significance of valley-fill complexes II and III is in their showing that a particular type of channel belt may occur at various levels of an evolving valley-fill and that the vertical succession of channel-belt types may not necessarily follow a predictable pattern. As discussed further in the next section, the evolution of a valley-fill system may be perturbed by internal and/or external factors, which results in considerable stratigraphic variation.

## 6. Discussion

### *6.1. The diversity of sinuous channel belts*

The analysis of seismic data from the offshore study area shows that deep-water sinuous channel belts can be differentiated on the basis of their planform, cross-sectional geometry and component architectural elements. The tentative classification of channel belts suggested in the study sheds some new light on the genetic relationships among various sinuous channels.

*Meandering channel belts* — These channel belts are typified by high-sinuosity, regular and smoothly-curved meander loops and a conduit with low banks and high width/depth ratio (Figs. 11 and 12). Their most characteristic architectural element are LAPs, indicating that the channel evolved from relatively straight and systematically increased its sinuosity by erosion and deposition in the lateral domain. The bases and tops of non-deformed LAPs are horizontal (Figs. 2, 5 and 13), as also evidenced elsewhere by seismic images (Abreu et al., 2003; Mayall et al., 2006; Kolla et al., 2007, figs. 10–12; Labourdette, 2007; Nakajima et al., 2009) and outcrop sections (Campion et al., 2000; Abreu et al., 2003; Lien et al., 2003; Shultz et al., 2005; Beaubouef et al., 2007; Cronin et al., 2007; O'Byrne et al., 2007; Wynn et al., 2007; Dykstra and Kneller, 2009; Janocko and Nemec, 2011), which suggests that the process of submarine channel meandering occurs when no significant aggradation takes place. The lack of vertical thalweg migration indicates that the system is dominated by equilibrium flows with the rate of lateral deposition balanced by the rate of lateral erosion (Kneller, 2003). Outer-bank bars/mounds are rare in meandering channels, probably because the cut-bank erosion and minimal thalweg aggradation render their preservation potential very low (Nakajima et al., 2009).

Another striking characteristic of the meandering channel belts in the present case is the apparent lack of recognizable levées or other localized overbank deposits in seismic sections and attribute maps. However, there is no doubt that the channelized flows were spilling out and spreading sediment in overbank areas. Coarse-grained LAPs, some of them fully conglomeratic (Janocko and Nemec, 2011), are clear indication that the flow height must have grossly exceeded the channel depth (Dykstra and Kneller, 2009). Overbank deposition is known to be associated with meandering channel belts

**Table 1.** Characteristics of the three examples of submarine valley-fill complexes from the study area in offshore West Africa (see seismic images in Figs. 15–17). U – valley upper reaches; L – valley lower reaches.

| Main characteristics | Valley-fill complex I (Fig. 15) | Valley-fill complex II (Fig. 16) | Valley-fill complex III (Fig. 17) |
|---|---|---|---|
| Mappable length | 50.2 km | 19 km | 40 km |
| Depth | 220 m (U) to 100 m (L) | 180 m (U) to 250 m (L) | 250 m (U) to 220 m (L) |
| Basal width | 700 m (U) to 1400 m (L) | 400 m (U) to 600 m (L) | 1470 m (U) to 1940 m (L) |
| Valley-wall inclination | 32° (U) to 12° (L) | 16° (U) to 18° (L) | 22° (U) to 25° (L) |
| Morphology of valley margins | U-part: slump scars and associated MTDs. L-part: external levees, slump scars | erosional terraces with LAPs, slump scars and associated MTDs | external levées, slump scars, and associated MTDs |
| Channel-belt types and MTD occurrences (numbered in ascending order) | (1) non-aggradational meandering channel belt (2)–(7) levéed sinuous channel belts. | (1) erosional cut-and-fill channel belt (2) MTDs (3)–(6) levéed sinuous channel belts | (1) meandering belt with deeply incised last-stage channel (2) non-aggradational meandering channel belt and MTDs (3) levéed sinuous channel belt (4) non-aggradational meandering channel belt (5) levéed sinuous channel belt (6) non-aggradational meandering channel belt (7) levéed sinuous channel belt |
| Upward change in channel sinuosity | 2.2 → 1.9 | 1.6 → 1.2 | 2.3 → 2.5 → 1.5 → 1.8 → 1.5 → 2.6 → 1.2 |
| Upward change in channel width/depth ratio | 3.6 → 2.0 | 3.0 → 2.8 | 2.1 → 4.3 → 2.2 → 1.9 → 3.3 → 2.0 → 2.7 |
| Upward change in channel migration style | lateral migration → aggradational lateral migration and lateral switching → aggradation and lateral switching | vertical aggradation → aggradation and lateral switching | lateral migration → aggradation and lateral switching → lateral migration → vertical aggradation → aggradation and lateral switching → lateral migration → aggradational lateral migration → lateral migration → aggradation and lateral switching |
| Upward change in channel-belt stacking pattern | U-part: orderly stacked → isolated disorderly offset L-part: orderly stacked → isolated orderly offset | orderly stacked → isolated disorderly offset | disorderly stacked → orderly stacked → isolated disorderly offset → orderly stacked → disorderly stacked |

(Lien et al., 2003; Arnott et al., 2007; Janbu et al., 2007; Dykstra and Kneller, 2009; Janocko and Nemec, 2011) and is a prerequisite for the formation of multi-storey, vertically-stacked meandering channel belts (e.g., Dykstra and Kneller, 2009, fig. 8). Nevertheless, seismically-recognizable levées have been reported mainly from non-meandering sinuous channels (e.g., Clark and Pickering, 1996; Nakajima and Satoh, 2001; Fildani and Normark, 2002). The excessive spill-out of equilibrium flows in meandering channel belts (Kneller, 2003) apparently renders the thickness/width aspect of levées very low and their relief beyond the seismic resolution.

*Levéed sinuous channel belts* — These channel belts have prominent, gull wing-shaped levées and an irregularly curved conduit with a low width/depth ratio, common sharp bends and outer-bank mounds/bars at the bend apices (Figs. 11–13). Isolated channel belts are generally typified by flat bases (Figs. 9A and 14B), whereas those stacked vertically in channel-belt complexes generally evolve from a pre-existing meandering channel (Fig. 9B, C and section A–A' in Fig. 15). The vertical stacking indicates that the channel evolved by a concurrent aggradation of its thalweg zone and levée, which makes it reasonable to infer that the formation of these channel belts is due to some better confined and fully depositional flows. If the flow is sufficiently confined by channel, its spill-out will be moderate and hence will dissipate within a relatively short distance from the channel, resulting in levée build-up.

Some initial incision may be required for the inception of isolated channel belts, even though they seem to form on an apparently flat substrate to aggrade by thalweg and levée accretion (Fig. 13B; see also Fonnesu, 2003; Gee and Gawthorpe, 2007; Clark and Cartwright, 2009; Hubbard et al., 2009). Experiments by Rowland et al. (2010) for a wide range of flows failed to produce a purely depositional self-confinement of turbidity current, which suggests that some incipient erosional confinement of flow may be needed to instigate the formation of aggradational levéed channels. However, the relief of this basal "inception" scour may well be of sub-seismic scale and hence unrecognizable in seismic sections.

Levéed channel belts may be laterally offset due to slight lateral migration in continuity with the underlying belt or to intermittent lateral switching (Figs. 15–17; see also McHargue et al., 2011). The latter mode may involve some incipient incision (see previous paragraph). The mode of lateral shifting depends probably upon the magnitude and velocity of channel-conveyed flows in addition to the system's net rate of aggradation and channel infilling. Channel migration in continuity with the underlying belt will likely occur when the aggradational channel remains sufficiently deep to confine a major part of flow volumes. According to Kane et al. (2008), flows that are more than five times thicker than the channel depth tend to deposit sediment at the outer banks, thereby potentially straightening the channel or causing its avulsion. Flows below this threshold tend to deposit sediment on the inner bank, forming aggradational LAPs in an aggrading channel belt.

Another prerequisite for the formation of aggradational point bars may be the cohesiveness of outer bank. Channel bends with aggradational LAPs are generally tangential to the valley walls (Fig. 15, profile A-A'; also see Posamentier et al., 2000; Posamentier and Kolla, 2003; Deptuck et al., 2007), which typically consist of compacted mud-rich deposits. Notably, aggradational LAPs in the study area occur in valley-confined channel-belt complexes, but are generally lacking in unconfined levéed channel belts.

Channel-belt stacking with intermittent lateral switching will occur where the channel becomes plugged with sediment to a point when it can no longer contain the flows and avulsion

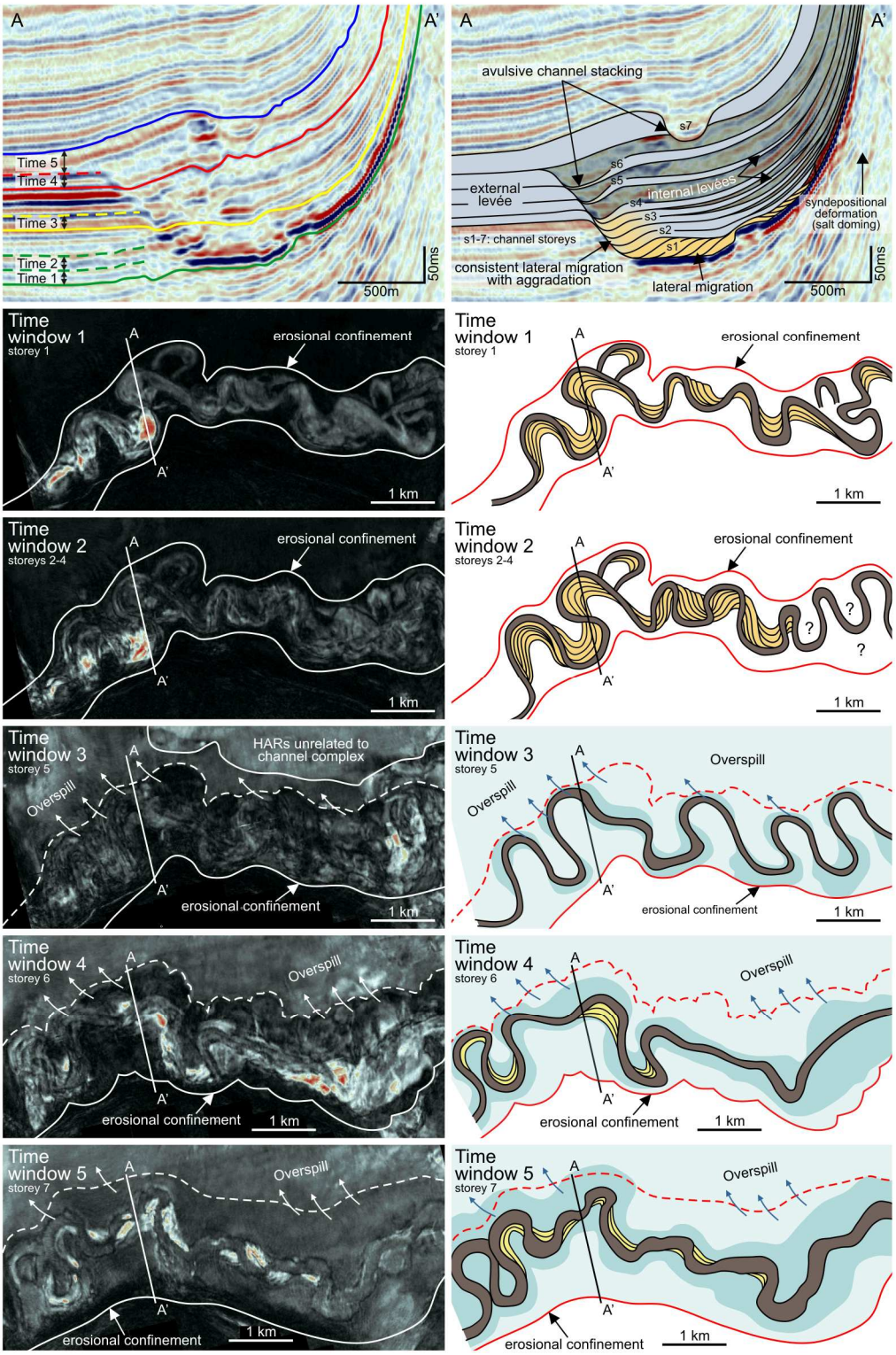


**Fig. 15.** Valley-fill complex I (Table 1) as an example of the typical submarine valley-fills in the study area; for description, see text. The seismic section and its interpretation (top row) indicate the time-window slices and channel-belt storeys displayed as maps below. Note that the valley-fill in this case developed under the influence of syndepositional salt-doming to the right, which resulted in formation of an extensive external levée on the other side of the valley. However, the doming does not seem to have much affected the stratigraphic evolution of the valley-fill channel system, as the succession resembles closely other cases where no such deformation was involved.

occurs. The new conduit may significantly deviate from the previous one, resulting in a disorderly directional stacking (McHargue et al., 2011).

Outer-bank mounds/bars are a characteristic architectural element of levéed channel belts. In seismic attribute maps, these deposits generally occur in the thalweg zone near the outer bank and are most notable at the bend apices (Fig. 6), but may extend either upstream or downstream from the apex (Fig. 18A, B) or occur at the outer- to inner-bank transition in a bend inflection zone (Fig. 18C). Deposition localized between the bend apex and downstream inflection point (Fig. 18A) is attributed to relatively well-confined flows, with the flow run-up on the outer bank at sharp bends causing abrupt deceleration and loss of capacity (Kane et al., 2008; Straub et al., 2008; Nakajima et al., 2009; Amos et al., 2010; Janocko et al., 2011). It has been also been suggested (Piper and Normark, 1983; Pickering et al.,

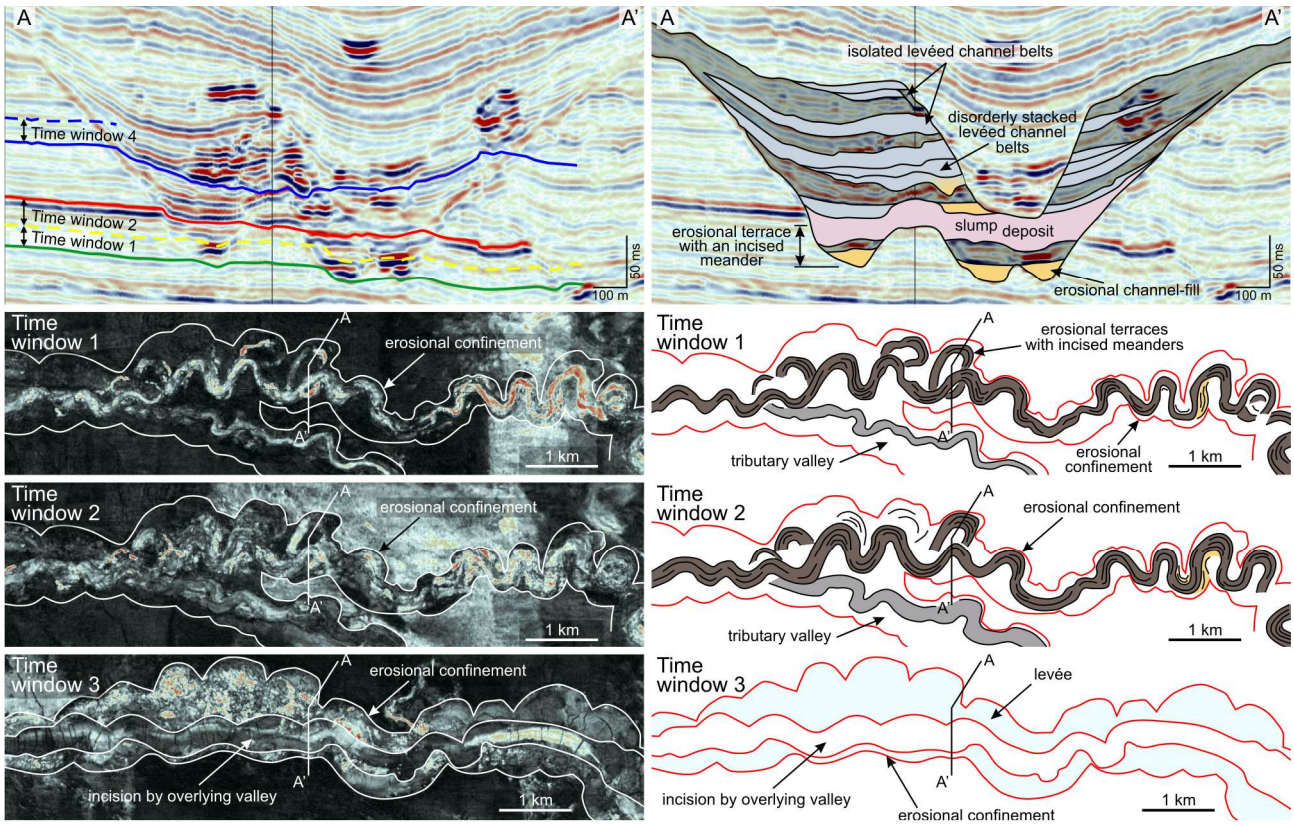


**Fig. 16.** Valley-fill complex II (Table 1) as an example of a relatively uncommon variety of submarine valley-fill in the study area; for description, see text. The seismic section and its interpretation (top row) indicate the time-window slices displayed as maps below. Note the erosionally superimposed younger incised valley-fill complex, which renders the whole stratigraphic succession a two-storey valley-fill complex set.

1989; Clark and Pickering, 1996; Peakall et al., 2000) that the intermittent decoupling of the upper part of the flow by overspill will likely decelerate the channel-confined part of the flow and cause rapid deposition at and directly downstream of the bend apex.

Deposition at the outer bank between the bend apex and upstream inflection point (Fig. 18B) is attributed to flows with a major overspill and its large part re-entering the channel at the adjacent bend and colliding with the channelized flow, which causes abrupt flow deceleration and rapid sediment dumping (Janocko et al., 2011). Deposition at the outer- to inner-bank transition in bend inflection zone (Fig. 18C) is attributed to high-discharge, poorly confined depositional flows that run down-valley across the channel bends and experience localized basal deceleration when crossing bend inflection zones (Janocko et al., 2011).

*Erosional channel belts* — These channel belts are formed by a simple cut-and-fill process, with little or no evidence of levées and with the last-stage channel-fill typically mud-prone, composed of heterolithic deposits (Figs. 10, 11 and 13). Other characteristic features of erosional channel belts include low to moderate sinuosity, outer-bank mound/bars at channel bends, low width/depth ratios and steep banks (Figs. 11–13). In fluvial geomorphology, such conduits are referred to as laterally inactive sinuous channels (Schumm, 1985; Nanson, 2010).

As discussed further below, the erosional channel belts in the study area probably evolved by incision of incipiently meandering or levéed channels, whose primary depositional elements were erased in the process by bank undercutting, slumping and erosion. Only the planform of the original conduit (sinuosity, bend shape and amplitude) would be inherited by the deepened and enlarged channel. The entrenchment was likely due to an allogenic factor, such as the growth of salt domes or continental slope tectonics, rather than to flow hydralics alone (see Sylvester et al., 2011), as these channel belts occur in only some valley-fills, most of them affected by halokinesis.

Once the incising channel reached an equilibrium profile, the erosion apparently ceased and sediment bypass prevailed. Although a channel at equilibrium would normally tend to meander, the odd hydraulic geometry of a deep and narrow conduit with cohesive banks and inherited sinuosity could not match flow helicoid or be readily adjusted, thus preventing lateral migration (see Nanson, 2010). Most flows were likely "undersized" with respect to the channel capacity, resulting in no major overspill and no significant levées. Sand-prone sediment patches at the bend apices resulted probably from localized deposition due to intermittent flow deceleration (Straub et al., 2008; Nakajima et al., 2009), rather than to flow stripping by overspill (cf. Piper and Normark, 1983).

*Hybrid channel belts* — The formation of hybrid channel belts, combining features of the three other categories, could theoretically be due to a whole range of factors, such as occasional "outsized" flows or major change in flow discharges, flow avulsions, channel confluences, variable substrate properties, base-level changes, halokinesis or slope tectonics. For example, occasional "outsized" flows may deposit outer-bank mounds/bars in a meandering channel (Fig. 7; Nakajima et al., 2009), straightening its path and instigating incision, or the growth of levées in a levéed channel belt may effectively increase the channel depth, leading to a better flow confinement and conduit lateral migration (Kane et al., 2008). As discussed further below, the hybrid channel belts in the study area are apparently products of various failed channel transformations of this kind.

*Genetic relationships among channel-belt types* — A cross-plot of the bend length and half-amplitude of sinuous channels (Fig. 19A) reveals two different styles of bend expansion: one dominantly transverse and the other dominantly longitudinal with respect to the channel-belt axis (see the inset sketches in

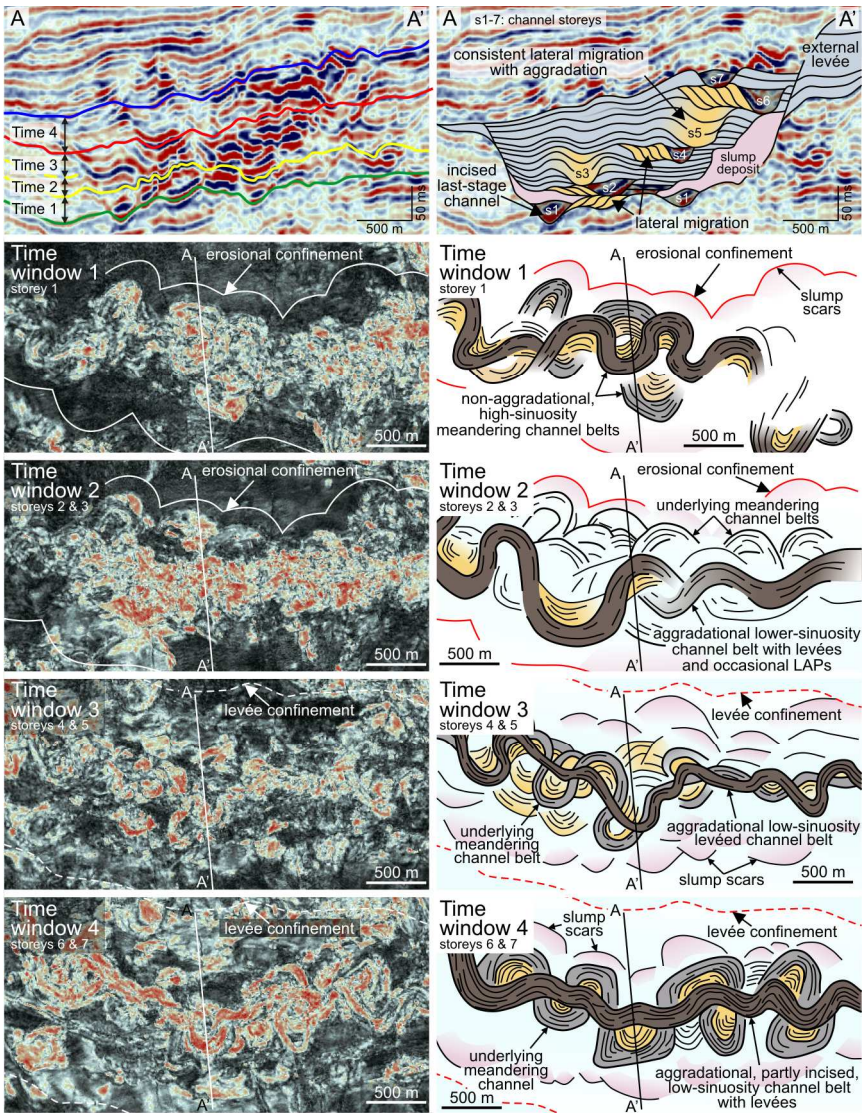


**Fig. 17.** Valley-fill complex III (Table 1) as an example of another uncommon variety of submarine valley-fill in the study area; for description, see text. The seismic section and its interpretation (top row) indicate the time-window slices and channel-belt storeys displayed as maps below.

Fig. 19A). The continuum of planform variation from nearly straight to highly sinuous horseshoe-shaped channels is thought to represent the evolutionary trend of meandering channels (Fig. 19B), because neither the levéed nor the erosional channels show any significant lateral expansion or sinuosity change in their development. The two-tier trend (Fig. 19A) thus implies that a developing meandering channel initially increases mainly its winding breadth (bend amplitude) by lateral expansion, before reaching a threshold above which the channel length and sinuosity increase without significant expansion. This means also that a meandering channel, if not perturbed and transformed, should invariably reach a mature or supermature planform, which is consistent with the evidence from all measured last-stage meandering channels and with their LAPs signifying considerable lateral migration.

Consequently, the levéed channels are thought to have evolved from immature or submature incipient meandering conduits, perturbed by system net aggradation, whereas the laterally inactive erosional channels are thought to have evolved by incision of either some moderately sinuous levéed channels or submature/mature meandering channels, from which they inherited their sinuosity. As to the hybrid channel belts, their most common variety (Fig. 14A) can be attributed to a failed transformation of levéed channel into erosional channel, whereas the less common varieties (Fig. 14B-D) can be attributed to a failed transformation of meandering channel into an aggradational levéed channel. The failed transformations can be attributed to a weak allogenic perturbation of the turbiditic system's profile, probably by minor salt movements or slope faulting.

The general characteristics of the main channel-belt types in the studied area of West African continental palaeoslope are summarized in Figure 20.

### *6.2. The development of submarine valley-fill complexes*

The majority of valley-fill complexes in the study area show a comparable stratigraphic pattern of channel-belt evolution. The basal part of the succession consists of meandering channel belts with a high sandstone net/gross (Figs. 15 and 20). They are typically overlain by local MTDs, which may range from mud-prone, valley wall-derived slide and slump deposits to coarser-grained deposits of co-genetic debris flows spawned by large high-density turbidity currents. The middle to upper part of the succession consists of multi-storey to isolated levéed aggradational channel belts with a decreasing sinuosity and moderate to low sandstone net/gross. The valley-fill succession as a whole is fining upwards, increasingly heterolithic and richer in mud.

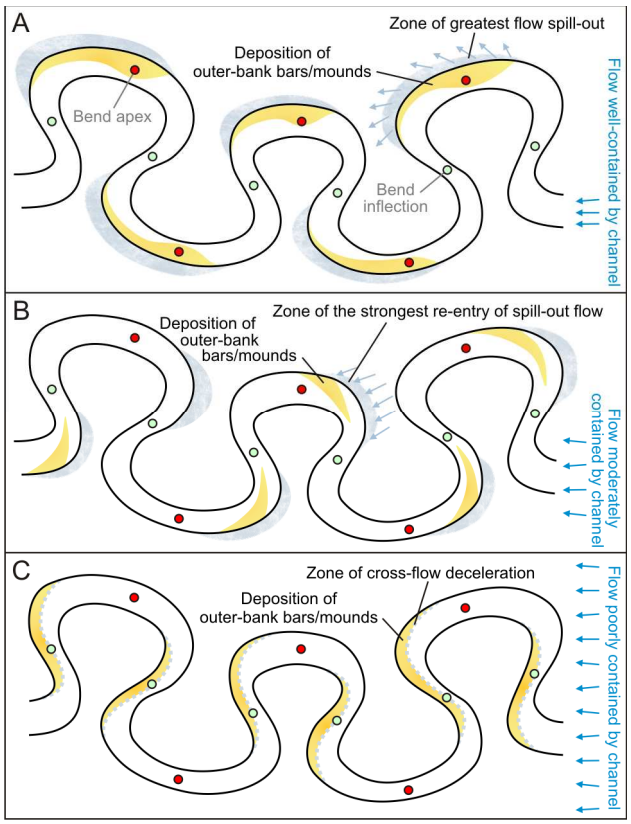


**Fig. 18.** Schematic diagrams showing variable location of outer-bank bars/mounds in submarine sinuous channels and its suggested causes (based on Janocko et al., 2011); for discussion, see text. (A) Mounds formed around and directly downstream of the bend apex. (B) Mounds formed between the bend apex and upstream inflection point. (C) Mounds form in the channel-bend inflection zone.

A similar stratigraphic trend has been documented from confined channel-belt complexes in offshore Borneo (Posamentier et al., 2000; Posamentier and Kolla, 2003), offshore Gulf of Mexico (Posamentier, 2003; Posamentier and Kolla, 2003; Posamentier et al., 2007), offshore Nigeria (Posamentier and Kolla, 2003; Deptuck et al., 2007), offshore Angola and Congo (Labourdette and Bez, 2010), offshore Egypt (Samuel et al., 2003, fig. 7; Cross et al., 2009) and the Delaware Basin of Texas, USA (Beaubouef et al., 2007). A net upward fining of confined channel-belt complexes, attributed to increasing aggradation rate, has been postulated also by recent models (McHargue et al., 2011; Sylvester et al., 2011), although the issue of channel-belt types is considered simplistically in these studies. The event-based model of McHargue et al. (2011) takes no account of the effects of lateral accretion and suggests that a greater lateral migration of channels, expected to be favoured by low sand/mud ratio, will likely occur at the latest stages of channel-complex development. In the model of Sylvester et al. (2011), high net/gross belts of laterally migrating channels are expected to be stacked disorderly in the basal part of channel-belt complex and to become more orderly stacked as the rate of aggradation increases. This latter suggestion matches roughly the pattern recognized in the present study, although the model assumes one channel-belt type with ever-present LAPs and no change in sinuosity with time.

Somewhat different models have been derived from studies in offshore Egypt (Samuel et al., 2003), offshore Gabon (Wonham et al., 2000), offshore Brazil and Angola (Mayall and Stewart, 2000, Mayall et al., 2006) and the Elazığ Basin of eastern Turkey (Cronin et al., 2005, 2007). Mayall and Stewart (2000) and Mayall et al. (2006) have postulated a model that consists of a basal erosional surface overlain by coarse sediment lag 1–2 m thick, deposited in low-sinuosity channel belt, covered with MTDs derived either locally or from distant sites; the higher part consists of laterally migrating aggradional channel belts with high sandstone net/gross, whereas laterally migrating high-sinuosity levéed channel belts with low net/gross occur at the top. In this model, submarine valleys are considered to be like giant channels scoured by powerful erosive flows, which is why the depositional succession is suggested to commence with a channel-fill element (basal lag), rather than a valley-floor channel belt.

Submarine valleys are similarly ascribed to large erosive flows in the models of Wonham et al. (2000) and Samuel et al. (2003, end-member B in fig. 10), where meandering channel belts are expected to occur in the upper part of channel-belt complex and aggradational levéed channel belts to occur in the lower part, with an overall upward fining due to decreasing sandstone net/gross. Samuel et al. (2003) also noted that the basal part of valley-fill may contain locally-derived MTDs and occasionally bears thin sands interpreted to be relic deposits of the erosive flows that incised the valley. A slightly different stratigraphic pattern is suggested in the model of Cronin et al. (2005, 2007), based on outcrops of several channel-belt complexes, where basal conglomeratic deposits of braided channel belts are overlain by finer-grained belts of erosional channels and covered by the low net/gross meander belts of small, high-sinuosity channels.

Despite their variation and interpretive discrepancies, submarine valley-fill complexes appear to have several main features in common – such as:

- an erosional base marking deep incision of turbiditic system;
- basal deposits indicative of considerable sediment bypass with little or no aggradation;
- common occurrences of MTDs in the lower part;
- aggradational succession of levéed sinuous channel belts, multi-storey to isolated;
- non-aggradational meandering channel belts which may occur in the basal and/or top part of valley-fill or occasionally also in the middle part;
- an overall upward fining with decreasing sandstone net/gross.

Submarine valley-fill complexes are clearly recording periods of a deep incision, aggradation and abandonment of a particular flow route of turbidity currents (Fig. 20). This development suggests a continuum of changes in the system profile, from deep erosion to an incipient “graded” state with basal lag or meandering channel belts, and further to aggradation with levéed channel belts and to eventual abandonment (Kneller, 2003). Most of the slope valley-fills in the study area and a majority of other reported cases show such a pattern of development, exemplified by valley-fill complex I (Table 1, Fig. 15).

The formation of a slope valley is thought to be due to either a rapid incision of an erosional channel belt or a slow gradual incision of a meandering channel belt (Fig. 20). In the former case, the rapid incision will prevent lateral migration and result in a V-shaped valley with a thalweg sinuosity similar to that of the original channel. In the latter case, the slow incision will only gradually restrain lateral migration, resulting in a wide-floor, U-shaped low-sinuosity valley with common terraces and a remnant, high-sinuosity meandering channel (Figs. 16 and 20; see also Sylvester et al., 2011). The onset of aggradation will produce multi-storey meander belts, so long as the aggradation rate is not too high (Dykstra and Kneller, 2009, fig. 8). As the system’s equilibrium profile begins to rise, the increased accommodation will enhance aggradation and result in levéed

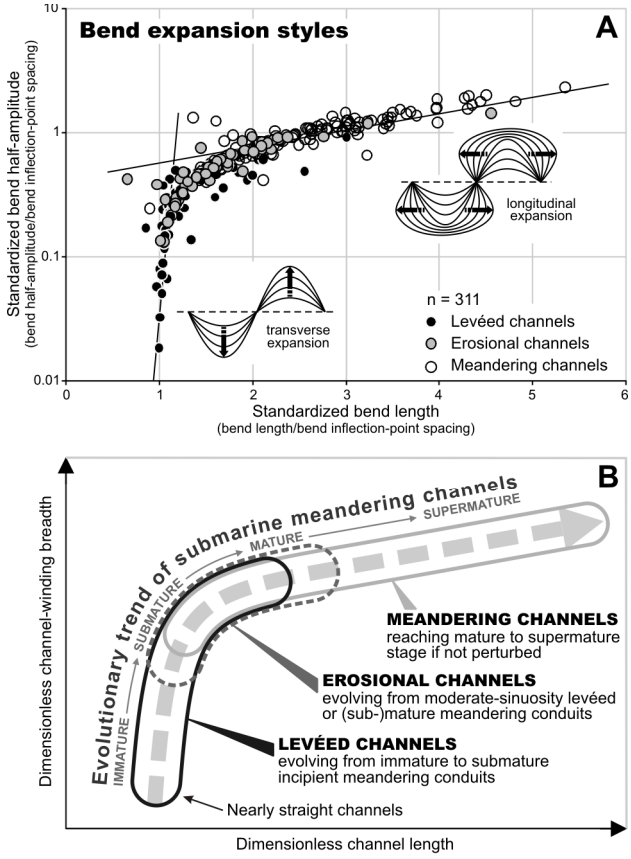


**Fig. 19.** (A) Cross-plot of the bend length vs. half-amplitude of sinuous channels (datasets as in Fig. 12), revealing two different styles of bend expansion: dominantly transverse or dominantly longitudinal with respect to the channel-belt axis, as shown by the inset planform sketches. (B) Interpretation of the upper plot, discussed in the text.

channel belts. With a gradual increase in aggradation rate, the vertically stacked channel belts will not only decrease their sand net/gross, but also assume a more orderly directional pattern (McHargue et al., 2011). The transition to abandonment phase will be marked by offset-stacked to isolated levéed channel belts (Figs. 15 and 16) and sheet-like deposits formed as crevasse splays or terminal splays/lobes (Gardner and Borer, 2000; Posamentier and Kolla, 2003; Cross et al., 2009).

Variation among valley-fills can be attributed to the effect of external factors (e.g., halokinesis, slope tectonics) or to an autogenic forcing due to the evacuation of sediment to the valley terminus and related base-level change, possibly accompanied by a major accretion of muddy deposits on the adjoining slope. A significant base-level rise will raise the potential equilibrium profile, whereby the aggrading valley-fill system will reach the valley top without attaining a "graded" state and will shift outside the valley before reaching an equilibrium. The valley-fill will then have isolated levéed sinuous channel belts at the top, as exemplified by the present study area (Figs. 15 and 16) and as seems to be the case in the majority of reported valley-fill complexes (see references above).

In the case of no major rise in base level or considerable sediment accretion in the valley neighbourhood, the aggrading valley-fill system may incidentally reach its equilibrium profile near the valley top, whereby non-aggradational meandering channel belts will form. Similar channel belts will form when the aggrading valley-fill system approaches the valley top and the spilling-out flows begin to spread sediment over a wider area, which may dramatically reduce the intra-valley effective aggradation rate. In other sporadic cases, the aggrading valley-fill system may reach a transient equilibrium profile much earlier, at a mid-depth height of the valley, before the resulting bypass of sediment raises further the base level and instigates renewed aggradation (Fig. 17).

The occurrence of MTDs in valley-fills is common, but by no means universal (Fig. 20). The emplacement of MTDs generally takes place at an early stage, when the valley has assumed its maximum relief (Fig. 20), but no valley-wall collapses must necessarily occur or they may be very local and their products may also tend to be removed by erosion. The preservation potential of MTDs increases with the onset of valley-floor aggradation.

## 7. Conclusions

The study was focused on the interpretation of seismic sections and attribute maps of sinuous channel-belt complexes from the continental slope in offshore West Africa, calibrated to well-core samples and supplemented with comparative outcrop cases from other ancient submarine slopes. Five main architectural elements of channel-belts were recognized:

- Lateral-accretion packages (LAPs) – interpreted as deposits formed by the accretion of sediment at the inner bank of channel bend in association with the lateral migration of channel thalweg.
- High-amplitude reflection patches in the thalweg zone near outer bank – interpreted as coarse sediment mounds or outer-bank bars resulting from the deceleration and/or overspill of turbidity currents at channel bends.
- Levées – recognizable as wedge-shaped sand-prone ridges at channel margins and attributed to the overspill of channel-conveyed flows.
- Mass-transport deposits (MTDs) – recognizable as odd-shaped "chaotic" units and ascribed to local slides, slumps or debris flows derived from the channel banks or valley walls.
- Last-stage channel-fills – recognizable as a mud-prone fill heralding and recording the abandonment of a channel.

These elements occur in various combinations, but no single channel belt combines all of them, which suggests that some elements may be mutually exclusive. Four categories of sinuous channel belts were distinguished on the basis of their planform and transverse geometry and the architectural elements involved:

- Meandering channel belts – characterized by the occurrence of LAPs, markedly erosional base, high-sinuosity conduit, horseshoe-shaped bends and negligible levées. They are formed by the lateral migration of sinuous channel and are dominated by flows combining erosion and deposition in their lateral domain, with the overbank flow in equilibrium with the substrate gradient and no significant lateral dissipation at the channel margins.
- Levéed channel belts – characterized by a slightly incised or depositional base, prominent levées, low-sinuosity conduit, irregular parabola-shaped and often sharp bends and common outer-bank bars/mounds. Aggradational LAPs may occur in belts where aggradation combined with significant lateral channel migration. Levées indicate overbank flows that rapidly dissipated at the channel margins.
- Erosional channel belts – characterized by concave-upwards erosional bases, moderate bulk sinuosity,

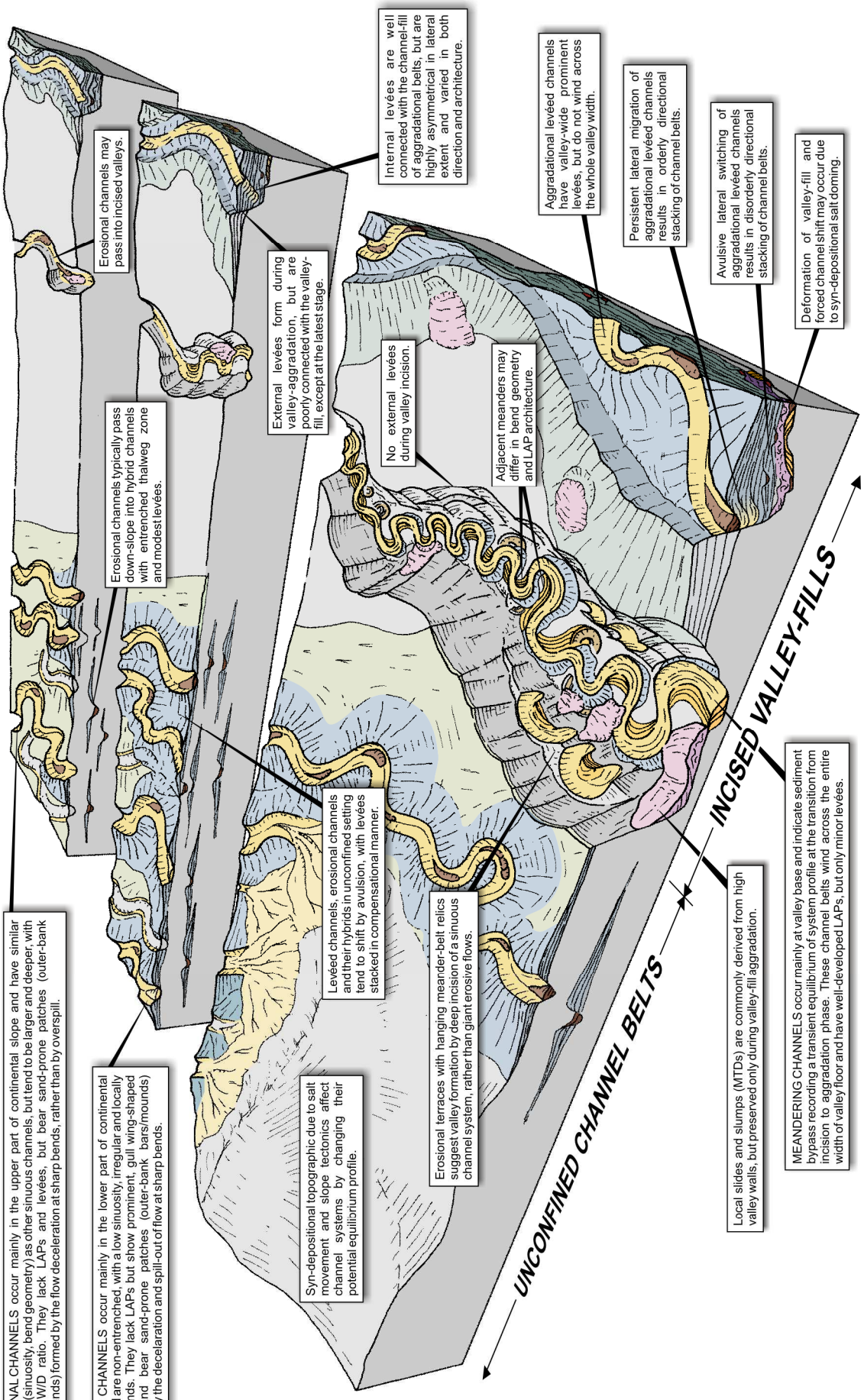


**Fig. 20.** Summary of the main characteristics of submarine channel belts and incised valley-fills in the studied area of West African Miocene continental slope (for discussion, see text).

smoothly-curved to sharp bends and a general lack of recognizable levées, LAPs or outer-bank mounds. They are formed by entrenchment of one the previous channel-belt types and filled by vertical aggradation, with the overbank flows negligible or non-dissipating at the channel margins.

- Hybrid channel belts – which are typically levéed and have erosional bases, showing characteristics of more than one of the other channel types. Their origin is attributed to channels that underwent "mutation" due to external perturbations involving either flow discharge or profile gradient.

Quantitative analysis indicates that meandering channels form when system is near its potential equilibrium profile. They evolve from nearly straight to highly sinuous by increasing first the bend amplitude and then the conduit length. Levéed channels are thought to evolve from incipient meandering conduits perturbed by aggradation and erosional channels to evolve from either moderately sinuous levéed or highly sinuous meandering conduits, inheriting their sinuosity. Hybrid channels signify a failed channel transformation.

The channel belts may occur isolated, but are commonly stacked upon one another, forming multi-storey channel-belt complexes that are either unconfined or developed within incised valleys. Unconfined channel-belt complexes, made of levéed channel belts stacked vertically in an offset "compensational" manner, are relatively uncommon in the study area. Confined channel-belt complexes predominate, with the confinement provided by valley relief and often also by the valley external levées at the late stage of infilling.

The majority of valley-fill complexes show a development from deep erosion to a transient equilibrium state with the deposition of coarse lag or non-aggradational meandering channel belts, and further to aggradation with levéed channel belts and eventual abandonment. Non-aggradational meandering channel belts may form in the basal and/or top part of valley-fill and sporadically in the middle part. MTDs tend to be emplaced when the valley assumes its maximum relief, but may not necessarily be present. The observed variation among valley-fills can be attributed to external factors (e.g., halokinesis, slope tectonics) or to an autogenic forcing related to the evacuation of sediment from the valley, base-level change and mud accretion on the adjoining slope.

## Acknowledgements

This study was a part of the first author's 3-year PhD research project funded by Statoil ASA. Statoil is also acknowledged for the permission to publish the selected seismic and well data. The study in its initial phase benefited from the stimulating discussions with Anna Pontén, Anjali Fernandes and Ben Kneller.

## References

Abreu, V., Sullivan, M., Pirmez, C., Mohrig, D., 2003. Lateral accretion packages (LAPs): an important reservoir element in deep water sinuous channels. Marine and Petroleum Geology, 20, 631−648.

Adeogba, A.A., McHargue, T.R., Graham, S.A., 2005. Transient fan architecture and depositional controls from near-surface 3-D seismic data, Niger Delta continental slope. AAPG Bulletin, 89, 627−643.

Amos, K.J., Peakall, J., Bradbury, P.W., Roberts, M., Keevil, G., Gupta, S., 2010. The influence of bend amplitude and planform morphology on flow and sedimentation in submarine channels. Marine and Petroleum Geology, 27, 1431−1447.

Armitage, D.A., Romans, B.W., Covault, J.A., Graham, S.A., 2009. The influence of mass transport-deposit surface topography on the evolution of turbidite architecture: The Sierra Contreras, Tres Pasos Formation (Cretaceous), southern Chile. Journal of Sedimentary Research, 79, 287−301.

Arnot, M.J., King, P.R., Browne, G.H. and Helle, K., 2007. Channelized, innermost, basin-floor-fan morphologies, Mount Messenger Formation Waikiekie South Beach and Inland, New Zealand. In: Nilsen, T., Shew, R., Steffens, G., Studlick, J. (Eds.), Atlas of Deep-Water Outcrops. AAPG Studies in Geology, 56, pp. 249–256.

Arnott, R.W.C., 2007. Stratal architecture and origin of lateral accretion deposits (LADs) and conterminuous inner-bank levee deposits in a base-of-slope sinuous channel, lower Isaac Formation (Neoproterozoic), East-Central British Columbia, Canada. Marine and Petroleum Geology, 24, 515−528.

Babonneau, N., Savoye, B., Cremer, M., Klein, B., 2002. Morphology and architecture of the present canyon and channel system of the Zaire deep-sea fan. Marine and Petroleum Geology, 19, 445-467.

Babonneau, N., Savoye, B., Cremer, M., Bez, M., 2004. Multiple terraces within the deep incised Zaire Valley (ZaïAngo Project): are they confined levees? In: Lomas, S.A., Joseph, P. (Eds.), Confined Turbidite Systems. Geological Society of London Special Publication, 222, pp. 91−114.

Badalini, G., Kneller, B.C., Winker, C.D., 2000. Architecture and processes in the late Pleistocene Brazos-Trinity Turbidite System, Gulf of Mexico. In: Weimer, P., Slatt, R.M., Coleman, J., Rosen, N.C., Nelson, H., Bouma, A.H., Styzen, M.J., Lawrence, D.T. (Eds.), Deep-Water Reservoirs of the World. SEPM Gulf Coast Section 20th Bob F. Perkins Research Conference, pp. 16−34.

Beaubouef, R.T., Rossen, C., Lovell, R.W.W., 2007. The Beacon Channel: a newly recognized architectural type in the Brushy Canyon Formation, Texas, USA. In: Nilsen, T., Shew, R., Steffens, G., Studlick, J. (Eds.), Atlas of Deep-Water Outcrops. AAPG Studies in Geology, 56, pp. 432−443.

Bouma, A.H., 1962. Sedimentology of Some Flysch Deposits: A Graphic Approach to Facies Interpretations. Elsevier, Amsterdam, 168 pp.

Brice, J.C., 1974. Evolution of meander loops. Geological Society of America Bulletin, 85, 581−586.

Bridge, J.S., 2003. Rivers and Floodplains: Forms, Processes and Sedimentary Record. Blackwell Publishing, Oxford, 491 pp.

Campion, K. M., Sprague, A. R., Mohrig, D., Lovell, R. W., Drzewiecki, P. A., Sullivan, M. D., Ardill, J. A., Jensen, G. N., Sickafoose, D. K., 2000. Outcrop expression of confined channel complexes. In: Weimer, P., Slatt, R.M., Coleman, J., Rosen, N.C., Nelson, H., Bouma, A.H., Styzen, M.J., Lawrence, D.T. (Eds.), Deep-Water Reservoirs of the World. SEPM Gulf Coast Section 20th Bob F. Perkins Research Conference, pp. 127−150.

Carlson, P.R., Bruns, T.R., Molnia, B.F., Schwab, W.C., 1982. Submarine valleys in the northeastern Gulf of Alaska: characteristics and probable origin. Marine Geology, 47, 217–242.

Cartigny, M.J.B., Postma, G., Van den Berg, J.H., Mastbergen, D.R., 2010. A comparative study of sediment waves and cyclic steps based on geometries, internal structures and numerical modeling. Marine Geology, 280, 40−56.

Clark, I.R., Cartwright, J.A., 2009. Interactions between submarine channel systems and deformation in deepwater fold belts: examples from the Levant Basin, Eastern Mediterranean sea. Marine and Petroleum Geology, 26, 1465−1482.

Clark, J.D., Pickering, K.T., 1996. Architectural elements and growth patterns of submarine channels: applications to hydrocarbon exploration. AAPG Bulletin, 80, 194–221.

Clemenceau, G.R., Colbert, J., Eddens, J., 2000. Production results from levee-overbank turbidite sands at Ram/Powell field, deepwater Gulf of Mexico. In: Weimer, P., Slatt, R.M., Coleman, J., Rosen, N.C., Nelson, H., Bouma, A.H., Styzen, M.J., Lawrence, D.T. (Eds.), Deep-Water Reservoirs of the World. SEPM Gulf Coast Section 20th Bob F. Perkins Research Conference, pp. 241−251.

Collinson, J.D., Thompson, D.B., 1982. Sedimentary Structures. Allen and Unwin, London, 207 pp.

Cook, T.W., Bouma, A.H., Chapin, M.A., Zhu, H., 1994. Facies architecture and reservoir characterization of a submarine fan channel complex, Jackfork Formation, Arkanas. In: Weimer, P., Bouma, A.H., Perkins, B.F. (Eds.), Submarine Fans and Turbidite Systems: Sequence Stratigraphy, Reservoir Architecture and Production Characteristics. SEPM Gulf Coast Section Foundation 15th Annual Research Conference, pp. 69–81.

Corney, R.K.T., Peakall, J., Parsons, D.R., Elliott, L., Amos, K.J., Best, J.L., Keevil, G.M., Ingham, D.B., 2006. The orientation of helical flow in curved channels. Sedimentology, 53, 249–257.

Cronin, B.T., Çelik, H., Hurst, A., Türkmen, I., 2005. Mud prone entrenched deep-water slope channel complexes from the Eocene of eastern Turkey. In: Hodgson, D.M., Flint, S.S. (Eds.), Submarine Slope Systems: Processes and Products. Geological Society of London Special Publication, 244, pp. 155–180.

Cronin, B.T., Çelik, H., Hurst, A., 2007. Sinuous channels in late stages of entrenched deep-water channel complexes: Hasret Mountain Main Channel, Turkey. In: Nilsen, T., Shew, R., Steffens, G., Studlick, J. (Eds.), Atlas of Deep-Water Outcrops. AAPG Studies in Geology, 56, pp. 368−372.

Cross, N.E., Cunningham, A., Cook, R.J., Taha, A., Esmaie, E., El Swidan, N., 2009. Three- dimensional seismic geomorphology of a deep-water slope-channel system: the Sequoia field, offshore west Nile delta, Egypt. AAPG Bulletin, 93, 1063−1086.

Das, H.S., Imran, J., Pirmez, C., Mohrig, D., 2004. Numerical modeling of flow and bed evolution in meandering submarine channels. Journal of Geophysical Research, 119, art. no. C10009.

Dalrymple, R.W., Boyd, R., Zaitlin, B.A., 1994. Incised-Valley Systems: Origin and Sedimentary Sequences. SEPM Special Publication, 51, 391 pp.

Demyttenaere, R., Tromp, J.P., Ibrahim, A., Allman-Ward, P., Meckel, T., 2000. The influence of bend amplitude and planform morphology on flow and sedimentation in submarine channels, In: Weimer, P., Slatt, R.M., Coleman, J., Rosen, N.C., Nelson, H., Bouma, A.H., Styzen, M.J., Lawrence, D.T. (Eds.), Deep-Water Reservoirs of the World. SEPM Gulf Coast Section Foundation 20th Annual Research Conference, pp. 304−317.

Deptuck, M.E., Steffens, G.S., Barton, M., Pirmez, C., 2003. Architecture and evolution of upper fan channel-belts on the Niger Delta slope and in the Arabian Sea. Marine and Petroleum Geology, 20, 649–676.

Deptuck, M.E., Sylvester, Z., Pirmez, C., O'Byrne, C., 2007. Migration-aggradation history and 3-D seismic geomorphology of submarine channels in the Pleistocene Benin-major Canyon, western Niger Delta slope. Marine and Petroleum Geology, 23, 406−433.

Droz, L., Bellaiche, G., 1985. Rhone Deep-Sea Fan: morphostructure and growth pattern. AAPG Bulletin, 69, 460–479.

Dykstra, M., Kneller, B.C., 2009. Lateral accretion in a deep-marine channel complex: implications for channelized flow processes in turbidity currents. Sedimentology, 56, 1411−1432.

Elliott, T., 2000. Depositional architecture of a sand-rich, channelized turbidite system: the Upper Carboniferous Ross Sandstone Formation, western Ireland. In: Weimer, P., Slatt, R.M., Coleman, J., Rosen, N.C., Nelson, H., Bouma, A.H., Styzen, M.J., Lawrence, D.T. (Eds.), Deep-Water Reservoirs of the World. SEPM Gulf Coast Section 20th Bob F. Perkins Research Conference, pp. 342−373.

Faulkenberry, L., 2004. High-resolution seismic architecture of upper slope submarine channel systems: Gulf of Mexico and offshore Nigeria. Unpublished Ph.D. Thesis, University of Leeds, 258 pp.

Ferry, J.-N., Mulder, T., Parize, O., Raillard, S., 2005. Concept of equilibrium profile in deep-water turbidite systems: effects of local physiographic changes on the nature of sedimentary process and the geometries of deposits. In: Hodgson, D.M., Flint, S.S. (Eds.), Submarine Slope Systems: Processes and Products. Geological Society of London Special Publication, 244, pp. 181−193.

Fildani, A., Normark, W.R., 2002. The stratigraphic evolution of Monterey Fan area and growth patterns of related channel complexes, AAPG Bulletin, Annual Meeting, Program, 12, pp. A54.

Fonnesu, F., 2003. 3D seismic images of a low-sinuosity slope channel and related depositional lobe (West Africa deep-offshore). Marine and Petroleum Geology, 20, 615−629.

Gardner, M.H., Borer, J. M., 2000. Submarine channel architecture along a slope to basin profile, Brushy Canyon Formation, West Texas. In: Bouma, A.H., Stone, C.G. (Eds.), Fine-Grained Turbidite Systems. AAPG Memoir 72/SEPM Special Publication 68, pp. 195−214.

Gee, M.J.R., Gawthorpe, R.L., 2007. Early evolution of submarine channels offshore Angola revealed by three-dimensional seismic data, In: Davies, R.J., Posamentier, H.W., Wood, L.J., Cartwright, J.A. (Eds.), Seismic Geomorphology: Applications to Hydrocarbon Exploration and Production. Geological Society of London Special Publication, 277, pp. 223−235.

Harms, J.C., Southard, J.B., Walker, R.G., 1982. Structures and Sequences in Clastic Rocks. SEPM Short Course No. 9 Lecture Notes. Society of Economic Paleontologists and Mineralogists, Tulsa, 250 pp.

Heiniö, P., Davies, R.J., 2007. Knickpoint migration in submarine channels in response to fold growth, western Niger Delta. Marine and Petroleum Geology, 24, 434−449.

Hodgson, D.M., 2009. Distribution and origin of hybrid beds in sand-rich submarine fans of the Tanqua depocentre, Karoo Basin, South Africa. Marine and Petroleum Geology, 26, 1940−1956.

Hubbard, S.M., De Ruig, M.J., Graham, S.A., 2009. Confined channel-levee complex development in an elongate depo-center: deep-water Tertiary strata of the Austrian Molasse Basin. Marine and Petroleum Geology, 26, 85−112.

Imran, J., Islam, M.A., Huang, H., Kassem, A., Dickerson, J., Pirmez, C., Parker, G., 2007. Helical flow couplets in submarine gravity underflows. Geology, 35, 659−662.

Islam, M.A., Imran, J., Pirmez, C., Cantelli, A., 2008. Flow splitting modifies the helical motion in submarine channels. Geophysical Research Letters, 35, L22603, doi:10.1029/2008GL034995.

Janbu, N.E., Nemec, W., Kırman, E., Özaksoy, V., 2007. Facies anatomy of a channelized sand-rich turbiditic system: the Eocene Kusuri Formation in the Sinop Basin, north-central Turkey. In: Nichols, G., Paola, C., Williams, E.A. (Eds.), Sedimentary Environments, Processes and Basins – A Tribute to Peter Friend. Internationaol Assocociation of Sedimentologists Special Publication, 38, pp. 457−517.

Janocko, M., Cartigny, M.J.B., Nemec, W., Hansen, E.W.M., 2011. Turbidity current hydraulics and sediment deposition in erodible sinuous channels: laboratory experiments and numerical simulations. Marine and Petroleum Geology (MS in review).

Janocko, M., Nemec, W., 2011. The facies architecture and formation of deep-water point bars: an outcrop perspective. Sedimentology (MS in review).

Kane, I.A., Hodgson, D.M., 2011. Sedimentological criteria to differentiate submarine channel levee subenvironments: exhumed examples from the Rosario Fm. (Upper Cretaceous) of Baja California, Mexico, and the Fort Brown Fm. (Permian), Karoo Basin, S. Africa. Marine and Petroleum Geology, 28, 807–823.

Kane, I.A., McCaffrey, W.D., Peakall, J., 2008. Controls on sinuosity evolution within submarine channels. Geology, 36, 287−290.

Kane, I.A., Dykstra, M., Kneller, B.C., Tremblay, S., McCaffrey, W.D., 2009. Architecture of a coarse grained channel-levee system: the Rosario Formation, Baja California, Mexico. Sedimentology, 56, 2207−2234.

Kane, I.A., McCaffrey, W.D., Peakall, J., Kneller, B.C., 2010. Submarine channel levee shape and sediment waves from physical experiments. Sedimentary Geology, 223, 75−85.

Kassem, A., Imran, J., 2004. Three-dimensional modeling of density current, II. Flow in sinuous confined and unconfined channels. Journal of Hydraulic Research, 42, 591−602.

Keevil, G.M., Peakall, J., Best, J.L., Amos, K.J., 2006. Flow structure in sinuous submarine channels: velocity and turbulence structure of an experimental submarine channel. Marine Geology, 229, 241−257.

Keevil, G.M., Peakall, J., Best, J.L., 2007. The influence of scale, slope and channel geometry on the flow dynamics of submarine channels. Marine and Petroleum Geology, 24, 487−503.

Kneller, B.C, 2003. The influence of flow parameters on turbidite slope channel architecture. Marine and Petroleum Geology, 20, 901−910.

Kneller, B.C. and Branney, M.J. (1995) Sustained high-density turbidity currents and the deposition of thick ungraded sands. Sedimentology, 42, 607−616.

Kolla, V., Posamentier, H.W., Wood, L.J., 2007. Deep-water and fluvial sinuous channels: characteristics, similarities and dissimilarities, and modes of formation. Marine and Petroleum Geology, 24, 388−405.

Labourdette, R., 2007. Integrated three-dimensional modeling approach of stacked turbidite channels. AAPG Bulletin, 91, 1603−1618.

Labourdette, R., Bez, M., 2010. Element migration in turbidite systems: random or systematic depositional processes? AAPG Bulletin, 94, 345−368.

Lien, T., Walker, R.G., Martinsen, O.J., 2003. Turbidites in the Upper carboniferous Ross Formation, western Ireland: reconstruction of a channel and spillover system. Sedimentology, 50, 113−148.

Lowe, D.R., 1982. Sediment gravity flows. II. Depositional models with special reference to the deposits of high-density turbidity currents. Journal of Sedimentary Research, 52, 279−297.

Lowe, D.R., 1988. Suspended-load fallout rate as an independent variable in the analysis of current structures. Sedimentology, 35, 765−776.

May, J.A., Warme, J.E., Slater, R.A., 1983. Role of submarine canyons on shelfbreak erosion and sedimentation: modern and ancient examples. In: Stanley, D.J., Moore, G.T. (Eds.), The Shelfbreak: Critical Interface on Continental Margins. SEPM Special Publication, 33, pp. 315−332.

Mayall, M., Stewart, I., 2000. The architecture of turbidite slope channels. In: Weimer, P., Slatt, R.M., Coleman, J., Rosen, N.C.,

Nelson, H., Bouma, A.H., Styzen, M.J., Lawrence, D.T. (Eds.), Deep-Water Reservoirs of the World. SEPM Gulf Coast Section 20th Bob F. Perkins Research Conference, pp. 578−586.

Mayall, M., Jones, E., Casey, M., 2006. Turbidite channel reservoirs – key elements in facies prediction and effective development. Marine and Petroleum Geology, 23, 821−841.

McHargue, T., Pyrcz, M.J., Sullivan, M.D., Clark, J., Fildani, A., Romans, B., Covault, J., Levy, M., Posamentier, H., Drinkwater, N., 2011. Architecture of turbidite channel system on the continental slope: patterns and predicitions. Marine and Petroleum Geology, 28, 728−743.

Métivier, F., Lajeunesse, E., Cacas, M.C., 2005. Submarine canyons in the bathtub. Journal of Sedimentary Research, 75, 6−11.

Miall, A.D., 1985. Architectural-element analysis: a new method of facies analysis applied to fluvial deposits. Earth-Science Reviews, 22, 261−308.

Mohrig, D., Buttles, J., 2007. Deep turbidity currents in shallow channels: Geology, 35, 155−158.

Morris, W.R., Normark, W.R., 2000. Sedimentologic and geometric criteria for comparing modern and ancient sandy turbidite elements. In: Weimer, P., Slatt, R.M., Coleman, J., Rosen, N.C., Nelson, H., Bouma, A.H., Styzen, M.J., Lawrence, D.T. (Eds.), Deep-Water Reservoirs of the World. SEPM Gulf Coast Section 20th Bob F. Perkins Research Conference, pp. 606−623.

Mutti, E., Normark, W.R., 1987. Comparing examples of modern and ancient turbidite systems: Problems and concepts. In: Legget, J.K., Zuffa, G.G. (Eds.), Deep Water Clastic Deposits: Models and Case Histories. Graham and Trotman, London, pp. 1−38.

Nakajima, T., Peakall, J., McCaffrey, W.D., Paton, D.A., Thompson, P.J., 2009. Outerbank bars: a new intra-channel architectural element within sinuous submarine slope channels. Journal of Sedimentary Research, 79, 872−886.

Nakajima, T., Satoh, M., 2001. The formation of large mudwaves by turbidity currents on the levees of the Toyama deep-sea channel, Japan Sea. Sedimentology, 48, 435–463.

Nanson, R.A., 2010. Flow fields in tightly curving meander bends of low width-depth ratio. Earth Surface Processes and Landforms, 35, 119−135.

O'Byrne, C.J., Barton, M.D., Steffens, G.S., Pirmez, C., Buergisser, H., 2007. Architecture of a laterally migrating channel complex: Channel 4, Isaac Formation, Windermere Supergroup, Castle Creek North, British Columbia, Canada. In: Nilsen, T., Shew, R., Steffens, G., Studlick, J. (Eds.), Atlas of Deep-Water Outcrops. AAPG Studies in Geology, 56, pp. 115−118.

O'Connell, S., McHugh, C., Ryan, W.B.F., 1995. Unique fan morphology in an entrenched thalweg channel on the Rhône Fan. In: Pickering, K.T., Hiscott, R.N., Kenyon, N.H., Ricci Lucchi, F., Smith, R.D.A. (Eds.), Atlas of Deep-Water Environments: Architectural Style in Turbidite Systems. Chapman and Hall, London, pp. 80−83.

Pacht, J.A., Bowen B.E., Schaefer B.L., Pottorf W.R., 1992. Systems tract, seismic facies, and attribute analysis within a sequence stratigraphic framework − Example from the offshore Louisiana Gulf Coast. In: Rhodes E.G., Moslow T., (Eds.), Marine Clastic Reservoirs. Springer-Verlag, New York, pp. 21−39.

Peakall, J., McCaffrey, W.D., Kneller, B.C., 2000. A process model for the evolution, morphology, and architecture of sinuous submarine channels. Journal of Sedimentary Research, 70, 434−448.

Peakall, J., Amos, K.J., Keevil, G.M., Bradbury, P.W., Gupta, S., 2007. Flow processes and sedimentation in submarine channel bends. Marine and Petroleum Geology, 24, 470−486.

Phillips, S., 1987. Dipmeter interpretation of turbidite-channel reservoir sandstones, Indian Draw Field, New Mexico. In: Tillman, R.W., Weber, K.J. (Eds.), Reservoir Sedimentology. SEPM Special Publication, 40, pp. 113−128.

Pickering, K.T., Hiscott, R.N., Hein, F.J., 1989. Deep-Marine Environments: Clastic Sedimentation and Tectonics. Kluwer Academic Publishers, London, 424 pp.

Piper, D.J.W., Normark, W.R., 1983. Turbidite depositional patterns and flow characteristics, Navy submarine fan, California Borderland. Sedimentology, 30, 681−694.

Pirmez, C., Imran, J., 2003. Reconstruction of turbidity currents in Amazon Channel. Marine and Petroleum Geology, 20, 823−849.

Pirmez, C., Beaubouef, R.T., Friedmann, S.J., Mohrig, D.C., 2000. Equilibrium Profile and base-level in submarine channels: examples from Late Pleistocene systems and implications for the architecture of deepwater reservoirs. In: Weimer, P., Slatt, R.M., Coleman, J., Rosen, N.C., Nelson, H., Bouma, A.H., Styzen, M.J., Lawrence, D.T. (Eds.), Deep-Water Reservoirs of the World. SEPM Gulf Coast Section 20th Bob F. Perkins Research Conference, pp. 782−805.

Posamentier, H.W., 2003. Depositional elements associated with a basinfloor channel–levee system: case study from the Gulf of Mexico. Marine and Petroleum Geology, 20, 667−690.

Posamentier, H.W., Kolla, V., 2003. Seismic geomorphology and stratigraphy of depositional elements in deep-water settings. Journal of Sedimentary Research, 73, 367−388.

Posamentier, H.W., Meizarwan, Wisman, P.S., Plawman, T., 2000. Deep water depositional systems – Ultra-deep Makassar Strait, Indonesia. In: Weimer, P., Slatt, R.M., Coleman, J., Rosen, N.C., Nelson, H., Bouma, A.H., Styzen, M.J., Lawrence, D.T. (Eds.), Deep-Water Reservoirs of the World. SEPM Gulf Coast Section 20th Bob F. Perkins Research Conference,, pp. 806−816.

Posamentier, H. W., Davies, R. J., Cartwright, J. A., Wood, L. J., 2007. Seismic geomorphology - an overview, In: Davies, R.J., Posamentier, H.W., Wood, L.J., Cartwright, J.A. (Eds.), Seismic Geomorphology: Applications to Hydrocarbon Exploration and Production. Geological Society of London Special Publication, 277, pp. 1−14.

Postma, G., Nemec, W. and Kleinspehn, K., 1988. Large floating clasts in turbidites: a mechanism for their emplacement. Sedimentary Geology, 58, 47−61.

Prather, B.E., 2003. Controls on reservoir distribution, architecture and stratigraphic trapping in slope settings. Marine and Petroleum Geology, 20, 529−545.

Rowland, J.C., Hilley, G.E., Fildani, A., 2010. A test of initiation of submarine leveed channels by deposition alone. Journal of Sedimentary Research, 80, 710−727.

Samuel, A., Kneller, B.C., Ralan, S., Sharp, A., Parsons, C, 2003. Prolific deep-marine slope channels of the Nile Delta, Egypt. AAPG Bulletin, 87, 541−560.

Schumm, S.A., 1985. Patterns of alluvial rivers. Annual Reviews of Earth and Planetary Science, 13, 5–27.

Schwab, A.M., Tremblay, S., Hurst, A., 2007. Seismic expression of turbidity-current and bottom-current processes on the Northern Mauritanian continental slope, In: Davies, R.J., Posamentier, H.W., Wood, L.J., Cartwright, J.A. (Eds.), Seismic Geomorphology: Applications to Hydrocarbon Exploration and Production. Geological Society of London Special Publication, 277, pp. 237−252.

Shanmugam, G., Moiola, R.J., 1988. Submarine fans: characteristics, models, classification, and reservoir potential. Earth-Science Reviews, 24, 383-428.

Shultz, M.R., Fildani, A., Cope, T.D., Graham, S.A., 2005. Deposition and stratigraphic architecture of an outcropping ancient slope system: Tres Pasos Formation, Magallanes Basin, southern Chile. In: Hodgson, D.M., Flint, S.S. (Eds.), Submarine Slope Systems: Processes and Products. Geological Society of London Special Publication, 244, pp. 27−50.

Skene, K.I., Piper, D.J.W., Hill, P.S., 2002. Quantitative analysis of variations in depositional sequence thickness from submarine channel levees. Sedimentology, 49, 1411−1430.

Skene, K.I., Piper, D.J.W., 2005. Late Cenozoic evolution of Laurentian Fan: Development of a glacially-fed submarine fan. Marine Geology, 27, 67−92.

Sprague, A.R., Sullivan, M.D., Campion, K.M., Jensen, G.N., Goulding, F.J., Sickafoose, D.K., Jenette, D.C., 2002. The physical stratigraphy of deep-water strata: a hierarchial approach to the analysis of genetically related stratigraphic elements for improved reservoir prediction. AAPG Annual Meeting Abstracts, Houston, pp. 10−13.

Straub, K.M., Mohrig, D., McElroy, B., Buttles, J., 2008. Interactions between turbidity currents and topography in aggrading sinuous submarine channels: a laboratory study. GSA Bulletin, 120, 368−385.

Straub, K.M., Mohrig, D., Buttles, J., McElroy, B., Pirmez, C., 2011. Quantifying the influence of channel sinuosity on the depositional mechanics of channelized turbidity currents: a laboratory study. Marine and Petroleum Geology, 28, 744−760.

Sylvester, Z., Pirmez, C., Cantelli, A., 2011. A model of submarine channel-levee evolution based on channel trajectories: Implications for stratigraphic architecture. Marine and Petroleum Geology, 28, 716-727.

Timbrell, G., 1993. Sandstone architecture of the Balder Formation depositional system, UK Quadrant 9 and adjacent areas. In: Parker, J.R. (Ed.), Petroleum Geology of Northwest Europe. Proceedings of the 4th Conference, Geological Society of London, pp. 107−121.

Vrolijk, P.J., Southard, J.B., 1997. Experiments on rapid deposition of sand from high-velocity flows. Geoscience Canada, 24, 45–54.

Weimer, P., Slatt, R.M., 2007. Petroleum Geology of Deepwater Settings. AAPG Studies in Geology, 57, 816 pp.

Wonham, J.P., Jayr, S., Mougamba, R., Chuilon, P., 2000. 3D sedimentary evolution of a canyon fill (Lower Miocene-age) from the Mandorove Formation, offshore Gabon. Marine and Petroleum Geology, 17, 175−197.

Wynn, R.B., Cronin, B.T., Peakall, J., 2007. Sinuous deep-water channels: genesis, geometry and architecture. Marine and Petroleum Geology, 24, 341−387.

# II

# Turbidity current hydraulics and sediment deposition in erodible sinuous channels: laboratory experiments and numerical simulations

Michal Janocko [a], Matthieu J.B. Cartigny [b], Wojciech Nemec [a], Ernst W.M. Hansen [c]

[a] *Department of Earth Science, University of Bergen, 5007 Bergen, Norway*
[b] *Department of Earth Sciences, University of Utrecht, 3508 TA Utrecht, the Netherlands*
[c] *Complex Flow Design A.S., 7462 Trondheim, Norway*

Submitted to *Marine and Petroleum Geology*

**Abstract**

The study combines laboratory experiments and 3D numerical simulations to identify key factors controlling the spatial pattern of sediment deposition in submarine sinuous channels and the process of channel meandering. By exploring a full range of possible circumstances, the study recognizes five types of channel bars and reveals conditions of their formation. These channel depocentres include meander bars (point bars), bars formed in the channel-bend inflection zone at the inner- to outer-bank or outer- to inner-bank transition, and outer-bank bars formed directly upstream or downstream of the bend apex. Every bar type requires particular flow conditions, but some bars may form concurrently or alternate with one another in certain circumstance. Many of the bars appear to be significantly thinner than the host channel depth, which may be due to their scaling with the thickness of the flow density core or to the use of monosized sediment.

The simulations indicate that the flow helicoid may rotate either inwards or outwards at channel bends, or may virtually lose its structure in the case of a grossly oversized flow. If the length scale of the flow helicoid matches the channel curvature, the flow rotates inwards irrespective of others conditions. If the flow is out of phase with the channel, the direction of the helicoid rotation depends on the flow velocity and the angle at which the flow velocity core approaches the outer bank. The elevation of the velocity core above the channel floor has an additional transient impact on the local sense of flow rotation. The study confirms and expounds on many previous laboratory observations pertaining to the flow of turbidity currents in sinuous non-meandering channels. However, the study also indicates that the meandering process may not be scale-independent and that the development of subaqueous meandering channels in small-scale laboratory or numerical experiments may be an impossible task. Inferences about the channel meandering conditions based on small-scale experiments should thus be considered with much caution.

*Keywords:* Turbidity currents, Sinuous channels, Laboratory experiments, Numerical simulations, Helicoidal flow, Meandering, Channel bars

## 1. Introduction

Laboratory experiments on turbidity-current flow in sinuous channels have thus far been limited to non-erodible, solid-wall conduits, while purporting to imitate the large-scale flows known from natural deep-water sinuous channels. Despite many interesting hydraulic observations derived from these experiments, the scaling of flow with sediment grain size remains an intractable problem and also no true meandering channels – with active lateral migration and point-bar accretion – have been reproduced in laboratory. Therefore, one of the moot points has been as to how reliable such small-scale experiments may actually be.

The aim of the present study was to monitor turbidity-current flows in an erodible laboratory channel and then to reproduce the flows by numerical CFD (computational fluid dynamics) simulation and to upscale them to natural conditions. In this way, the qualitative correspondence of laboratory and natural flows could be verified, particularly when it comes to the loci of preferential sediment deposition. The rationale was to focus on the key factors controlling flow in sinuous channels, including conditions favouring the meandering process as well as a full range of departures from such conditions.

The CFD simulations are most insightful in revealing the corresponding spectrum of flow behaviours and sediment deposition patterns, shedding light on the architectural diversity of submarine sinuous channels and adding to the potential range of their architectural elements. The results confirm and expound on previous laboratory observations regarding turbidity currents in non-meandering sinuous channels. However, the requirements for turbidity-current meandering appear to be unattainable in laboratory conditions, and this puts in doubt at least some of the laboratory-derived notions about flow in deep-water meandering channels. The CFD simulations are more reliable in this respect, revealing the particularity of submarine meandering phenomenon.

## 2. Rationale

Submarine sinuous channels can be classified into three end-member categories: non-aggradational meandering channels, aggradational levéed channels and erosional, cut-and-fill channels (Kneller, 2003; Janocko et al., 2011). They differ in their planform and width/depth ratio, and more importantly, in the type and combination of architectural elements. Previous research has indicated that the meandering channels are the least common channel variety on the modern seafloor and in the ancient record (Pyles et al., 2010), which suggests that the conditions required for the formation of meandering channels are more specific and reached less frequently than conditions favouring the development of other sinuous channels.

In the light of the previous experimental, outcrop and seismic studies (see references below), the development of submarine sinuous channels is controlled by the following key factors (Fig. 1):

- The relationship between the flow's desired equilibrium ("graded") substrate profile and the conduit's actual profile.
- The relationship between the rotating flow's inherent hydraulic curvature and the conduit's pre-existing curvature.
- The relationship between the flow thickness and the conduit depth (topographic relief).
- The degree of conduit bank erodibility by the conveyed flows.

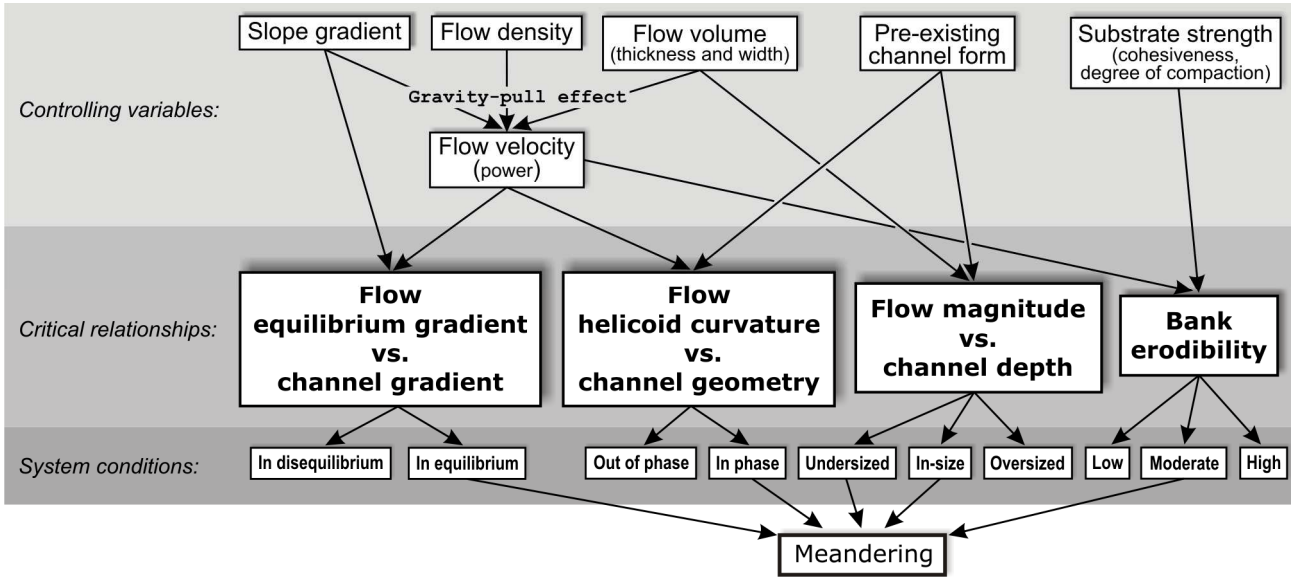


**Fig. 1.** Figure showing the relationship between factors influencing the development of submarine sinuous channels. Channel types result from a particular combination of the system conditions, which are determined by the critical relationships between the flow and substrate properties.

Each of these factors has its particular "optimal" state that potentially favours meandering as well as two alternative departures from this state, which disfavour the meandering processes. As a prerequisite for the formation of meandering channels, the existing studies have indicated a combination of the following optimal states of the four factors:

*Slope-equilibrium flow* – Submarine channels evolve through the adjustment to an equilibrium profile along which turbidity currents are conveyed down-slope with minimum substrate aggradation or degradation (Pirmez et al., 2000; Kneller, 2003). The equilibrium profile desired by a flow depends chiefly upon the flow velocity, effective density and thickness (Fig. 1; Kneller, 2003). Once the channel-floor gradient is in equilibrium with the prevalent flows, the erosion and deposition occur mainly in the lateral domain, causing the channel to increase its curvature and develop meanders. In ancient submarine meander belts, the slope-equilibrium of flows is indicated by the flat, originally horizontal bases and tops of point bars (Abreu et al., 2003; Campion et al., 2000; Lien et al., 2003; Shultz et al., 2005; Mayall et al., 2006; Beaubouef et al., 2007; Cronin et al., 2007; Kolla et al., 2007, figs. 10–12; Labourdette, 2007; O'Byrne et al., 2007; Wynn et al., 2007; Dykstra and Kneller, 2009; Nakajima et al., 2009; Janocko et al., 2011; Janocko and Nemec, 2011). The negligible aggradation of meandering channel belts is indicated also by the lack of significant levées (Kneller, 2003; Dykstra and Kneller, 2009; Janocko et al., 2011; Janocko and Nemec, 2011). Flows that are not in equilibrium with the channel-floor gradient can be either aggradational or degradational (erosive).

*In-phase flow* – Fluvial hydraulic research has shown that the phenomenon of meandering is an intrinsic property of fluid flow and that a water current tends to assume a meandering flow pattern even in the absence of a pre-existing channel or an erodible substrate (Gorycki, 1973). The inception of meandering is considered to be a function of the flow discharge and hydraulic drag, resulting in helicoidal flow geometry that is sinuous in planform. A change in the flow curvature, or planform amplitude and wavelength, can be regarded as being roughly proportional to the flow discharge (Fig. 1). As suggested by Dykstra and Kneller (2009), analogous hydraulic parameters may be responsible for the meandering of turbidity currents. However, the hydraulic geometry of a river channel is continuously adjusted by the perennial flow, whereas turbidity currents are discrete flows and the channel adjustment made by one flow may not necessarily meet the hydraulic geometry of a subsequent flow. Lateral channel migration can be maintained only if the prevalent turbidity currents are "in phase" with the channel's hydraulic geometry (i.e., curvature and cross-sectional area). If the hydraulic geometry of prevalent flows fails to match the host channel geometry, the growth of meanders is inhibited.

*In-size flow* – The thickness of turbidity current is a function of the flow volume (Fig. 1). The degree of flow confinement by conduit has a significant effect on the flow hydraulic structure and the loci of sediment deposition in both fluvial and subaqueous sinuous channels (Shiono and Muto, 1998; Loveless et al., 2000; Islam et al., 2008; Kane et al., 2008). In the present study, a turbidity current is considered to be "in-size" with the channel capacity if the flow thickness is between ½ and 1½ of the channel depth. Flows thicker than 1½ of the channel depth are considered to be "oversized", whereas flows thinner than ½ of the channel depth are considered to be "undersized". The latter category does not include cases of extremely undersized flows, as may occur in deep channels with low aspect ratios, where flow spill-out is inhibited. Poorly-confined flows tend to deposit sediment at the outer bank, whereas well-confined, in-size flows accrete sediment to the inner bank (Loveless et al., 2000; Kane et al., 2008). Well-confined flows also tend to be more sinuous and more effective in bypassing their sediment load (Mohrig and Buttles, 2007; Kane et al., 2008), which suggests that they can reach faster a slope-equilibrium state.

*Moderate bank erodibility* – It has long been recognized in fluvial research that the key to producing experimental meandering channels is a proper scaling of bank strength relative to flow power (Kleinhans, 2010; and references therein). Banks that are too weak will promote avulsion and the development of a braided channel, whereas banks that are too strong will render the channel laterally inactive. Actively meandering channels thus require banks sufficiently strong to prevent avulsion, but weak enough to allow systematic erosion of the outer bank and hence lateral migration of the channel. The issue of bank strength has thus far been little explored in turbiditic research, but it seems logical to assume that the banks of submarine meandering channels must fulfil similar requirements as their fluvial counterparts.

In order to explore the flow hydraulics and architectural diversity of submarine sinuous channels, a series of laboratory experiments and numerical simulations have been designed for a full range of possible flow scenarios, including conditions

**Table 1.** Review of the laboratory and numerical-simulation experiment conditions with the resulting architectural elements of sinuous channel belts.

| Experiments | | Flow conditions | | | | | | | | The resulting architectural elements of sinuous channel belts |
|---|---|---|---|---|---|---|---|---|---|---|
| Laboratory run # | Simulation run # SS – small scale LS – large sclae | Slope-equilibrium flow | In-phase flow | In-size flow | Slope-aggrading flow | Out-of-phase too large flow | Out-of-phase too small flow | Oversized flow | Undersized flow | |
| | LS1 | • | • | • | | | | | | point bars and inner- to outer-bank transition bars |
| | LS2 | | • | • | • | | | | | vertical channel-filling |
| 7[B] 8[B] | SS3[A] LS3[B] | • | | • | | • | | | | outer- to inner-bank transition bars[A], down-apex outer-bank bars [B] and inner- to outer-bank transition bars[B] |
| | LS4 | • | | • | | | • | | | - |
| | LS5 | • | • | | | | | • | | inner- to outer-bank transition bars |
| | LS6 | • | • | | | | | | • | point bars and inner- to outer-bank transition bars |
| 9[A] | LS7[A] SS7[B] | • | | | | • | | • | | outer- to inner-bank transition bars[A] and down-apex outer-bank bars[B] |
| | LS8 | • | | | | | • | • | | - |
| | SS9[A] SS9[B] LS9[B] | • | | | | • | | | • | outer- to inner-bank transition bars[A], down-apex outer-bank bars[B] and inner- to outer-bank transition bars[B] |
| | LS10 | • | | | | | • | | • | - |
| | SS11 | | • | | • | | | • | | vertical channel-filling |
| | SS12 | | • | | • | | | | • | vertical channel-filling |
| 6[A] 10[A] | SS13[A] SS13[B] SS13[C] | | | • | • | • | | | | down-apex outer-bank bars[A,B], inner- to outer-bank transition bars[A], up-apex outer-bank bars[C] and vertical channel-filling |
| | SS14 | | | • | • | | • | | | vertical channel-filling |
| 3–5[A] | LS15[A] SS15[B] SS15[C] LS15[C] | | | | • | • | | • | | down-apex outer-bank bars[A,B], inner- to outer-bank transition bars[A], up-apex outer-bank bars[C] and vertical channel-filling |
| | SS14 | | | | • | | • | • | | up-apex outer-bank bars and vertical channel-filling |
| | SS17[A] SS17[B] LS17[B] SS17[C] | | | | • | • | | | • | down-apex outer-bank bars[A,B], inner- to outer-bank transition bars[A], up-apex outer-bank bars[C] and vertical channel-filling |
| | SS18 | | | | • | | • | | • | vertical channel-filling |

optimal for the meandering process. Both aggradational and equilibrium slope conditions are taken into account in the simulations, but degradational conditions are disregarded as a relatively trivial scenario. A degradational channel, when incising rapidly, bears an inherited planform and acts as a bypass conduit where little or no sediment can be accumulated. When incising slowly, the channel can accumulate sediment, but in a manner similar as in the original, pre-incision conduit.

Channel-bank strength is not regarded as an independent variable in the numerical simulations, as the bank erodibility in the CFD model can readily be regulated by adjusting the erosional capacity of the flow. With the number of controlling variables effectively reduced to three, a total of eighteen scenarios have been analysed, including simulations of ten different laboratory flows (see the variants of flow conditions in Table 1).

## 3. Descriptive terminology

Dunes and ripples are hydraulic bedforms related strictly to sediment transport and flow regime, dependent solely on the flow power and grain size, and scaling with the thickness of flow and its inner boundary layer (Allen, 1982; Harms et al., 1982). In contrast, the larger bedforms referred to as bars – the macroforms of Jackson (1975) – are local sediment depocentres. They are constructional features resulting from sediment accumulation, independent of the flow regime, formed due to local flowline perturbation and scaling with the flow width, rather than thickness (see also Nakajima et al., 2009).

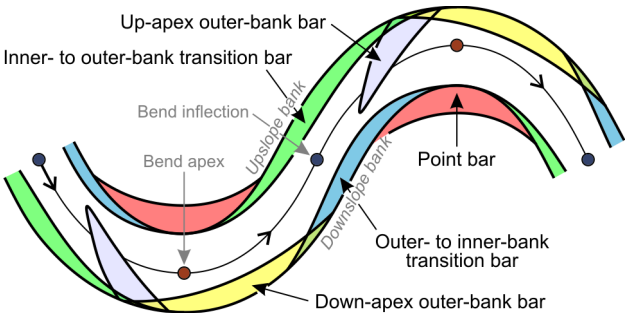


**Fig. 2.** Descriptive terminology of channel bars and banks used in the present paper.

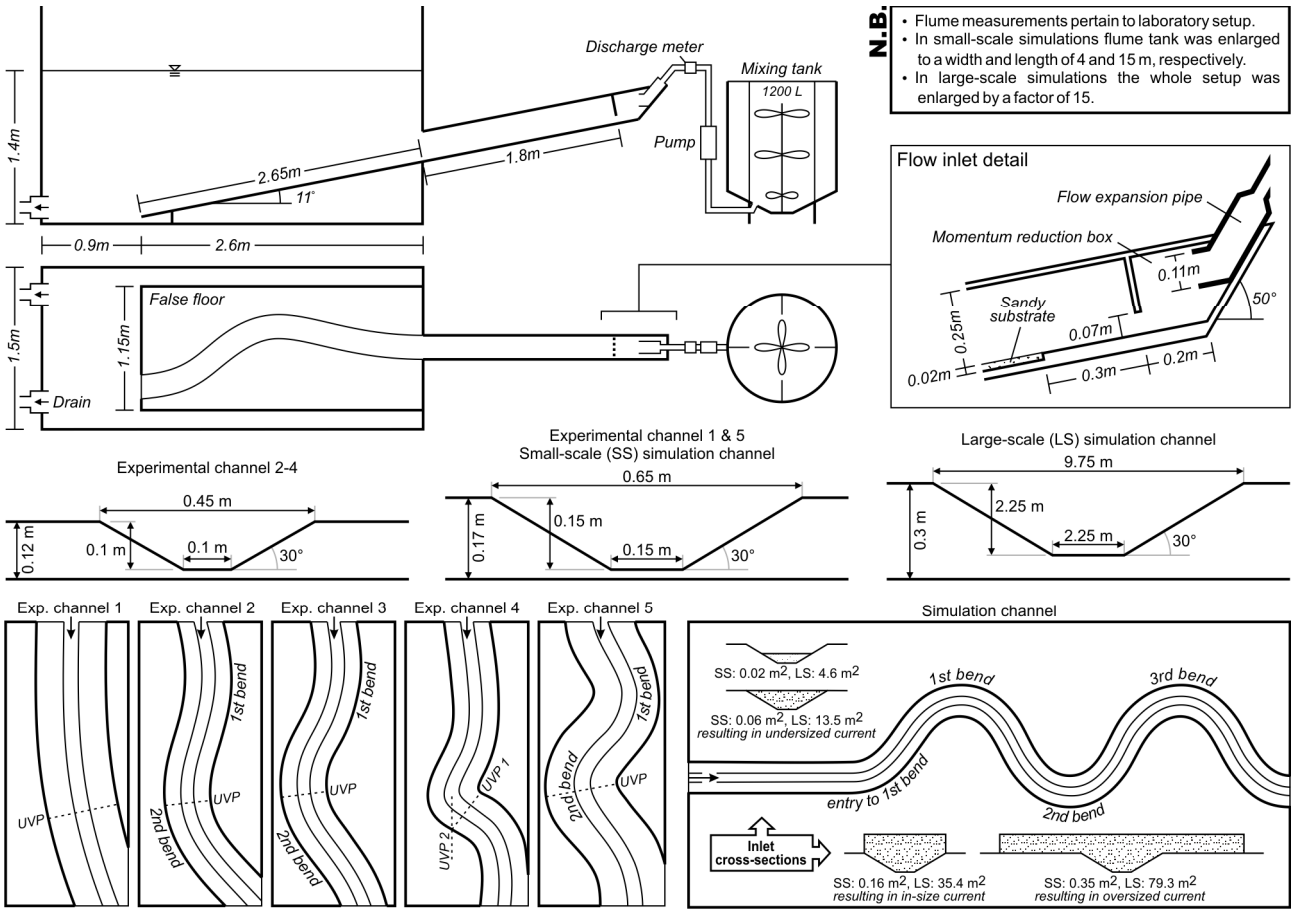


**Fig. 3.** Laboratory and simulation setup. For further explanation, see text.

Point bars are the characteristic attribute of meandering channels, where flowlines rotate in a holicoidal manner at the channel bends (Bridge, 2003). However, the turbiditic currents in sinuous channels are variously superelevated and their flowlines can be perturbed in other ways, resulting in pronounced sediment accumulation at other locations (e.g., see the nested mounds of Phillips, 1987; Timbrell, 1993; the outer-bank bars of Nakajima et al., 2009). Instead of using arbitrary labels for these other bar varieties, we refer to them descriptively according to their position at the outer bank relative to the channel bend apex and according to their location at the upslope or downslope bank of the bend inflection zone (i.e., at the inner-to-outer bank or outer-to-inner bank transition). This terminology for channel bars is defined further in Fig. 2. Whereas point bars typify meandering channels, the other bar types are generally characteristic of sinuous non-meandering channels, albeit may also form in a conduit between the episodes of its lateral migration.

The rotating flow helicoid rising against the inner bank (or point-bar flank) at a channel bend is referred to also as the inward-directed helicoid, whereas the flow helicoid rising against the outer bank is accordingly referred to as the outward-directed helicoid (see also Keevil et al., 2007; Peakal et al., 2007; Giorgio Serchi et al., 2011).

## 4. Laboratory experiments

The main purpose of conducting laboratory experiments was to calibrate and validate the numerical CFD model, which was to be used further for a wider range of flow simulations. The laboratory effort focused on producing a meandering channel that would migrate laterally by outer-bank erosion with sediment deposition on the inner bank. In an attempt to meet the requirements for channel meandering, the following parameters were varied in combination: the flow discharge and sediment concentration and the channel curvature and cross-sectional area.

### *4.1. The method of laboratory experiments*

Twelve separate experiments were conducted at the Eurotank Flume Laboratory, University of Utrecht. The experimental setup consisted of a raised 1.15 × 2.65 m expansion table placed inside a rectangular flume tank (1.5 × 3.5 m in area and 2 m deep) with a 2-m long, straight input channel centred on one side of the table (Fig. 3). The inclination of both the input channel and the expansion table was set to 11°. On the expansion table, five sinuous channels were consecutively moulded using wet fine-grained quartz sand ($D_{median}$ = 160 µm). The channel forms differed in sinuosity (1.05-1.15) and depth (0.10 and 0.15 m) (Fig. 3). To avoid channel-floor scouring at flow inlet, the sandy substrate in the area was replaced with a wooden plate (see inset in Fig. 3).

The flume tank was filled with fresh water, and all turbidity currents released into the flume were composed of fresh water and fine-grained quartz sand ($D_{10}$ = 103 µm, $D_{50}$ = 160 µm, $D_{90}$ = 251 µm, standard deviation 58 µm, grain density 2,650 kg/m$^3$). The volumetric concentration of sand varied from 5 to 15 % among runs, which corresponded to absolute flow density of 1,132.5–1,397.5 kg/m$^3$ and an excess density of 13.25–39.75 % relative to the ambient water. The sediment-water mixture was pumped from a mixing tank (1.2 m$^3$ volume) via an electromagnetic discharge-meter into a flow expansion pipe and further into a momentum-reduction box, from which it was released into the input channel through an inlet 0.22 × 0.07 m in cross-section. All flows released from the inlet were fully

**Table 2.** Summary of flow properties, channel forms and the resulting velocity and depositional patterns in the laboratory experiments.

| Lab. run # | Channel # | Discharge [$m^3$/hr] | Concentration [volume %] | Duration [min] | The observed pattern of erosion and deposition in laboratory erodible channel, with the direction of cross-stream velocity vector at the base of flow (BCSV) at channel bends |
|---|---|---|---|---|---|
| 1 | 3 | 12 | 5 | 1 | ~95% of sediment load deposited in the input channel, thin (<1 cm) levees develop downstream of inlet and outer banks, directly downstream of inlet channel substrate is reworked into ripples, no evident erosion or deposition on the expansion table, BCSV towards outer bank |
| 2 | 3 | 16 | 5 | 1 | ~60% of sediment load deposited in the input channel, deposition occurs mainly at inner bank of 2nd bend (<2 cm), deposit is rippled upstream and smooth downstream of bend apex, significant erosion of outer bank at 2nd bend apex (8 cm) and around inlet (5 cm on both sides), moderate (<2 cm) levees develop downstream of inlet and outer banks, BCSV towards outer bank |
| 3 | 3 | 20 | 5 | 1 | ~30% of sediment load deposited in the input channel, deposition occurs mainly on the downstream end of the outer bank (<2 cm), deposits are rippled, moderate erosion of outer bank at bend apex (5 cm) and around inlet (5 cm on both sides), thick (<3 cm) rippled levees develop downstream of inlet and outer banks, BCSV towards outer bank |
| 4 | 3 | 22 | 5 | 1 | ~30% of sediment load deposited in the input channel, depositional and erosional pattern similar to Run 3, BCSV towards outer bank |
| 5 | 2 | 15 | 5 | 2 | ~60% of sediment load deposited in the input channel, deposition occurs in the downstream part of inner bank at the 2nd bend (<2 cm) and the overbank area downstream of the 1st bend (<4 cm), both intra-channel and levee deposits are smooth, moderate erosion of outer bank at bend apex (5 cm) and around inlet (5 cm on both sides), BCSV towards outer bank |
| 6 | 2 | 15 | 10 | 2 | ~40% of sediment load deposited in the input channel, deposition occurs in the thalweg (<3 cm), moderate rippled levees (<2 cm) develop on both sides of the channel, high erosion of downstream end of outer bank at the 2nd bend (10 cm), and moderate erosion around inlet (3 cm on both sides), BCSV towards outer bank |
| 7 | 5 | 17 | 15 | 2 | ~15% of sediment load deposited in the input channel, deposition occurs in the thalweg (<4 cm), downstream part of inner bank at the 2nd bend (<3 cm; smooth deposit), thick rippled levees (<3 cm) develop on both sides of the channel, high erosion of outer bank and inner bank (10 cm), and around inlet (5 cm on both sides), BCSV towards outer bank |
| 8 | 5 | 15 | 15 | 1 | ~20% of sediment load deposited in the input channel, deposition occurs in the thalweg (<6 cm), downstream part of inner bank at the 2nd bend (<2 cm; smooth deposit), thick rippled levees (<3 cm) develop on both sides of the channel, high erosion of outer bank and inner bank (8 cm), and around inlet (3 cm on both sides), BCSV towards outer bank |
| 9 | 4 | 16 | 15 | 1 | ~20% of sediment load deposited in the input channel, deposition occurs in the thalweg (<6 cm, rippled deposit), in outer- to inner-bank transitions (<5 cm, smooth deposit), thick rippled levees (<3 cm) develop on both sides of the channel, high erosion of outer bank at bend apex (10 cm), inner bank (5 cm) and around inlet (5 cm on both sides), BCSV towards outer bank |
| 10 | 1 | 15 | 7 | 2 | ~60% of sediment load deposited in the input channel, deposition occurs in thalweg and on the downstream end of the outer bank (<1 cm, smooth deposit), thin (<0.5 cm) smooth levees develop downstream of inlet and outer bank, directly downstream of inlet channel substrate is reworked into ripples, 2 cm erosion on both sides of the channel around inlet, BCSV towards outer bank |
| 11 | 1 | 10 | 5 | 3 | ~95% of sediment load deposited in the input channel, thin (<0.5 cm) levees develop downstream of inlet and outer bank, directly downstream of inlet channel substrate is reworked into ripples, no evident erosion or deposition on the expansion table, BCSV towards outer bank |
| 12 | 1 | 5 | 5 | 3 | ~99% of sediment load deposited in the input channel, no evident erosion or deposition on the expansion table, BCSV towards outer bank |

turbulent, with Reynolds numbers ranging from 4,460 to 17,119. Flows varied in discharge from 5 to 22 $m^3$/hr and had duration of one to three minutes (Table 2).

Flow velocity profiles at channel bends were measured by five ultrasonic probes (UVP Duo MX, 0.5 MHz) mounted 0.12 m apart on a glass frame from which the probes looked down into the flow at an angle of 45° (for exact probe location, see Fig. 3). The glass frame was mounted 0.3 m above the channel base, ensuring that the probes did not interact with the channelized flow. Single two-dimensional velocity profiles were constructed by combining measurements from two identical runs, between which the probe orientation was rotated by 90° in horizontal plane. After two runs, this procedure would yield 10 time-integrated one-dimensional velocity profiles which, after interpolation, formed two-dimensional velocity profiles of flow cross-sections.

The flume tank had an installed camera, and the topography was measured by a photomapping technique taking advantage of the water-surface migration during the filling and draining of the tank. Topographic isolines, formed by the intersection of the water surface and sediment surface on the expansion table, were systematically captured on camera for the vertical increments of water-level change of 0.02 m. The individual photographs were rectified for tilt and lens distortion using established control points on the sediment surface. The isolines were then digitized and distributed in the vertical domain, and subsequently interpolated into a 3D topographic map.

Although the banks of submarine meandering channels generally contain significant amounts of cohesive sediment (Janocko and Nemec, 2011), the ratio of bank strength to flow power in the laboratory experiments appeared to be qualitatively satisfactory when using the clay-free quartz sand, as the sinuous channels showed lateral erosion while preventing flow avulsion. The bank apparent strength is attributed to the low erosional capacity of small-scale turbidity currents.

### *4.2. The results of laboratory experiments*

The flow parameters and channel forms used and the resulting velocity-vector orientation and sedimentation pattern for the individual runs are summarized in Table 2. Examples illustrating the observed range of results are shown in Fig. 4. The velocity profiles and topographic photomaps from runs 8 and 9 (Figs. 5 and 6) were used further to calibrate and validate the CFD simulation model.

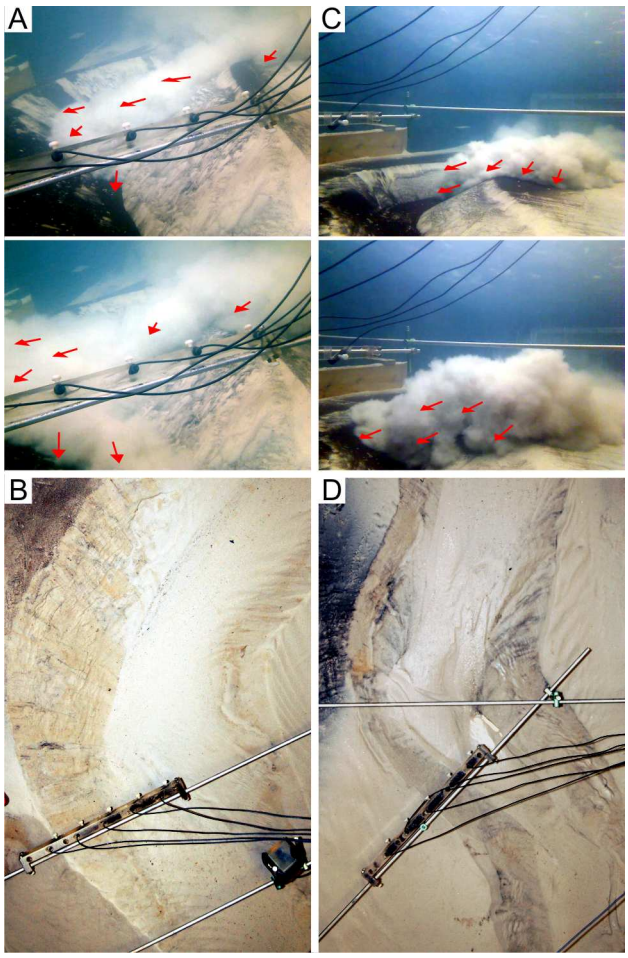


**Fig. 4.** Photographs showing the flow pattern and the resulting depocentres in the laboratory runs 8 and 9 (see Tables 1 and 2). (A) Flow of a well-confined turbidity current around a channel bend. Note the superelevation of the flow on the outer bank and its separation from the inner bank downstream of the bend apex. Arrows indicate flow direction. (B) Depositional pattern resulting from a well-confined current. The thickest deposits form in the thalweg and on the inner bank downstream of the bend apex, with minor deposition at the outer bank. (C) Flow of a poorly-confined turbidity current around a channel bend. Note that the flow travels downslope across the bend and spills out at bend inflections. Arrows indicate flow direction. (D) Depositional pattern resulting from a poorly-confined current. Sediment is deposited mainly in the thalweg and in the outer- to inner-bank transition.

Despite the considerable variation in experimental setup among the individual flow runs, the behaviour of turbidity currents in the erodible sinuous channels was largely similar. However, the degree of flow confinement by channel varied, resulting in somewhat different patterns of the flow interaction with the sinuous conduit. Flows with a relatively low input discharge, low initial concentration or a significant sediment loss by deposition in the input channel appeared to be well-confined, despite overspill through outer-bank run-up (runs 1, 2, 5, 8 and 10–12 in Table 2). The flow core part of highest concentration and velocity moved with super-elevation along the bend outer bank, resulting in near-bottom flow separation at the inner bank directly downstream of the bend apex (Fig. 4A). These flow separation zones in channels with more than one bend were further accentuated by the re-entering of overspill flow. The near-bottom cross-channel velocity vector at the measurement sites at channel bends was directed towards the outer bank (Fig. 5A), indicating a flow helicoid rising against the outer, rather than the inner bank.

Flows with a higher input discharge or a higher initial concentration and insignificant sediment loss in the input channel (runs 3, 4, 6, 7 and 9 in Table 2) were poorly confined by the sinuous conduit. A large part of the flow travelled straight down slope across the channel bends, spilling out of the channel and re-entering it in the bend inflection zones and causing flow separation at the inner- to outer-bank transition (Fig. 4C). The channel-contained core part of the flow moved along the bend outer bank, similarly forming a zone of flow separation at the inner bank directly downstream of the bend apex. Likewise, the near-bottom cross-channel velocity vector at channel bends was directed towards the outer bank (Fig. 6A), with no evidence of flow helicoid rise against the inner bank.

In all the experiments, the channelized flow deposited a downslope-thinning continuous belt of sediment in the channel thalweg zone, while depositing sediment also by overspill in the outer overbank areas directly downstream of the bend apices (Fig. 4B, D). The thalweg-zone deposit was generally rippled in the upper reaches of the channel and smooth in the lower reaches, where the flow power declined. On the account of the experiment small scale, the rippled and smooth bed configurations are thus likely to represent tractional deposition and non-tractional dumping of sediment, respectively. Notably, the overbank deposits of poorly-confined, grossly overspilling flows were rippled, whereas those formed by well-confined flows were smooth. The well-confined flows formed smooth deposits at the outer banks downstream of bend apices, apparently due to local deceleration during outer-bank runup (Fig. 4B). Similarly, the poorly-confined flows formed smooth deposits at the outer- to inner-bank transition in bend inflection zones, attributed to local deceleration in areas where major overspill occurred (Fig. 4D). Smooth deposits were also formed, particularly by the well-confined flows, in the inner-bank flow separation zones downstream of bend apices (Fig. 4B).

Despite using a range of erodible sinuous channel forms and flow parameters, the laboratory study came short of producing a laterally-migrating, true meandering channel. The reason was that the four prerequisites for flow meandering, discussed in section 2, could not be fulfilled in a single experimental run. Flows that were closest to attain equilibrium with the channel slope (runs 7–9 in Table 2) had too high a moment of inertia to be hydraulically in phase with the channel curvature. Perhaps the momentum of a slope-equilibrium flow might have been adjusted by reducing its sediment concentration and steepening of the slope, but the flume-tank construction did not allow the expansion table to be steeper than 11°. Alternatively, the channel wavelength might have possibly been adjusted to match the phase of the flow's intrinsic curvature, but the expansion table was too short to allow such morphometric adjustments for a multi-bend sinuous channel. Anyway, these are purely conceptual speculations and the fact remains that a meandering turbiditic channel has been impossible to produce in laboratory conditions.

The laboratory study as a whole confirms most of the observations from previous small-scale studies using non-erodible sinuous channels (e.g., Peakall et al., 2007; Amos et al., 2010). However, it is doubtful that any of the earlier-reported laboratory flows came even close to meandering conditions, and hence the laboratory-derived inferences about flow in deep-water meandering channels may not be reliable and should be considered with much caution.

## 5. Numerical CFD simulations

The main thrust of the study was on numerical CFD simulations, which offer greater precision and flexibility when it comes to the choice of flow properties and experimental setup. The greatest advantage of numerical simulations is that they allow all the main hydraulic characteristics of turbidity current and its responses to topography to be continuously monitored in three dimensions over the whole flow and its entire duration.

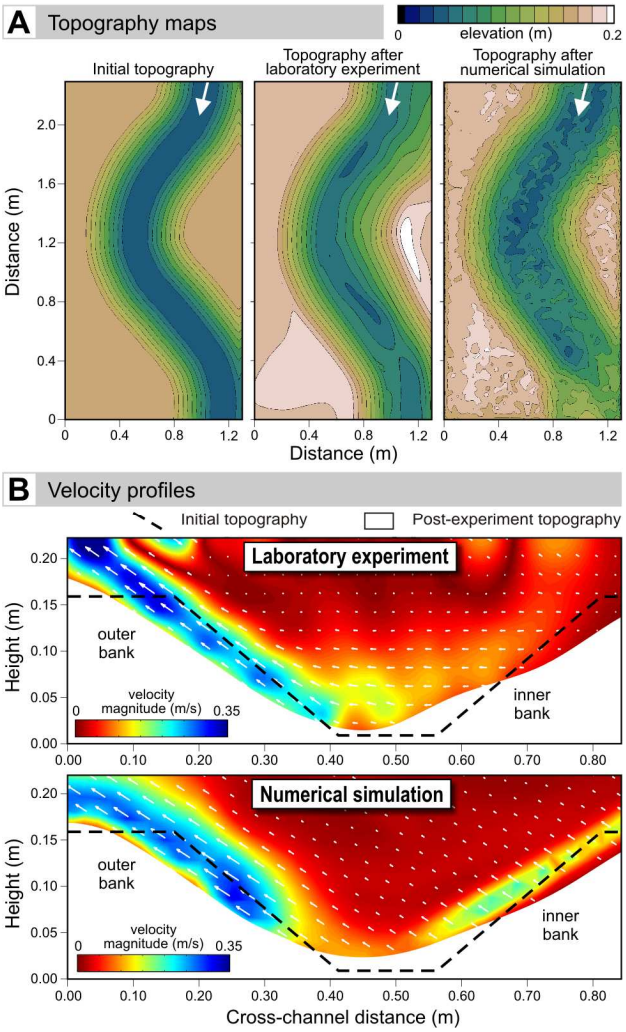


**Fig. 5.** Comparison of simulation results with measured data from the experimental run 8. (A) Maps showing the changes in topography. Note that the erosion occured at the inner bank and deposition occured in the thalweg and in the overbank area in both laboratory experiments and numerical simulations. (B) 2D velocity profiles across the channel in the 2nd bend. For location, see Fig. 3, experimental channel 5. Note the superelevation of the current on the outer bank and up-bank directed cross-flow velocity. The physical and numerical experiments show similar velocity distribution.

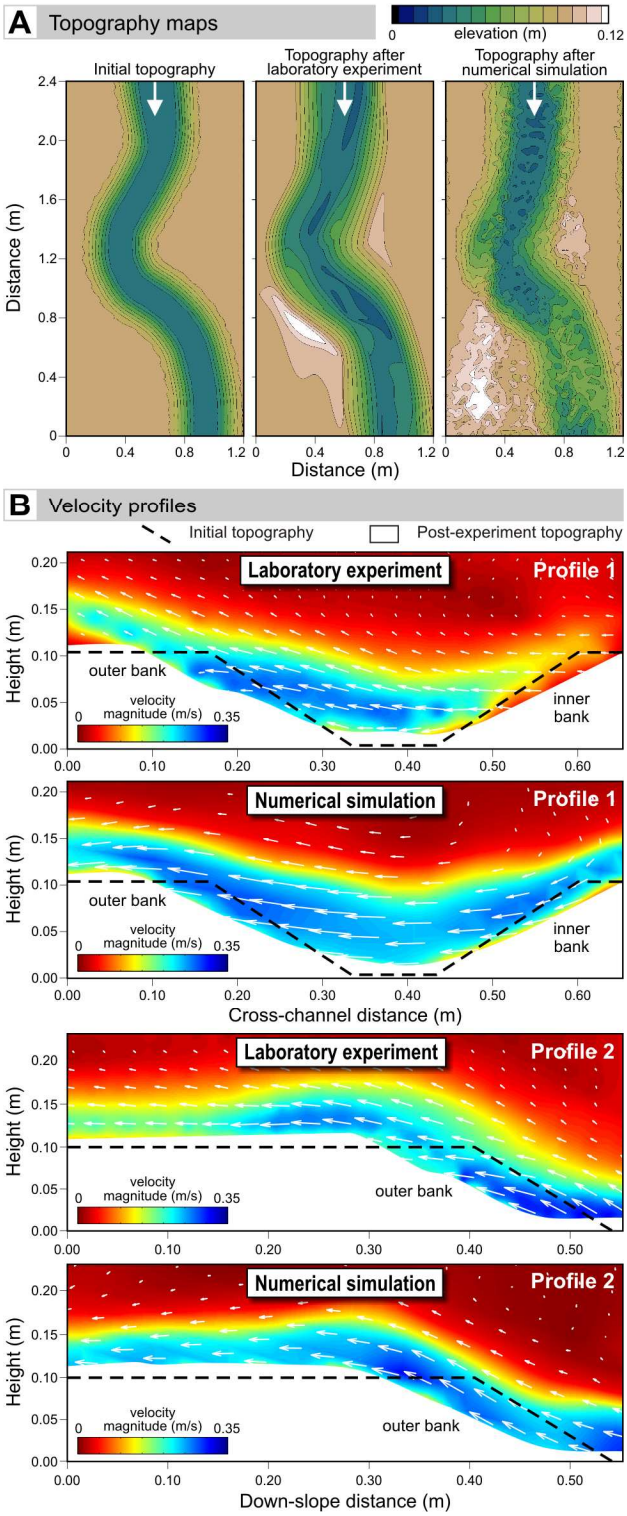


**Fig. 6.** Comparison of simulation results with measured data from the experimental run 9. (A) Maps showing the changes in topography. Note that the erosion occured at the inner bank and deposition occured in the thalweg and at the outer bank in both laboratory experiments and numerical simulations. (B) Velocity profiles of cross-channel (Profile 1) and overbank flow (Profile 2) in the 2nd bend. For location, see Fig. 3, experimental channel 4. Note the superelevation of the current on the outer bank and up-bank directed cross-flow velocity. The physical and numerical experiments show similar velocity distribution.

The flow parameters possible to display with full spatial and temporal continuity include: the x-y-z velocity components, velocity magnitude (geometric mean as a measure of turbulence intensity), vorticity, volumetric sediment concentration and bulk density, dynamic viscosity, shear-strain rate and bottom shear stress. No laboratory facility allows such a multi-parametric insight into flow behaviour.

The aim of CFD simulations was first to imitate most of the laboratory flows and verify the hydraulic correspondence, and then to extend the range of experiments performed in the laboratory by varying further the slope inclination, flow discharge and channel wavelength. Substrate strength was regulated by a pre-set erosiveness parameter of the flow, selected on a trial-and-error basis to allow lateral channel activity but prevent flow avulsion (i.e., the substrate would still consist of fine-grained quartz sand, but its erodibility was adjusted). Some of the flow simulations were additionally upscaled to natural conditions (as specified in Table 1) in order to assess whether the flow hydraulics and sediment deposition pattern in small-scale experiment mimicked sufficiently the behaviour of a natural-scale system.

### *5.1. The MassFlow-3D™ numerical model*

Computational fluid dynamics deals with the numerical solution, by computational methods, of the governing equations

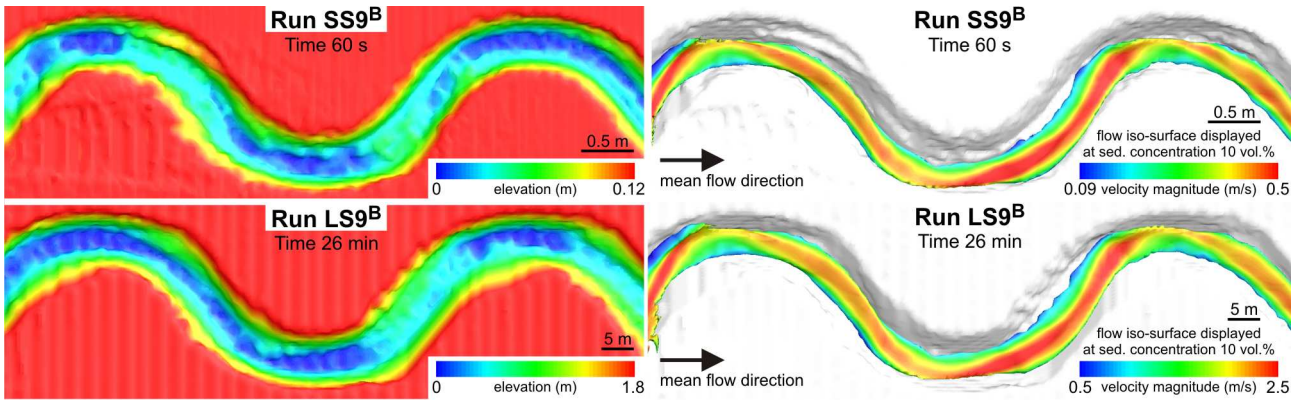


**Fig. 7.** The comparison between a small-scale and a large-scale simulation with similar system conditions (see Table 1). The location and geometry of the resulting deposits, as well as their size in relation to the channel and the velocity distribution of their formative flow, are very similar, indicating that the small-scale runs that have a large-scale equivalent are a good approximation of flow and deposition in natural channels.

describing fluid flow (Wesseling, 2001). The CFD software MassFlow-3D™ used in the present study is a customized version of the commercial software Flow-3D™, adopted by the Flow Science Inc. and Complex Flow Design A.S. to simulate sediment gravity flows including the transport, deposition and erosion of sediment by turbidity currents. The software was verified by replication of laboratory and natural flows (Heimsund, 2007; Heimsund et al., 2007), and was utilized in several recent studies (Heimsund, 2007; Hansen et al., 2008; Aas et al., 2010a, b; Basani et al., 2011).

MassFlow-3D™ simulates fluid motion by solving a 3D set of Navier–Stokes transient differential equations by a finite-volume, finite-difference method in a fixed Eulerian rectangular grid. The effects of flow turbulence are simulated by using the renormalization group (RNG) model with explicitly derived equation constants (Yakhot and Orszag, 1986). The RNG model is considered to be superior to the commonly used $k$-$\varepsilon$ model, as it more accurately describes flows with low-intensity turbulence and strong shear regions (Yakhot and Smith, 1992). The dispersion of mono- or poly-sized cohesionless sediment is treated as a continuous phase and its variable spatial volumetric concentration and density are calculated. Both bedload and suspension transport are considered. The bedload transport, simulated as the rolling and saltating motion of coarser particles along the bed, is predicted by using the models of Meyer-Peter and Müller (1948) and Rijn (1984). The transport equations for sediment in suspension account for advection, sediment drift and the effects of particle interaction. The drift (settling) velocity of suspended particles is approximated by a non-linear model, allowing a more precise account of coarser and faster-settling sediment. The interaction of particles in suspension (i.e., hindered settling, particle collisions, interlocking of grains) is accounted for by using the Richardson and Zaki (1954) correlation. Sediment entrainment (erosion) is calculated on the basis of the Mastbergen and Van den Berg (2003) model, in which the critical Shields parameter is predicted by using the Shields-Rouse equation (Guo, 2002). The critical Shields parameter is modified for inclined surfaces by integrating the angle of repose and is corrected for particle armouring effect by using the Egiazaroff formula (Kleinhans and Rijn, 2002).

The system initial topographic geometry is either constructed directly in the MassFlow-3D™ or imported as a stereolithographic file, and is processed for simulation by the FAVOR™ (fractional area-volume obstacle representation) software (Hirt and Sicilian, 1985). FAVOR™ determines the fractional areas of grid cell faces and the corresponding cell volumes that are exposed to flow. It thus defines the boundaries of objects independently of the grid design, avoiding stair-step boundaries and the use of body-fitted grids. The channel topographic surface used for both small- and large-scale simulations in the present study was produced with the 3D-modelling software Rhinoceros™ and imported into MassFlow-3D™ as a stereolithographic file.

### *5.2. The simulation setup*

The geometry of the flow inlet and the input channel in the CFD simulation setup was designed to imitate the laboratory experimental setup. However, the flume tank was enlarged to a width of 4 m and length of 15 m to accommodate a sinuous channel with greater wavelength and amplitude. As in the laboratory experiments, the digital channel substrate consisted of a packed (64 vol. %) fine-grained quartz sand. The simulation grid containing the input channel and flume tank had a pressure-specified upper boundary equal to the height of the flow expansion pipe that served as the input source. The whole geometric setup would then be enlarged by an arbitrary factor of 15 for upscaled simulations imitating natural deep-sea conditions at a scale of many ancient meander belts (Janocko and Nemec, 2011).

The pressure at the upper boundary was set to represent hydrostatic pressure at a water column of 1 m high in laboratory-scale simulations, but was increased to represent an arbitrary water-column height of 1000 m in natural-scale simulations. The simulation numerical grid had a total cell count of up to five millions, although the cell count varied with the inclination of the expansion table and input channel. As to the resolution, the cell x-y-z dimensions were 0.04 × 0.04 × 0.01 m in laboratory-scale simulations and 0.6 × 0.6 × 0.15 m in the upscaled simulations. The sediment-water mixture at the grid input boundary was defined by the inlet cross-sectional area, flow velocity, volumetric sediment concentration and the turbulent kinetic energy calculated on the basis of the mean input velocity. The grain size and density were the same as in the laboratory experiments, but the input sediment concentration was kept constant at 10 vol.%. All simulated flows were continuous without any breaks or surge-like behaviour. Three sizes of inlet cross-section were used (Fig. 3) in order to generate undersized, in-size and oversized flows.

### *5.3. The calibration of numerical model to laboratory experiments*

The MassFlow-3D™ software requires pre-setting of two flow parameters that cannot be directly measured in the laboratory, namely the flow entrainment coefficient and turbulence length scale. The entrainment coefficient specifies the sediment-particle lift velocity, or sediment flux from substrate erosion, whereas the turbulence length scale specifies

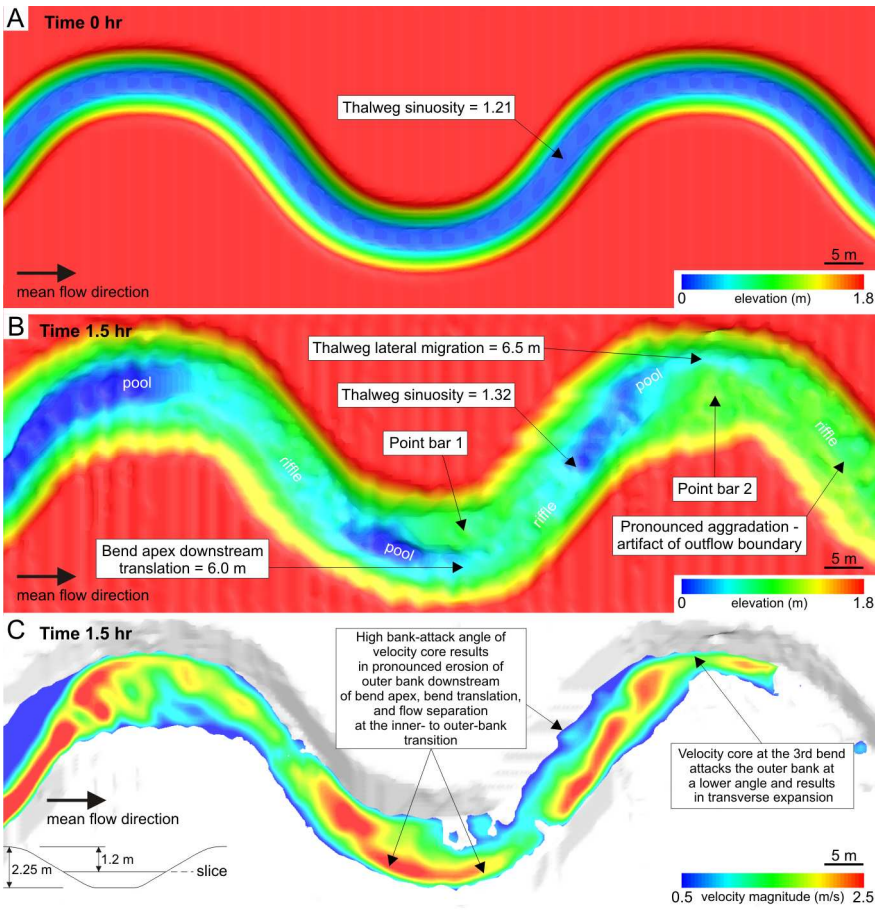


**Fig. 8.** Development of a meandering channel with point bars in simulation run LS6. (A) Topography map of the pre-defined channel form prior to experiment. The experimental surface has been rotated to horizontal. (B) Post-experiment topography map. (C) Flow velocity slice extracted 1.05 m above the channel floor.

the maximum size of eddies in the flow. For the simulations to be realistic, these parameters were estimated empirically on a qualitative trial-and-error basis by comparing the flow hydraulic structure, amount of erosion and thickness of deposit in the simulation experiment and its laboratory prototype.

The calibration of the numerical model to laboratory experiments was done in two steps. First, the entrainment coefficient and turbulence length scale were defined by using the laboratory run 8 (Table 2) as a reference. The criterion for comparison was the similarity of the flow velocity magnitude and the direction of flow-transverse velocity vector, as well as the amount of substrate erosion and the location of sediment depocentres (Fig. 5). Second, the flow simulation was performed to imitate the laboratory run 9 (Table 2) – involving somewhat different channel geometry and a slightly higher flow discharge – with a similar comparative assessment of the result. The comparisons show a satisfactory similarity between the laboratory and the CFD simulation results (Fig. 6), which suggests that the numerical model can be used to simulate realistically a wider range of experimental conditions.

### *5.4. Upscaling of numerical model*

Due to the scarcity of flow measurements from prototype natural channels, laboratory experiments are either non-scaled or scaled on the basis of the dimensionless Froude number (e.g., Keevil et al., 2006; Peakall et al., 2007; Islam et al., 2008; Kane et al., 2008; Straub et al., 2008). The experiments have managed to reproduce to some extent the flow characteristics and depositional features of natural channels, although the parameters of laboratory models – such as sediment grain size, turbulence intensity, critical shear stress for sediment motion and slope gradient – are expected to differ considerably from prototype conditions (Postma et al., 2008). However, it is these parameters and their combination that may play a crucial role in such complex systems as the turbidity-current flow in meandering channels.

An upscaling of laboratory experiments by using numerical formulae such as the Froude number in combination with a simple geometrical scaling is thus unlikely to represent the flow and depositional processes at a natural scale. Instead of attempting to upscale numerically the physical parameters of laboratory flows, the focus in the present study was therefore to reproduce the spatial characteristics of flow behaviour and sedimentation pattern. On a trial-and-error basis, the input flow parameters in the upscaled simulations were conditioned by comparing the resulting spatial pattern of erosion and deposition with the topographic changes observed in the corresponding laboratory runs. As a rule, the small-scale and upscaled simulations that resulted in similar topographic changes did also result in similar flow pattern (Fig. 7). The sediment entrainment coefficient and turbulence length scale established for the upscaled simulations of laboratory experiments were used further in the large-scale simulations that did not have small-scale laboratory or numerical equivalents (simulation runs LS1, LS2, LS4−LS6, LS8 and LS10 in Table 1).

Apart from a simple enlargement of the channel and tank geometry, the input parameters that required adjustment in the upscaling process were the slope inclination, flow velocity, turbulence length scale and simulation time. Satisfactory results were obtained when the slope inclination was reduced by 0.5,

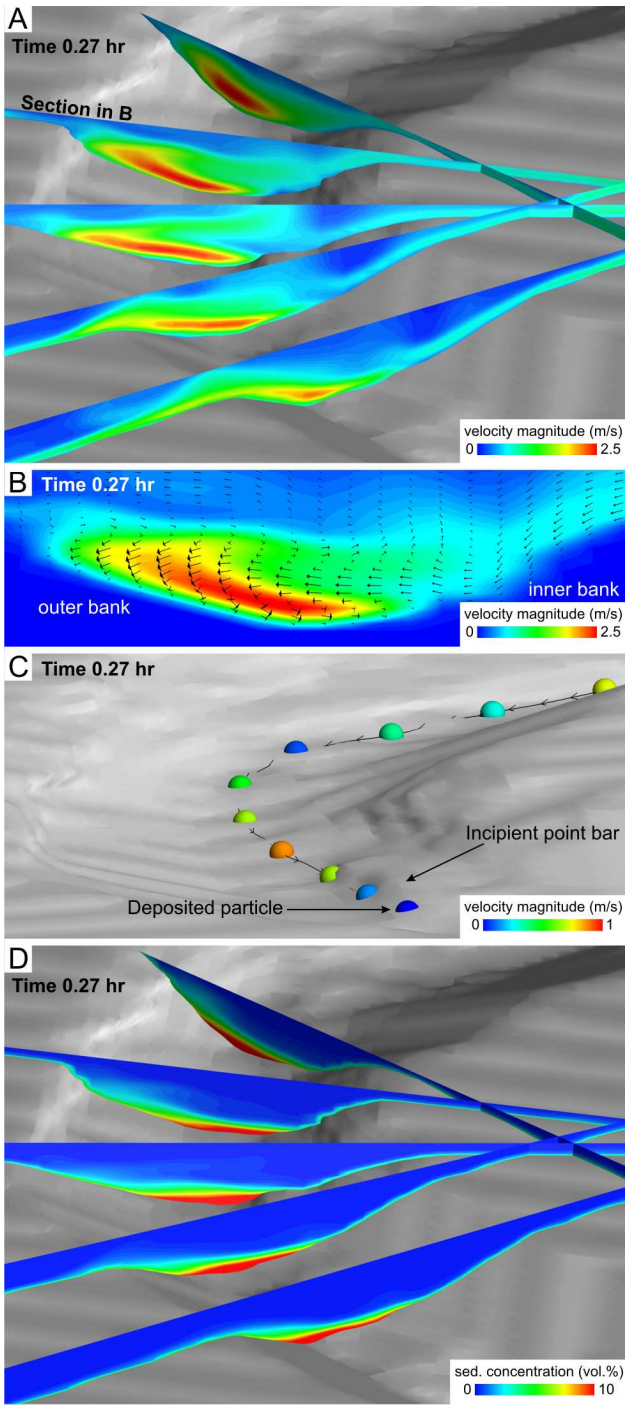


**Fig. 9.** Flow properties and point bar formation at the 2nd bend in simulation run LS6. (A) Profiles of velocity magnitude showing the turbidity current travelling superelevated on the outer-bank. Flow is towards the viewer. (B) Profile across the channel bend displaying a colour map of velocity magnitude overlain by 3D velocity vectors. Note the inward-directed helicoidal cell in which the basal flow decelerates upon meeting the inner bank. Also note the developing point bar at the toe of the inner bank. Flow is towards the viewer. Location of the profile is displayed in (A). (C) Simulated transport path of a single fine-grained quartz particle. The (not-to-scale) particle markers are coloured with velocity magnitude. Note the particle travels along the channel floor from the thalweg towards the point bar where it decelerates due to up-bank climbing and is subsequently deposited. (D) Sediment concentration profiles showing the undersized current travelling around the 2nd bend. Note that the density core passes from outer towards the inner bank upstream of bend apex and hugs the inner bank where the point bar forms. Also note that the thickness of the developing point bar equals the thickness of the flow. Flow is towards the viewer.

the flow velocity at inlet was increased 3 to 4 times, and the turbulence length scale was increased by a factor of 15. To match the size of deposits and the amount of erosion with respect to laboratory channels, the simulation time had to be increased by a factor of 12 to 60, depending on the flow capacity. The grain size and volumetric concentration of sediment were kept constant.

## 6. The results of CFD simulations

Systematic numerical variation of the critical flow/channel relationships (see system conditions in Fig. 1) resulted in a wide spectrum of sedimentation patterns in the channel (Table 1). The present section gives detailed description of the simulation runs in which the intra-channel deposits might qualify as channel bars. The description focuses on the individual varieties of bars (see terminology in Fig. 2), shedding light on the hydraulic circumstances of their formation. Although the same type of bar often formed under different combinations of flow conditions, the hydraulic circumstances of bar formation were similar and are characterized on the basis of a representative case.

### *6.1. The formation of point bars*

A lateral migration of channel and formation of point bars occurred when the turbidity currents were in equilibrium with the channel slope and in phase with the channel curvature, and were in-size or moderately undersized with respect to the channel depth (Table 1). Such conditions were reached in the large-scale simulations LS1 and LS6, where the slope inclination was 3°, the flow velocity at the inlet was 2 m/s and the flow inlet cross-sectional area was between ½ and 2 of the channel cross-section (resulting in discharges in the range of 33,410–255,100 $m^3$/hr). No analogous conditions could be reached in the laboratory, where it was impossible to produce flows that would simultaneously be in slope-equilibrium and in-phase state. The flow in simulation run LS1 was in size with the channel and in run LS6 was undersized, but the flow pattern and channel evolution were similar and are described from the latter run.

Over a period of 1.51 hour, the channel sinuosity increased from 1.21 to 1.32 as a result of the lateral migration of the channel at its 2nd and 3rd bend by outer-bank erosion and a lateral accretion of sediment at the inner bank (Fig. 8A, B). Before the lateral migration occurred (first ~5 minutes), the channel assumed an asymmetrical erosional profile at the bends, with a steeper outer bank and a gentler-inclined inner bank. After 1.51 hour, the apex of the 2nd bend in the channel thalweg was displaced by 6 m in the downslope direction, while the channel thalweg at the 3rd bend migrated by 6.5 m sideways due to transverse expansion. The channel also developed a riffle and pool morphology similar to meandering rivers (Fig. 8B). The differential planform development of the two adjacent bends is attributed to a dissimilar bank-attack angle (*sensu* Straub et al., 2011) and the velocity magnitude of the flow core. The flow velocity core approached the 2nd bend at a low angle and met the outer bank directly upstream of the bend apex, from which point it travelled superelevated along the outer bank until reaching the bend inflection point (Figs. 8C and 9A). In the bend down-apex zone, the velocity core experienced the highest outer-bank run-up, which corresponded to the maximum of outer-bank erosion. At the 3rd bend, the flow velocity core approached the outer bank at a higher angle and farther upstream of the apex, resulting in the maximum bank run-up and erosion in the bend apex zone and subsequently detaching itself from the outer bank upstream of the bend inflection point (Fig. 8C). The flow density (sediment concentration) core, in

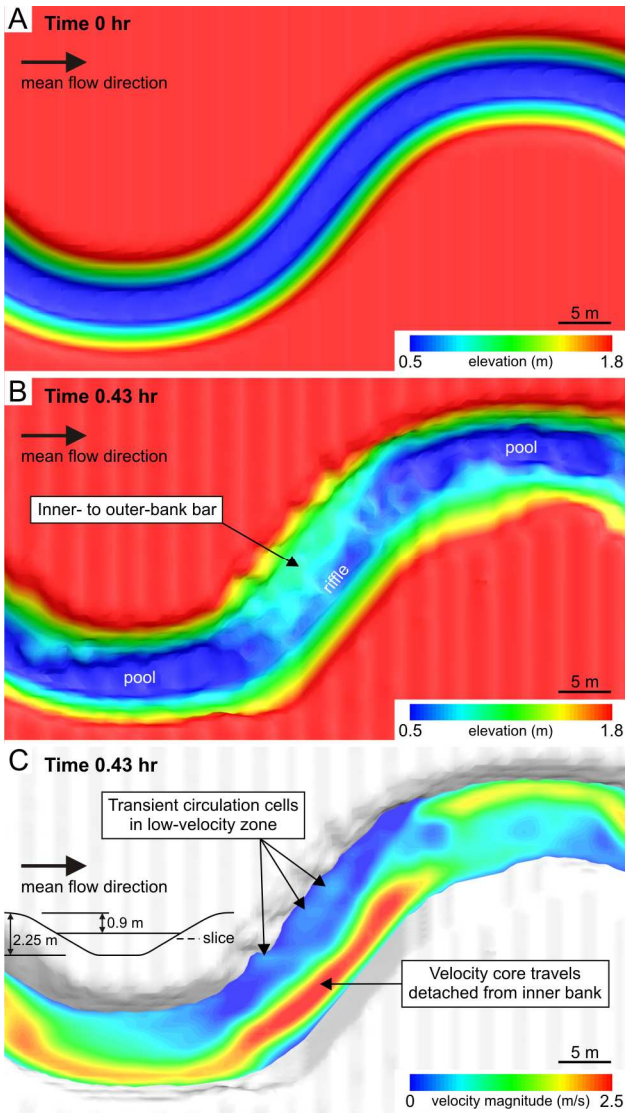


**Fig. 10.** Development of an inner- to outer-bank transition bar in simulation run LS9$^{B}$. (A) Topography map of the pre-defined channel form prior to experiment. Detail of inflection between the 2$^{nd}$ and the 3$^{rd}$ bend. The experimental surface has been rotated to horizontal. (B) Post-experiment topography map. (C) Flow velocity slice extracted 1.35 m above the channel floor.

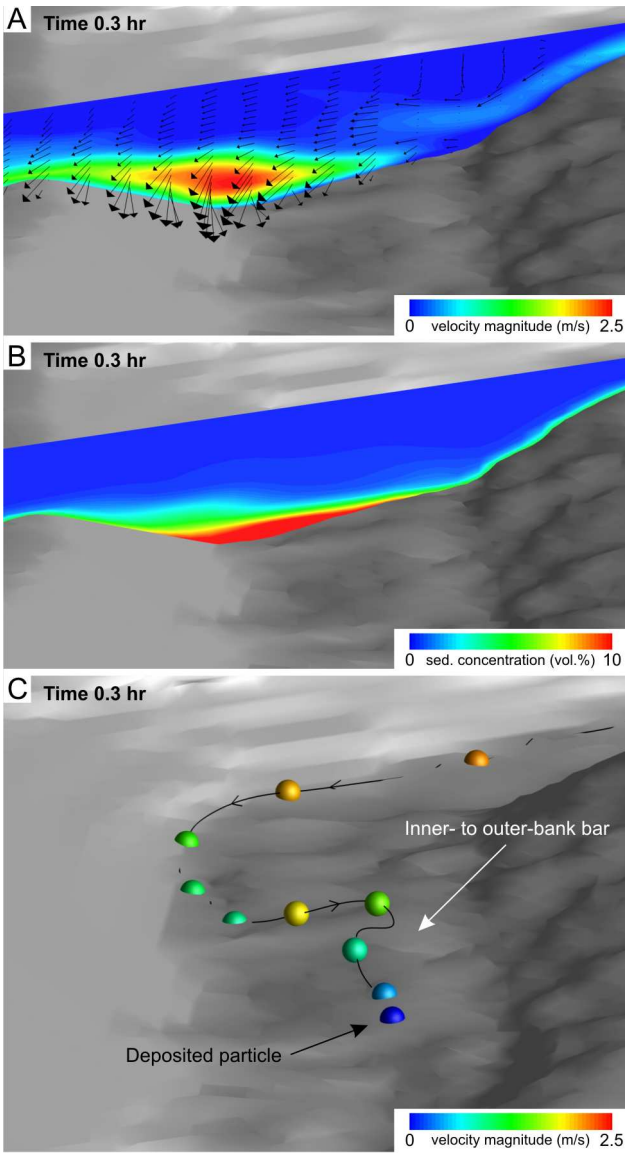


**Fig. 11.** Flow properties and deposition at the inflection between the 2$^{nd}$ and the 3$^{rd}$ bend in simulation run LS9$^{B}$. (A) Profile across the channel showing a colour map of velocity magnitude overlain by 3D velocity vectors. The velocity core travels superelevated on the downslope bank and shows an inward-directed helicoid with basal flow in the thalweg directed towards the upslope bank. Flow is towards the viewer. (B) Sediment concentration profile showing the undersized current. Note the thickness of the bar is equal to the thickness of the flow. (C) Simulated transport path of a single fine-grained quartz particle. The (not-to-scale) particle markers are coloured with velocity magnitude. Note the particle travels along the floor of the channel from the downslope bank towards the transition bar where it is lifted up and deposited in the low-velocity zone.

contrast, travelled attached to the outer bank at each bend and was crossing over to the inner bank upstream of the bend apex (Fig. 9D).

The helicoidal circulation of the rotating flow at the channel bends involved an inward-directed cell (Fig. 9B). The flow rotation was most pronounced in the upstream part of the bends and gradually weakened down channel before reversing its direction at the bend inflection points.

Point bars formed as a result of the inward helicoidal circulation and the path of the flow velocity core, which in turn affected the path of the density core (Fig. 9). Sediment tended to be transferred along the channel floor towards the inner bank by the inward-directed flow helicoid, resulting in inner-bank accretion by the climbing and decelerating flow (Fig. 9C).

The thickness of point bars in run LS6 was lower than the channel depth, but equal to the undersized flow thickness (Fig. 9D). In run LS1, the in-size flow produced point bars of similar thickness, apparently because of its greater spill-out and loss of volume. The channel in this case developed a less asymmetrical profile, but the extent of its lateral migration and the spatial distribution of flow velocity and density were similar.

### *6.2. The formation of inner- to outer-bank transition bars*

Apart from deposition at other sites in the channel, the accumulation of sediment at the inner- to outer-bank transition – on the upslope sides of bend inflection zones (Fig. 2) – occurred when the turbidity currents were in equilibrium with the channel slope and slightly exceeding the phase of the channel curvature. These inflection-zone bars formed either as a downstream extension of translational point bars (Fig. 8B) or as a self-standing depocentre on the upslope side of the channel-bend inflection zone, whether solitary or accompanied by the formation of down-apex outer-bank bars (Fig. 7). Changes in flow thickness appeared to play no significant role. All these bars were lower than the channel depth and typically also lower

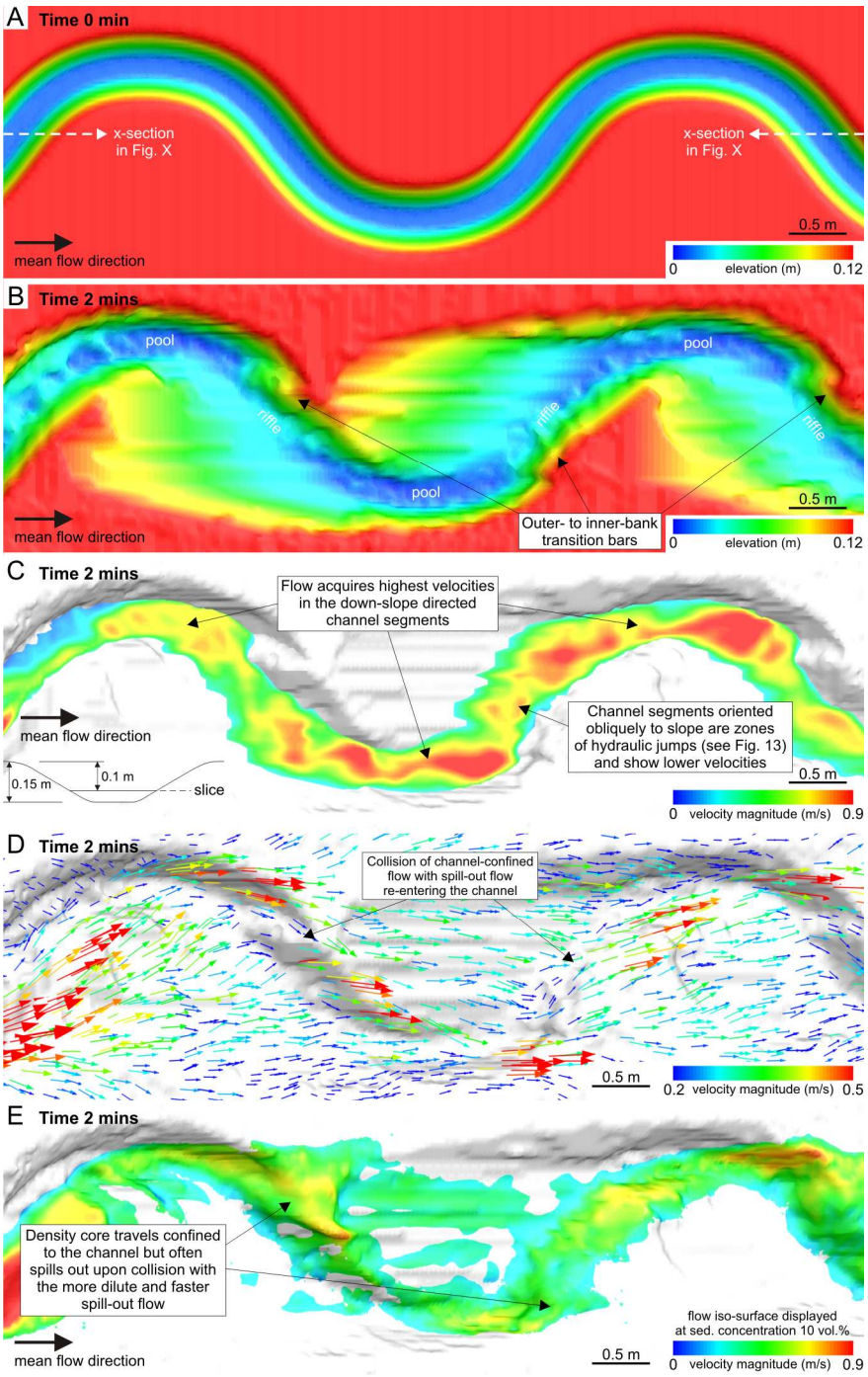


**Fig. 12.** Development of outer- to inner-bank transition bars in simulation run SS3$^{A}$. (A) Topography map of the pre-defined channel form prior to experiment. The experimental surface has been rotated to horizontal. (B) Post-experiment topography map. (C) Flow velocity slice extracted 5 cm above the channel floor. (D) Near-bottom velocity vectors coloured with velocity magnitude. (E) Flow iso-surface displayed at sediment concentration 10 vol.% coloured with velocity magnitude.

than the other bars.

Bars of this type formed in simulations LS1, LS3$^{B}$, LS5, LS6, SS9$^{B}$, LS9$^{B}$, SS13$^{A}$, LS15$^{A}$ and SS17$^{A}$ (Table 1), and the hydraulic conditions of their formation can be characterized on the basis of simulation run LS9$^{B}$ (Figs. 10 and 11). The slope inclination in this run was set to 3°, the inlet/channel cross-section ratio was ½, the input flow velocity was 3 m/s (discharge 71,710 m$^{3}$/hr) and the simulation time required for the formation of distinct bars was 6 minutes. The bars formed in the bend inflection segment between the 2$^{nd}$ and the 3$^{rd}$ bend (Fig. 10A, B), where the superelevated flow-velocity core was hugging the outer- to inner-bank transition, while leaving a low-velocity zone along the opposite bank (Figs. 10C and 11A). The low-velocity zone involved two to four smaller, transient circulation cells that migrated obliquely against the bank and tended to be perturbed by the low-density spill-out flow that was re-entering the channel at the bend inflection and enhancing turbulence there (Fig. 10C). Unlike the velocity core, the flow density core remained attached to the inner- to outer-bank transition, causing sediment deposition (Fig. 11B).

All flows depositing sediment at the inner- to outer-bank transition showed a local inward-directed rotational helicoid (Fig. 10C, F). The turn-over site of the flow helicoid in the bend-inflection zone oscillated, affecting the downstream extent of the bars. Flows that were only slightly out of phase with the channel curvature showed their helicoid reversal shortly

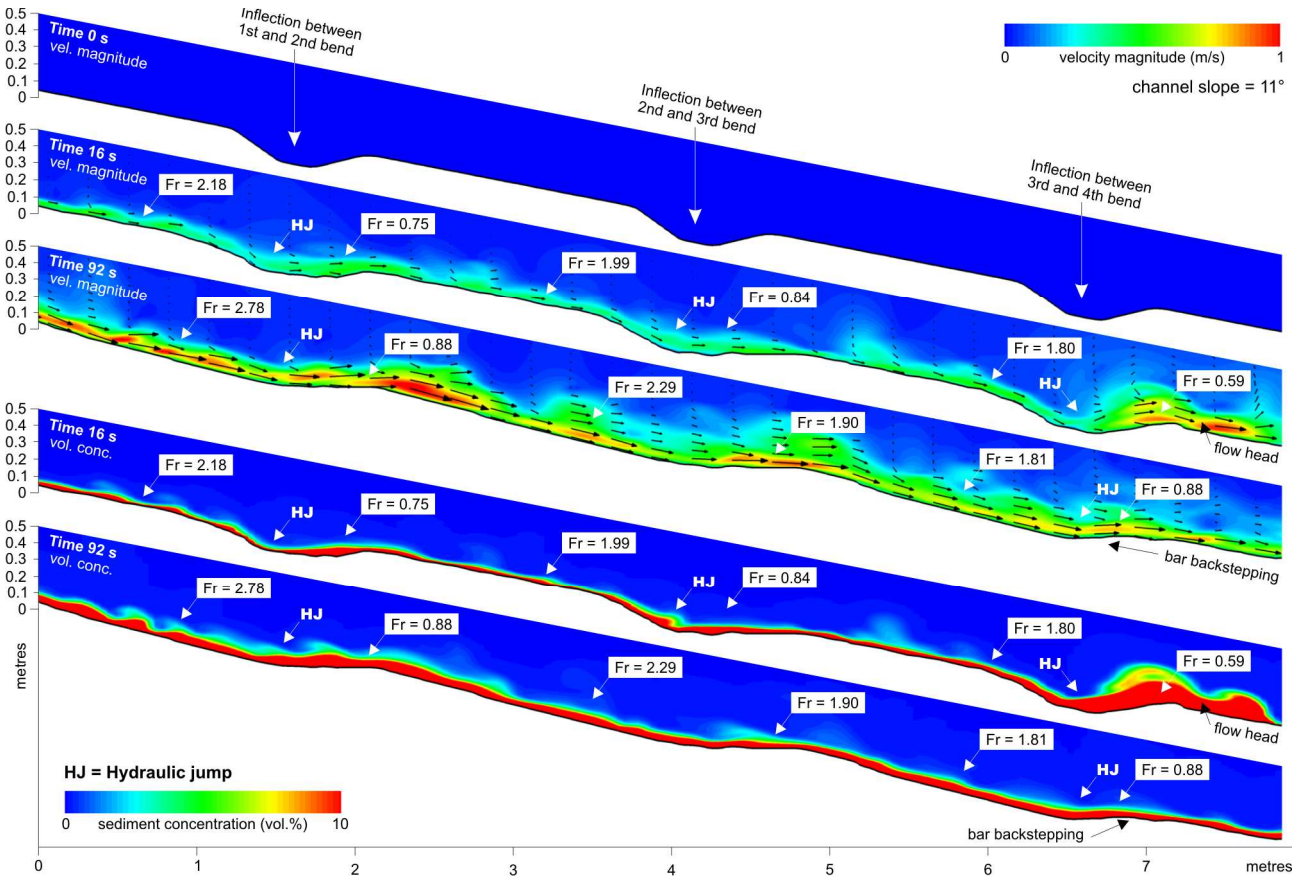


**Fig. 13.** Velocity and sediment concentration profiles along the channel belt in simulation run SS3$^{A}$ showing the generation of hydraulic jumps at bend inflection zones. Location of cross-section is displayed in Fig. 12A.

downstream of the bend inflection point, whereas flows with a greater phase offset had the helicoid reversal delayed – occurring directly upstream of the next bend apex, where the flow velocity core was crossing over from the inner to the outer bank (Fig. 10C). The inward-directed flow helicoid at a channel bend was transporting sediment along the channel floor into the low-velocity zone where the sediment was incorporated in the transient circulation cells colliding with the upslope bank of the channel's bend-inflection segment. The sediment was apparently dumped from the dissipating turbulent eddies, forming the bars (Fig. 11C). The bars showed slight lateral accretion, owing to the re-entering spill-out flow that tended to sweep sediment from the bar towards the channel thalweg (Fig. 11A).

### *6.3. The formation of outer- to inner-bank transition bars*

Sediment deposition at the outer- to inner-bank transition of bend inflection zones – on the upslope sides of channel inflection segments (Fig. 2) – occurred when the turbidity currents were at equilibrium with the channel slope, but the phase of their rotation helicoid considerably exceeded the conduit's curvature. The flow was poorly confined and travelled down slope across the channel bends, while eroding the up-slope bank of the channel bend-inflection segment (Table 1, Fig. 12A, B). Changes in flow thickness played no significant role in the pattern of flow and sediment deposition.

Bars of this type formed in both small-scale (runs SS3$^{A}$ and SS9$^{A}$) and large-scale simulations (run LS7$^{A}$). The favourable conditions in small-scale runs were reached with a slope inclination of 11°, the inlet cross-section to channel cross-section ratio between ½ and 2, and the flow input velocity of 1 m/s (discharge 72−785 m$^3$/hr). The simulation time required was less than 2 minutes. In large-scale simulation, similar deposits formed in a run with the slope inclination of 6°, the inlet/channel cross-section ratio of 3.5, the flow input velocity of 3 m/s (discharge 856,800 m$^3$/hr) and a simulation time of 0.33 hour. The pattern of flow and sediment deposition was similar, and thus only one example, run SS3$^{A}$, is described here.

The turbidity current in this small-scale simulation was an in-size flow, by was poorly confined by the channel due to the relatively high input discharge and steep slope (Fig. 12C−E). When entering the 1$^{st}$ bend, the flow split in two parts due to its spill-out at the outer bank. The channel-confined, higher-density part of the flow decreased its velocity by half, while the velocity of its more dilute spill-out part remained unchanged. A new spill-out of the confined flow at the next bends was instigated by the re-entry of the earlier spill-out flow (Fig. 12E). The flow pattern at channel bends showed a poorly-developed helicoid with the basal flow directed down-channel (Fig. 12D) and the top flow directed orthogonally towards the outer bank. The helicoid was limited to the flow density core, with sediment concentration of 10–15 vol. %, and was discontinued in the bend's down-apex zone by the channelized-flow collision with the re-entering spill-out flow. The spill-out flow, owing to its higher velocity, travelled down slope across the channel bends and extended laterally over the whole width of the channel belt (Fig. 12E). The flow was subject to a hydraulic jump when crossing the bend inflection zones, which was manifested by its abrupt local deceleration with an increase in flow thickness (Fig. 13).

These bank-attached bars, formed at the outer- to inner-bank transition in channel-bend inflection zones, were thickest at the bends where the channel-confined flow collided with the re-entering spill-out flow travelling down the slope (Fig. 12B, D, E). The amount of sediment accreted to the bank declined gradually downstream of the bend inflection point. The

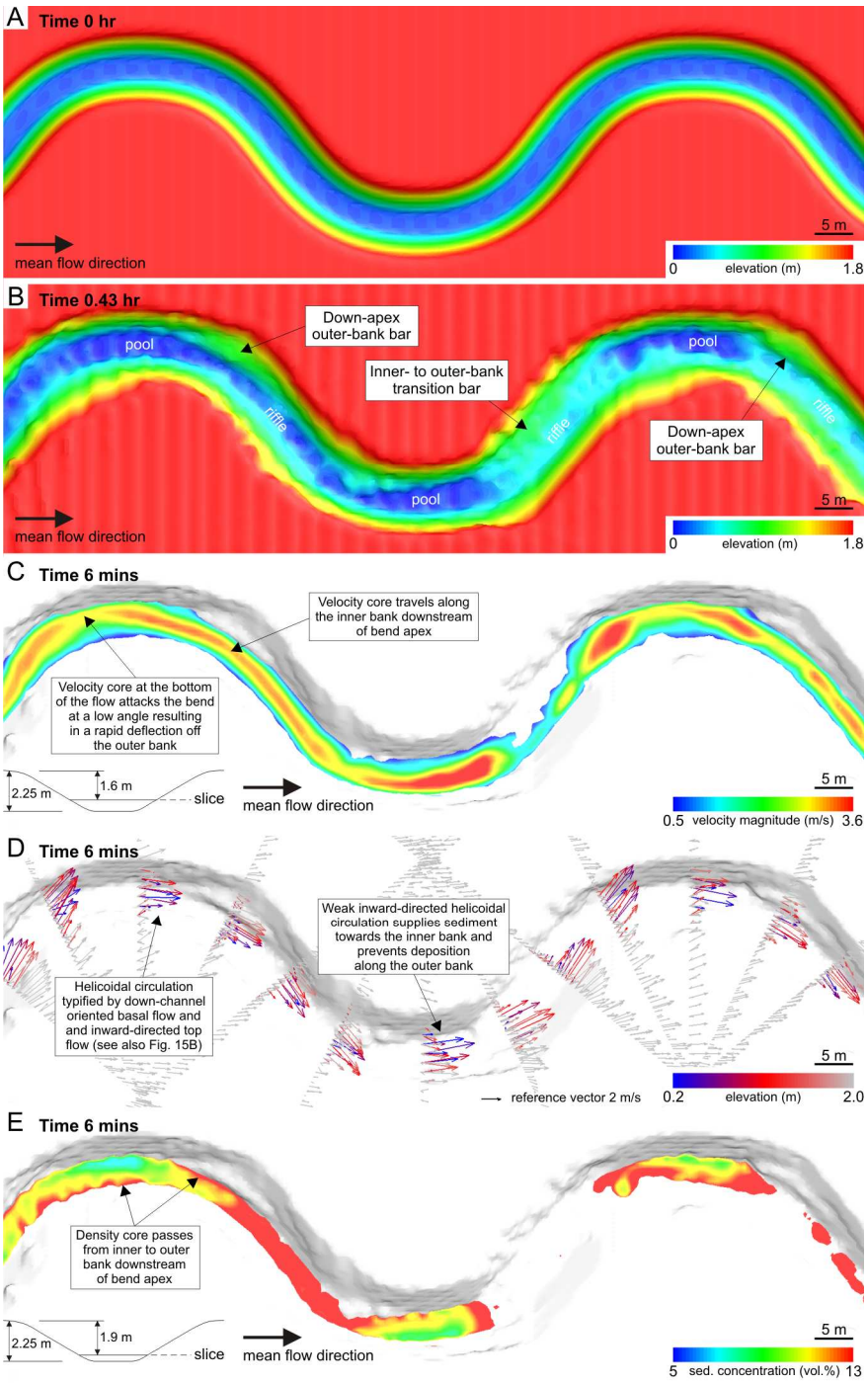


**Fig. 14.** Development of down-apex outer-bank bars in simulation run LS9$^{B}$. (A) Topography map of the pre-defined channel form prior to experiment. The experimental surface has been rotated to horizontal. (B) Post-experiment topography map. (C) Flow velocity slice extracted 0.65 cm above the channel floor. (D) Channel cross-sections showing velocity vectors coloured by elevation. (E) Flow slice extracted 0.35 cm above the channel floor showing sediment concentration.

sediment was delivered chiefly by the channel-confined denser flow, but its deposition was instigated by the flow's collision with the overbank low-density flow re-entering the channel in its bend inflection zone and experiencing local hydraulic jump. The sediment dropped by flow in the collision zone tended to be swept downstream, resulting in a more pronounced bar growth in that direction.

### *6.4. The formation of down-apex outer-bank bars*

These outer-bank bars, deposited directly downstream of the channel-bend apex (Fig. 2), were formed under a wide range of flow conditions in both small- and large-scale simulations. The main prerequisite for their formation seems to be a high-velocity turbidity current whose intrinsic flow helicoid exceeds the phase of pre-existing channel curvature and cannot cause meandering, but whose volume is insufficient to cause an excessive spill-out and storage of sediment in the bend inflection zones. The flow thickness and slope gradient did not seem to affect the location of the sediment depocentres, but had an effect on the resulting bar thickness and accretion architecture.

The flow in the simulation runs SS7$^{B}$, SS9$^{B}$, LS3$^{B}$ and LS9$^{B}$ (Table 1) was in equilibrium with the channel slope and produced such bars by a lateral accretion of sediment at the 1$^{st}$

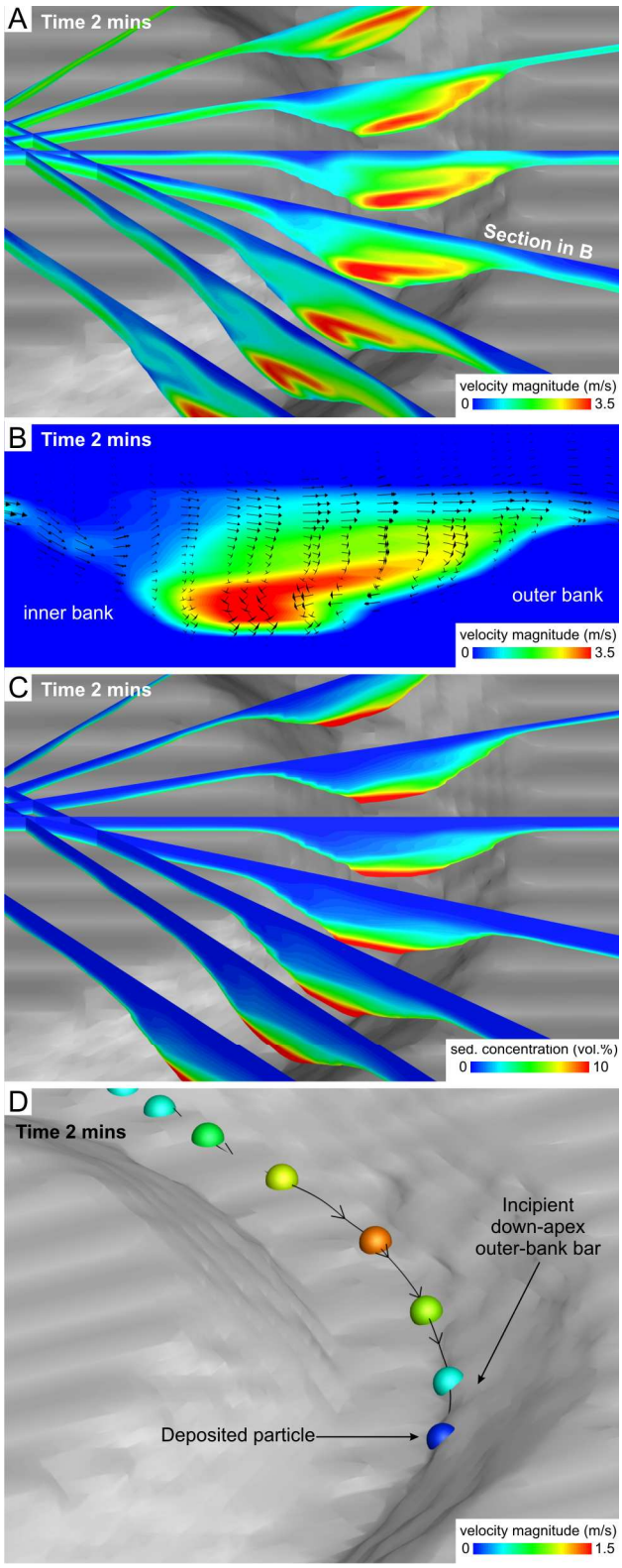


**Fig. 15.** Flow properties and deposition of down-apex outer-bank bar at the 1st bend in simulation run LS9B. (A) Profiles of velocity magnitude showing the splitting of the velocity core into two parts. The lower part of the core, that governs deposition at outer bank, bounces off the outer bank and travels further by hugging the inner bank. Flow is towards the viewer. (B) Profile across the channel bend displaying a colour map of velocity magnitude overlain by 3D velocity vectors. Note the weak outward-directed helicoidal cell. Also note the developing bar at the toe of the outer bank. Flow is towards the viewer. Location of the profile is displayed in (A). (C) Sediment concentration profiles showing the undersized current travelling around the 1st bend. Note that the superelevation of the density core passes from the inner towards the outer bank dowstream of the bend apex. Also note that the thickness of the developing bar is roughly ½ the thickness of the flow. Flow is towards the viewer. (D) Simulated transport path of a single fine-grained quartz particle. The (not-to-scale) particle markers are coloured with velocity magnitude. Note the particle travels along the channel floor from the thalweg towards the outer bank where it decelerates due to up-bank transport and is subsequently deposited.

and the 3rd bend. In the small-scale simulations, the favourable conditions for the formation of these bars were reached with a slope inclination of 6°, the inlet/channel cross-section ratio of ½ to 3½, the input flow velocity of 0.5 m/s (discharges of 36−635 $m^3$/hr) and a simulation time of 1 minute. In the large-scale simulations, the appropriate slope inclination was 3°, the flow velocity at the inlet was 3 m/s (discharges of 71,710−382,600 $m^3$/hr) and the simulation time required for the formation of analogous bars was 6 minutes. The flow thickness controlled to some extent the bar thickness, but the latter had never reached the top of the channel. The bars varied in their thicknesses, but all were considerably lower than the channel depth.

The flow pattern in the large-scale run LS9B can serve as an example of the flow conditions needed for the formation of down-apex outer-bank bars (Fig. 14). Prior to the development of these bars, the turbidity current flowed well-confined by the channel with only minor spill-out at the bend outer bank. The outer-bank bars formed at the 1st and the 3rd bend (Fig. 14A, B), where the flow velocity core approached the outer bank at a low angle (Fig. 14C) and split itself into two parts upon meeting the bank (Fig. 15A). The higher-density lower part of the flow core bounced off the outer bank before reaching the bend apex and travelled further by hugging the inner bank (Figs. 14C and 15A). The lower-density upper part of the flow core travelled superelevated against the outer bank, losing momentum due to partial overspill. The lower and the upper part of the flow were rejoining each other at the bend inflection points.

Velocity vectors show that the channel-confined flow at the bends comprised a weak outward-directed rotational cell transporting sediment along the channel floor towards the outer bank (Figs. 14D and 15B). The flow density core entered the channel bend superelevated against the inner bank and crossed over to the outer bank downstream of the bend apex (Figs. 14E and 15C). The outer-bank bars thus formed because the helicoid cell was delivering sediment to the outer bank, where the sediment was laterally accreted by the decelerating, up-bank directed flow (Fig. 15D). The velocity of the channel-confined flow became subsequently reduced due to an increased spill-out at its entry to the 1st and 2nd bend, accompanied by the outer-bank erosion. The helicoidal flow circulation at the 1st and 3rd bend was consequently weakened and the rate of sediment accretion at the outer bank declined, although the flow pattern remained unchanged. The bars ceased to grow after ~26 minutes, when the flow began to bypass its sediment load.

Similar outer-bank bars formed by the aggradational flows in runs SS13A, LS15A and SS17A (Table 1). The bars first were relatively thin, compared to the channel depth, but had subsequently aggraded to the height of the levée crest. They formed during the first minute at the 1st and 3rd bend in run SS17A, with the slope inclination of 4°, the inlet/channel cross-section ratio of ½ and the input flow velocity of 1 m/s (discharge 72 $m^3$/hr). As in the large-scale simulation LS9B, the flow velocity core approached the 1st bend at a relatively low angle, but the flow had a lower velocity and – instead of undergoing a rapid deflection towards the inner bank – passed the entire bend superelevated against the outer bank. As an effect of the superelevation, the flow stretched laterally by increasing its width and decreasing its thickness. The flow velocity core travelled along the toe of the outer bank, showing an outward-directed helicoidal circulation. At the bend apex, the elevated upper part of the flow travelling along the outer bank

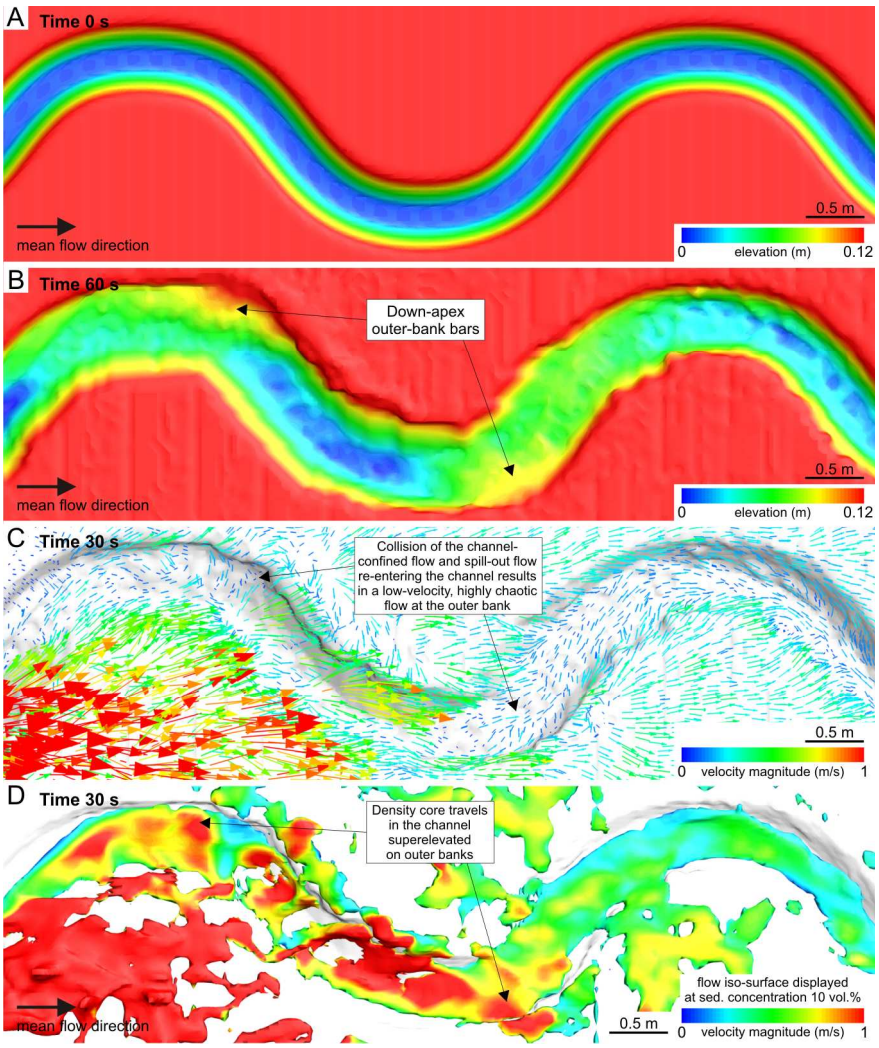


**Fig. 16.** Development of down-apex outer-bank bars in simulation run SS17$^{A}$. (A) Topography map of the pre-defined channel form prior to experiment. The experimental surface has been rotated to horizontal. (B) Post-experiment topography map. (C) Near-bottom velocity vectors coloured with velocity magnitude. (E) Flow iso-surface displayed at sediment concentration 10 vol.% coloured with velocity magnitude.

decelerated to a point at which it began to collapse in itself and descend the bank, thus forming a secondary, inward-directed circulation cell. Outer-bank bars began forming where the bank-descending fluid met the flow velocity core. This confluence caused local deceleration of the current and deposition of sediment, which was transported along the channel floor towards the outer bank by the primary, outward-directed flow helicoid.

At a simulation time of 0.5 minute, the bars ceased expanding laterally and began to aggrade together with the channel floor until they reached the height of the levée crest in the next 0.5 minute. Longer simulation times resulted in channel backfilling.

Another variety of outer-bank bars was observed forming in the simulation runs SS13$^{B}$, SS15$^{B}$, SS17$^{B}$ and LS17$^{B}$ under aggradational slope conditions (Fig. 16A, B; Table 1). The thicknesses of these bars were comparable to the channel depth and did not vary significantly with the flow thickness. The hydraulic conditions of their formation are illustrated here from the small-scale run SS17$^{A}$. The slope inclination in this case was 1°, the inlet/channel cross-section ratio was 1, the input flow velocity was 5 m/s (discharge 1,962 m$^{3}$/hr) and the simulation time was 1 minute. The rotational helicoid of the fast flow had a phase considerably greater than the channel curvature, and thereby the majority of the flow spilled out when entering the 1$^{st}$ bend (Fig. 16C & D). As a result, the flow remaining in the channel decreased in thickness to ¼ and decelerated to 1 m/s, while its sediment concentration increased to 15 vol.%. The flow passed the 1$^{st}$ bend with an inward-directed circulation helicoid (Fig. 17A). The more voluminous, low-density spill-out flow also rapidly decelerated, spreading across the point bar in a radial manner while moving towards the inflection zone of the 1$^{st}$ and the 2$^{nd}$ bend (Fig. 16C). The spill-out flow re-entered the channel in the down-apex zone of the 1$^{st}$ bend, pushing the channel-conveyed flow towards the outer bank and partly out of the channel (Fig. 17A). The collision resulted in a low-velocity flow zone with secondary circulation cells migrating against the outer bank. An outer-bank bar formed in this zone by sediment dumping from the collapsing dissipative cells. The spill-out flow collided again with the channel-conveyed flow at the 2$^{nd}$ bend after being obliquely deflected from the inner towards the outer bank (Fig. 16C). Sediment was thus deposited at the outer bank in the same manner as in the 1$^{st}$ bend.

Simulation times longer than 1 minute in runs SS13$^{A}$, SS15$^{A}$ and SS17$^{A}$, and longer than 30 minutes in run LS17$^{A}$, resulted in a progressive backfilling of the channel and deposition of thick levées next to the outer-bank bars.

### *6.5. The formation of up-apex outer-bank bars*

Deposits that might also qualify as outer-bank bars were formed in the up-apex zone of channel bends in the simulation

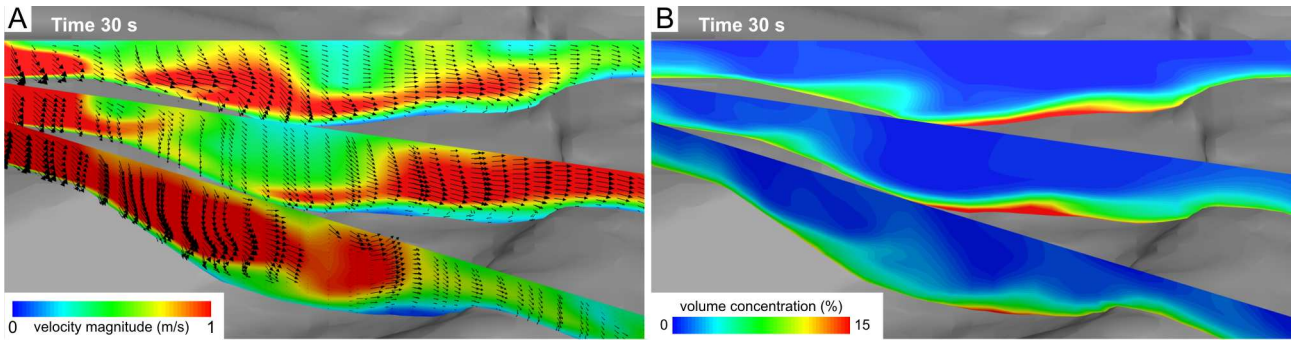


**Fig. 17.** Velocity magnitude (A) and sediment concentration (B) profiles illustrating the formation of down-apex outer-bank bars in simulation run SS17$^{A}$. The profiles show how the spill-out flow re-entering the channel pushes the high-density channel-confined flow towards the outer bank where it decelerates and deposits sediment. The high-density channelized flow travelling at the toe of the outer bank shows a weak inward-directed helicoidal circulation.

runs SS13$^{C}$, SS14, SS15$^{C}$, LS15$^{C}$ and SS17$^{C}$. The bars grew and thickened obliquely across the channel, from the inner bank at a bend inflection to the outer bank upstream of the next bend apex. They formed regardless of the thickness by the slope-aggrading flows, provided that their velocity was either high enough to generate a flow-helicoid phase significantly exceeding that of the pre-existing channel curvature or a flow-helicoid phase smaller than that of the channel. (Table 1). The hydraulic conditions of their formation are explained here on the basis of runs SS13$^{C}$ and LS15$^{C}$ (Fig. 18).

In the small-scale run SS13$^{C}$, the slope inclination was 1°, the input flow velocity was 2 m/s, the inlet/channel cross-section ratio was 1.5 (discharge 785 m$^3$/hr) and the simulation time needed for the development of bars was 0.5 minute. In the large-scale run LS15$^{C}$, the slope inclination was 0.5°, the input flow velocity was 6 m/s, the inlet/channel cross-section ratio was 3.5 (discharge 171,3000 m$^3$/hr) and the simulation time was 6 minutes. These simulations thus involved flows with a considerably lower velocity than that of the flows that produced the down-apex outer-bank bars in simulations SS13$^{B}$, SS15$^{B}$, SS17$^{B}$ and LS17$^{B}$ (see previous section).

The up-apex outer-bank bars formed at the channel 2$^{nd}$ bend in simulation SS13$^{C}$ (Fig. 18A) and at the 3$^{rd}$ and 4$^{th}$ bends in simulation LS15$^{C}$ (Fig. 18B). The formation of the bars was instigated by a collision of the higher-density, lower-velocity channel-conveyed flow with the lower-density, higher-velocity spill-out flow re-entering the channel (Fig. 18C, D). Their confluence resulted in a cross-channel low-velocity flow zone with secondary circulation cells moving and dissipating against the outer bank. The sediment deposited there was delivered by the channel-conveyed part of the flow. The sediment, after being incorporated in the collision-zone circulation cell, was carried in dense turbulent suspension towards the outer bank and dumped there from the dissipating eddies (Fig. 18E, F).

A prerequisite for the formation of these bars was apparently a comparable magnitude of the channel-conveyed and the spill-out flow, making the two flows collapse upon their collision. If the power of the spill-out flow is considerably greater, this part of flow tends to be deflected towards the down-slope bank of inflection zone and may even force the channel-confined flow out of the channel, whereby sediment deposition occurs in the down-apex zone of the outer bank (as seen in the simulation runs SS13$^{B}$, SS15$^{B}$, SS17$^{B}$ and LS17$^{B}$, Fig. 16 & 17; and runs SS3$^{A}$, SS9$^{A}$ and LS7$^{A}$, Fig. 12). If the spill-out flow instead is too weak, the channel-conveyed flow will not be decelerated enough to deposit its load. In the present simulated cases (SS13$^{C}$, SS14, SS15$^{C}$, LS15$^{C}$ and SS17$^{C}$), the channel-conveyed flow had a low power and hence was easily halted by collision with the spill-out flow. This localized deceleration resulted in vertical accretion of sediment directly downstream of the up-apex outer-bank bars (Fig. 18A, B) and eventually led to a gradual backfilling of the channel.

## 7. Discussion

### *7.1. The factors governing sedimentation in submarine sinuous channels*

The diversity of sediment depocentres in erodible sinuous channels revealed by the laboratory experiments and numerical simulations supports the notion that the crucial factors controlling the sediment deposition pattern in submarine sinuous channels are (Fig. 1): (1) the relationship between the flow's desired equilibrium gradient and the pre-existing channel gradient; (2) the relationship between the flow's intrinsic helicoid curvature and the pre-existing channel curvature; (3) the relationship between the flow size (magnitude) and the channel depth; and (4) the relationship between the flow power and the strength of channel banks, which means bank erodibility (Fig. 19). The study sheds light on the diversity of submarine sinuous channels (e.g., Kneller, 2003; Janocko et al., 2011) and also clarifies the contradictory laboratory reports on the flow structure and sediment depocentres in such channels (e.g., Peakall et al., 2007; Islam et al., 2008; Straub et al., 2008). The hydraulic circumstances leading to the formation of particular depocentres and channel bar types have been recognized from fully three-dimensional simulations, which allow for more reliable inferences than those based on laboratory 2D flow-velocity profiles and overhead camera imagery.

The meandering channels, increasing in sinuosity by outbound lateral migration, form when the turbidity currents are in equilibrium with the slope, in phase with the channel curvature, in size or moderately undersized with respect to the channel depth, and are moderately erosive with respect to the channel banks (Table 1, Fig. 19). The characteristic deposits of meandering channels are point bars, formed at the inner bank of channel bends by lateral sediment accretion. The simulations show that the lateral accretion occurs when the sediment is transported towards the inner bank along the channel base and deposited on the point-bar flank. The deposition of sediment from a gradually decelerating basal flow suggests tractional bedload transport.

This observation is consistent with inferences from ancient meander belts. For example, Dykstra and Kneller (2009) and Janocko and Nemec (2011) have demonstrated that the palaeotransport direction in point bars is obliquely up the bar flank, with the laterally-accreted beds fining up dip and reflecting a lateral decline in flow competence. The outcrop studies also show that the majority of point-bar deposits are stratified, which indicates tractional deposition.

The conditions for channel meandering could only be satisfied in large-scale simulations imitating natural conditions, because it proved to be impossible to produce a small-scale current that would be in equilibrium with the channel slope and simultaneously fast enough to be in phase with the channel

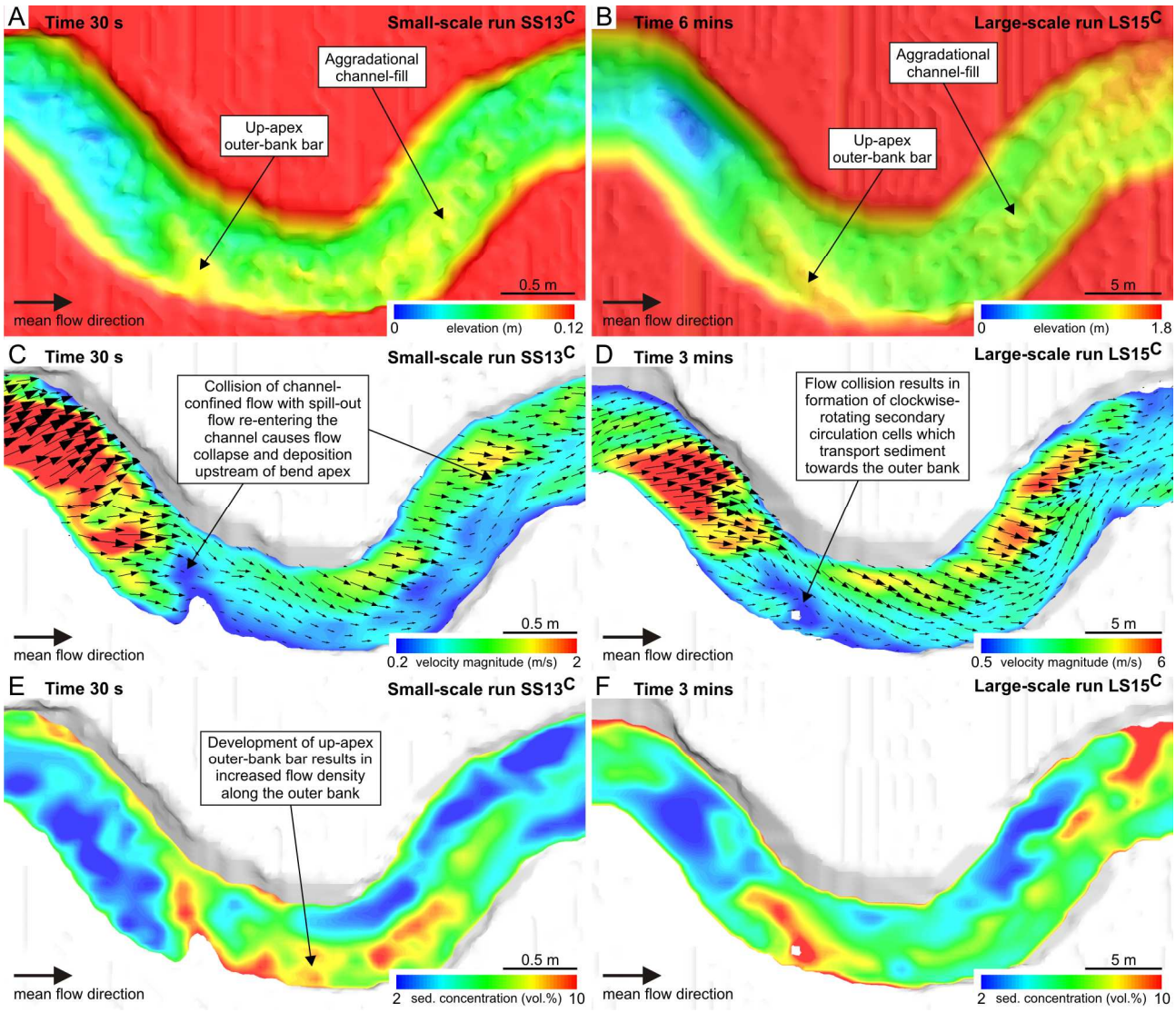


**Fig. 18.** Development of up-apex outer-bank bars in the 2nd bend of simulation run SS13C and the 3rd bend of simulation run LS15A. (A and B) Post-experiment topography maps. The experimental surfaces have been rotated to horizontal. (C and D) Channel slices coloured with velocity magnitude and overlain by velocity vectors. (E and F) Channel slices displaying sediment concentration. In (C) and (E) the slice is extracted 7 cm above the channel floor, in (D) and (F) 1.125 m above the channel floor.

curvature. Although the experimental setup (the grain size and density and the input sediment concentration used) might possibly be blamed, the results suggest that the hydraulic conditions required for channel meandering are not scale-independent. The fact is that no laterally-migrating sinuous subaqueous channels have thus far been produced in either laboratory conditions or small-scale numerical simulations.

The hydraulic conditions favouring formation of translational point bars also seem to allow the development of point bar-attached, inner- to outer-bank transition bars (Table 1, Fig. 19). However, these bars develop also when the phase of the current helicoid is large enough to produce down-apex outer-bank bars. The main prerequisite for the formation of the bank-transition bars thus seems to be an out-of-phase large flow, which leads to a significant detachment of the flow velocity core from channel bank at the inner- to outer-bank transition. The sediment is dragged into the velocity-core separation zone either by convection or by an inward-directed bottom flow, in which case the amount of sediment entrapped in the low-velocity zone is greater. The sediment there is then taken over by the secondary circulation cells that travel towards and dissipate against the upslope bank, where sediment deposition causes formation and vertical accretion of a bar.

The formation of inner- to outer-bank transition bars has been shown in a number of previous studies (Peakall et al., 2007; Straub et al., 2008; Amos et al., 2010) and eloquently described from experiments by Straub et al. (2011). The bars in these experiments formed by sediment fallout from turbulent suspension in the flow separation zones extending from the inner-bank apex to the next bend's outer-bank apex. Although the experiments did not provide details as to how the sediment was supplied into the separation zone, the formation mode, geometry and location of these depocentres is similar to the bars produced in the laboratory experiments and numerical simulations in the present study.

Another pattern of sedimentation in sinuous channels, shown by the numerical simulations and recognized in several previous studies (Straub et al., 2008; Nakajima et al., 2009; Amos et al., 2010), is the development of outer-bank bars. In the simulation scenarios, these bars formed when the phase of the current rotation exceeded that of the channel curvature (Table 1, Fig. 19), in both slope-equilibrium and aggradational conditions and irrespective of the flow size. Three mechanisms for bar deposition in the down-apex zone of outer banks have been recognized. In the first case, the outer-bank bars formed in slope-equilibrium conditions by a flow whose velocity core travelled along the inner bank. The velocity core showed an

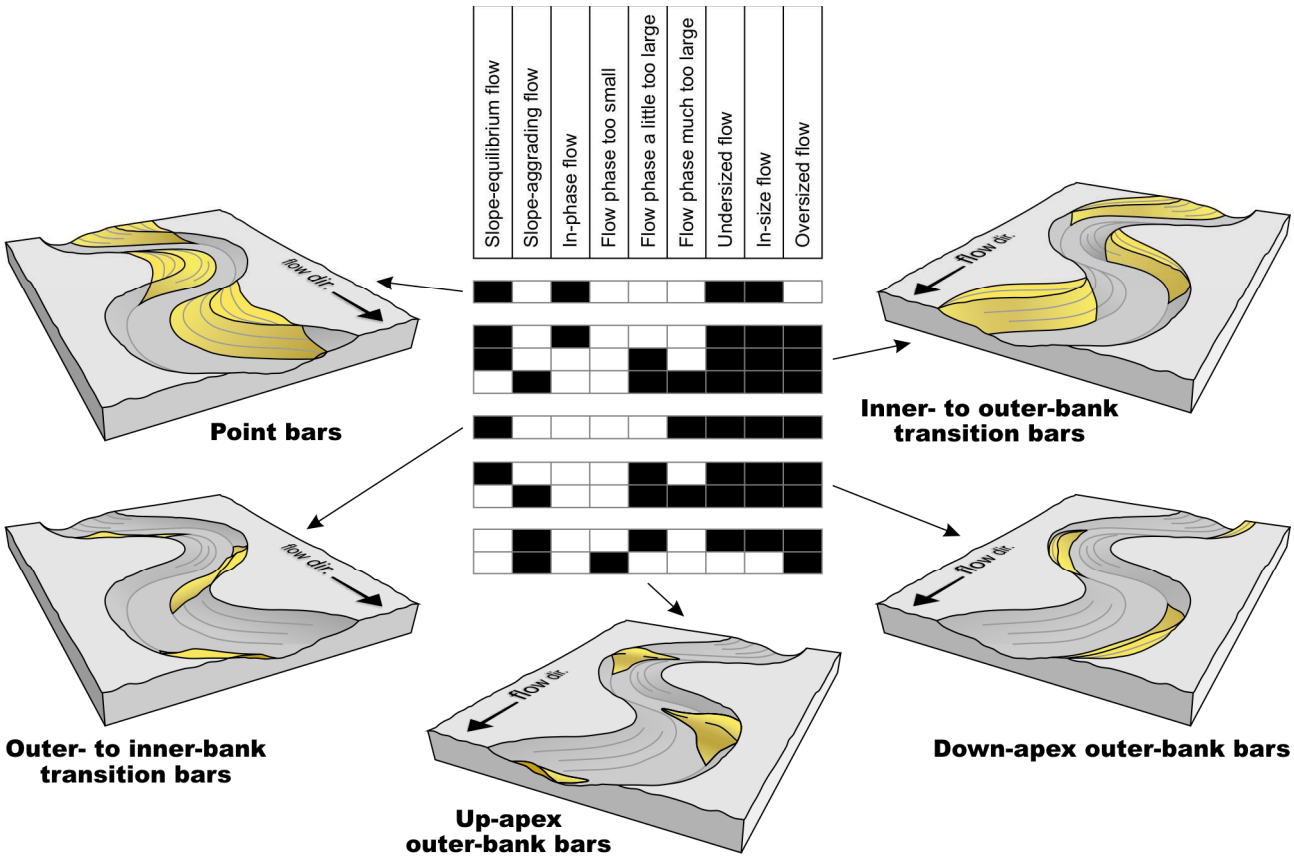


**Fig. 19.** Summary of the investigated system conditions that result in deep-water channel bars.

outward-directed helicoidal circulation, which carried sediment along the channel floor towards the outer bank – where the sediment was laterally accreted due to the flow deceleration against the bank. In the second case, the bars formed in aggradational conditions. The flow travelled superelevated against the outer bank along the entire bend, with an outward-directed rotation helicoid. The superelevation spread the flow laterally and reduced its thickness, which led to deceleration at the flow margins. The elevated flow at the outer bank soon collapsed, descending the bank and colliding with the flow velocity core travelling along the bank foot. The collision effectively decelerated the flow and led to sediment deposition at the outer bank, where it was delivered along the channel base by the outward-directed helicoid. In the third case, the outer-bank bars formed in aggradational conditions when the phase of the flow helicoid exceeded considerably the channel curvature and resulted in collision of the channel-conveyed flow with the spill-out flow re-entering the channel at its bends.

The previous studies on outer-bank bars suggested that the key factor for the formation of these bars was the superelevation of turbidity currents, irrespective of the direction of their helicoidal rotation at the channel bends (Straub et al., 2008; Nakajima et al., 2009; Amos et al., 2010). In aggradational conditions, such as in the experiments of Straub et al. (2008), the localized deposition of sediment at the outer bank was inferred to have occurred simply due to the flow loss of capacity in its bank run-up (Nakajima et al., 2009). However, no deposition due solely to the flow run-up on outer bank has been recognized in the laboratory experiments and numerical simulations in the present study. The origin of outer-bank bars apparently depends on more than one factor and seems to require an outward-directed flow helicoid. This notion is supported by the palaeocurrent measurements in an outer-bank stratified sediment mound described by Janocko and Nemec (2011) from a meander belt in the Rosario Formation, Mexico.

The seismic analysis of outer-bank bars in a sinuous palaeochannel of the Amazon fan, by Nakajima et al. (2009), indicates a decrease in the channel sinuosity as a result of outer-bank sediment accretion. This observation implies that the flows depositing sediment at the outer bank were concurrently eroding the inner bank of the channel bends, making the channel thalweg migrate towards the channel-belt axis and effectively straightening the conduit. No such process has been observed in the present numerical simulations. Instead, the flows in slope-equilibrium conditions – after the development of bars – had reached a bypass stage where no sediment was eroded or deposited. In aggradational conditions, the channel – in contrast –was eventually backfilled with sediment. However, the velocity structure of slope-equilibrium flows (simulation runs $LS3^B$, $SS7^B$, $SS9^B$ and $LS9^B$) might potentially allow inner-bank erosion, because the flow velocity core travelled attached to the inner bank of channel bend and showed an outward-directed helicoid transporting sediment along the floor towards the outer bank. Therefore, it remains unclear why the currents reached a bypass stage instead of causing inward lateral migration and straightening of the channel thalweg. More research is needed to clarify the mechanism which would allow a sinuous channel to accrete sediment on its bend outer banks while systematically decreasing its sinuosity.

The formation of outer- to inner-bank transition bars apparently requires quite specific conditions: flows that are in equilibrium with the channel slope and have a rotational helicoid phase considerably larger than the phase of the channel curvature (Table 1, Fig. 19). Prolonged flows are likely to result in a straight broader channel, as the flow in such conditions is poorly confined and causes significant erosion at the inner- to outer-bank transition in bend inflection zones. The preservation of these inflection-zone bars thus requires short-lived or highly episodic flows. Bars attached to the downslope bank of bend inflection zones as well as features similar to the up-apex outer-bank bars have previously been recognized in natural sinuous

channels (Nakajima et al., 2009), which proves that these bars do occur in nature, despite the lack of their earlier recognition.

A peculiar aspect of many bars in both laboratory experiments and numerical simulations is that their thickness was smaller than the depth of the host channel, including point bars and irrespective of the flow size. The thickness of bars apparently scales with the thickness of the flow density core, which is determined by the channel confinement and thus is comparable in undersized, oversized and in-size flows. It is worth noting that the density core of the in-size and oversized flows in the channel is considerably smaller than at the inlet, owing to the flow spill-out at the outer bank of the first bend. As the thickness of channel-conveyed flow becomes abruptly reduced there, the flow's vertical density profile is immediately altered and the thickness of its density core is adjusted. The channel-confined flow effectively becomes semi-independent of the dilute spill-out flow, albeit interacting with it at confluences, especially if the spill-out is volumetrically large.

Another possible reason why many bars are thinner than the host channel depth may be the use of monosized sediment in the laboratory and numerical flows. If the flow carried a wider range of grain sizes, it might appear powerful enough to transport finer particles to the height of the channel bank and deposit bars as thick as the channel depth.

### *7.2. The differences in flow helicoidal circulation*

One of the most contentious issues concerning the flow of turbidity currents in sinuous channels has been the direction of rotation of the current's primary helicoidal circulation cell at the channel bends. As in the case of a meandering fluvial channel, the pattern of flow rotation can be expected to play a crucial role in the spatial partitioning of sediment and the formation of local depocentres in a submarine sinuous channel. Previous laboratory and numerical studies have been inconclusive, reporting both an inward-directed (Kassem and Imran, 2004; Imran et al., 2007; Islam et al., 2008) and an outward-directed flow helicoid (Corney et al., 2006; Keevil et al., 2006; Keevil et al., 2007; Peakall et al., 2007; Amos et al., 2010; Giorgio Serchi et al., 2011). The 3D numerical simulations conducted in the present study show that the direction of the flow rotation at channel bends can be either way, depending on the circumstances.

Corney et al. (2008) and Giorgio Serchi et al. (2011) have suggested that the direction of the flow rotation depends on the elevation of the flow velocity core entering the channel bend. If the velocity core is perched sufficiently high above the channel floor, it will sink upon meeting the outer bank and give rise to an inward-directed rotation cell. If the flow velocity core is close to the floor, it will rise against the outer bank and generate an outward-directed helicoid at the bend. These authors have also indicated that the elevation of the flow core of maximum velocity may play an important role, as this zone will be closer to the floor in the conditions of a steeper channel gradient, higher density and stronger density-layering of the flow, as well as a higher flow Froude number.

Following the observations by Gorycki (1973) and suggestions of Dykstra and Kneller (2009), an inward-directed rotation at channel bends is considered here to reflect the inherent helicoidal circulation of turbidity current. Flows that show such a sense of rotation are thought to be in phase with the hydraulic geometry of the host channel, which means that the channel profile and curvature do not affect the flow intrinsic helicoid in any significant way.

The phase (or length scale) of the current helicoid is controlled by the flow velocity magnitude, and hence depends indirectly on the slope inclination, flow density and thickness, which jointly determine the velocity. As pointed out by Gorycki (1973) and shown in the present study, if the length scale of the flow helicoid does not match the hydraulic geometry of the channel − its intrinsic structure will be perturbed. In flows that are out of phase with the channel and are little affected by the re-entry of spill-out flow, the direction of the helicoidal rotation will depend on the velocity magnitude and the bend-attack angle of the flow. These two variables also determine the path of the flow velocity core around the channel bend, which seems to be directly related to the direction of the helicoidal rotation. The elevation of the velocity core above the floor is a secondary factor, as it affects the formation of secondary circulation cells upon the flow collision with the outer bank, but does not determine the path of the flow velocity core, which may lead to a reversal of the secondary circulation in the downstream part of the bend.

Flows that are significantly out-of-phase with respect to the channel typically show an outward-directed helicoidal rotation at the bends. However, if the flow's phase is excessively large or the flow is excessively thick and poorly confined, the pattern of flow rotation tends to be more complicated or virtually chaotic.

## 8. Conclusions

The laboratory experiments and numerical CFD simulations conducted in the present study suggest that the pattern of sediment deposition in submarine sinuous channels and their meandering depend on the following critical relationships (Fig. 19):

- The relationship between the flow's desired substrate equilibrium gradient and the host channel's actual slope gradient.
- The relationship between the length scale of the flow's rotational helicoid and the channel's pre-existing curvature.
- The relationship between the flow thickness and the channel depth.
- The relationship between the flow power and the channel bank strength (i.e., erodibility).

The study explored a whole spectrum of possible combinations of the circumstances, revealing the formative conditions for a range of sediment depocentres that can be regarded as channel bars. The following bar types have been distinguished:

- Point bars – deposits accreted laterally on the inner bank of channel bend, of sediment brought in along the channel floor by an inward-directed flow helicoid and lain down due to the flow deceleration on the bar flank. These bars typify meandering channels and are formed by flows that are in hydraulic equilibrium with the channel slope, but in phase with the channel curvature and are in size or undersized relative to the channel depth.
- Inner- to outer-bank transition bars – deposits attached to the upslope bank of channel-bend inflection zone and formed by the vertical accretion of sediment in a low-velocity zone of flow detachment from the bank, with sediment delivery from the flow velocity core along the channel floor by an inward-directed flow helicoid. These bars are formed by the out-of-phase flows with a helicoid length scale exceeding the channel curvature. They thus occur in non-meandering channels, but may also be formed in a meandering channel by excessively fast episodic flows.
- Outer- to inner-bank transition bars – deposits attached to the downslope bank of channel-bend inflection zone and formed by a rapid deceleration of the channel-conveyed flow, when colliding with the spill-out flow re-entering the channel and subject to a hydraulic jump. These bars form

formed by slope-equilibrium flows with a helicoid phase considerably exceeds the channel curvature. Such flows, if prolonged or repetitive, can widen and straighten the channel.

- Down-apex outer-bank bars – deposits attached to the channel bend's outer bank in its down-apex zone due to: (1) detachment of the flow velocity core from the outer bank; (2) deceleration of the velocity core perched on the outer bank; or (3) collision of the channel-conveyed flow and the spill-out flow re-entering the channel. The formation of these bars requires outward-directed flow helicoid transporting sediment along the channel floor towards the outer bank. These bars form in non-meandering channels in slope-equilibrium or aggradational conditions and require relatively fast, out-of-phase currents.
- Up-apex outer-bank bars – deposits attached to the channel bend's outer bank in its up-apex zone, resulting from the sediment entrapment in a low-velocity zone formed by collision of the channel-conveyed flow with the spill-out flow re-entering the channel. These bars form in strongly aggradational conditions and require a velocity of channel-conducted flow that are low enough to be locally halted by a re-entry of the low-density spill-out flow.

Many of the bars formed in the laboratory experiments and numerical simulations, including point bars, were significantly thinner than the host channel depth, which suggests that the bar thickness either scales with the thickness of the channel-confined flow density core or is an artefact of the use of monosized sediment. If the sediment included a range of finer grain fractions, these might have been spread to the bank top and form bars as thick as the channel depth.

The simulations indicated that the flow rotation helicoid can be either inward- or outward-directed at channel bends, or may virtually lose its structure in the case of a grossly oversized flow. If the length scale of the flow helicoid matches the channel curvature, the flow rotation at a channel bend is directed inwards irrespective of the other conditions. If the flow is out of phase with the channel, the direction of the helicoid rotation depends on the flow velocity and the angle at which the flow velocity core approaches the bend's outer bank. A transient, local impact on the direction of flow rotation is exerted by the elevation of the flow velocity core above the channel floor.

The study confirms and expounds on many previous laboratory inferences about the flow of turbidity currents in sinuous non-meandering channels, while showing also that most aspects of such flows can be numerically simulated without the necessity to upscale the system and increase greatly the computer calculation time. However, the study indicates that the process of channel meandering may not be scale-independent and that the formation of subaqueous meandering channels in small-scale laboratory or numerical experiments may be an impossible task. Therefore, inferences about the channel meandering conditions based on small-scale experiments should be considered with much caution.

## Acknowledgements

The study was a part of the first author's doctoral research project funded by Statoil ASA. George Postma is thanked for helping with the laboratory experiments, Riccardo Basani for practical advice regarding CFD simulations and Sverre Henriksen for useful discussions. Natalie Portman is thanked for inspiring some of the interpretations.

## References

Aas, T.E., Howell, J.A., Janocko, M., Midtkandal, I., 2010. Re-created Early Oligocene seabed bathymetry and process-based simulations of the Peïra Cava turbidite system. Journal of the Geological Society, 167, 857–875.

Aas, T.E., Howell, J.A., Janocko, M., Jackson, C., 2010. Control of Aptian palaeobathymetry on turbidite distribution in the Buchan Graben, Outer Moray Firth, Central North Sea. Marine and Petroleum Geology, 27, 412–434.

Abreu, V., Sullivan, M., Pirmez, C., Mohrig, D., 2003. Lateral accretion packages (LAPs): an important reservoir element in deep water sinuous channels. Marine and Petroleum Geology, 20, 631−648.

Amos, K.J., Peakall, J., Bradbury, P.W., Roberts, M., Keevil, G., Gupta, S., 2010. The influence of bend amplitude and planform morphology on flow and sedimentation in submarine channels. Marine and Petroleum Geology, 27, 1431−1447.

Allen, J.R.L., 1982. Sedimentary Structures: Their Character and Physical Basis. Developments in Sedimentology, 30. Unabridged One-Volume Edition, Elsevier, Amsterdam, 1256 pp.

Basani, R., Janocko, M., Cartigny, M., Hansen, E.W.M., Dirkx, R., Postma, G., Eggenhuisen, J., 2011. MassFlow-3D$^{TM}$ as a simulation tool for turbidity currents: some preliminary results. In: Martinius, A. et al. (Eds.), From Depositional Systems to Sedimentary Successions on the Norwegian Continental Shelf. IAS Special Publication (MS in review).

Beaubouef, R.T., Rossen, C., Lovell, R.W.W., 2007. The Beacon Channel: a newly recognized architectural type in the Brushy Canyon Formation, Texas, USA. In: Nilsen, T., Shew, R., Steffens, G., Studlick, J. (Eds.), Atlas of Deep-Water Outcrops. AAPG Studies in Geology, 56, pp. 432−443.

Bridge, J.S., 2003. Rivers and Floodplains: Forms, Processes and Sedimentary Record. Blackwell Publishing, Oxford, 491 pp.

Campion, K. M., Sprague, A. R., Mohrig, D., Lovell, R. W., Drzewiecki, P. A., Sullivan, M. D., Ardill, J. A., Jensen, G. N., Sickafoose, D. K., 2000. Outcrop expression of confined channel complexes. In: Weimer, P., Slatt, R.M., Coleman, J., Rosen, N.C., Nelson, H., Bouma, A.H., Styzen, M.J., Lawrence, D.T. (Eds.), Deep-Water Reservoirs of the World. SEPM Gulf Coast Section 20th Bob F. Perkins Research Conference, pp. 127−150.

Corney, R.K.T., Peakall, J., Parsons, D.R., Elliott, L., Amos, K.J., Best, J.L., Keevil, G.M., Ingham, D.B., 2006. The orientation of helical flow in curved channels. Sedimentology, 53, 249–257.

Corney, R. K. T., Peakall, J., Parsons, D., Elliott, L., Best, J. L., Thomas, R. E., Keevil, G. M., Ingham, D. B., Amos, K. J., 2008. Reply to discussion of Imran et al. on "The orientation of helical flow in curved channels" by Corney et al., Sedimentology, 55, 241–247.

Cronin, B.T., Çelik, H., Hurst, A., 2007. Sinuous channels in late stages of entrenched deep-water channel complexes: Hasret Mountain Main Channel, Turkey. In: Nilsen, T., Shew, R., Steffens, G., Studlick, J. (Eds.), Atlas of Deep-Water Outcrops. AAPG Studies in Geology, 56, pp. 368−372.

Dykstra, M., Kneller, B.C., 2009. Lateral accretion in a deep-marine channel complex: implications for channelized flow processes in turbidity currents. Sedimentology, 56, 1411−1432.

Giorgio Serchi, F., Peakall, J., Ingham, D. B., Burns, A. D., 2011. A unifying computational fluid dynamics investigation on the river-like to river-reversed secondary circulation in submarine channel bends. Journal of Geophysical Research, 116, paper C06012, doi:10.1029/2010JC006361.

Gorycki, M.A., 1973. Hydraulic drag: a meander-initiating mechanism. Geological Society of America Bulletin, 84, 175–186.

Guo, J., 2002. Hunter Rouse and Shields diagram. Proceedings of the IAHR-APD Congress, Singapore, 2, 1069−1098.

Hansen, E.W.M., Nemec, W., Heimsund, S., 2008. Numerical CFD simulations – a new tool for the modelling of turbidity currents and sand dispersal in deep-water basins. Extended Abstract, NPD Production Geoscience Conference, Norwegian Petroleum Directorate, Stavanger.

Harms, J.C., Southard, J.B., Walker, R.G., 1982. Structures and Sequences in Clastic Rocks. SEPM Short Course No. 9 Lecture Notes. Society of Economic Paleontologists and Mineralogists, Calgary, 851 pp.

Heimsund, S., 2007. Numerical simulation of turbidity currents: a new perspective for small- and large-scale sedimentological experiments. M.Sc. Thesis, University of Bergen, 129 pp.

Heimsund, S., Xu, J., Nemec, W., 2007. Numerical simulation of recent turbidity currents in the Monterey canyon system, offshore California. Poster Abstract OS33A-0996, American Geophysical Union Fall Meeting, San Francisco.

Hirt, C.W., Sicilian, J.M., 1985. A Porosity Technique for the Definition of Obstacles in Rectangular Cell Meshes. Proceedings of the Fourth International Conference on Numerical Ship Hydrodynamics, National Academy of Science, Washington, DC.

Imran, J., Islam, M.A., Huang, H., Kassem, A., Dickerson, J., Pirmez, C., Parker, G., 2007. Helical flow couplets in submarine gravity underflows. Geology, 35, 659−662.

Islam, M.A., Imran, J., Pirmez, C., Cantelli, A., 2008. Flow splitting modifies the helical motion in submarine channels. Geophysical Research Letters, 35, L22603, doi:10.1029/2008GL034995.

Jackson, R.G., 1975. Hierarchical attributes and a unifying model of bed forms composed of cohesionless material and produced by shearing flow. Geol. Soc. Am. Bull., 86, 1523−1533.

Janocko, M., Nemec, W., 2011. The facies architecture and formation of deep-water point bars: an outcrop perspective. Sedimentology (MS in review).

Janocko, M., Nemec, W., Henriksen, S., Warchoł, M., 2011. The diversity of deep-water sinuous channel belts and slope valley-fill complexes. Marine and Petroleum Geology (MS in review).

Kane, I.A., McCaffrey, W.D., Peakall, J., 2008. Controls on sinuosity evolution within submarine channels. Geology, 36, 287−290.

Kassem, A., Imran, J., 2004. Three-dimensional modeling of density current, II. Flow in sinuous confined and unconfined channels. Journal of Hydraulic Research, 42, 591−602.

Keevil, G.M., Peakall, J., Best, J.L., Amos, K.J., 2006. Flow structure in sinuous submarine channels: velocity and turbulence structure of an experimental submarine channel. Marine Geology, 229, 241−257.

Keevil, G.M., Peakall, J., Best, J.L., 2007. The influence of scale, slope and channel geometry on the flow dynamics of submarine channels. Marine and Petroleum Geology, 24, 487−503.

Kleinhans, M., van Rijn, L.C., 2002. Stochastic prediction of sediment transport in sand-gravel bed rivers. Journal of Hydraulic Engineering, 128, 412−25.

Kleinhans, M.G., 2010. Sorting out river channel patterns. Progress in Physical Geography, 34, 287−326.

Kneller, B.C, 2003. The influence of flow parameters on turbidite slope channel architecture. Marine and Petroleum Geology, 20, 901−910.

Kolla, V., Posamentier, H.W., Wood, L.J., 2007. Deep-water and fluvial sinuous channels: characteristics, similarities and dissimilarities, and modes of formation. Marine and Petroleum Geology, 24, 388−405.

Labourdette, R., 2007. Integrated three-dimensional modeling approach of stacked turbidite channels. AAPG Bulletin, 91, 1603−1618.

Lien, T., Walker, R.G., Martinsen, O.J., 2003. Turbidites in the Upper carboniferous Ross Formation, western Ireland: reconstruction of a channel and spillover system. Sedimentology, 50, 113−148.

Loveless, J. H., Sellin, R. H. J., Bryant, T. B., Wormleaton, P. R., Catmur, S., Hey, R., 2000. The effect of overbank flow in a meandering river on its conveyance and the transport of graded sediments. Water and Environment Journal, 14, 447−455.

Mastbergen, D.R., Van den Berg, J.H., 2003. Breaching in fine sands and the generation of sustained turbidity currents in submarine canyons. Sedimentology, 50, 625−637.

Mayall, M., Jones, E., Casey, M., 2006. Turbidite channel reservoirs – key elements in facies prediction and effective development. Marine and Petroleum Geology, 23, 821−841.

Meyer-Peter, E., Mueller, R., 1948. Formulas for bed-load transport. Proceedings of the 3rd Conference, International Association of Hydraulic Research, Stockholm, Sweden, 39−64.

Mohrig, D., Buttles, J., 2007. Deep turbidity currents in shallow channels: Geology, 35, 155−158.

Nakajima, T., Peakall, J., McCaffrey, W.D., Paton, D.A., Thompson, P.J., 2009. Outerbank bars: a new intra-channel architectural element within sinuous submarine slope channels. Journal of Sedimentary Research, 79, 872−886.

O'Byrne, C.J., Barton, M.D., Steffens, G.S., Pirmez, C., Buergisser, H., 2007. Architecture of a laterally migrating channel complex: Channel 4, Isaac Formation, Windermere Supergroup, Castle Creek North, British Columbia, Canada. In: Nilsen, T., Shew, R., Steffens, G., Studlick, J. (Eds.), Atlas of Deep-Water Outcrops. AAPG Studies in Geology, 56, pp. 115−118.

Peakall, J., Amos, K.J., Keevil, G.M., Bradbury, P.W., Gupta, S., 2007. Flow processes and sedimentation in submarine channel bends. Marine and Petroleum Geology, 24, 470−486.

Phillips, S., 1987. Dipmeter interpretation of turbidite-channel reservoir sandstones, Indian Draw Field, New Mexico. In: Tillman, R.W., Weber, K.J. (Eds.), Reservoir Sedimentology. SEPM Special Publication, 40, pp. 113−128.

Pirmez, C., Beaubouef, R.T., Friedmann, S.J., Mohrig, D.C., 2000. Equilibrium Profile and base-level in submarine channels: examples from Late Pleistocene systems and implications for the architecture of deepwater reservoirs. In: Weimer, P., Slatt, R.M., Coleman, J., Rosen, N.C., Nelson, H., Bouma, A.H., Styzen, M.J., Lawrence, D.T. (Eds.), Deep-Water Reservoirs of the World. SEPM Gulf Coast Section 20th Bob F. Perkins Research Conference, pp. 782−805.

Postma, G., Kleinhans, M., Meijer, P., Eggenhuisen, J., 2008. Sediment transport in analogue flume models compared with real-world sedimentary systems: a new look at scaling evolution of sedimentary systems in a flume. Sedimentology, 55, 1541−57.

Pyles, D. R., Jennette, D. C., Tomasso, M., Beaubouef, R. T., Rossen, C., 2010. Concepts Learned from a 3D Outcrop of a Sinuous Slope Channel Complex: Beacon Channel Complex, Brushy Canyon Formation, West Texas, U.S.A. Journal of Sedimentary Research, 80, 67−96.

Richardson, J.F., Zaki, W.N., 1954. Sedimentation and fluidization: Part I. Transactions of the Institute of Chemical Engineers, 32, pp. 35–53.

van Rijn, L. C., 1984. Sediment transport, Part I: Bed load transport. Journal of Hydraulic Engineering, 110, 1431−1456.

Shiono, K., Muto, Y., 1998. Complex flow mechanisms in compound meandering channels with overbank flow. Journal of Fluid Mechanics, 376, 221−261.

Shultz, M.R., Fildani, A., Cope, T.D., Graham, S.A., 2005. Deposition and stratigraphic architecture of an outcropping ancient slope system: Tres Pasos Formation, Magallanes Basin, southern Chile. In: Hodgson, D.M., Flint, S.S. (Eds.), Submarine Slope Systems: Processes and Products. Geological Society of London Special Publication, 244, pp. 27−50.

Straub, K.M., Mohrig, D., McElroy, B., Buttles, J., 2008. Interactions between turbidity currents and topography in aggrading sinuous submarine channels: a laboratory study. GSA Bulletin, 120, 368−385.

Straub, K.M., Mohrig, D., Buttles, J., McElroy, B., Pirmez, C., 2011. Quantifying the influence of channel sinuosity on the depositional mechanics of channelized turbidity currents: a laboratory study. Marine and Petroleum Geology, 28, 744−760.

Timbrell, G., 1993. Sandstone architecture of the Balder Formation depositional system, UK Quadrant 9 and adjacent areas. In: Parker, J.R. (Ed.), Petroleum Geology of Northwest Europe. Proceedings of the 4th Conference, Geological Society of London, pp. 107−121.

Wesseling, P., 2001. Principles of Computational Fluid Dynamics. Springer-Verlag, Berlin, 644 pp.

Wynn, R.B., Cronin, B.T., Peakall, J., 2007. Sinuous deep-water channels: genesis, geometry and architecture. Marine and Petroleum Geology, 24, 341−387.

Yakhot, V., Orszag, S.A., 1986. Renormalization group analysis of turbulence, I. Basic theory. Journal of Scientific Computing, 1, 1−51.

Yakhot, V., Smith, L.M., 1992. The renormalization group, the e-Expansion and derivation of turbulence models. Journal of Scientific Computing, 7, 35−61.

III

# The facies architecture and formation of deep-water point bars: an outcrop perspective

MICHAL JANOCKO and WOJCIECH NEMEC
*Department of Earth Science, University of Bergen, 5007 Bergen, Norway*

Submitted to *Sedimentology*

**ABSTRACT**

The study analyses outcrop examples of a wide range of deep-water point bars and reviews earlier-published cases with the aim to give insights in the meandering process of turbiditic channels. Six point-bar types are distinguished on descriptive basis. The main differences are in the facies of laterally accreted beds, which may be sand-mud couplets, sand beds, couplets of mudclasts rudite and sand, gravel-sand couplets, beds with updip-segregated gravel and sand or gravel beds. Beds vary in thickness, but represent a different persistent variety of the depositing currents. Point bars also vary in size (thickness, width), reflecting the channel depth and bend radius, and in the stacking pattern of beds – reflecting planform evolution of meander bend. Meander belts differ further in the infilling mode of their last-stage channel.

Despite these major differences, the deep-water point bars have several features in common. Their horizontal or gently inclined erosional bases indicate meander-belt formation in quasi-equilibrium slope conditions, with erosion and deposition in lateral domain. Sparse levées indicate bypassing spill-out flows. The encasing cohesive deposits point to the importance of bank strength, as in meandering fluvial channels. The laterally accreted beds show updip fining and tractional oblique updip transport, which indicate a rotating flow helicoid rising against the inner bank, spreading its bedload over the point-bar flank and segregating laterally grain sizes. The downdip parts of beds indicate a higher sediment concentration in the flow.

The differences among meander belts bear importantly on their heterogeneity, but are unrecognizable from seismic images. However, the six point-bar types are readily identifiable from a well-core sample, and their detailed characteristics provided by the study can serve as a useful guide for the recognition and characterization of ancient meander belts and for the development of their models as hydrocarbon reservoirs.

**Keywords** Point bar, meandering, channel bend, lateral accretion, deep water, turbidites

## INTRODUCTION

Point bars are the single most important element of meander belts, testifying to channel meandering – a process still poorly understood in relation to deep-water realm. Inferences about deep-water meandering channels based on rivers and laboratory flows are unreliable. The usefulness of meandering river channels as analogues is questionable, not least because the deep-water sediment gravity flows are rheologically and hydraulically different from an open-channel water flow. Laboratory experiments with turbidity currents have thus far failed to produce meandering channels and shed light on their formation, and also insights from numerical simulations are yet to be seen.

The deposits of deep-water point bars in outcrop sections remain the only reliable source of information on the behaviour of meandering turbidity currents and the conditions in which sinuous channels migrate by lateral accretion. Unlike other palaeochannel types, the meandering channel belts in outcrops are readily recognizable due to the characteristic lateral-accretion bedding of point bars and an associated last-stage channel-fill. Outcrops of point-bar deposits allow their facies architecture to be studied in detail and the bedding attitude and local palaeocurrent direction to be measured, which gives insights in the formative deep-water flows. The number of documented point-bar outcrops in deep-water successions is now considerable, allowing comparisons to be made and case-unbiased inferences to be drawn about the development of turbiditic meandering channels.

The general scope of the present study was to analyse in detail a wide range of deep-water point bars in outcrop sections and to review, on a comparative basis, the earlier-published outcrop examples. The study had four specific aims: (1) to describe the component facies of deep-water point bars and draw inferences about the depositing flows; (2) to determine the vectorial direction of bedload transport on point-bar surface and recognize the gross pattern of flow helicoid at channel bends; (3) to analyse the cross-sectional geometry and spatial

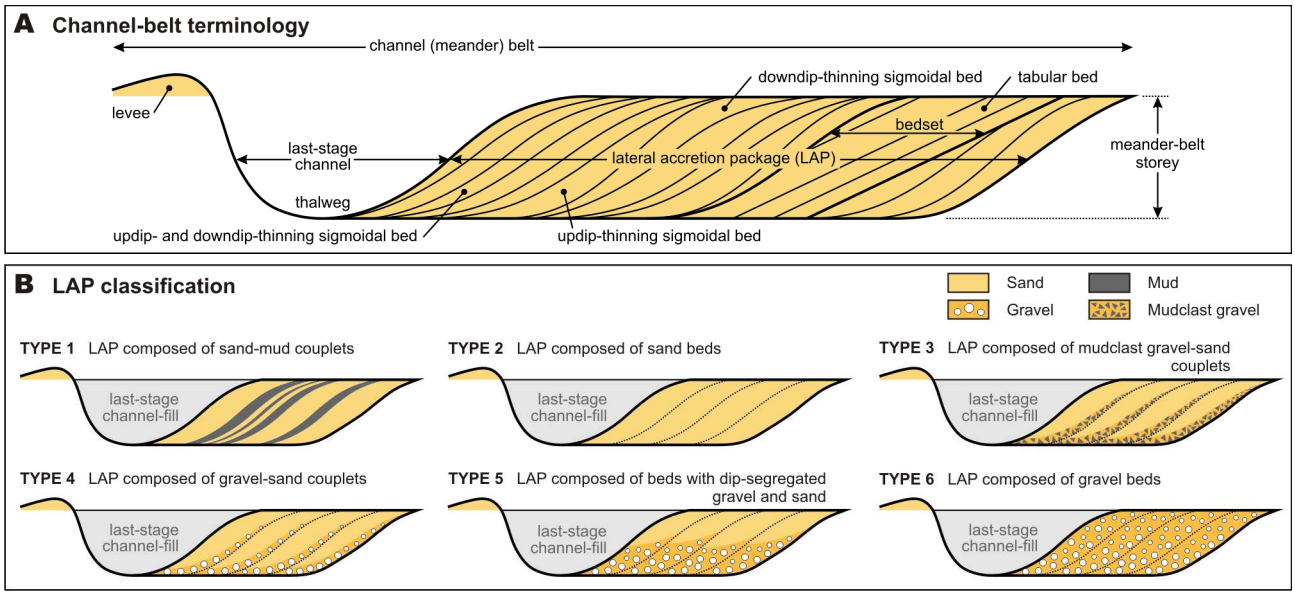


**Fig. 1.** Definition diagrams. (A) Terminology for a meander belt and its elements. (B) Classification of deep-water point-bar LAPs based on the content and spatial partitioning of gravel, sand and mud.

attitude of laterally-accreted beds in order to recognize point-bar planform evolution; and (4) to distinguish main common varieties of deep-water point bars in attempt to provide their tentative classification. On the basis of the extensive evidence from outcrops, inferences are also drawn as to the physical conditions for channel meandering in deep-water realm.

## TERMINOLOGY

A submarine channel is defined as a long-term conduit for down-slope transport of sediment, formed by turbidity currents (Mutti, 1977). A meandering channel is a laterally-active sinuous channel that systematically migrates by bend growth. Its deepest, axial hydraulic zone is referred to as the channel thalweg (Bridge, 2003). The migrating conduit in its final, abandonment-phase position is called the 'last-stage' channel (Fig. 1A).

Deposits that filled the last-stage channel are referred to as the channel-fill (Fig. 1A). The broader term 'channel belt' refers jointly to the channel-fill and deposits intimately associated with the channel (Fig. 1A; Bridge, 2003), such as point bars and levées, as well as possible outer-bank bars, nested mounds and mass-transport (slide, slump or debris-flow) deposits buried by the growing point bars. A meandering channel belt is also called shortly 'meander belt'. In an aggrading system, successive channel belts may be stacked upon one another to form channel-belt complexes.

Lateral accretion packages (LAPs) (Abreu *et al.*, 2003) consist of inclined beds deposited by the lateral accretion of sediment at channel banks. Lateral accretion as such may occur at various locations relative to a channel bend (Nakajima *et al.*, 2009; Fernandes *et al.*, 2011), but the term LAP in the present paper is limited to deposits accreted at the inner bank and potentially representing a point bar (Fig. 1A). The LAPs in the present study are classified descriptively into six types on the basis of the volumetric content and spatial partitioning of gravel, sand and mud (Fig. 1B), but with no claim that this classification must necessarily be exhaustive on a global scale. The LAP beds in dip section have a sigmoidal or nearly tabular geometry, forming broad lenses that are thinning updip or downdip or in both directions (Fig. 1B). A set of relatively conformable LAP beds is referred to as 'bedset' (Fig. 1B).

The geomorphological terminology for channel-bend planform transformation (i.e., expansion, translation and

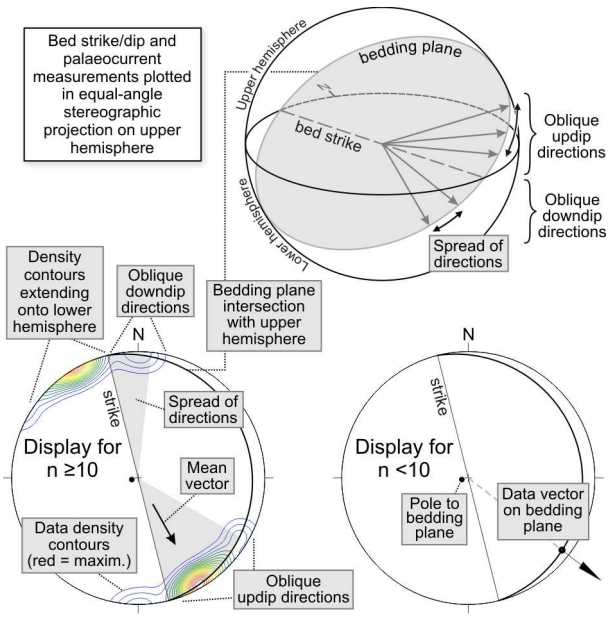


**Fig. 2.** The stereographic display of bedding attitude and palaeocurrent direction used in the present study. Note that the upper hemisphere projection is used for convenience and that two alternative displays are used (lower diagrams), depending on the number of data (*n*).

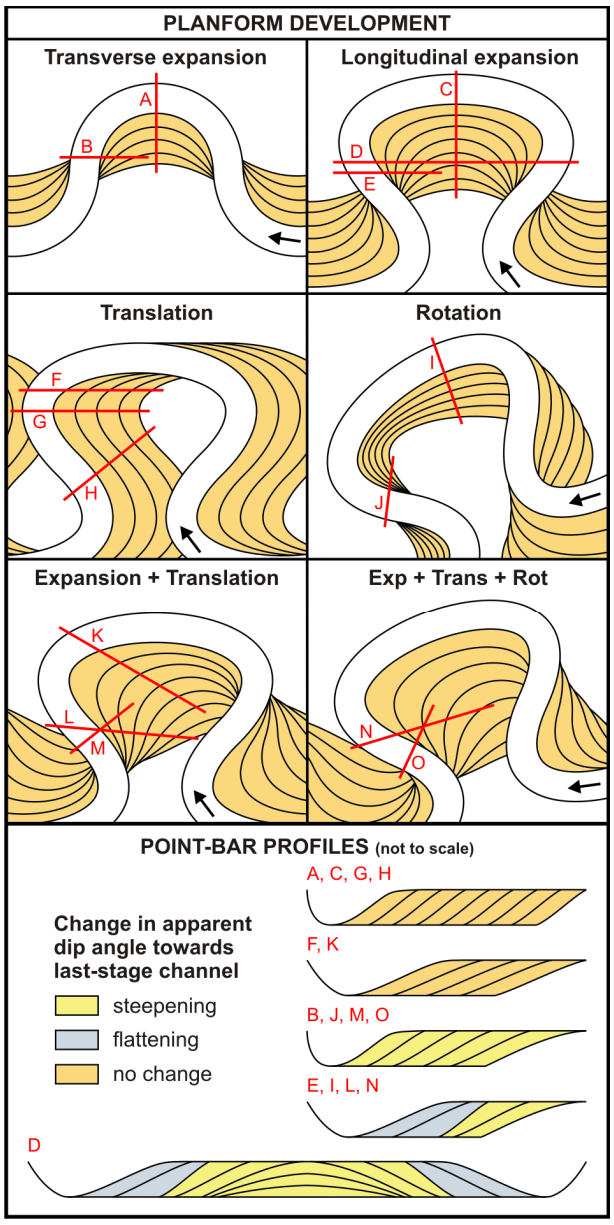


**Fig. 3.** Terminology for meander-bend planform transformation. The planform development of point bars in the present study is reconstructed mainly on the basis of the true (measured) and apparent (seen in outcrop wall) bedding attitude. However, this approach has considerable limitations, because different styles of planform development may result in similar strike or dip patterns in an arbitrary 2D outcrop section. The diagrams show how the bedding strike and apparent dip may vary in random 2D sections for the most common planform transformation styles; the true dip of LAP beds is assumed to be constant.

rotation) is after Brice (1974). Descriptive sedimentological terminology, including clast fabric notation, is after Harms *et al.* (1975, 1982). In the description of deposits, cementation is disregarded and sediment is referred to by its primary name as clastic material (i.e., conglomerate is referred to as gravel, sandstone as sand and mudstone as mud). The distinction between low- and high-density turbidity currents is according to Lowe (1982), with the evidence of a non-tractional deposition of coarse sediment as a criterion. The tractional divisions of 'classical' turbidites are labelled with the Bouma (1962) letter code, whereas the additional divisions formed by high-density turbidity currents are denoted with the code of Lowe (1982). Following Blikra & Nemec (1998, 2000) and Lønne & Nemec (2004), the one-word label 'debrisflow' is used to denote sediment gravity flows with plastic rheology.

## METHODS

The point-bar LAPs in outcrop sections were studied by using the outcrop photomosaic, with an overlay drawing of LAP geometry and bedding architecture, and by direct observations in the outcrop – with the measurement of bedding attitude, transport direction and representative facies logs. Palaeocurrent directions were measured on the basis of imbricate gravel fabric, bed solemarks (flute casts) and ripples or dunes exposed on bedding surfaces. The dispersion of local clast-fabric data was treated numerically by the eigenvector method (Mark, 1973), with the eigenvector of dataset defining the direction of the maximum concentration of data vectors and with the primary eigenvalue ($S_1$) defining the fabric strength, or the degree of data-vector concentration around the eigenvector. The $S_1$-value can range from 0 to 1, with $S_1 = 0$ indicating a disorderly dataset and $S_1 = 1$ denoting a set of perfectly parallel data vectors.

The measurements of palaeocurrent direction and bedding attitude (strike and dip) were collected systematically across the LAP in a large number of selected 'stations'. The raw data were subsequently rotated to correct for the tectonic tilt of sedimentary succession, using the mean attitude of adjacent sheet-like overbank turbidites as an approximation of palaeo-horizontal reference level. The rotated datasets are displayed in an equal-angle stereographic projection on upper hemisphere (for detailed explanation, see Fig. 2).

The measurements of LAP bedding attitude derived from same palaeo-horizontal level across the outcrop section were additionally plotted in map view to recognize possible changes in the strike of point-bar bedding. These plan-view plots, together with the inclination and relative thicknesses of beds seen in the outcrop section, were used to infer the probable planform development of the channel meander (i.e., the channel-bend growth by expansion, translation, rotation or a combination of these modes; Fig. 3). However, these inferences are hypothetical and should be considered with caution, because – in terms of a single outcrop section – different modes of meander planform evolution may result in similar bedding patterns (Fig. 3). Nevertheless, the data allow discerning changes in meander growth, even if the actual mode of growth is uncertain.

**Table 1.** The geological settings of deep-marine sedimentary successions from which the LAP examples 1–9 are described in the present study.

| LAP example | Formation and age | Location | Basin type | Feeder system | Depositional system |
|---|---|---|---|---|---|
| 1, 7 & 9 | Kırkgecit Fm., Eocene | Elaziğ Basin, Turkey | Back-arc basin with topography affected by basement block-faulting | River delta | Channelized slope fairway encountering a submarine high, including channels, levées, crevasse splays and extensive packages of turbidite sheets |
| 2 | Rocchetta Fm., Oligocene | Piedmont Basin, Italy | Fore-arc basin with topography affected by basement block-faulting | Shelf-edge collapses | Base-of-slope system in a narrow, elongate sub-basin, including channels and ponded depositional lobes |
| 3 | Mount Messenger Fm., Miocene | Taranaki Basin, New Zealand | Foredeep trough between a fold-and-thrust belt and volcanic arc | Shelf-edge collapses, possibly delta | Base-of-slope channel-belt complex incised in an older basin-floor complex of channel belts and depositional lobes |
| 4–6 & 8 | Rosario Fm., Late Cretaceous | Peninsular Ranges Basin, Mexico | Fore-arc basin with strike-slip margin | River delta | Channelized fairway in the lower part of an upper-slope submarine valley |

## THE POINT-BAR LAP CATEGORIES

The six categories of point-bar LAPs distinguished in the present study (Fig. 1B) and documented with outcrop examples (Table 1) are described in detail and interpreted in the ensuing section. The description of each outcrop case is given in three portions (bedding architecture, sedimentary facies and palaeocurrent pattern), with the evidence clearly separated from its interpretation. The field examples are supplemented with earlier-published cases and/or outcrop cases which the authors visited without making detailed documentation. The review of the LAP categories is followed by a brief description of less common cases, which differ from the majority and invite possible distinction of additional categories.

### Point-bar LAPs composed of sand-mud couplets

This point-bar category is illustrated by the LAP example 1 (Table 1), one of several point bars exposed at the Hasret Mountain in the north-eastern part of the Elaziğ Basin, eastern Turkey. The meandering channel belts there form a relatively short, delta-fed submarine slope system that was redirected almost orthogonally by underwater structural high ~3 km away from the Late Miocene shelf edge (Cronin *et al.*, 2007b). The deep-water system, comprising several channel-belt complexes confined by incision and/or topography, evolved through three main depositional phases (Cronin *et al.*, 2000, 2007a, b). The deposits of phase 1 are amalgamated lenses of clast-supported cobble gravel originally attributed to submarine braided channels, but possibly representing the bedload lags of sediment-bypassing low-sinuosity conduits. The deposits of phase 2 consist mainly of sand-supported pebble gravel and pebbly sand, representing channels filled by aggradational lateral accretion. The deposits of phase 3, represented by the LAP example 1 (Fig. 4), consist of isolated meandering channel belts with laterally accreted sand-mud couplets.

*LAP example 1*

*Bedding geometry* – The point-bar LAP and associated last-stage channel-fill are exposed in an outcrop section trending NE–SW (052-232°). The meander belt is 1.5 m thick and ~35 m wide, it has a flat top and a palaeo-horizontal erosional base. The LAP formed in the basal part of a valley-fill incised in similar underlying deposits and covered with sheet-like, mud-capped turbidites (Fig. 4A, B). The channel belt occupies more than a third of the palaeovalley width. The valley-fill 'background' deposits are sheet-like sand beds (8–50 cm thick) capped with thin (< 15 cm) mud layers (Fig. 4A, B). Their mean attitude (220/12°NW) served as an estimate of palaeo-horizontal reference level for the rotation of local directional data.

The meander belt in cross-section consists of three prominent, laterally-accreted lenticular sand beds, of which the last one represents the last-stage channel-fill (Fig. 4A, B). The first two beds, in the NE part of the LAP, have a maximum thickness of 1 m and a shape of sigmoidal symmetrical lenses thinning both updip and downdip. The third bed is up to 2.1 m thick and sigmoidal in shape, but thinning mainly in updip direction. The lenticular beds are separated by uniform packages, ~50 cm thick, of thin (<15 cm) sand-mud couplets. The LAP is underlain by heterolithic deposits composed of thin (<10 cm), cross-laminated sand sheets alternating with mud.

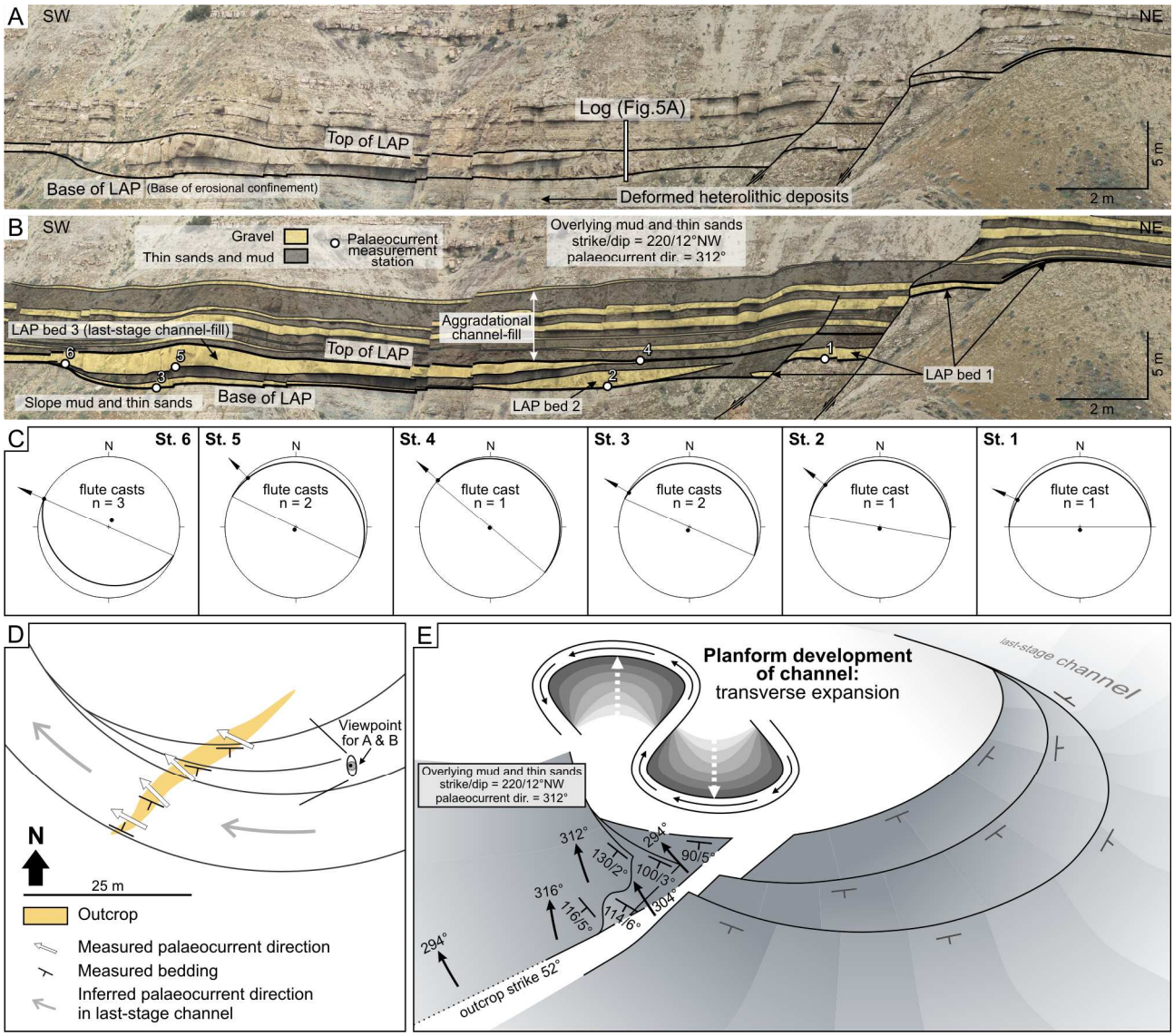


**Fig. 4.** Example of a point-bar composed of sand-mud couplets (LAP example 1 in Table 1), Elaziğ Basin, Turkey. (A) Outcrop photograph and (B) overlay drawing of the LAP. Note the three thick beds, of which the latest initiated the aggradational infilling of last-stage channel. Beds 1 and 2 have the shape of symmetrical sigmoidal lenses and are separated by a tabular unit of thin heterolithic turbidites. The log is shown in Fig. 5A. (C) The attitude of LAP bedding and the corresponding palaeocurrent direction from stations 1–6, plotted in upper-hemisphere stereographic projection. The local directions of bedload transport range from strike-parallel to updip-deviated. (D) Interpretive horizontal slice through the LAP, showing the measured bedding attitude and palaeocurrent directions. The convergence of bedding strikes towards the west (into the outcrop), suggests point-bar transverse expansion. (E) Schematic 3D planform reconstruction of the point-bar LAP, showing the bedding attitude and palaeocurrent directions in the outcrop section.

The LAP bedding surfaces have a maximum dip angle of 6° towards 180–220°. The measured attitude of the base and top surfaces of the two symmetrical sand lenses converge towards WNW, indicating these beds pinch out into the outcrop. Similar convergence is shown by the rotated measurements from all three beds collected at one height above the LAP base and plotted in map view (Fig. 4C, D). The channel belt trends towards SW and the mean palaeocurrent direction is towards NW (Fig. 4C), which suggests that the planform geometry of the LAP bedding in the outcrop section may represent the downstream end of an expansional point bar (Fig. 4D, E).

*Sedimentary facies* – The three lenticular sand beds have conformable bases and show grain-size fining both normal to base and in updip direction. The coarsest part of the first and the third lens consists of planar parallel-stratified, normally-graded very coarse to medium sand with scattered granules and pebbles at the base and a ripple cross-laminated top part. The middle lens consists of normally-graded fine to very fine sand (Fig. 5A), with the lower two-third of the bed thickness showing plane-parallel stratification and the upper part being ripple cross-laminated. The thin sand-mud couplets in the intervening heterolithic packages consist of very fine-grained, ripple cross-laminated sand grading into laminated mud.

The lenticular sand beds are considered to be tractional turbidites T*bc(d)* plastered to the point-bar surface by relatively large, low-density currents. The

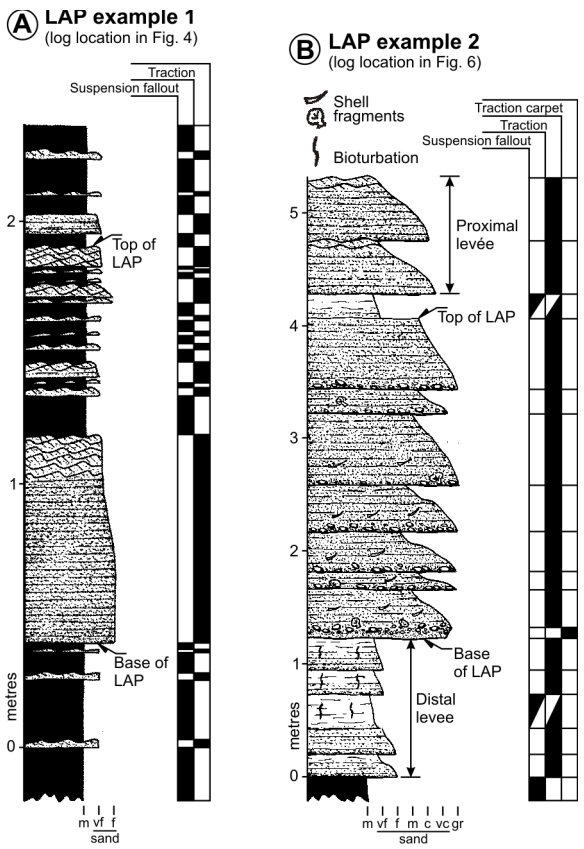


**Fig. 5.** Interpreted facies logs from the point-bar LAP example 1 (Fig. 4) and example 2 (Fig. 6); for comments, see text.

updip fining of beds suggests a lateral reduction of flow competence on the point-bar flank. The thin sand-mud couplets are turbidites T*c(d)e* draped uniformly across the channel by much smaller and more dilute currents, each followed by fallout of mud suspension. Notably, the lateral plastering of sand was chiefly due to the sporadic large flows, which indicates that the point-bar growth was highly episodic.

*Palaeocurrent pattern* – Palaeocurrent directional indices in the LAP example 1 are limited to flute casts and ripple crests, which are only rarely exposed. The palaeocurrent data here are such much sparser than in the remaining LAP cases. The mean palaeocurrent direction for the channel belt is towards the SW (Cronin *et al.*, 2000), whereas the direction in the LAP-covering heterolithic deposits is towards 312°. Measurements from the three sand lenses in the NE part of the LAP (points 1, 2 and 4 in Fig. 4B) indicate a mean flow azimuth of 305° and show an updip deviation of 2° to 28° from the corresponding LAP bedding strike (Fig. 4C). Flute casts in the thalweg zone in SW part of the outcrop show a mean palaeocurrent azimuth of 303° and up-bar deviation of 0–20°. The tractional sediment transport was thus directed obliquely up the point-bar flank (Fig. 4E), which suggests a secondary flow helicoid rising along the channel base against the inner bank.

*Other examples*

A similar spatial partitioning of sediment grain size was described from a LAP of the Solitary Channel in the Miocene Tabernas Basin, SE Spain (channel-complex set 4 of Abreu *et al.*, 2003; also see Wynn *et al.*, 2007). The LAP there is only partly preserved, ~10 m thick and > 50 m wide. It has an originally horizontal erosional base and consists of medium to coarse, massive sand beds (10–90 cm thick) with scattered pebbles in the lower part, and of fine to very fine, massive to stratified sand beds (5–30 cm thick) in the upper part. The sand beds are capped with mud layers 10–25 cm thick and have an updip- and downdip-thinning shape of sigmoidal lenses or are nearly tabular in shape. The beds have conformable bases, and the bed maximum inclination in its thickest part reaches 15°. The last-stage channel-fill is muddy. The LAP was interpreted by Abreu *et al.* (2003) as a 'suspension-dominated' deep-water point bar; the label is potentially misleading, but was presumably meant to denote that the largely massive sand beds indicate deposition by rapid dumping directly from turbulent suspension (Lowe, 1988; Vrolijk & Southard, 1997), as is typical of high-density turbidity currents (Lowe, 1982).

Another example of a deep-water LAP composed of sand-mud couplets is afforded by the Rehy Cliffs outcrop of the Late Carboniferous Ross Fm. in the Clare Basin of western Ireland. The LAP has been described by several authors, albeit inconsistently, probably due to the poor accessibility of the coastal cliff. Elliott (2000) and Wynn *et al.* (2007) described the LAP as being composed of medium to thick sand beds, commonly amalagamated, but generally interlayered with heterolithic units comprising thin, silt- or mud-capped sand layers. Lien *et al.* (2003) and Abreu *et al.* (2003), in contrast, described these heterolithic units as mudclast gravels. Abreu *et al.* (2003) described also the thicker sand beds as massive, whereas Wynn *et al.* (2007) described them as comprising a lower massive division, often non-graded, and a planar parallel-stratified upper division (turbidites $T_{ab}$).

The Rehy meander belt is ~7.5 m thick and ~380 m wide, with the late-stage channel width of ~130 m (Elliott, 2000). The sand beds in outcrop section are sigmoidal lenses thinning both updip and downdip and downlapping the LAP's basal palaeo-horizontal erosional surface. The beds are dipping at 8–12° towards the last-stage channel and extend laterally for ~85 m. The bedding architecture involves thinning-upwards sets to inclined parallel beds separated by truncation surfaces, occasionally onlapped by a relic set of subhorizontal beds. One of the LAP bedsets is reported by Elliott (2000) to show slump folding. The massive or massive-to-stratified sand beds imply episodic deposition from high-density turbidity currents. The relatively thick intervening units of heterolithic deposits indicate a predominance of relative small, discrete low-density flows (Elliott, 2000). However, if

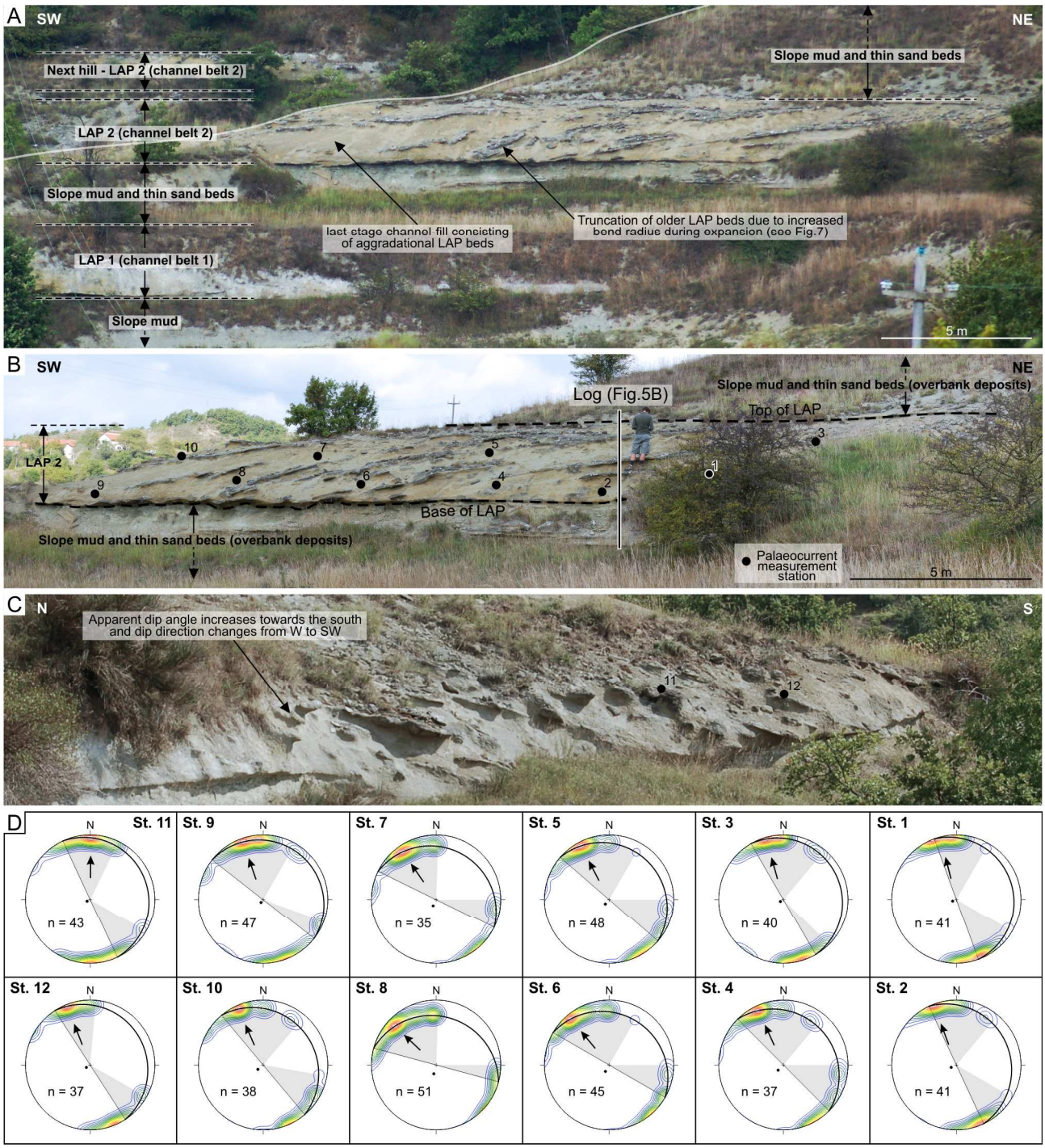


**Fig. 6.** Example of a point-bar composed of sand beds (LAP example 2 in Table 1), Piedmont Basin, Italy. (A) The channel belt 2 is part of a meander-belt complex exposed in several adjacent hills and comprising point bars, last-stage channel-fills and inter-channel overbank deposits. Note the internal truncation in LAP 2 and the gradual flatting of beds in the last-stage channel-fill. (B) The SW–NE outcrop section of LAP 2 with indicated measurement stations of the bedding attitude and palaeocurrent direction. The log is shown in Fig. 5B). Note the undulating horizontal base of the LAP, reflecting incremental lateral migration of the channel thalweg. (C) The N–S outcrop section of LAP 2, showing additional measurement stations and a lateral increase in bedding inclination towards the south; the bedding strike is nearly parallel to the outcrop strike in the northern part of the section. (D) Measurements of the LAP bedding attitude and the corresponding palaeocurrent directions from stations 1–12, plotted in upper-hemisphere stereographic projection ($n$ = number of data in their local sets). The local transport directions vary from nearly strike-parallel to deviated updip.

the intervening units are indeed composed of mudclast gravel, the point bar would appear to have been formed by a more consistent series of higher-energy and high-density flows, some of them charged with locally-derived mudclasts.

### Point-bar LAPs composed of sand beds

This point-bar category is illustrated by the LAP example 2 (Table 1) from one of the many deep-water meander belts cropping out in the hills between the villages of Mioglia and Miogliola in NW Italy

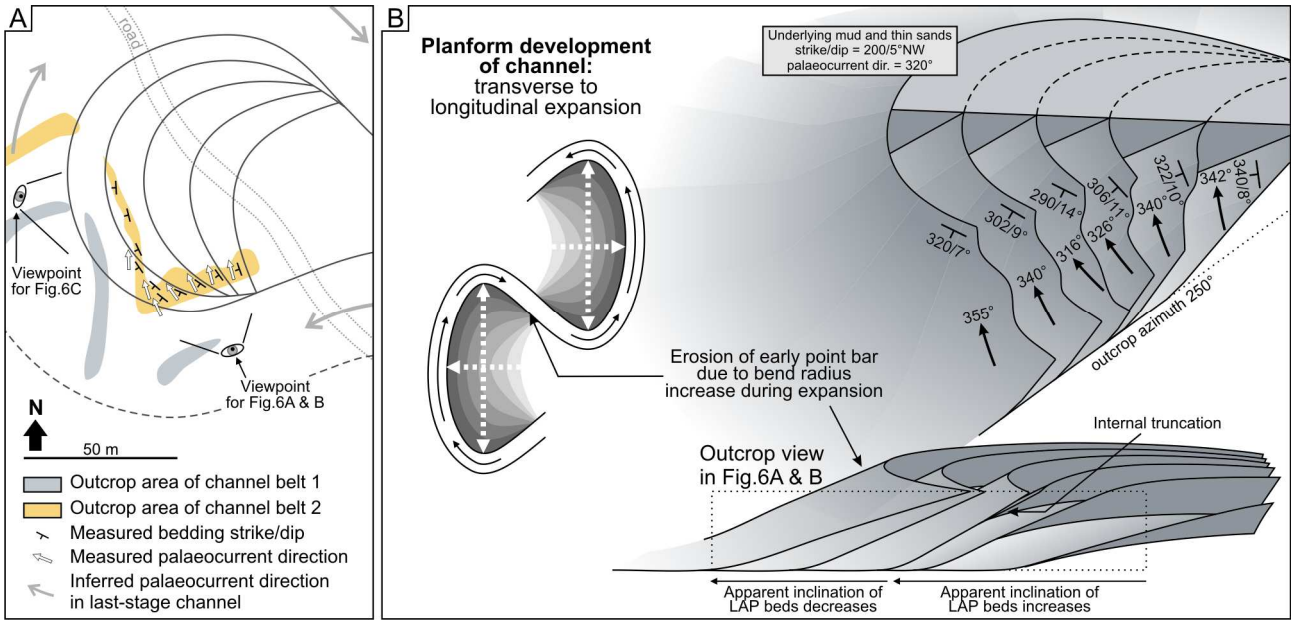


**Fig. 7.** (A) Interpretive horizontal slice through the upper part of LAP 2 (Fig. 6B, C), showing the measured local bedding attitude and mean palaeocurrent direction (Fig. 6D). The convergence of bedding strikes towards the upstream end of point bar (and perhaps similarly towards the downstream end) results in erosional truncation and a systematic bedding-dip shift towards the last-stage channel (see Fig. 6A, B). (B) Schematic 3D planform reconstruction of the LAP, showing the local bedding attitude and mean palaeocurrent directions in the outcrop section. The changes in bedding attitude suggest that the point bar evolved by transverse to longitudinal expansion.

*LAP example 2*

*Bedding geometry* – The point-bar LAP crops out on both sides of a narrow spur with walls trending NE–SW (70–250°) and N–S (350–170°) (Figs 6A–C & 7A). The meander-belt thickness is ~2.6 m and its apparent width is 35 m in the NE–SW outcrop wall and 45 m in the N–S wall. The LAP has a horizontal original top and also a broadly horizontal, slightly uneven erosional base. The LAP beds have thicknesses of up to 70 cm and dip angle of up to 16°, with dip direction in the range of 195–250°. The underlying, thinly-bedded heterolithic turbidites have an attitude of 200/5°NW, which served as an estimate of palaeo-horizontal reference level for measurement rotation.

The NE–SW outcrop section shows distinct lateral changes in the LAP bedding architecture. In the NE part of the outcrop, the LAP consists of sigmoidal beds that are thinning in the downdip or both downdip and updip direction and show an apparent decrease in dip angle towards the last-stage channel (Fig. 6A). This package of beds is truncated in the central part of the outcrop and followed by a package of updip-thinning sigmoidal beds whose apparent dip angle similarly decreases towards the last-stage channel. The last few beds in the SW part of the outcrop are very gently inclined and seem to be the initial, laterally-accreted part of the aggradational last-stage channel-fill. The same LAP exposed in the N–S outcrop section shows a progressive increase of the bedding dip angle towards the south (Fig. 6C). At the northern end of the section, the bedding strike is nearly parallel to the strike of the outcrop (Fig. 7A).

The measurements of bedding attitude, when corrected for tectonic tilt and plotted in plan view, reveal the following picture of the LAP architecture: The bed strikes in the NE part of the outcrop section converge towards the SE, whereas the strikes in the SW part tend to converge towards NW (Figs 6D & 7A, B). The change occurs at the apparent truncation unconformity in the mid-part of the NE–SW outcrop section (Fig. 6A). On the account of the northward flow direction (Fig. 6D), the planform evolution of the LAP can be attributed to a transition from transverse to longitudinal expansion of the channel bend (see Janocko et al., 2011b), with the internal unconformity marking the limit of transverse expansion and recording truncation of inner point-bar deposits (Fig. 7B).

*Sedimentary facies* – The LAP sand beds have erosional undulating bases and are normally graded and planar parallel-stratified (Fig. 5). Bed grain size ranges from very coarse to very fine sand, but shows little lateral change in the updip direction. However, the downdip parts of beds bear scattered small pebbles (size ≤ 2 cm) and/or shell fragments at the base, whereas their updip basal parts contain only scattered granules. The LAP is underlain by a composite, undulating subhorizontal sand layer ~10 cm thick, which is mainly parallel stratified, but locally massive and inversely graded, coarsening upwards from medium to very coarse sand with scattered small pebbles. The layer apparently represents an amalgamation of the downdip portions of LAP beds. The meander belt is encased in a flat-bedded heterolithic succession composed of normally-graded and stratified, fine- to very fine-grained sand sheets, 15–50 cm thick, alternating with massive or laminated mud layers 20–40 cm thick.

The LAP sand beds are considered to be tractional turbidites T*b*. The undulating basal layer is thought to be an amalgam of tractional deposits and inversely-

graded traction carpets (*sense* Lowe, 1982) formed at the downdip termini of LAP beds. The top-missing turbidites T*b* and the occurrence of traction-carpet deposits at the LAP toe indicate that the laterally-migrating channel was conveying large and powerful turbidity currents, bypassing most of their sediment load and occasionally becoming overcharged with sediment in the thalweg zone. The coarse-tail updip fining of beds reflects lateral reduction of flow competence on point-bar flank. The lack of mud cappings indicates that the bypassing flows followed closely one another or were erosive, removing mud. The surrounding heterolithic deposits are thought to be an overbank facies comprising hemipelagic mud interspersed with turbidites T*bc(d)* and T*c(d)* formed by waning low-density currents.

*Palaeocurrent pattern* – Palaeocurrent directions were measured on the basis of flute casts and imbricate gravel clasts at the bases of sand beds. The mean palaeoflow direction for the channel belt is towards the NNE (Smith, 1995). Directions measured in the LAP are in the range of 313–360° (Figs 6D & 7A, B) and those in the underlying overbank deposits have a mean of 320°. The $S_1$ eigenvalues for clast orientation datasets are in the range of 0.69 to 0.82, indicating high fabric strength. Palaeocurrent directions are obliquely up the LAP bedding surfaces (Figs 6D & 7A), deviating from bed strike by 5–33°. The deviation is up to 5° greater in the updip parts of LAP beds. The data indicate that the bedload transport at the channel bend was directed obliquely up the point-bar surface (Fig. 7B), with the particle paths increasingly steeper towards the bar top.

*Other examples*

An example of sandy LAP was described by Beaubouef *et al.* (2007) and Pyles *et al.* (2010) from the Beacon Channel in the Permian Brushy Canyon Fm., Texas. The LAP is only partly preserved, but has a subhorizontal erosional base and shows sigmoidal sand beds that thin in both updip and downdip direction, but are thickest in their lower parts. The beds show also internal updip differences. The lower parts of beds consist of planar parallel-stratified, medium to fine sand which becomes also through cross-stratified in updip direction before passing into a massive fusilinid rudite with fine-sand matrix. The thin uppermost parts of beds consist of fine sand and silt with plane-parallel stratification and ripple cross-lamination. The LAP beds are onlapped by a package of thin subhorizontal beds of very fine-grained, ripple cross-laminated sand and silt, probably representing the last-stage channel-fill. The LAP top and most of the channel-fill are truncated by an overlying channel belt.

The outcrop of Beacon Channel allowed Pyles *et al.* (2010) to reconstruct the channel-belt planform. The channel associated with the LAP was 103 m wide and at least 5 m deep, and had a sinuosity of 1.26 and bend amplitude of 149 m. Bedding-attitude measurements and outcrop correlations indicated that the channel underwent bend expansion combined with downstream translation. Palaeocurrent on the point-bar flank was directed obliquely downwards, which suggests a reverse flow helicoid rising against the outer bank.

Other documented examples of sandy point bars include: the Baumgardner quarry LAP in the Jackfork Group, Arkansas (Abreu *et al.*, 2003); LAPs in the Sobrarbe and Morillo formations of the Hecho Group, Spain (Crumeyrolle *et al.*, 2007); LAPs in the Gull Island Fm. exposed in the Ballybunion section and Moher Cliffs, Ireland (Martinsen *et al.*, 2000); LAPs in the Rinevella Point outcrop of the Ross Fm., Ireland (Sullivan *et al.*, 2000; Abreu *et al.*, 2003); and LAP in the Dad Sandstone Member of the Lewis Shale Fm., Wyoming (Slatt *et al.*, 2007). Sandy LAP-like features interpreted as possible deep-water point bars were also reported from the Ainsa-1 Channel quarry in the Pyrenean Foreland (Clark & Pickering, 1996; Wynn *et al.*, 2007) and the Solitary Channel in the Tabernas Basin, Spain (Wynn *et al.*, 2007). These packages in cross-section have palaeo-horizontal erosional bases and consist of sigmoidal, updip-fining stratified beds with varied geometry. The lowest parts of beds in some cases are massive and amalgamated, forming a uniformly massive basal part of the LAP (Abreu *et al.*, 2003). The height of these LAPs ranges from 0.5 to 10 m and their width from a couple of metres to tens of metres. Their facies architecture suggests lateral accretion by low-density turbidity currents, possibly much denser in the thalweg zone, and their planform development varies.

## Point-bar LAPs composed of mudclast gravel-sand couplets

This LAP variety is illustrated by the point-bar example 3 (Table 1) exposed in a beach cliff by the mouth of the Waikiekie stream in North Taranaki, New Zealand. The channel belt belongs to a base-of-slope turbiditic succession of the Late Miocene Mount Messenger Fm., Taranaki Basin (Arnot *et al.*, 2007), and occurs at the base of an erosionally confined, sandy channel-belt complex. This erosional palaeo-fairway is the upper part of a moderately wide (~1.7 km width) channel-belt complex set ~60 m thick. The channel belt cut across a slope-derived muddy slump unit and incised into the underlying channel-belt complex with similar sandy deposits (Fig. 8). It is overlain by sheet-like sandy turbidites and a complex of simple erosional (cut-and-fill) palaeochannels.

*LAP example 3*

*Bedding geometry* – The LAP is 6 m thick and its incomplete width exposed in the N-trending outcrop is 62 m (Fig. 8). The LAP has a horizontal original top and also its erosional base is horizontal in the northern half of the outcrop. In the southern half, the basal surface is uneven, showing undulations and first rising slightly and then falling towards the last-stage channel. The undulations are basal indentions reflecting incremental migration of channel thalweg by cut-bank erosion, with slight variation in scour depth.

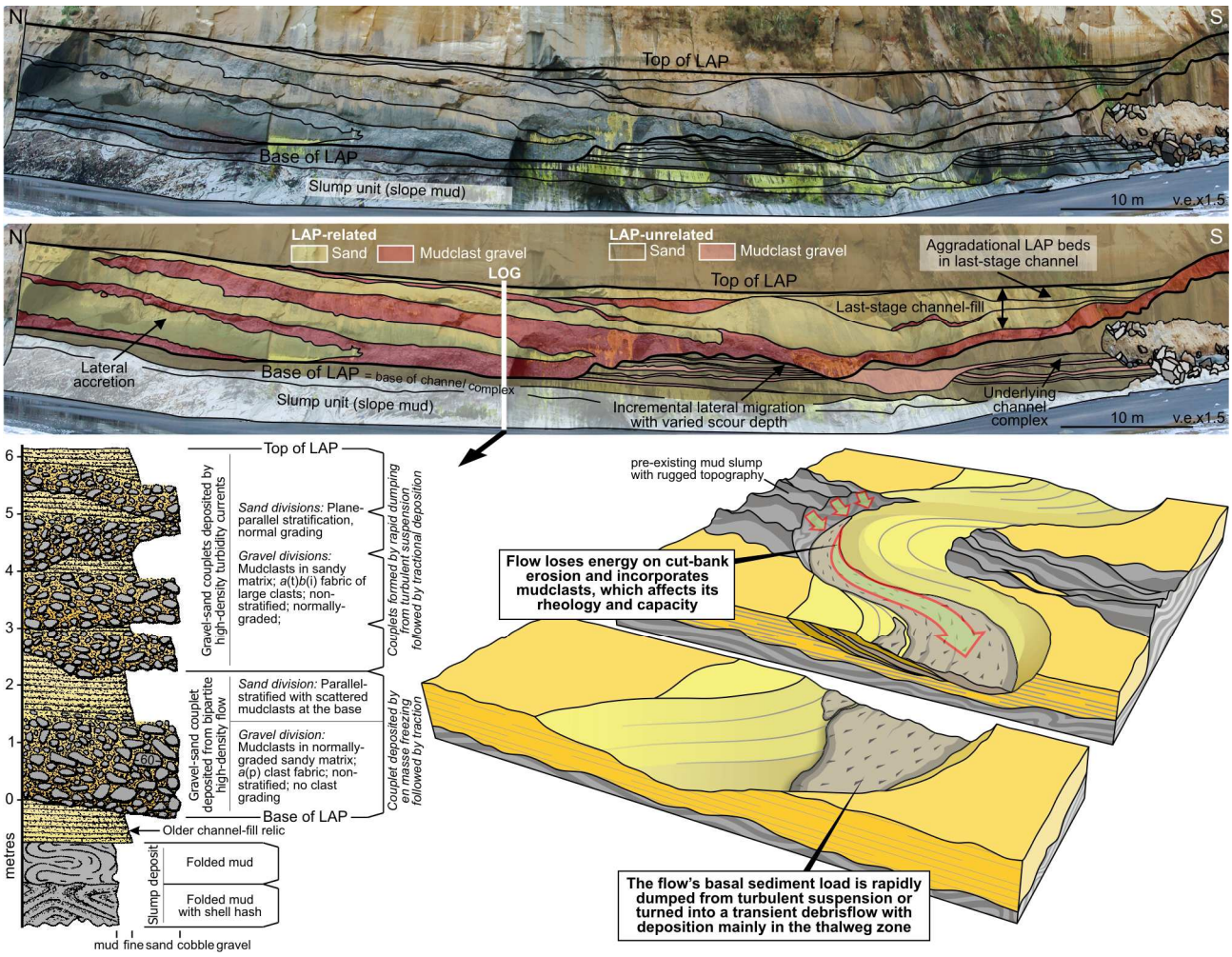


**Fig. 8.** Example of a point-bar composed of mudclast gravel-sand couplets (LAP example 3 in Table 1), Taranaki Basin, New Zealand. In the outcrop photomosaic (top) and the corresponding overlay drawing, note the tabular geometry and downdip thickening of mudclasts gravel divisions and thinning of sand divisions of the beds. The LAP's undulating base, originally subhorizontal, indicates incremental lateral migration of the channel thalweg. The log shows interpreted facies details and the blockdiagram shows the inferred origin of mudclasts gravel, derived from a mud-slump deposit cross-cut by the meandering channel.

The LAP consists of thick bipartite beds with erosional, undulating and locally loaded bases, each comprising a mudclast gravel division overlain by sand division (Fig. 8). The downdip parts of gravel divisions tend to be thicker, up to 1.5 m, and amalgamated. The sand divisions are up to 2.8 m thick and thinning downdip, truncated by the overlying bed and commonly also deformed by it in the pinchout part. The apparent dip of beds in the outcrop is 8°, decreasing slightly towards the last-stage channel. The bedding architecture of last-stage channel-fill (Fig. 8) shows aggradational lateral accretion of sand beds, which means a combination of lateral accretion and pronounced vertical aggradation leading to the channel abandonment.

*Sedimentary facies* – The gravel divisions of bipartite beds (see log in Fig. 8) consist of intraformational mudclasts and sandy matrix. They are massive, clast- to matrix-supported. Clasts are angular to subrounded, ranging in size from small pebbles to rip-up slabs up to 30 cm long. Matrix is fine to very fine sand, often visibly rich in disseminated mud. These divisions show normal grading in their updip parts, but are non-graded in the middle and downdip parts or locally showing crude coarse-tail inverse grading. Clast imbrication indicates an *a*(p)*a*(i) fabric. The sand divisions are normally-graded and planar parallel-stratified, showing a sharp contact to the underlying gravel, but a textural transition to its matrix. Both divisions show slight updip fining. The sand beds in last-stage channel-fill are similarly graded and stratified, but only the lowest beds include a subordinate, lenticular basal division of mudclast gravel. All beds lack mud caps.

The mudclasts are thought to have been derived from erosion of the underlying mud-slump unit, by channel incision and lateral migration. The mud debris would conceivably be derived and incorporated by flow in its thalweg zone. The debris was thus carried in the densest lower part of sand-laden turbidity current, raising its concentration and viscosity, suppressing turbulence and causing rheological flow bipartition. Upon the current deceleration at channel bends, its high-concentration load was then either dumped directly from turbulent suspension or deposited as a current-spawned, transient co-genetic debrisflow. The abundance of angular and subangular clasts indicates short transport, perhaps just over a couple of channel bends (see blockdiagram in

Fig. 8). The updip thinning of the gravelly divisions indicates that the rotating current at channel bend lacked sufficient competence to spread its heavy basal load evenly over the point bar flank.

The downdip pinchout of the upper sandy divisions is at least partly due to their differential erosion by subsequent flow, but may also indicate a more limited accretion of sand in the lower part of point-bar flank, since the thalweg zone would generally favour erosion and sediment bypass in the case of low-density current. This is evidenced by the LAP base formed as a roughly horizontal surface. The bipartite beds lack mud caps or relics of such, which suggests closely consecutive flows with little or no intervening deposition of mud.

The aggradational lateral-accretion filling of the last-stage channel indicates a decrease in flow discharges, although the lack of bed mud caps suggests that the flows followed closely one another. The last-stage flows were highly depositional and still plastering sediment on the inner bank, but were unable to erode the outer bank to maintain channel migration, thereby causing aggradation.

*Palaeocurrent direction* – The outcrop surface is too flat to allow measurements of exact bedding attitude and detailed palaeocurrent directions. The palaeo-fairway general trend is estimated at ~320° (Arnot *et al.*, 2007), but the bedding architecture, channel geometry and clast imbrication in the studied outcrop indicate local channel-belt trend towards the SW.

*Other examples*

One of the best-exposed LAPs made of mudclast gravel-sand couplets is in the outcrop of the Carboniferous Jackfork Fm. in the Big Rock quarry, Arkansas. A description of the LAP was given by Abreu *et al.* (2003). The meander belt is ~5 m thick and ~200 m wide, forming the upper part of an equally narrow (200–300 m width) channel-belt complex ~10 m thick. A third of channel-belt width is occupied by last-stage channel-fill. The LAP has an undulating base and flat top, originally horizontal. It consists of unconformably stacked sets of irregularly-shaped sigmoidal beds which are similarly bipartite, but whose mudclast gravel divisions are thickening and the upper sand divisions thinning in the updip direction. Bed inclination increases towards the last-stage channel, reaching 16°, and the channel-fill consists of sub-horizontal sand beds. Similar LAP deposits form the underlying meander belt. The high cliff outcrop is inaccessible on foot and facies details are unavailable, but the sand divisions are reportedly massive, attributed to high-density currents. The structure of mudclast gravel divisions is unspecified, but Abreu *et al.* (2003) interpreted them to be tractional deposits. Irrespective of the actual mode of sediment deposition, the flow-transverse partitioning of gravel and sand in this case is clearly different than in the LAP example 3, implying different flow conditions. The flows in the Big Rock case were apparently large and powerful enough to spread their mudclasts-laden basal load to the top of point-bar flank, while simultaneously eroding and bypassing sediment along the channel thalweg and also depositing relatively little in the adjoining lower part of bar flank. The mud debris was probably derived and carried by the turbidity current's head and deposited directly behind it. Sand would then be dumped rapidly from the current's decelerated body, with highest sediment concentration in the flow axial zone, whereas the low-concentration upper part and tail of the flow would virtually bypass the channel bend.

An example of LAP composed of mudclast-rich sand beds was reported by O'Byrne *et al.* (2007) from the Proterozoic Isaac Fm. The lower- to middle-slope channel belt, ~20 m thick and ~250 m wide, is exposed in the Castle Creek area of the Cariboo Mountains in British Columbia, Canada. The channel belt is incised in a succession of alternating thick packages of sand sheets and mud-rich, thin-bedded heterolithic deposits. The LAP consists of updip- and downdip-thinning sigmoidal beds downlapping its flat, originally horizontal erosional surface. Bed inclination increases towards the last-stage channel and reaches 12°. Beds near the last-stage channel show an aggradational lateral accretion, with 'gull-wing' shape at the channel margin, and the upper two-third of the channel is plugged with mud. The downdip parts of the LAP beds are normally-graded from granules to fine sand, massive to cross-stratified. The mean grain size decreases updip, where the graded beds are massive to planar parallel-stratified. Their thin upper tips are parallel-stratified to ripple cross-laminated. The sand beds have a laterally discontinuous basal division of clast-supported mudclast gravel, up to 1 m thick, and are capped with thin silt/mud layers or erosional relics of such. The beds have erosional bases and the LAP abounds in internal truncations, with angular bedding unconformities and common amalgamation of beds. Hydroplastic deformation is also common, including sand injections and slump folds.

O'Byrne *et al.* (2007) attributed the LAP to a repetitive cut-and-fill process with a systematic lateral offset of successive sinuous channels, mimicking one another. The LAP in this interpretation would then not be a point bar of laterally migrating channel, but rather a package of the laterally-stacked erosional relics of consecutive channel-fills (i.e., a multi-lateral channel-belt complex). However, the LAP has a flat common base and resembles deep-water point bars described here (LAP example 3) and by other authors (e.g., Abreu *et al.*, 2003; Eschard *et al.* 2003; Euzen *et al.*, 2007). Internal truncations and angular unconformities can be expected in point-bar LAPs, particularly when formed by flows with highly varied discharges, and are common in both fluvial (Willis, 1993; Bridge, 2003) and many deep-water meander belts (e.g., see the LAP examples 2 & 9; Elliott, 2000; Abreu *et al.*, 2003; Dykstra & Kneller, 2009). Deep-water meander belts generally lack levées and the levéed last-stage channel in the Castle Creek case might seem unusual. However, the development of last-stage channel commonly differs from the meander belt's previous evolution, and the

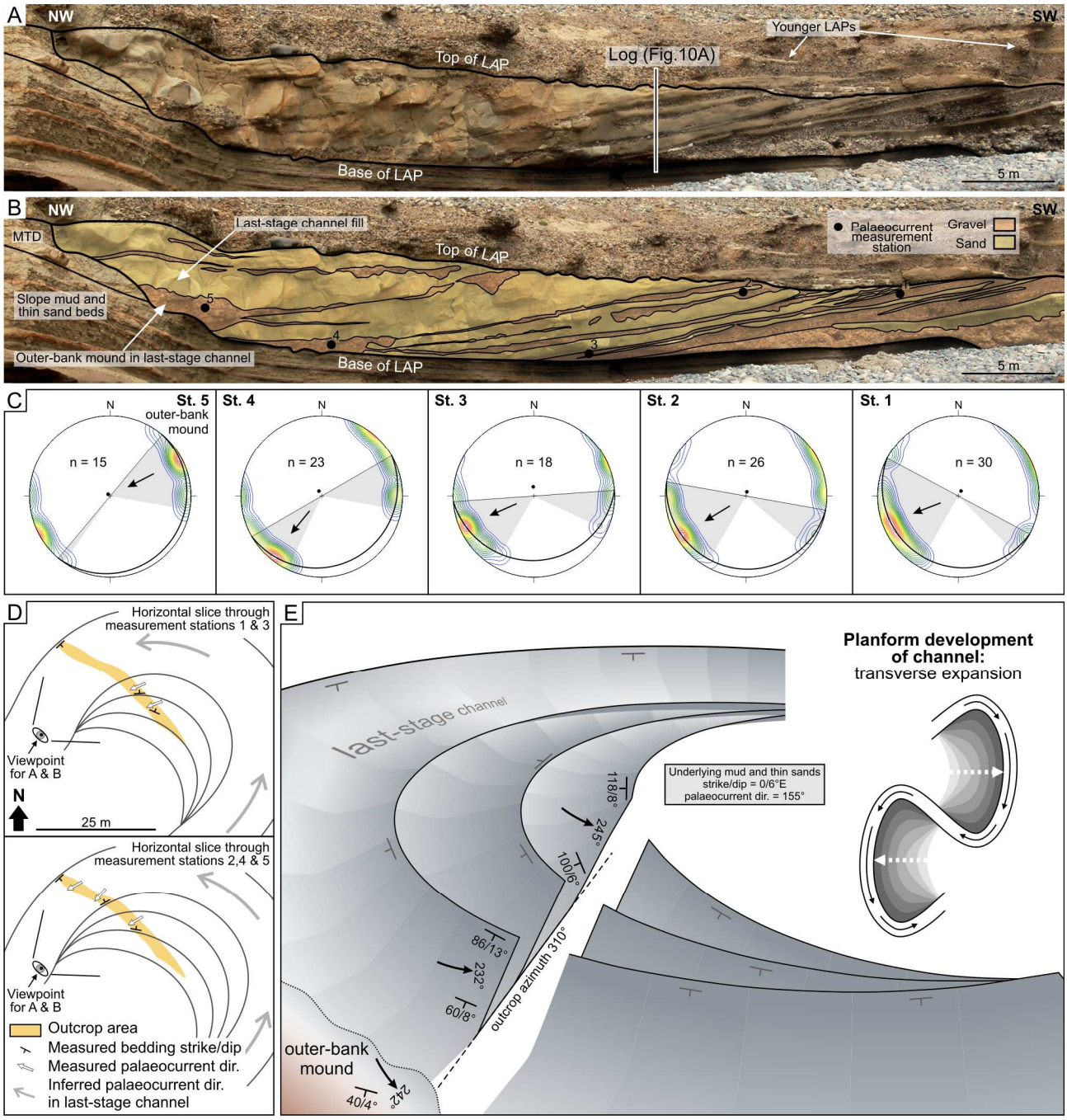


**Fig. 9.** Example of a point bar composed of gravel-sand couplets (LAP example 4 in Table 1), Rosario Fm., Mexico. (A) Outcrop photograph and (B) overlay drawing of the LAP. Note the location of measurement stations 1–5, the pockets of loaded gravel in the LAP upper part and the gravelly outer-bank mound in last-stage channel-fill. (C) Measurements of the LAP bedding attitude and the corresponding palaeocurrent directions from stations 1–5, plotted in upper-hemisphere stereographic projection (*n* = number of data in their local sets). Note that the prevalent direction of bedload transport is obliquely updip for the LAP beds, but different for the outer-bank gravel mound. (D) Interpretive horizontal slices through the lower and upper part of the LAP. The westward convergence bedding strikes (out of the outcrop) suggests point-bar transverse expansion. (E) Schematic 3D planform reconstruction of the LAP, showing the local bedding attitude and mean palaeocurrent directions measured in the outcrop section.

formation of levées may indicate little more than an increased aggradation. In short, there is no compelling evidence in the O'Byrne *et al.* (2007) description that would prevent the Castle Creek LAP from being interpreted as a point bar.

Another example of LAP belonging to the present category was described by Eschard *et al.* (2003) and Euzen *et al.* (2007) from the Late Cretaceous Pab Fm. of Pakistan. The meander belt is ~45 m thick and more than 200 m wide, forming the basal part of a thicker channel-belt complex. The LAP consists of mudclast gravel-sand couplets that vary from tabular to lenticular, thinning both updip and downdip. The beds are inclined at 10–15° towards the last-stage channel, and their mudclast gravel divisions are generally pinching out in updip direction. The LAP has aggradational lateral-accretion architecture and its erosional base rises towards the last-stage channel. The mudclast gravel divisions consist of angular mud debris and a sandy matrix, showing a clast-supported texture and normal

grading. Sand divisions are reportedly massive and non-graded, with local dewatering features and basal traction-carpet layers. The sand beds lack mud caps and are amalgamated in the absence of gravel division. The facies suggest deposition by high-density, closely successive turbidity currents or flows with multiple surges. The last-stage channel is poorly preserved, incised by an aggradational succession of levéed, cut-and-fill channels offset laterally relative to one another.

The earlier-mentioned LAP example from the Ross Fm. in the Rehy Cliffs of Ireland would also fall in the present category if the sand layers there are indeed coupled with mudclast gravel layers, as reported by Abreu *et al.* (2003) and Lien *et al.* (2003).

### Point-bar LAPs composed of gravel-sand couplets

Some of the best outcrops of LAPs composed of gravel-sand couplets are afforded by the Late Cretaceous Rosario Fm. in the San Fernando Canyon on the Pacific margin of Baja California, Mexico. The meander belts occur in the lower part of a large, mid-slope valley-fill trending N–S, confined by incision and external levées. The individual meander belts are encased in a succession comprising thick units of mud and silt, heterolithic packages of mud intercalated with thin sand sheets and gravel-sand beds, as well as heterolithic mass-transport deposits. Three selected cases (LAP examples 4–6 in Table 1) are presented here to illustrate this LAP category and show its variation. The first example, along with some adjacent other LAPs, was described by Dykstra & Kneller (2009), but the present study adds crucial details, particularly a more thorough analysis of palaeocurrent directions and their implications for flow pattern.

*LAP example 4*

*Bedding geometry* – This meander belt is ~2.6 m thick and ~35 m wide, exposed in a beach cliff trending NW–SE (130–310°) (Fig. 9A, B & D). It is cut in a heterolithic succession of thin (1–10 cm) mud, silt and sand sheets, whose mean bedding attitude (0/6°E) has been used as a reference palaeo-horizontal level. In the NW part of the outcrop, the meander belt also overlies erosionally a mass-transport unit of deformed thin sand-mud layers. The meander belt is overlain by another, comparable channel belt.

The LAP has a flat top and a flat erosional base roughly parallel to substrate bedding. It consists of tabular gravel-sand couplets 10–80 cm thick (Figs 9A, B & 10). Both the sand and particularly the gravel division in some beds are discontinuous, with the gravel forming lenses or loaded pockets. In the SE half of the LAP, the beds are inclined at up to 13° with dip direction in the range of 340–028°. Bed inclination decreases towards the last-stage channel, as the bed gravel divisions also become increasingly thicker in downdip direction. In the downdip part of one of the beds, its gravel division passes into a gravel mound that extends and thickening towards the stepped outer bank (Fig. 9A, B). The gravel planar stratification changes laterally from paralleling the LAP beds to dipping away from the outer bank. The overlying sand division has a sub-horizontal top and its thickness compensates for the irregular morphology of the gravel mound. The last-stage channel-fill shows aggradational lateral accretion of updip-thinning beds with decreasing inclination.

When plotted in a map view, the corrected strike directions of the LAP bedding converge increasingly towards the west, suggesting point-bar expansion (Fig. 9D). On the account of south-westerly flow direction (Fig. 9C), the LAP outcrop may thus be interpreted as a longitudinal section through the downstream part of an expansional point bar (Fig. 9E). Alternatively, it may be an oblique section through the downstream part of an expansional-translational or rotational point bar or possibly a point bar combining all three modes of planform transformation (Fig. 3).

*Sedimentary facies* – The LAP beds are bipartite, comprising extraformational polymict gravel and sand (Fig. 10A). Mud caps are lacking. The gravel divisions are normally-graded and planar parallel-stratified, with a clast-supported texture. Clasts are subrounded to rounded, of pebble to cobble size, and the matrix is sandy. Clast imbrication indicates a 'rolling' *a*(t)*b*(i) fabric. The sand divisions have a gradational contact with the underlying gravel and commonly contain scattered mudclasts in the lower part. The sand is normally-graded and shows plane-parallel stratification, often hydroplastically deformed and/or showing dewatering features. The gravel divisions are locally amalgamated at the LAP toe, forming a composite, coarsening-upwards basal layer ~20 cm thick. The individual beds show only slight updip fining, marked by a decrease in gravel mean size and the disappearance of mudclasts in sand division.

The stratified gravel-sand couplets are tractional deposits of low-density turbidity currents. Dykstra & Kneller (2009) estimated that the flows could be anywhere from 3 to 27 times thicker that the channel relief of ~2.6 m. Gravel was likely carried in the flow head and deposited when lagging behind it, whereas sand would be deposited from the flow body. The majority of transported gravel probably bypassed the channel bend, being only locally entrapped by loading in soft sandy substrate (see Nemec *et al.*, 1999, fig. 7). The lack of mud caps may be due to the bypass of flow tail or to subsequent erosion, but may as well indicate flows that followed closely one another. Both gravel and sand were spread sideways to the top of point-bar flank, and only the updip fining of gravel reflects a lateral reduction of flow competence on the bar-flank slope.

The gravel mound at the base of last-stage channel (Fig. 9B) is attributed to the deposition of coarse bedload against the outer bank – a process postulated for the formation of outer-bank bars (Nakajima *et al.*, 2009).

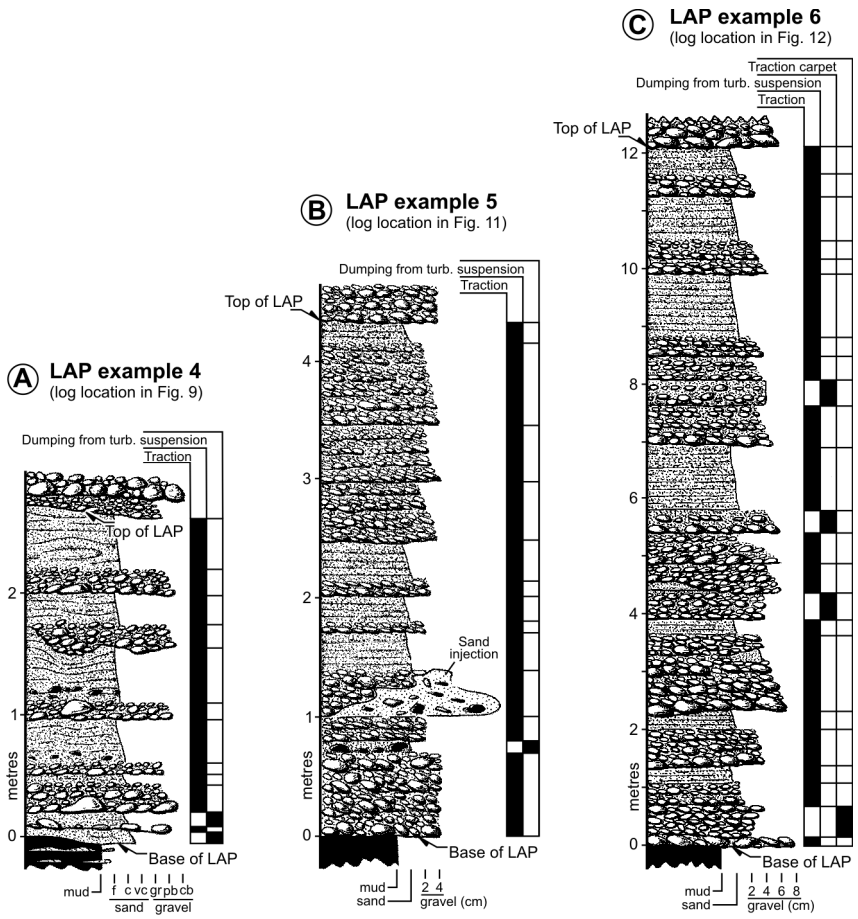


**Fig. 10.** Interpreted facies logs from the point-bar LAP example 4 (Fig. 9), example 5 (Fig. 11) and example 6 (Fig. 12); for comments, see text.

*Palaeocurrent pattern* – Local palaeocurrent directions were determined from imbricate clast fabric. The channel-belt axis was likely more-or-less parallel to the hosting valley (Dykstra & Kneller, 2009), which would mean a southerly trend. The underlying heterolithic deposits show indeed a mean palaeocurrent direction towards 155° (Dykstra & Kneller, 2009). The mean local palaeocurrent direction in the LAP outcrop, based on 112 measurements, is towards 240° (Fig. 9C), which can be attributed to the channel curvature (Fig. 9D). The strength of clast-fabric datasets is high, with the $S_1$ eigenvalues in the range of 0.74 to 0.81. The local palaeocurrent vectors in the LAP beds diverge from the corresponding bed strike by 20–48° towards the south, more strongly in the NW part of the outcrop section (Fig. 9C). The divergence in the downdip and updip parts of beds differs by 20–28°, with more southward skewness in the updip parts. Taken together, the data indicate that the bedload transport direction at the channel bend was obliquely up the point-bar flank (Fig. 9E) and increasingly deviated from the channel axis towards the bar top (Fig. 9D). This evidence implies a flow helicoid rising against the inner bank at the meander bend.

However, the clast fabric of the outer-bank gravel mound in last-stage channel indicates local palaeocurrent direction towards 242° (Fig. 9C, E), which means that the depositing flow in this instance was rising against the outer bank.

*LAP example 5*

*Bedding geometry* – This meander belt is exposed in two adjoining outcrop walls trending NE–SW (50–230°) and NNW–SSE (160–340°) (Fig. 11A, B & D). The channel belt is incompletely preserved, as its top and margins were eroded by the overlying channel-belt complex. The belt's maximum preserved thickness is 4.3 m, and its apparent widths exposed in the two outcrop walls are 15 m and 10 m, respectively. The LAP has an erosional base roughly parallel to the bedding attitude (350/4°E) of the underlying heterolithic succession of sand-mud sheets 5–20 cm thick, used as an estimate of palaeo-horizontal reference level.

The LAP in outcrop section consists of sigmoidal beds up to 1 m thick, thinning either downdip or updip or in both directions (Fig. 11A, B). Both the gravel and the sand divisions of beds are generally thinning in downdip direction, with local deformation due to loading, and the sand often also pinches out updip. The inclination of beds increases from 3° to 12° towards the (unpreserved) last-stage channel and their dip direction varies randomly in the range of 240–288° from one bedset to another.

The corrected measurements of bedding strike in plan view suggest that the development of the point-bar LAP involved several episodes of meander-bend expansion and translation (Fig. 11D), which is consistent with the cross-sectional geometry of the LAP beds. On the account of the SSE trend of channel belt (Fig. 11C), the

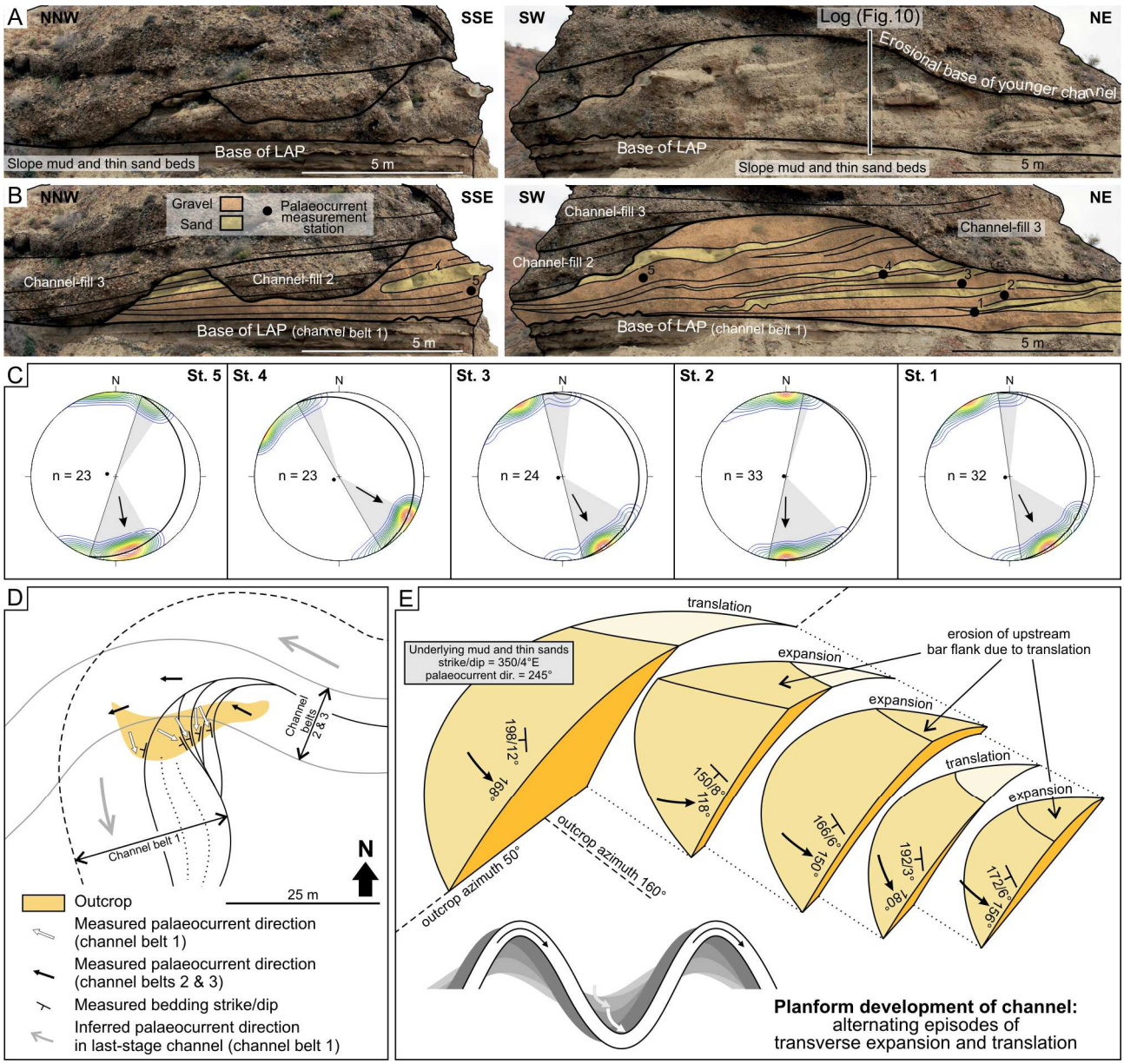


**Fig. 11.** Example of a point bar composed of gravel-sand couplets (LAP example 5 in Table 1), Rosario Fm., Mexico. (A) Outcrop photographs and (B) overlay drawings of the LAP. Note that the sand beds in cross-section are updip-thickening or symmetrical lenses and that the LAP lower part consists mainly by gravel beds. Local measurement stations are numbered 1–5. (C) Measurements of the LAP bedding attitude and the corresponding palaeocurrent directions from stations 1–5, plotted in upper-hemisphere stereographic projection ($n$ = number of data in their local sets). Note that the prevalent direction of bedload transport is obliquely updip for the LAP beds. (D) Interpretive horizontal slice through the LAP. The bedding strikes vary, but diverge to the south (out of the outcrop) and suggest point-bar expansion combined with episodic translation. (E) Schematic 3D planform reconstruction of the LAP, showing the local bedding attitude and mean palaeocurrent directions measured in the outcrop section. The geometry of bed sets is a result of the meander-bend expansion or translation regulated by erosion.

pattern of bedding strike (Fig. 11D) and the lateral change in bedding dip angle (Fig. 11A, B), the NE–SW outcrop wall may be a longitudinal section through the downstream end of a point bar combining expansion and translation (Fig. 11E).

*Sedimentary facies* – The LAP beds are gravel-sand couplets lacking mud caps (Fig. 10B). Their lower division consists of pebble-grade polymict extraformational gravel, subrounded to rounded, with a medium-sand matrix. The gravel commonly shows normal grading, plane-parallel stratification and a tractional $a$(t)$b$(i) fabric. The sand division is generally thinner and laterally less continuous (Fig. 11A,B) or is virtually missing in some beds. The sand is normally-graded and planar parallel-stratified. The gravel/sand contact is rather sharp, although the sand divisions locally bear scattered small pebbles and intraformational mudclasts in the lower part. The updip fining of beds is weak, recognizable only by a lateral decrease of maximum clast size in the gravelly divisions and the disappearance of gravel clasts in the sand divisions. The flat-bedded heterolithic deposits below the meander belt are sheets of planar parallel-stratified to ripple cross-laminated, fine to very fine sand capped with massive or sporadically laminated silt and mud.

The LAP beds are tractional deposits of low-density turbidity currents, which were large and powerful enough to spread both sand and pebble gravel to the top of the point-bar flank, despite some lateral reduction of the flow competence. The sharp bipartition of beds suggests that gravel was likely deposited directly behind the flow head and sand was subsequently emplaced from the overpassing flow body, which was entraining small pebbles and carrying locally-drived mudclasts. The lack of mud caps suggests closely successive or multi-surge flows, although the erosional bases of amalgamated LAP beds indicate that mud caps and cross-laminated bed tops, if originally present, might possibly be removed by erosion.

*Palaeocurrent pattern* – Local palaeocurrent directions were measured from gravel clast fabric. Based on 135 measurements, the mean paleocurrent direction for the point-bar LAP is towards 155° (Fig. 11C, D). The $S_1$ eigenvalues of individual datasets are in the range of 0.71–0.90, indicating high fabric strength. The bedload palaeocurrent directions are obliquely updip with respect to the bedding plane (Fig. 11C, D & E), deviating from bed strike by 12–30°, which indicates a rotating flow helicoid rising against the inner bank. The overall variation of palaeocurrent directions in the LAP is 60°. Measurements based on ripples and flutes in the underlying sheet-like turbidites indicate mean transport direction towards the SW (245°).

*LAP example 6*

*Bedding geometry* – This meander belt (Fig. 12) crops out in a mountain side trending NNE–SSW (030–210°) and is ~12 m thick and >200 m wide, but only its 80-m section – including the last-stage channel-fill – is well-exposed and described here. The channel belt is underlain by slope mud interspersed with thin sheets of silt and sand turbidites, whose structural attitude (355/8°E) has been used as an estimate of palaeo-horizontal reference level. The LAP base is erosional and slightly aggradational, showing several rising steps (Fig. 12A, B) formed by an incremental thalweg migration. The LAP top is the erosional base of an overlying channel belt, deepening slightly towards the NE.

The LAP in cross-section consists of updip- and downdip-thinning sigmoidal beds, up to 1.5 m thick, comprising gravel and sand divisions. In the early (SSW) part of the LAP, the gravel divisions tend to be amalgamated in the basal part and are thinning in the updip direction, where they are overlain by sand divisions that are thinning and pinching-out downdip (Fig. 12A, B). The sand divisions are often deformed and laterally discontinuous. In the later part of the LAP, the gravel divisions are thinner and virtually lacking in the uppermost part. The beds here are capped with silt and mud, and pinching out towards the last-stage channel. The channel-fill consists of mud intercalated with the pinch-out toes of LAP sand beds.

The outcrop is a steep cliff and the bedding attitude was possible to measure only from the lower part of the LAP. The beds here are dipping at 5–16° towards the ENE (52–80°). It is also apparent from the outcrop that the LAP beds are steepening towards the last-stage channel (Fig. 12A, B). The bedding strike measurements, corrected and plotted in map view, appear to converge towards the NW (Fig. 12D). On the account of the southward flow direction (Fig. 12C, D), the steepening of LAP beds towards the last-stage channel and their changing strike, the outcrop may be interpreted to be a longitudinal section through the upstream end of an expansional point bar (Fig. 12E).

*Sedimentary facies* – The majority of LAP beds are bipartite, comprising a gravel division overlain by sand division (Fig. 10C). Bed bases are erosional and locally deformed by loading. The gravel divisions are laterally less extensive, lenticular or virtually lacking in the last-deposited few beds. Gravel clasts are rounded to well-rounded, with a mean size of 3 to 12 cm. Matrix is coarse/medium sand. The gravel is mainly normally-graded, weakly parallel-stratified and showing tractional *a*(t)*b*(i) fabric, but in some beds is massive, graded or non-graded, and appears to be inversely graded in the thin downdip parts of many beds. The sand divisions are normally-graded, massive and/or planar parallel-stratified, occasionally bearing scattered small pebbles and mudclasts. Updip fining is shown mainly by the gravel divisions. The surrounding deposits are massive mud interspersed with thin sheets of ripple cross-laminated sand and silt, commonly deformed by loading.

Most of the LAP gravel-sand couplets are tractional deposits of low-density tubidity currents, spread across the height of point-bar flank. However, some flows were decelerated abruptly enough at the channel bend to dump gravel directly from turbulent suspension, or to generate a traction carpet or a transient debrisflow overriding the point-bar toe. The updip fining of gravel reflects a lateral decline of flow competence on the bar flank. The lack of mud caps may be due to closely-successive flows or erosion, as the last few beds are capped and indicate discrete, isolated flows.

*Palaeocurrent pattern* – Palaeocurrent measurements (126 data) indicate channel-belt trend towards 180° (Fig. 12C, D), parallel to the host valley (Dykstra & Kneller, 2009). Flute casts in the underlying heterolithic turbidites show transport direction to the SE (150°). The strength of gravel fabric in the LAP beds is relatively low, with the $S_1$ eigenvalues of 0.60 to 0.79. The local palaeocurrent directions vary by 36° and deviate by 14–22° updip from the bed strike (Fig. 12C–E), indicating a rotating flow helicoid rising against the inner bank (Fig. 12E). The oblique transport directions are towards the SSE at the LAP toe, but diverge by 8–34° towards SSW in its updip part, which indicates a corresponding increase in flow-transverse velocity component.

*Another example*

A detailed description of another LAP with gravel-sand couplets in the Rosario Fm. was given by Dykstra & Kneller (2009). The meander belt is ~5 m thick and

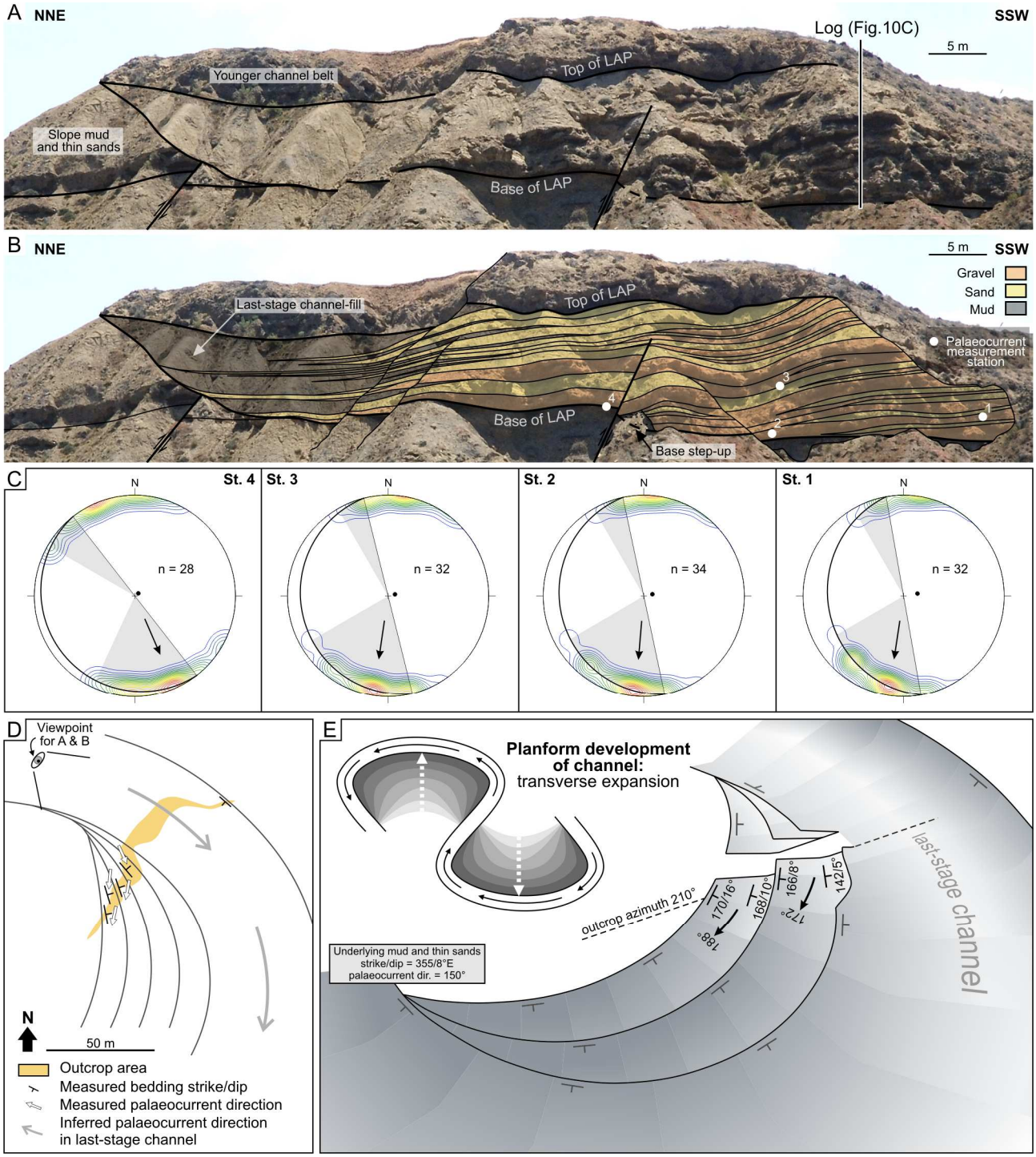


**Fig. 12.** Example of a point bar composed of gravel-sand couplets (LAP example 6 in Table 1), Rosario Fm., Mexico. (A) Outcrop photograph and (B) overlay drawing of the LAP. Note that the gravel divisions of beds predominate in the LAP lower part and many thicken downdip before abruptly pinching out, whereas sand divisions predominate in the last-stage channel-fill. The log is shown in Fig. 10C. Local measurement stations are numbered 1–4. (C) Measurements of the LAP bedding attitude and the corresponding palaeocurrent directions from stations 1–4, plotted in upper-hemisphere stereographic projection (*n* = number of data in their local sets). Note that the prevalent direction of bedload transport is obliquely updip for the LAP beds. (D) Interpretive horizontal slice through the LAP lower part. The northward convergence of bed strikes (out of the outcrop) suggests transverse expansion of meander bend. (E) Schematic 3D planform reconstruction of the LAP, showing the local bedding attitude and mean palaeocurrent directions measured in the outcrop section.

~60 m wide, exposed in an outcrop trending NW–SE stratigraphically below our LAP example 4. It is cut in sheet-like deposits comprising gravel and gravel-sand beds, interpreted to be the aggradational fill and levée of an older channel belt. The LAP top is originally horizontal, whereas its erosional base is rising gently towards the last-stage channel on the NW side of the outcrop. The LAP consists of two successive bedsets separated by an erosional angular unconformity. The first set comprises south-striking beds inclined at 6–8° to the west, whereas the second set consists of west-striking beds inclined to the north and significantly

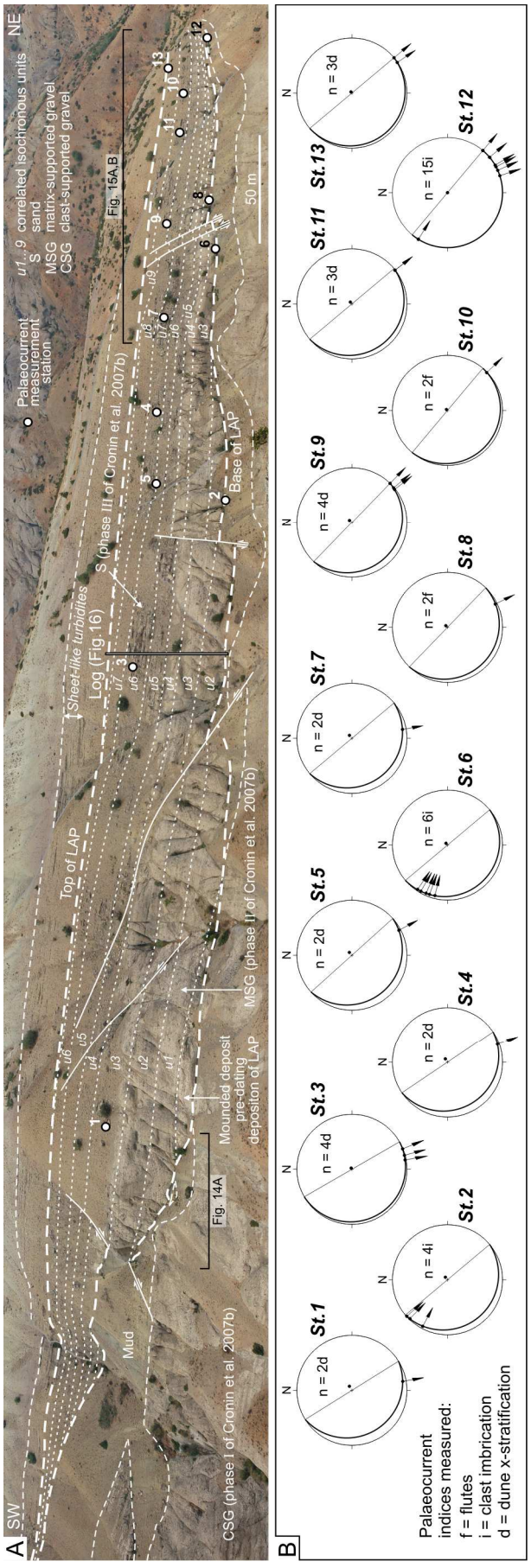


**Fig. 13.** Example of a point bar composed of beds with dip-segregated gravel and sand (LAP example 7 in Table 1), Elaziğ Basin, Turkey. (A) Outcrop photograph with an overlay line-drawing showing the successive accretion units of the LAP (labelled *u*1-*u*9). The lateral accretion is more apparent towards the NE, where the LAP erosional base is also stepping up due to the incremental lateral migration and decreasing scour depth of the channel thalweg. Note the location of local measurement stations 1–13. (B) Measurements of the LAP bedding attitude and the corresponding palaeocurrent directions from stations 1–13, plotted in upper-hemisphere stereographic projection (*n* = number of data in their local sets). Note that the prevalent direction of bedload transport is strike-parallel or obliquely updip in the LAP beds, but obliquely downdip in the thalweg deposits.

steeper (~12°). Beds in the first set are updip- and downdip-thinning sigmoidal lenses followed towards the NW by mainly updip-thinning ones, whose extended subhorizontal toes are stacked aggradationally upon one another instead of downlapping the LAP basal surface. The updip tips of gravel divisions are horizontal, interfingering with flat-bedded sand. The bedset is gently truncated towards the north and followed by the second set, whose beds are thinning updip and downdip-steepening, downlapping the LAP's gently rising basal surface. As a result, the beds are stacked in an aggradational manner, filling the channel to its top.

The channel-belt local trend is towards the SW (222°) and the palaeocurrent direction of the majority of beds, particularly in their second set, is obliquely updip. The LAP gravel beds and gravel-sand couplets show normal grading and plane-parallel stratification, and the sand divisions are often deformed by loading. Although Dykstra & Kneller (2009) describe the inclined beds as being coarsest in their middle section and fining both updip and downdip, our own observation from the outcrop is that the mean grain size of the majority of beds decreases consistently in the updip direction. The LAP as a whole is also fining laterally towards the last-stage channel.

The LAP is considered to be a point bar formed by the lateral migration of a single sinuous channel. Dykstra & Kneller (2009) interpreted the lateral change in bedding attitude across the LAP as an indication of the channel-bend downstream translation combined with expansion. Alternatively, the erosional truncation of the first bedset with an abrupt change in the bedding strike and higher inclination may be attributed to changes from point-bar expansion (lateral accretion of sediment) to translation (bar upstream erosion) and back to expansion. The gently rising base of the LAP and its lateral fining indicate that the flows were becoming less competent, gradually filling the channel, as in many other LAP cases (e.g., Figs 6, 8 & 9). The LAP sedimentary facies indicate tractional deposition by low-density currents. Palaeocurrent data indicate bedload transport obliquely up the point-bar surface, suggesting a flow helicoid rising against the inner bank.

**Point-bar LAPs composed of dip-segregated gravel and sand**

The point-bar LAPs of this category consist of beds that show striking downdip segregation of gravel and sand, often at a similar height. A detailed description is given for the LAP example 7 (Table 1), and another illustrative example is only briefly described.

*LAP example 7*

This channel belt occurs in the Eocene Kırkgecit Fm. of the Elazığ Basin, eastern Turkey (Table 1), and belongs to a topographically confined channel-belt complex formed on a deep-water slope terminated by submarine high – a setting characterized by slope flattening, increased channel sinuosity, flow overspill and possibly confluences or bifurcation of channels (see Mayall & Stewart, 2000). The sedimentary body was originally interpreted as two vertically-stacked cut-and-fill levéed channel belts, the lower gravelly with flat-bedded aggradational architecture and the upper sandy with evidence of lateral accretion (Cronin *et al.*, 2000, 2007b). Our field study has led us to reinterpret the bipartite sedimentary body as the meander belt of a single, erosionally-confined aggradional channel, whose LAP shows pronounced downdip segregation of gravel from sand. The channel belt is underlain by thin-bedded heterolithic turbidites and locally also cut in the older cobble gravel (phase-1 deposits of Cronin *et al.*, 2007b) interpreted by the latter authors as a deep-water complex of braided channel-belts. The LAP is overlain by a fining-upward succession of sand sheets capped with mud.

*Bedding geometry* – The channel belt is ~60 m thick and ~1200 m wide, exposed in an outcrop section trending NNE–SSW (026–206°). Buried low-amplitude normal and reverse faults indicate a declining syndepositional tectonic deformation (Fig. 13A). The belt is trending to the SE and the measured dip of its LAP bedding is 3–10° towards the NW (40–58°) (Fig. 13B). The structural attitude of the covering turbidite sheets is 230/20°NW, taken as an estimate of palaeo-horizontal reference level. The erosional base of the wide channel belt is stepped at both margins, but rising much steeper at the southern margin, where also the LAP bedding appears to be subhorizontal and highly aggradational (Fig. 14A). The LAP's northward accretion becomes apparent ~300 m away from the southern margin, where the sigmoidal bedding visibly increases its inclination before flattening again in downdip direction and onlapping the northern margin (Figs 13A & 15A, B). The LAP thus consists of broadly sigmoidal, updip- and downdip-thinning beds showing aggradation lateral accretion. Notably, the bed bases fit neatly into the rising steps of the basal surface at the northern margin, whereas the analogous steps at the southern margin seem to be unrelated to the onlapping beds, suggesting burial of a pre-existing erosional topography (Fig. 14B).

The stepped southern margin is thus interpreted to have recorded the initial stepwise down-cutting of channel (Fig. 14B). Channel meandering commenced at the subsequent stage of aggradation, when the flows in the down-cut channel started to erode the outer (N) bank while depositing sediment at inner (S) bank and burying it. The meandering channel was probably much smaller in relief than the primary down-cut conduit (~60 m deep), since the height span of the LAP's individual sigmoidal beds does not exceed 15 m. The secondary meandering conduit was aggrading while actively migrating by bend expansion. The basin was tectonically active and the change from channel-belt degradation to aggradation might have been caused by uplift of the adjoining structural high, which would raise the slope base and trigger channel back-filling.

The base of the channel belt in the southern part of the outcrop is covered with a flat-lying mounded gravelly unit, ~100 m wide and ~5 m thick (Fig. 13A), considerably coarser than the overlying LAP deposits. This basal unit is thought to comprise the lag deposits of bypassing flows in the down-cut channel, accumulated prior to the LAP development. The channel-belt base at the southern margin is also overlain by bank-derived slump deposits, apparently emplaced at the stage of channel down-cutting and bank steepening.

The corrected strike measurements of the LAP bedding in map view are alternating in their downstream convergence and divergence (Fig. 15C). The dispersion of bed strikes is low, and the outcrop is thought to be an oblique section through the point bar's central part (Fig. 15C, D). The planform development of the point bar is attributed to the channel-bend transverse expansion combined with episodic upstream rotation (Fig. 15D).

*Sedimentary facies* – The basal mounded unit (Fig. 13A), interpreted as amalgamated lag deposits of the primary down-cut channel, consists of the erosional uneven layers of crudely stratified, sandy cobble to pebble gravel and pebbly very coarse sand with scattered cobbles and boulders. The beds in the overlying LAP units u1 and u2 (Fig. 13A) are normally-graded and planar parallel-stratified, composed of sandy pebble gravel in their downdip parts and pebbly sand in the updip parts. The gravel is extraformational and polymict, subangular to subrounded, with a mean clast size of 3 cm and maximum size of 40 cm and with a matrix dominated by very coarse sand and granules. Clast fabric is tractional, of *a*(t)*b*(i) type. The gravel pinches out updip, giving way to sand that is also very coarse-grained, bearing granules and small pebbles.

In the subsequent units u3–u8 (Figs 13A & 15A, B), the LAP beds similarly consist of dip-segregated gravel and sand, but the textural separation occurs at a variable height and also the gravel size varies (Fig. 16). The downdip parts of beds are similarly composed of normally-graded, parallel-stratified sandy pebble gravel, which grades updip into pebbly very coarse sand before passing abruptly into trough cross-stratified very coarse sand with scattered pebbles and sporadic small cobbles. The sand becomes finer-grained farther updip, pinching

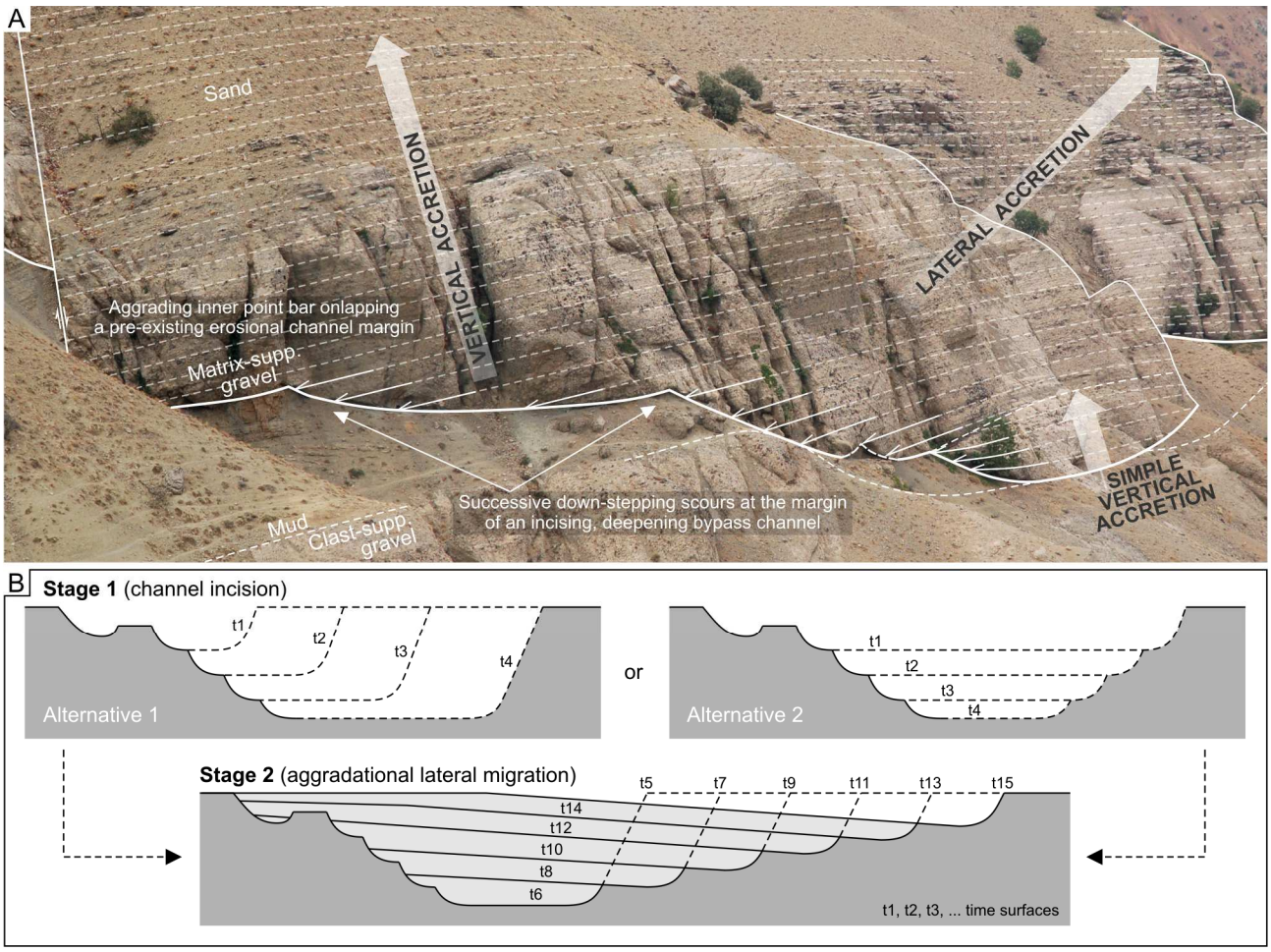


**Fig. 14.** (A) An oblique close-up view of the SW inner margin of LAP 7 (Fig. 13). Note that the LAP beds are aggradational, onlapping the stepped erosional margin, but show lateral accretion towards the NE. (B) Schematic interpretation of the LAP development: stage 1 – an erosional growth of channel by incremental down-cutting, forming a stepped erosional base (two alternative possibilities); and stage 2 – the infilling of the channel by lateral accretion with the thalweg zone migrating incrementally while reducing its scour depth. The channel effectively becomes shallower and narrower and is eventually filled and abandoned.

out in the thin-bedded subhorizontal heterolithic deposits of the aggrading point-bar top (Fig. 15A). The LAP unit u9 is only locally exposed, but its beds seem to resemble the underlying ones. The stratified LAP beds indicate deposition from low-density turbidity currents, fully turbulent and powerful enough to carry cobble gravel in traction.

The aggradational character of the LAP suggests that the channel-conveyed flows were depositional and resulting in net aggradation, yet capable of eroding the outer bank and causing lateral migration of the sinuous channel. This apparent paradox is explained by the LAP beds, showing concurrent lateral deposition of gravel and sand. It was probably the flow head that was doing the erosional work, whereas the flow body was depositing sediment – with the lateral segregation of gravel and sand reflecting the lateral decrease in flow competence on the point-bar flank. The updip termini of LAP beds are capped with mud, which indicates discrete erosive flows.

*Palaeocurrent pattern* – The measurements of palaeocurrent direction were based on the imbricate gravel fabric, flute casts and the bedding-plane exposure of trough cross-strata sets or dune forms. Based on 56 measurements (Fig. 13B), the mean palaeoflow direction in the outcrop is towards 146° (Fig. 15C), with a bulk dispersion of 56°. The underlying heterolithic turbidites and remnant older channel belt similarly indicate a mean palaeocurrent direction towards the SE (152°). However, the LAP local directions of bedload transport are highly varied (Fig. 13B). In most beds, the gravel fabric, flutes and sand dunes indicate a consistent oblique updip transport, deviating by 2–30° from the bed strike and suggesting a rotating flow rising against the inner bank. The clast fabric in thalweg gravel deviates locally by 10–26° towards the outer bank, indicating an oblique reverse flow in the outer thalweg zone.

*Another example*

A similar point-bar LAP, composed of beds showing downdip segregation of sand and gravel, is exposed in the Eocene Makarska Flysch of southern Croatia (Fig. 17). The outcrop has a E–W orientation and the meander belt is trending towards southwards. The meander belt is ~6 m thick and ~40 m wide, with a nearly flat top and a gently concave-upwards base rising towards the last-stage channel. The meander belt is

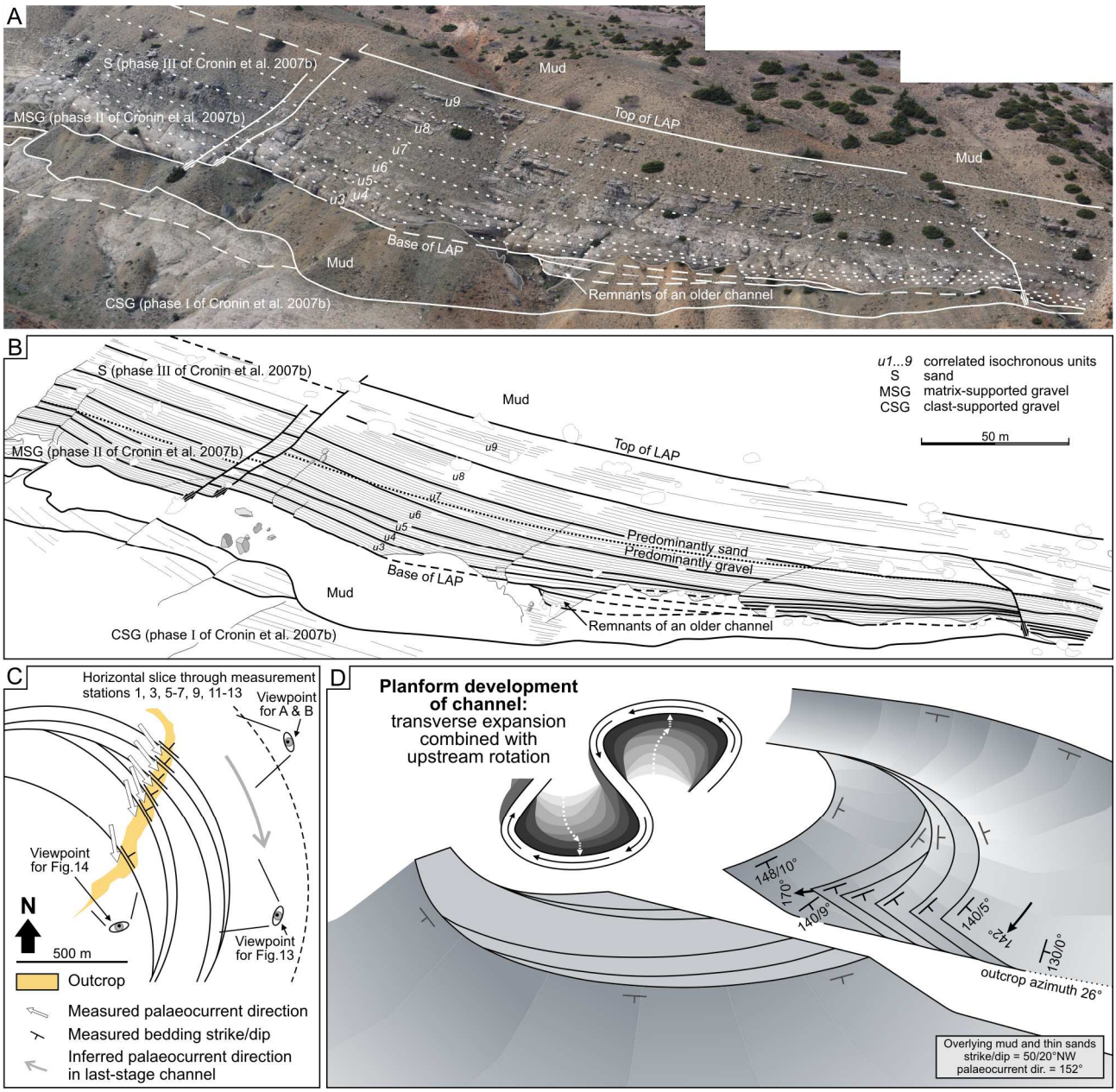


**Fig. 15.** (A) An oblique close-up view of the NW outer margin of LAP 7 (Fig. 13). Note that the LAP beds show aggradation, onlapping the rising erosional base of the meander belt. (B) The corresponding overlay line-drawing of the LAP bedding architecture. Note that the gravel-sand lithofacies boundary is diachronous, crossing the LAP bedding. (C) Interpretive horizontal slice through the LAP upper part. The divergence of bed strikes towards the SE (out of the outcrop) suggests channel-bend transverse expansion combined with upstream rotation . (D) Schematic 3D planform reconstruction of the LAP, showing some the local measurements of the bedding attitude and mean palaeocurrent directions from the outcrop section.

encased in a muddy slope succession interspersed with thin sandy turbidites, locally deformed by slumping. In the vertical section, the sigmoidal LAP beds are normally-graded and thinning updip, composed of crudely stratified pebble gravel passing abruptly updip into planar parallel-stratified, medium to fine sand. The laterally-accreted beds are generally conformable, only locally separated by gentle erosional unconformities. The consistent lateral segregation of sand and gravel renders the downdip and updip parts of beds amalgamated, making the LAP seemingly bipartite – gravelly in the lower part and sandy in the upper part. The last-stage channel is filled with laterally-accreted aggradational sand beds.

The LAP is considered to represent a deep-water point bar. The LAP beds were deposited from traction by low-density turbidity currents that resembled closely one another. The lack of mud caps suggests closely successive flows with bypassing tails. As in the case of LAP example 7, the lateral grain-size segregation suggests concurrent deposition of gravel and sand, with the former spread only to a certain height on the bar flank.

### Point-bar LAPs composed of gravel beds

The point-bar LAPs of this category consist of gravel beds, usually with a distinct downdip segregation of

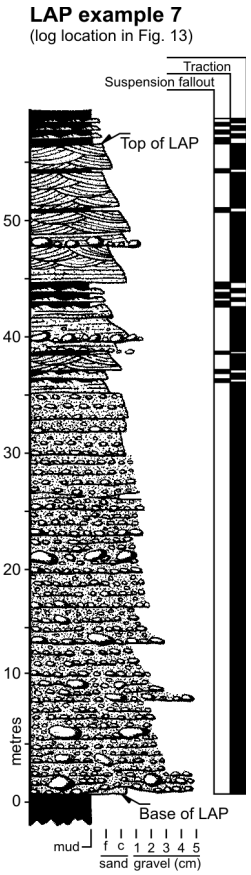


**Fig. 16.** Interpreted facies log from the point-bar LAP example 7 (Fig. 13); for comments, see text.

clast sizes. Two such outcrop cases (LAP examples 8 and 9 in Table 1) are described here for illustration and to show variation in their development.

*LAP example 8*

This LAP example is from the Canyon San Fernando valley-fill in the Late Cretaceous Rosario Fm., Mexico. The meander belt occurs stratigraphically above the earlier-described LAP examples 4–6, in the middle part of the submarine valley-fill, confined by the valley's external levée on one side and slope topography on the other (Morris & Busby-Spera, 1990; Dykstra & Kneller, 2007). The succession comprises isolated and multi-storey channel-belts encased in muddy heterolithic deposits and composed of gravel or gravel-sand beds with common evidence of lateral accretion.

*Bedding geometry* – The studied outcrop (Fig. 18A) is trending NW–SE (70–250°) and shows three vertically-stacked channel belts, the lower two with point bars (LAPs I & II in Fig. 18B). These meander belts are ~50 m wide and have erosional tops, with preserved thicknesses of 1–3 m. Their bases are stepping gently towards the last-stage channel and are uneven, showing erosional indentions by discrete shifts of channel thalweg. The channel-belt complex is underlain and surrounded by heterolithic deposits comprising of sand sheets, 5–25 cm thick, separated by mud layers 10–50 cm thick. Their mean structural attitude (320/8°NE) served as an estimate of palaeo-horizontal reference level. The third, uppermost storey is an asymmetrical cut-and-fill channel with flat and inclined gravel beds, gravel-sand couplets and muddy slump deposits.

LAPs I and II (Fig. 18A, B) consist of weakly sigmoidal to tabular gravel beds, 20–50 cm thick, inclined at 8–12° towards the ENE (azimuth 34–86°). The inclination of LAP beds in each case increases slightly towards the last-stage channel. The fill of last-stage channel consists of laterally-accreted aggradational gravel beds in case I, but is a massive sandy plug in case II. The bed strikes of LAP I converge towards the south in map view, whereas those of LAP II converge towards the southeast (Fig. 18C, D). The pattern suggests meander-bend expansion towards the NW and N, with a slight directional offset of meander II relative to meander I. Palaeocurrent data indicate channel-belt trend towards the south (Fig. 18C), which suggests that the outcrop section shows downstream ends of expansional point bars (Fig. 18D). Alternatively, the LAP bedding pattern might represent meander-bend rotation or combined expansion and translation, or perhaps a combination of all three modes of planform change (see Fig. 3).

*Sedimentary facies* – The LAP beds consist of well-rounded, polymict extraformational gravel with a mean clast size of ~6 cm and maximum size of 14 cm (Fig. 19A). Its clast-supported framework is filled with a fine- to medium-sand matrix. The gravel beds in LAP II are also locally separated by thin sand lenses. Beds are generally planar parallel-stratified, with little or no normal grading, but the downdip parts of beds in LAP I are mainly massive and occasionally show inverse grading. Imbricate clast fabric *a*(t)*b*(i) is recognizable in stratified gravel, whereas massive gravel shows an disorderly or non-imbricate *a*(p) fabric. The beds are fining updip, which gives the LAP an overall fining-upwards trend. The last-stage channel-fill associated with LAP I has a stepped base profile, consists of gravel beds and shows horizontal injections of gravel into the heterolithic muddy deposits of the outer bank. The last-stage channel-fill associated with LAP II consists of a medium-grained massive sand with floating large (20–70 cm), subrounded mudclasts. The underlying and laterally adjacent heterolithic deposits consist of a massive or laminated mud interbedded with thin, normally-graded sheets of fine to very fine, stratified sand.

The stratified gravel beds are tractional deposits of low-density turbidity currents, which were sufficiently powerful to spread their coarsest bedload laterally across the point-bar flank. In the case of LAP I, the near-bed concentration of sediment load in the flow axial zone was commonly high enough to cause a non-tractional dumping of gravel (Lowe, 1988; Vrolijk & Southard, 1997) or formation of a gravelly traction carpet (*sensu* Lowe, 1982). The high competence of flows is also evidenced by the general lack of gravel-capping sand divisions, apart from the sparse relics of such in LAP II. The bulk of sand and mud load was

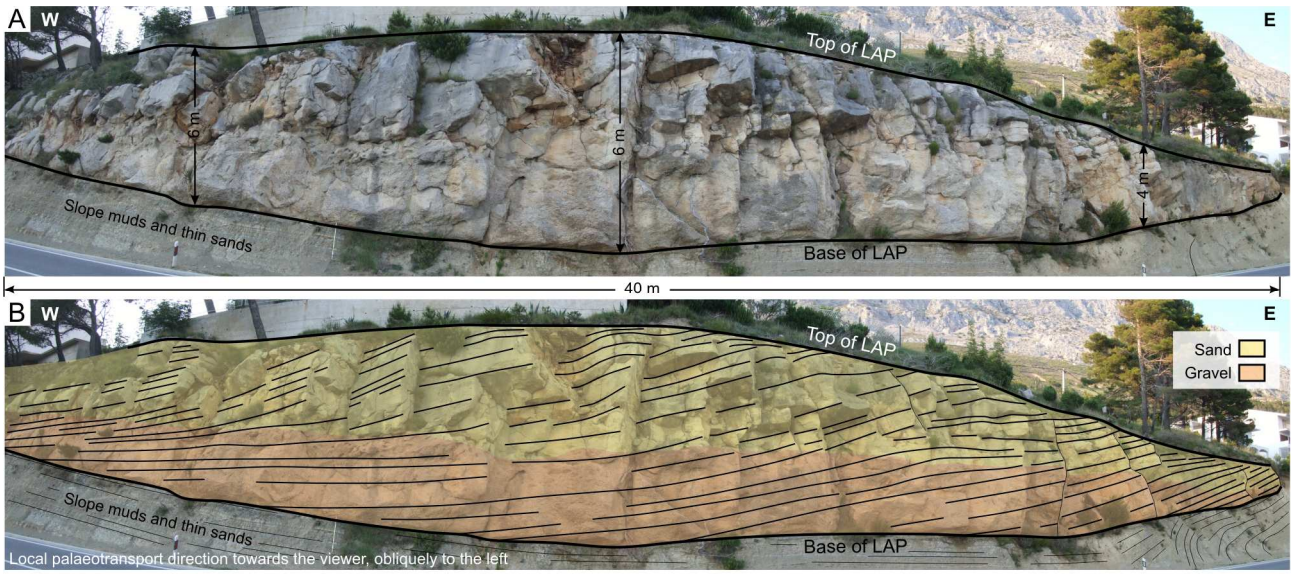


**Fig. 17.** Example of a point-bar LAP composed of beds with dip-segregated gravel and sand in the Eocene Makarska Flysch, southern Croatia. Road-cut outcrop in Bilići, ~22 km NW of the town of Makarska. (A) Outcrop photomosaic and (B) explanatory overlay drawing (for details, see text). The wide-angle photomosaic shows a deformed picture, as the LAP top in reality is flat and originally horizontal and so is also the erosional base in most of its lateral extent.

*LAP example 9*

This meander belt is exposed on the SW side of the Hasret Mountain in the Elazığ Basin of eastern Turkey. The belt occurs in the middle stratigraphic part (deposition phase 2 of Cronin *et al.*, 2000, 2007a) of a delta-fed, upper-slope channelized turbiditic system of the Eocene Kırkgecit Fm. This point-bar LAP example corresponds stratigraphically to the earlier-described LAP example 7 (Table 1), which most likely represents a tributary channel belt. According to the basin reconstruction by Cronin *et al.* (2000), the meander bend represented by LAP example 9 is located directly downstream of channel confluence, where the main channel was deflected obliquely to the slope by a submarine fault-block high. It is likely, therefore, that the channel bend was at least partly enforced by the basin-floor topography, rather then formed spontaneously by meandering currents. Nevertheless, this outcrop example shows a gravelly point bar formed by spectacularly powerful flows. The channel here had cut down deeper, overlying erosionally the older succession of clast-supported cobble gravel (see the preceding description of LAP example 7). The meander belt is overlain by a succession of channel belts with LAPs composed of sand-mud couplets (see the LAP example 1 described earlier in the text).

*Bedding geometry* – Large parts of the LAP are exposed in a spur with a 20-m wide wall facing the NE (125–305° trend) and a 50-m wide wall facing the SE (55–235° trend) (Fig. 20B, C). The LAP consists of three bedsets bounded by erosional angular unconformities and having a mean bedding attitude of 230/20°NW. The meander belt has an uneven, stepped erosional base, attributed to discrete shifts of the channel thalweg. The surrounding heterolithic sheet-like turbidites have a structural attitude of 204/14°NW, taken to approximate palaeo-horizontal reference level.

The three successive bedsets of the LAP (Fig. 20A) consist of tabular beds 0.4-5 m thick, which have erosional bases and are paralleling one another. The earliest set includes at least six beds that pinch out against the outer bank over some bank-attached, wedge-shaped mounds of considerably coarser gravel (Fig. 20A). The two sets of NW-dipping and steeper-inclined (≤14°) beds downlapping the channel belt's erosional base are attributed to the meander-bend expansion, whereas the intervening set of W-dipping and less-inclined beds is attributed to the bend's downstream translation. The LAP would then represent the consecutive episodes of the meander-bend expansion, translation and resumed expansion (Fig. 20A).

*Sedimentary facies* – The LAP beds generally show normal grading and consist of planar parallel-stratified, sand-supported cobble to pebble gravel (Fig. 19B), although some of the stratified beds are inversely graded and yet others are clast-supported and show little or no grading. The polymict extraformational gravel is subrounded to well-rounded, and matrix is fine to medium/coarse sand. The LAP dip-section is relatively narrow and poorly accessible, and it is unclear as to whether all the individual beds are fining updip. However, the LAP as a whole shows an upward fining, with the mean clast size decreasing from ~15 to ~5 cm and the maximum size from 52 to 30 cm. The mounded wedges of coarse gravel attached to the outer bank (Fig. 20A) consist of massive, normally-graded and clast-supported cobble gravel filled with coarse-sand matrix. Some of them are underlain by wedge-shaped erosional relics of deformed fine-grained sand with sporadic mudclasts. The surrounding heterolithic deposits comprise thin sheets (<10 cm) of cross-laminated fine sand alternating with mud layers 15–50 cm thick.

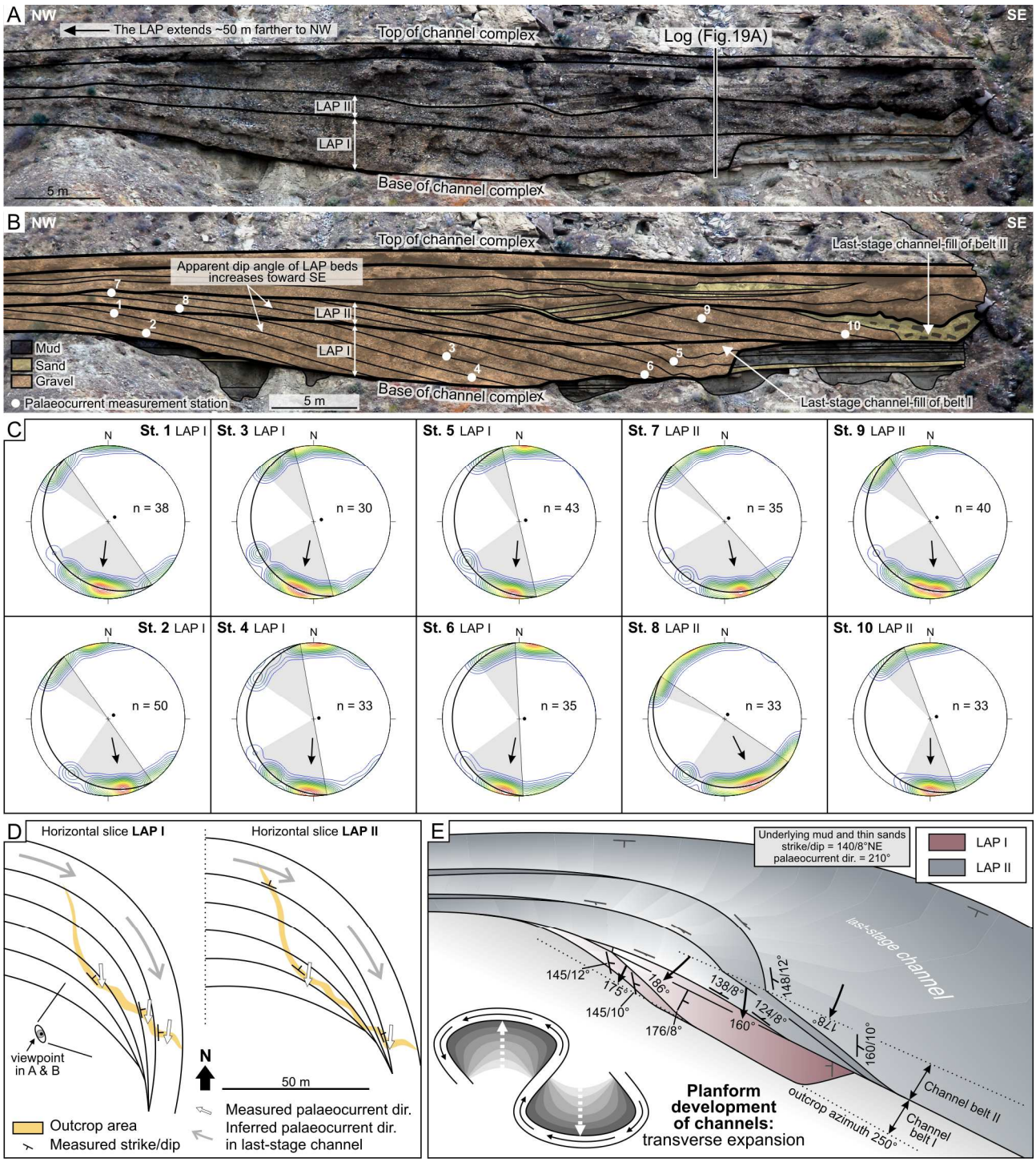


**Fig. 18.** Example of a point bar composed of gravel beds (LAP example 8 in Table 1), Rosario Fm., Mexico. (A) Outcrop photograph and (B) overlay drawing of three, erosionally superimposed channel-belt storeys. The lower two storeys consist of LAPs and an associated last-stage channel-fill. Note that the inclination of successive LAP beds increases towards the last-stage channel. Note also the location of measurement stations 1–10. (C) Measurements of the LAP bedding attitude and the corresponding palaeocurrent directions from stations 1–10, plotted in upper-hemisphere stereographic projection ($n$ = number of data in their local set). Note that the prevalent direction of bedload transport for the LAP beds is obliquely updip. (D) Interpretive planform slices through LAPs I and II. The southward convergence of bed strikes (out of the outcrop) suggests transverse expansion in both meander-belt storeys. (E) Schematic 3D planform reconstruction of the two vertically-stacked LAPs, showing the local bedding attitude and mean palaeocurrent directions measured in the outcrop section.

The LAP beds are tractional gravelly deposits of low-density turbidity currents (amalgamated turbidite divisions $R_1$ of Lowe, 1982). Their updip fining indicates a lateral decrease of flow competence on the point-bar flank. The lack of sandy divisions suggests that the bulk of sand load was carried in turbulent suspension and bypassing the meander bend. Bank-attached wedges of deformed sand are thought to be relics of slump deposits derived from the channel cut-bank. The lack of mud caps may indicate closely successive flows or be due to erosion. The bank-attached mounded wedges of coarse gravel are

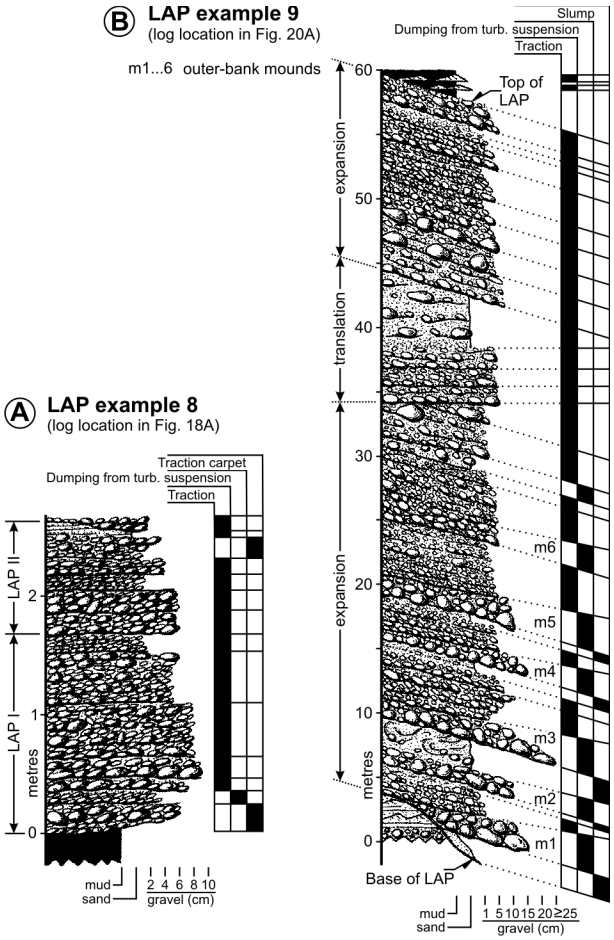


**Fig. 19.** Interpreted facies logs from the point-bar LAP example 8 (Fig. 18A) and example 9 (Fig. 20A); for comments, see text.

considered to be outer-bank mounds analogous to the so-called nested mounds (Phillips, 1987; Timbrell, 1993) or outer-bank bars (Nakajima *et al.*, 2009), comprising sediment dumped from an abruptly-decelerated basal part of the flow. Their location, shape and facies render the wedges similar to the thalweg mound in the LAP example 4 (Fig. 9B). Like the non-tractional downdip tips of beds in the LAP example 8 (see earlier description and Fig. 18B), these deposits indicate an excessive near-bed sediment concentration of flow in the thalweg zone (i.e., an axial development of transient high-density stream within an otherwise fully turbulent, low-density current).

*Palaeocurrent direction* – The outcrop surface is fairly flat, making it difficult to measure the attitude of individual beds and the corresponding gravel fabric. Therefore, no detailed palaeocurrent data have been derived from the LAP. The channel-belt is estimated to be trending NE–SW and the net local palaeoflow direction of the meander bend is towards the west.

## Other point-bar LAP varieties

The six descriptive categories of deep-water LAPs (Fig. 1B) reviewed and documented in the preceding sections include all common examples of such deposits found in outcrops, but may probably fall short of exhausting the natural spectrum of submarine point-bar varieties. There is a notable variation within some of the tentative categories, and the flow conditions may vary greatly from channel to channel and from one bend to another, which means that an even wider range of possible point-bar hybrids can be expected. One such example is described briefly below.

An uncommon LAP variety attributed to deep-water point bar was documented by Arnott (2007) from the Neoproterozoic Isaac Fm. of British Columbia, Canada. The meander belt is ~400 m wide and 12.5 m thick, has an originally horizontal erosional base and is encased in a muddy succession of sheet-like heterolithic deposits. The LAP consists of sand, but its coarser- and finer-grained beds form distinct bundles – referred to, respectively, as the coarse- and fine-grained units (Fig. 21A). The beds are inclined at 7–12° towards the last-stage channel (unexposed). The coarse-grained units are amalgamated in the lower half of the LAP and pinch updip in its upper half, interfingering with the fine-grained units which in turn are amalgamated near the LAP top. The coarse-grained units have erosional bases, in some cases covered with a lens of mudclast gravel or polymict pebble gravel (Fig. 21A). The erosional relief decreases updip and is onlapped by the bundle's component beds (Fig. 21B). The downdip parts of the component beds are >1 m thick, massive and composed of very coarse- to medium-grained sand, whereas their updip parts are thinner, finer-grained and planar parallel-stratified. The fine-grained units, in contrast, are considerably thinner (<15 cm), comprising turbidites T*bcd* and T*cd* made of medium-grained sand and silt. These units drape conformably the uneven tops of the coarse-grained units in the upper part of the LAP (Fig. 21B).

The peculiar grain-size segregation in the LAP was attributed by Arnott (2007) to a density-layering of the meandering currents. The coarse-grained units would be deposited by flows that were in hydraulic disequilibrium with the channel, becoming highly concentrated in lower part and dumping sediment at the bend, while the less-concentrated part of the flow was bypassing the channel bend. The fine-grained units would be deposited from the low-density tails of flows that were in equilibrium with the channel and bypassing its bend. The LAP in this interpretation would thus be formed by the alternating series of flows that were consistently either in equilibrium or in disequilibrium with the channel. The flows could be similar and the change in their behaviour was attributed to episodic changes in the channel perimeter due to cut-bank failures.

As an alternative scenario, we suggest that the alternating coarse- and fine-grained turbidite bundles may possibly represent primary differences in the successive flows. The system is thought to have been supplied with sediment from a collapsing shelf edge (R.W.C. Arnott, pers. comm. 2011), and the sediment yield in such a setting may be highly variable. For example, an episode of semi-continuous retrogressive slumping on upper slope may undercut the shelf-edge

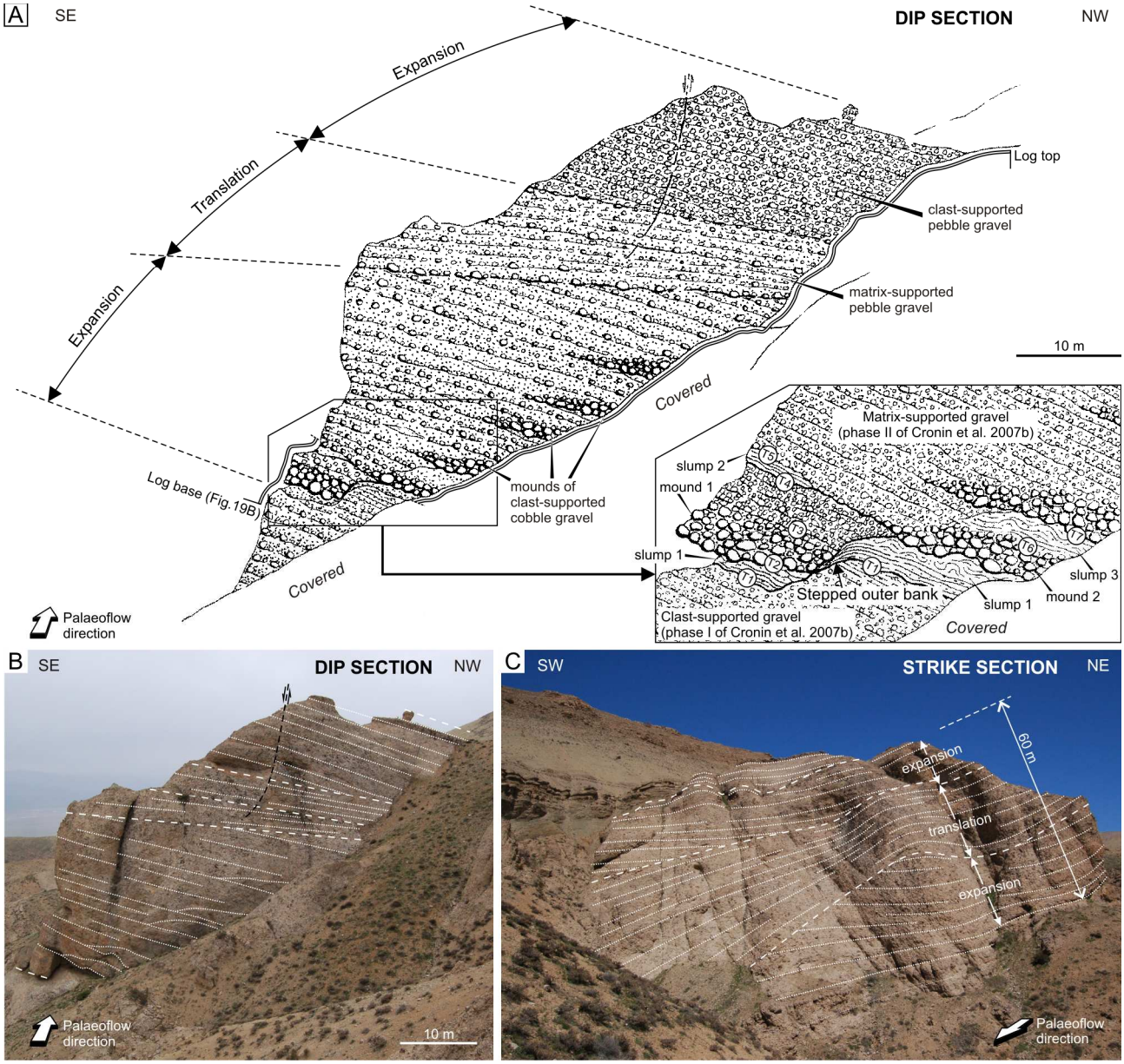


**Fig. 20.** Example of a point bar composed of gravel beds (LAP example 9 in Table 1), Elaziğ Basin, Turkey. (A) An overlay drawing of outcrop dip-section, showing three unconformable bedsets attributed to the point-bar transverse expansion, translational and resumed expansion. The lower unit includes wedge-shaped mounds of cobble gravel attached to the outer bank and overlying sandy slump deposits (see the inset detailed sketch) attributed to the outer-bank collapses. In the inset sketch, note that the LAP's erosional base steps up due an incremental lateral shifting of the channel thalweg and its decreasing scour depth; symbols T1–7 denote time surfaces. (B) Photograph of the outcrop dip-section shown in A. (C) Outcrop strike-section of the LAP, showing its three unconformable component bedsets.

deposits, trigger major failures and cause delivery of coarser sediment. The shelf would probably be narrow, on account of the sand grain size and occasional gravel admixture. The fine-grained turbidite bundles in the LAP may thus be deposits of less competent, low-density meandering flows, perhaps sustained and involving multiple surges, which were plastering sediment over the point-bar flank while gradually eroding the outer bank. Their action would be interrupted by an erosive outsized flow, which enlarged the conduit by scouring the previous deposits and eroding the outer bank, while possibly leaving a lag of bank-derived mudclasts or shelf-derived gravel at the point-bar toe. A short series of comparably large flows might follow and the modified conduit would then invite deposition, giving rise to an accretionary bundle of coarse-grained turbidites onlapping the scour surface. This notion is consistent with the amalgamation and gentler inclination of the coarse turbidites, implying large bypassing flows. The flows would unlikely be identical and their locus of maximum deposition would shift relative to the bend apex, resulting in variable scour and bed thicknesses. With the shelf edge temporarily stabilized by large collapses, the retrogressive sloughing of upper slope would resume – resulting in another bundle of fine-grained turbidites, draping the pre-existing morphology of the point-bar flank.

Other plausible scenarios might possibly be suggested, but would merely emphasize the fact that

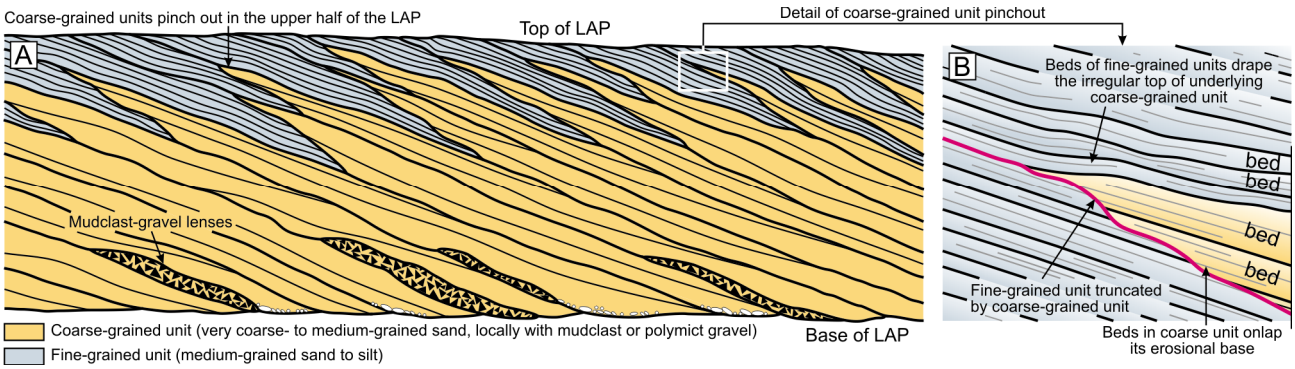


**Fig. 21.** Schematic representation of the hybrid point-bar case documented by Arnott (2007) from the Isaac Fm., Canada. (A) Sketch showing how the coarse-grained units pinch out and interfinger with fine-grained units in the upper part of the LAP. Note that both units consist of multiple turbidites. (B) Detail of the updip pinchout-out of coarse-grained unit. Note that the unit's erosional basal surface truncates the underlying fine-grained units and is onlapped by coarse-grained turbidites unit. The overlying fine-grained units drape the morphology of the coarse-grained unit.

the pattern of flows that formed the Isaac Fm. hybrid LAP remains unclear from the available evidence. Nevertheless, this point-bar LAP clearly differs from the other reviewed examples.

## IMPLICATIONS FOR CHANNEL MEANDERING

The preceding review of outcrop cases is concluded with a summary of features that seem to typify deep-water point bars as well as the principal features that determine their variability (Fig. 22). The characteristics of point-bar LAPs bear significant implications for the meandering process of deep-water channels, discussed in the ensuing section. The discussion focuses on the physical factors whose combination apparently promotes the meandering phenomenon in a deep-sea environment.

### Equilibrium slope conditions

Channels on submarine slope tend to reach a 'graded' equilibrium profile, along which turbidity currents can be conveyed down the system with minimum aggradation or degradation of the channel's longitudinal profile (Mayall & Stewart, 2000; Pirmez *et al.*, 2000; Kneller, 2003). When the channel is at grade, the amount of sediment deposited by flows is balanced by the amount removed by them, without significant change in the channel profile. The erosion and deposition of sediment then occur in the lateral domain, causing channel meandering and formation of point bars (Kneller, 2003, Ferry *et al.*, 2005).

The majority of point bars seen in outcrop show evidence of such equilibrium conditions. The lack of significant aggradation and degradation in the laterally migrating channel is indicated by the subhorizontal, flat erosional base of the resulting point-bar LAP. The point bar's flat top and the lack of prominent 'gull-wing' levées indicate that the voluminous spill-out flow of the dominating superelevated currents (Dykstra & Kneller, 2009) is largely bypassing the meander belt. Only limited overbank deposition occurs, but is a prerequisite for the formation of multi-storey meander belts (see cases in Figs 6A, 9A & 18A).

It is worth noting that channel meandering may occur also in the conditions of weak aggradation or degradation, as shown by the LAP examples 6–8 (Figs. 12A, 13A & 18A; see also Posamentier, 2003; Posamentier & Kolla, 2003; Cross *et al.*, 2009; Pyles *et al.*, 2010; Fernandes *et al.*, 2011; Janocko *et al.*, 2011b). However, such channel belts generally evolve from a 'graded' meandering channel, and their continued lateral accretion of sediment and migration are arguably an inherited property, imposed on the flows by the pre-existing sinuous channel, rather than their intrinsic hydraulic property. Turbidity currents do not seem to form point bars spontaneously in either aggradational or degradational conditions (Janocko et al., 2011a).

### Strength of channel banks

The ratio of flow power to bank strength is now widely recognized as an important factor controlling the planform of fluvial channels (Kleinhans, 2010; and references therein). For a river to meander, the ratio must be sufficiently low to prevent the flow from breaching the banks, but high enough to allow outer-bank erosion and lateral migration of the channel. The documented deep-water meander belts are invariably encased in cohesive mud or muddy heterolithic deposits, or a well-compacted older channel belt in some cases, which suggests a similar requirement for the meandering of submarine channels.

For a meandering channel belt to aggrade, not only must the accretion of its levées keep pace with the vertical accretion of sediment in the channel thalweg, but also the levée deposits must be sufficiently cohesive to prevent flow avulsion. Such conditions can seldom be reached in submarine settings. The extreme spill-out of superelevated turbidity currents in an aggrading channel forms levées made of coarse non-cohesive sediment (Straub *et al.*, 2008; 2011), as is shown also by the seismic facies of levées in aggradational non-meandering channels (Mayall & Stewart, 2000; Fonnesu, 2003; Clark & Cartwright, 2009; Janocko *et*

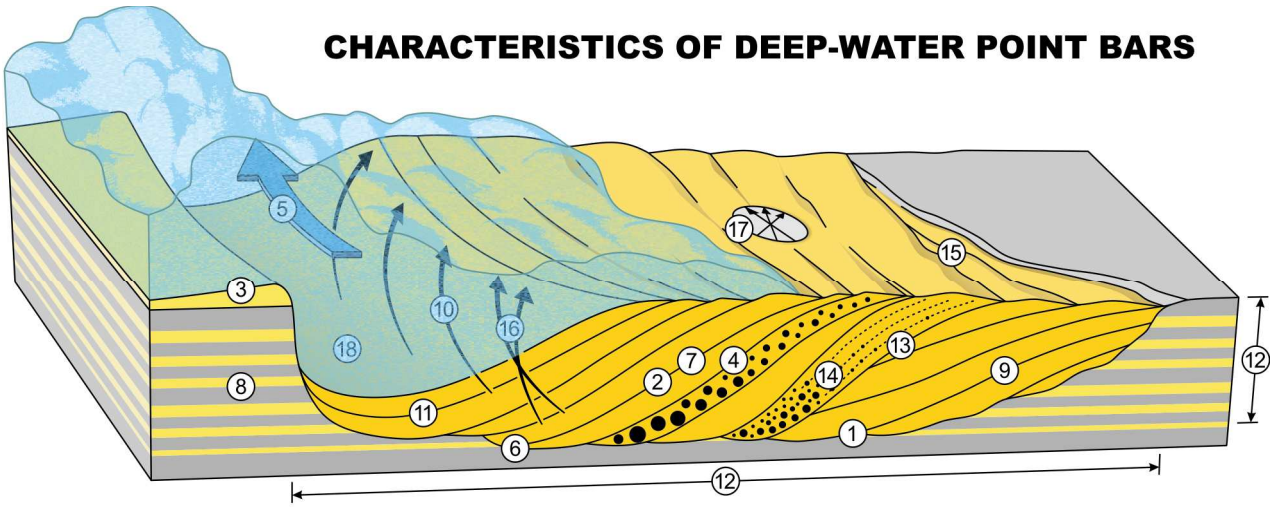


## Universal features

① Erosional, horizontal or gently inclined base
② Beds dipping towards the last-stage channel and downlapping the erosional base
③ Modest or absent levées
④ Beds fining updip
⑤ Deposition by channel-conveyed turbidity currents of low to high density, possibly spawning transient co-genetic debrisflows

## Other common features

⑥ Stepped base profile
⑦ Sigmoidal shape of beds in cross-section
⑧ Encasing in muddy heterolithic deposits
⑨ General lack of mud layers/caps
⑩ Bedload transport direction obliquely up the point-bar flank, increasingly deviating with height
⑪ Aggradational lateral accretion in last-stage channel

## Variable features

⑫ The thickness and width of meander belt
⑬ Prevalent bed geometry and bed-stacking style (conformable or unconformable)
⑭ The depositional sedimentary facies and their lateral change on point-bar flank
⑮ The strike and dip angle of beds in outcrop section
⑯ The degree of updip deviation of bedload transport direction from the bar-flank strike
⑰ The general dispersion of palaeoflow directions in the LAP
⑱ The infilling mode (facies) of last-stage channel

**Fig. 22.** A summary of features shared by deep-water meander belts, as well as features that render meander belts different from one another (for discussion, see text).

### Flow rotation pattern

One of the most contentious issues regarding deep-water channels was the hydraulic pattern of turbidity-current rotation at meander bends: Is the flow helicoid of superelevated current rising against the inner bank, as does the flow in meandering rivers, or is it governed by the large spill-out and rising against the outer bank? Laboratory experiments have been inconclusive, failing to produce meandering channels. Dilute turbidity currents were run through non-erodible conduits with a predefined moderate or high sinuosity, in some cases showing sediment deposition at the inner bank (Peakall *et al.*, 2007; Kane *et al.*, 2008; Amos *et al.*, 2010; Straub *et al.*, 2011). In the few cases with reported flow-velocity pattern, the flow helicoid in bend apex zone was rising against the outer bank, but the inner-bank deposition occurred only in a flow separation zone at the downstream end of the bend (Peakall *et al.*, 2007; Amos *et al.*, 2010; Straub *et al.*, 2011). Contradictory evidence came from the two previous outcrop studies with sufficiently detailed palaeocurrent data, one case indicating a flow ascending obliquely on the point-bar flank (Dykstra & Kneller, 2009) and the other indicating an obliquely descending flow (Pyles *et al.* (2010).

The detailed palaeocurrent data from the wide range of point-bar LAPs described in the present study indicate consistently a rotating-flow helicoid rising

against the inner bank. The bedload transport directions deviate obliquely updip by 2–48° from the LAP local strike, with the deviation commonly increasing in updip direction. Data from thalweg deposits generally indicate transport parallel to the channel local axis. In at least one instance (LAP example 7) there is also evidence of a transient secondary flow-cell driving bedload obliquely towards the outer bank, probably owing to a relatively wide thalweg with the main flow helicoid perching episodically on the bar flank (see Janocko *et al.*, 2011a). The outer-bank mounds made of graded massive gravel (LAP example 9) indicate episodic dumping of coarsest load at the foot of outer bank, whereas the isolated case of a stratified gravel mound (see LAP example 4) indicates tractional deposition by flow with a reverse helicoid, attributed to an excessively powerful turbidity current.

The evidence and inferences from outcrops are supported by the results of numerical CFD simulations (Janocko *et al.*, 2011a), which indicate that the flow helicoid in meander bend rises against the inner bank, transporting bedload obliquely up the point-bar flank. Flows that are too powerful and out of phase (i.e., flows whose intrinsic helicoid does not match the hydraulic curvature of pre-existing channel) tend to rise against the outer bank, which may explain the laboratory observations on flows in prefabricated sinuous channels and the sporadic outcrop evidence of flows with reverse helicoid (our LAP example 4; Pyles *et al.*, 2010). The flows with a reverse helicoid tend to be non-depositional in their descend on the point-bar flank, stripping or reworking its sediment, while forming deposits attached to the outer bank (Nakajima *et al.*, 2009). The Beacon LAP example of Pyles *et al.* (2010) thus likely represents tractional reworking of a pre-existing bar flank, rather than simple accretion of sediment brought in by the flow.

## The transport and partitioning of sediment

The outcrop evidence from point-bar LAPs indicates sediment accretion by tractional transport directed obliquely upslope on the point-bar flank. In addition to their upward fining due to the waning of flow, the LAP beds also show an updip lateral fining which indicates a sideways partitioning of sediment grain sizes by the flow on the point-bar flank. As explained in detail in the Appendix, a particle arriving in a meander bend is subject to radial centripetal force, which is proportional to the particle mass and square of its velocity and inversely proportional to the radius of the particle path. The bedload particles arriving on the point-bar flank will be distributed laterally according to their arrival velocity, path radius and the inclination and roughness of the bar surface. For the particle to be drifted upslope, its velocity ($v$) must fulfil the following condition:

$$v > \sqrt{\frac{g \cdot R(\sin\theta + f \cdot \cos\theta)}{\cos\theta - f \cdot \sin\theta}}$$

where $R$ is the bend radius of particle path; $\theta$ is the inclination angle of point-bar flank; $f$ is the coefficient of dynamic friction; and $g$ is the constant of gravitational acceleration. As the particle is drifted up-flank, the radius of its path effectively decreases and the particle may encounter a less-rough surface (i.e., suffer lesser frictional retardation), which enhances the up-drift and renders the particle path increasingly steeper. The up-drift will be enhanced also by a smaller, sharper bend and/or less inclined point-bar slope. Sand particles have small mass and are drifted easier against their gravity, but also gravel can be drifted high on the point-bar flank and even reach its top (see our LAP examples 4–6, 8 & 9). Gravel clasts have a greater mass, but when arriving at sufficiently high velocity, they are pulled stronger by centripetal force, while the frictional effect of finer-grained substrate is lower for the rolling, sliding and bouncing (sub-)rounded clasts.

Four varieties of the up-flank segregation of sediment characterize the point-bar LAP types (Fig. 1B) documented in the present study:

- Gradual updip fining of sand beds by a decrease of mean and/or maximum grain size, as is characteristic of the LAP types 1 and 2 (see examples 1 & 2, Fig. 5).
- Pronounced updip fining of gravel-sand couplets manifested by a compensational lateral offset of the bed's gravel and sand divisions, each showing also some internal updip fining, as is characteristic of the LAP types 3 and 4 (see example 3 in Fig. 8 and examples 4–6 in Fig. 10).
- Strong updip fining of gravel-sand beds manifested by a virtual updip separation of sand from gravel, each with internal updip fining, as is characteristic of the LAP type 5 (see example 7, Fig. 16).
- Gradual updip fining of gravel beds by a decrease of mean and/or maximum grain size, as is characteristic of the LAP type 6 (see examples 8 & 9, Figs 18–20).

The updip fining of beds indicates a lateral decline of flow competence on the point-bar flank, and there is also common evidence of a greater sediment concentration in the downdip part of the depositing flow (see descriptions of the LAP examples 2–6 & 8).

The point bars were formed by the same process – the action of meandering turbidity currents – and the observed variation in LAP development thus reflects differences in the character of the depositing flows. The LAPs composed of sand-mud couplets or sand beds (types 1 & 2, Fig. 1B) indicate gravel-free flows capable of spreading their sandy bedload laterally to the height of the developing point bar. The LAPs composed of gravel-sand beds (types 3–5, Fig. 1B) show marked lateral segregation of the two components, indicating flows capable of spreading gravel to a certain height on the point-bar flank, while spreading their sand load to the bar top. The transition from gravel to sand suggests that the deposition of sand followed the deposition of gravel and might initially be coeval, but the

**Table 2.** Meander-bend radii calculated for the point-bar LAP examples on the basis of Rozovskiĭ's (1961) formula. For explanation, see text.

| LAP example | LAP thickness (*D*) | Mean angular deviation (*β*) | Calculated bend radius (*R*) | *D/R* |
|---|---|---|---|---|
| 1 | 1.5 m | 16° | 58 m | 0.0258 |
| 2 | 2.6 m | 19° | 83 m | 0.0313 |
| 4 | 2.6 m | 34° | 42 m | 0.0619 |
| 5 | 4.3 m | 21° | 123 m | 0.0349 |
| 6 | 12.0 m | 18° | 406 m | 0.0295 |
| 7 | 15.0 m* | 16° | 576 m | 0.0260 |
| 8 LAP I | 1.5 m | 27° | 33 m | 0.0455 |
| 8 LAP II | 1.5 m | 25° | 35 m | 0.0428 |

For comparison: *D/R* ratios derived from the 3D seismic dataset studied by Janocko et al. (2011b) are in the range of 0.0235−0.0854 (based on measurements of *D* and *R* from 65 meander bends).

*Measured as the maximum hight-span of the LAP sigmoidal beds.

oblique updip transport direction implies that their lateral partitioning – though stemming from the intrinsic segregation of grain sizes in turbidity current – reflects the updip drift of particles on the bar flank, rather then the primary height of gravel/sand segregation in the current (cf. Arnott, 2007). The LAPs composed of gravel beds (type 6, Fig. 1B) indicate highly competent flows that carried their sand load in turbulent suspension and were capable of bypassing it through the channel bend. The up-bar fining of gravel similarly indicates segregation by the updip drift of particles, according to their sizes, with the gravel spread up to the point-bar height. It should be noted that the formation of such gravelly point bars does not mean that the turbidity currents were necessarily loaded with gravel to the height of the point bar. The current's gravelly bedload in reality was thin, relative to the channel relief, and it was the flow power that allowed the gravel to be drifted to the bar-flank top and the sand to bypass the meander bend.

### Implications for petroleum-reservoir models

The deep-water point bars of the six types (Fig. 1B) differ greatly in their heterogeneity, which includes both the range and spatial distribution of the main sediment fractions and the variety and architecture of the depositional sedimentary facies. These differences bear important implications for a reservoir model of submarine meander belt, where the primary heterogeneity plays crucial role and thus needs to be recognized and taken into account. The present study has provided detailed characteristics of the individual LAP varieties, which all differ sufficiently from one another to be identifiable from a well-core sample. The study can thus serve as a useful guide for the recognition and characterization of diverse meander belts and for the development of their models as hydrocarbon reservoirs.

Other useful inferences can also be made. The measured angular deviation of bedload transport direction from the corresponding strike of LAP beds may allow estimation of the channel-bend radius. The following relationship has been established for fluvial meanders (Rozovskiĭ, 1961):

$$\tan\beta = 11D/R \quad \text{or} \quad R = 11D/\tan\beta$$

where $\beta$ is the angular deviation, $D$ is the flow (channel) depth and $R$ is the channel-bend radius. Numerical CFD simulations (Janocko et al., 2011a) indicate that the development of point bars in deep-water channel is controlled chiefly by the channel-confined main part of flow, which allows the $D$ value to be approximated from the LAP thickness. The estimates of channel-belt radius calculated for the described LAP examples are given in Table 2. The outcrops do not allow for direct verification of the values, but the estimates seem to be realistic, because the corresponding D/R ratios are fully comparable to those derived independently for a range of meander belts from 3D seismic images (see Table 2).

The estimation of channel-bend radius allows further the meander-belt width, wavelength and point-bar volume to be estimated, which are some of the crucial features for a reconstruction of the submarine meander belt and for the development of its model as a reservoir.

## CONCLUSIONS

Outcrop studies have shown that the deep-water point bars, despite their formation by 'simple' lateral accretion, are not only varying in size (thicknesses and width), but differing greatly in the character of their bedding. The point-bar LAPs differ in the geometry and sedimentary facies of their component beds, as well as in the bedding inclination, the degree of erosion at bed bases and the occurrence of erosional truncations marking point-bar planform transformation (e.g., translation or rotation). As a tentative descriptive classification of outcrop cases, six main types of point-bar LAPs have been distinguished (Fig. 1B), although other hybrids are not precluded.

Apart from their major differences, the deep-water point bars have a number of key features in common (Fig. 22) – from which inferences have also been drawn about the meandering process:

- A horizontal top and an erosional, horizontal or gently inclined base, indicating quasi-equilibrium slope conditions of channel-belt development.

- Modest or absent levées, indicating a bypass of spill-out flows and supporting the notion of channel-belt equilibrium profile.
- LAP bedding inclined towards the last-stage channel and downlapping the erosional base, indicating persistent lateral accretion by channelized flows.
- An updip fining of LAP beds, indicating lateral segregation of bedload grain sizes by flow on the point-bar flank.
- LAP bed facies indicating tractional deposition by low-density turbidity currents, with a variable degree of substrate erosion and a higher flow density on the point-bar lower flank.

Other common features include:

- A stepped basal profile, reflecting an incremental lateral migration of the meandering channel thalweg and its decreasing scour depth.
- Sigmoidal cross-sectional shape of LAP beds, reflecting a gradual decline in sediment deposition towards both the channel thalweg and the point-bar top.
- Cohesive encasing deposits, supporting the notion that bank strength is a prerequisite for channel meandering.
- The lack of mud caps in the majority of LAP turbidites, indicating bypass of flow tails or removal of mud by subsequent flows.
- Bedload transport directed obliquely up the point-bar flank and increasingly deviated towards the bar top, indicating differential up-drift of sediment particles.
- Aggradational lateral-accretion architecture of the last-stage channel-fill, indicating increasingly depositional flows.

Features that render meander belts differing from one another include:

- The thickness and width of point-bar LAP, reflecting the depth and bend radius of the meandering channel.
- The prevalent cross-sectional geometry of LAP beds and the style of their erosional stacking (conformable or unconformable), reflecting the response of successive flows to the pre-existing morphology of point-bar flank.
- The depositional sedimentary facies of LAP beds and their updip changes, which reflect the character of flows and are quite consistent in a particular point bar, but differ greatly from one meander belt to another.
- The variable local strike and dip angle of LAP beds, reflecting changes in the point-bar planform and its flank morphology.
- The dispersion of local palaeocurrent directions, reflecting further the above-mentioned changes.
- The infilling mode and sedimentary facies of the last-stage channel-fill.

The observed differences among meander belts have an important bearing on their heterogeneity, but are beyond the seismic resolution and indiscernible from seismic images. However, the six main categories of point-bar LAPs are readily identifiable from a well-core sample, and their detailed characteristics provided by the present study can thus serve as a useful guide for the recognition and characterization of ancient meander belts and for the development of their models as hydrocarbon reservoirs.

## ACKNOWLEDGEMENTS

The study was a part of the first author's doctoral project funded by Statoil ASA, with Sverre Henriksen as advisor on the company's behalf. The following other researchers offered invaluable practical advice, discussions and field guidance to outcrops: Ben Kneller in Mexico; Bryan Cronin and Ibrahim Türkmen in the eastern Turkey; Peter King in New Zealand's North Island; Enrico Bonamini in Italy's Piedmonte; and Ervin Mrinjek in Croatia's Makarska region. Additional field assistance was kindly offered by Mehmet Cihat Alçiçek, Carlo Messina and Anna Pontén in Turkey, and by Juraj Janocko and Juraj Oslanec in Mexico.

## REFERENCES

**Abreu, V., Sullivan, M., Pirmez, C.** and **Mohrig, D.** (2003) Lateral accretion packages (LAPs): an important reservoir element in deep water sinuous channels. *Mar. Petrol. Geol.*, **20,** 631–648.

**Amos, K.J., Peakall, J., Bradbury, P.W., Roberts, M., Keevil, G.,** and **Gupta, S.** (2010) The influence of bend amplitude and planform morphology on flow and sedimentation in submarine channels. *Mar. Petrol. Geol.*, **27,** 1431–1447.

**Arnot, M.J., King, P.R., Browne, G.H.** and **Helle, K.** (2007) Channelized, innermost, basin-floor-fan morphologies, Mount Messenger Formation Waikiekie South Beach and Inland, New Zealand. In: *Atlas of Deepwater Outcrops* (Eds T.H. Nilsen, R.D. Shew, G.S. Steffens and J.R.J. Studlick), *AAPG Stud. Geol.*, **56,** 249–256.

**Arnott, R.** (2007) Stratal architecture and origin of lateral accretion deposits (LADs) and conterminous inner-bank levee deposits in a base-of-slope sinuous channel, lower Isaac Formation (Neoproterozoic), east-central British Columbia, Canada. *Mar. Petrol. Geol.*, **24,** 515–528.

**Beiser, A.** (2004) *Schaum's Outline of Applied Physics*. 4th Edn., McGraw-Hill, New York, 467 pp.

**Bouma, A.H.** (1962) *Sedimentology of Some Flysch Deposits: A Graphic Approach to Facies Interpretations*. Elsevier, Amsterdam, 168 pp.

**Beaubouef, R.T., Rossen, C.,** and **Lovell, R.W.W.** (2007) The Beacon Channel: a newly recognized architectural type in the Brushy Canyon Formation, Texas, USA. In: *Atlas of Deepwater Outcrops* (Eds T.H. Nilsen, R.D. Shew, G.S. Steffens and J.R.J. Studlick), *AAPG Stud. Geol.*, **56,** 432–443.

**Blikra, L.H.** and **Nemec, W.** (1998) Postglacial colluvium in western Norway: depositional processes, facies and palaeoclimatic record. *Sedimentology*, **45**, 909−959.

**Blikra, L.H.** and **Nemec, W.** (2000) Postglacial colluvium in western Norway: depositional processes, facies and palaeoclimatic record. Reply to Discussion by P. Bertran & V. Jomelli. *Sedimentology*, **47**, 1058−1068.

**Brice, J.C.** (1974) Evolution of meander loops. *Bull. Geol. Soc. Am.*, **85**, 581–586.

**Bridge, J.S.** (2003) *Rivers and Floodplains: Forms, Processes and Sedimentary Record*. Blackwell Publishing, Oxford, 491 pp.

**Clark, I.R.,** and **Cartwright, J.A.** (2009) Interactions between submarine channel systems and deformation in deepwater fold belts: examples from the Levant Basin, Eastern Mediterranean Sea. *Mar. Petrol. Geol.*, **26,** 1465–1482.

**Clark, J.D.,** and **Pickering, K.T.** (1996) Architectural elements and growth patterns of submarine channels: applications to hydrocarbon exploration. *AAPG Bull.*, **80,** 194–221.

**Cronin, B. T., Hurst, A., Çelik, H.** and **Türkmen, I.** (2000) Superb exposure of a channel, levee and overbank complex in an ancient deep-water slope environment. *Sed. Geol.*, **132,** 205–216.

**Cronin, B.T., Çelik, H.,** and **Hurst, A.** (2007a). Sinuous channels in late stages of entrenched deep-water channel complexes: Hasret Mountain Main Channel, Turkey. In: *Atlas of Deepwater Outcrops* (Eds T.H. Nilsen, R.D. Shew, G.S. Steffens and J.R.J. Studlick), *AAPG Stud. Geol.*, **56,** 368–372.

**Cronin, B.T., Çelik, H., Hurst, A., Gul, M., Gürbüz, K., Mazzini, A.** and **Overstolz, M.** (2007b). Slope-channel complex fill and overbank architecture, Tinker channel, Kırkgecit Formation, Turkey. In: *Atlas of Deepwater Outcrops* (Eds T.H. Nilsen, R.D. Shew, G.S. Steffens and J.R.J. Studlick), *AAPG Stud. Geol.*, **56,** pp. 363–367.

**Cross, N.E., Cunningham, A., Cook, R.J., Taha, A., Esmaie, E.** and **El Swidan, N.** (2009) Three- dimensional seismic geomorphology of a deep-water slope-channel system: the Sequoia field, offshore west Nile delta, Egypt. *AAPG Bull.*, **93,** 1063–1086.

**Crumeyrolle, E., Renaud, I.** and **Suiter, J.** (2007) The use of two- and three-dimensional seismics to understand sediment transfer from fluvial to deep water via sinuous channels: example from the Mahakam shelf and comparison with outcrop data (south-central Pyrenees). In: *Seismic Geomorphology: Applications to Hydrocarbon Exploration and Production* (Eds R.J. Davies, H.W. Posamentier, L.J. Wood and J.A. Cartwright), *Geol. Soc. London Spec. Publ.*, **277,** 85–103.

**Dykstra, M.** and **Kneller, B.** (2009) Lateral accretion in a deep-marine channel complex: implications for channelized flow processes in turbidity currents. *Sedimentology*, **56,** 1411–1432.

**Elliott, T.** (2000) Depositional architecture of a sand-rich, channelized turbidite system: the Upper Carboniferous Ross Sandstone Formation, Western Ireland. In: *Deep-water Reservoirs of the World* (Eds P. Weimer, R.M. Slatt, A.H. Bouma and D.T. Lawrence), pp. 342–373. Proceedings of the Gulf Coast Section SEPM Foundation 20th Annual Research Conference, Houston.

**Eschard, R., Albouy, E., Deschamps, R., Euzen, T.** and **Ayub, A.** (2003) Downstream evolution of turbiditic channel complexes in the Pab Range outcrops (Maastrichtian, Pakistan). *Mar. Petrol. Geol.*, **20,** 691–710.

**Euzen, T., Eschard, R., Alboyuy, E.** and **Deschamps, R.** (2007) Reservoir architecture of a turbidite channel complex in the Pab Formation, Pakistan. In: *Atlas of Deepwater Outcrops* (Eds T.H. Nilsen, R.D. Shew, G.S. Steffens and J.R.J. Studlick), *AAPG Stud. Geol.*, **56,** CD-ROM Suppl., 20 pp.

**Fernandes, A.M., Mohrig, D., Steel, R., Buttles, J.** and **Henriksen, S.** (2011) Three dimensional geometries of bank-attached bar-forms in sinuous submarine channels. (MS in prep.)

**Ferry, J.-N., Mulder, T., Parize, O.** and **Raillard, S.** (2005) Concept of equilibrium profile in deep-water turbidite systems: effects of local physiographic changes on the nature of sedimentary process and the geometries of deposits. In: *Submarine Slope Systems: Processes and Products* (Eds D.M. Hodgson and S.S. Flint), *Geol. Soc. London Spec. Publ.*, **244,** 181–193.

**Fonnesu, F.** (2003) 3D seismic images of a low-sinuosity slope channel and related depositional lobe (West Africa deep-offshore). *Mar. Petrol. Geol.*, **20,** 615–629.

**Harms, J.C., Southard, J.B., Spearing, D.R.** and **Walker, R.G.** (1975) *Depositional Environments as Interpreted from Primary Sedimentary Structures and Stratification Sequences*. SEPM Short Course No. 2 Lecture Notes, Society of Economic Paleontologists and Mineralogists, Dallas, 161 pp.

**Harms, J.C., Southard, J.B.** and **Walker, R.G.** (1982) *Structures and Sequences in Clastic Rocks*. SEPM Short Course No. 9 Lecture Notes, Society of Economic Paleontologists and Mineralogists, Calgary, 851 pp.

**Janocko, M., Cartigny, M., Nemec, W.** and **Hansen, E.W.M.** (2011a) Turbidity current hydraulics and sediment deposition in erodible sinuous channels: laboratory experiments and numerical simulations. *Mar. Petrol. Geol.* (MS in review).

**Janocko, M., Nemec, W., Henriksen, S.** and **Warchoł, M.** (2011b) The diversity of deep-water sinuous channels and their architectural elements. *Mar. Petrol. Geol.* (MS in review).

**Kane, I.A., McCaffrey, W.D.** and **Peakall, J.** (2008) Controls on sinuosity evolution within submarine channels. *Geology*, **36,** 287–290.

**Kleinhans, M.G.** (2010) Sorting out river channel patterns. *Prog. Phys. Geogr.*, **34,** 287–326.

**Kneller, B.C.** (2003) The influence of flow parameters on turbidite slope channel architecture. *Mar. Petrol. Geol.*, **20,** 901–910.

**Lerner, L.S.** (1997) *Physics for Scientists and Engineers*. Jones & Bartlett, Boston, 1138 pp.

**Lien, T., Walker, R.G.** and **Martinsen, O.J.** (2003) Turbidites in the Upper Carboniferous Ross Formation, western Ireland: reconstruction of a channel and spillover system. *Sedimentology*, **50,** 113–148.

**Lowe, D.R.** (1982) Sediment gravity flows, II. Depositional models with special reference to the deposits of high-density turbidity currents. *J. Sed. Res.*, **52,** 279–297.

**Lowe, D.R.** (1988) Suspended-load fallout rate as an independent variable in the analysis of current structures. *Sedimentology*, **35**, 765–776.

**Lønne, I.** and **Nemec, W.** (2004) High-arctic fan delta recording deglaciation and environment disequilibrium. *Sedimentology*, **51**, 553−589.

**Mark, D.M.** (1973) Analysis of axial orientation data, including till fabrics. *Geol. Soc. Am. Bull.*, **84,** 1369–1374.

**Martinsen, O. J., Lien, T.** and **Walker, R. G.** (2000) Upper carboniferous deep water sediments: Analogues for passive margin turbidite plays. In: Deep-water Reservoirs of the World (Eds P. Weimer, R. M. Slatt, A. H. Bouma and D. T. Lawrence), pp. 533–555. Proceedings of the Gulf Coast Section SEPM Foundation 20th Annual Research Conference, Houston.

**Mayall, M.** and **Stewart, I.** (2000) The architecture of turbidite slope channels. In: *Deep-water Reservoirs of the World* (Eds P. Weimer, R.M. Slatt, A.H. Bouma and D.T. Lawrence), pp. 578–586. Proceedings of the Gulf Coast Section SEPM Foundation 20th Annual Research Conference, Houston.

**Middleton, G.V.** and **Southard, J.B.** (1984) *Mechanics of Sediment Movement*. SEPM Short Course No. 3 Lecture Notes, 2nd Edition, Society of Economic Paleontologists and Mineralogists, Providence.

**Morris, W.R.** and **Busby-Spera, C.J.** (1990) A submarine fan valley-levee complex in the Upper Cretaceous Rosario Formation, Baja California: implications for turbidite facies models. *Geol. Soc. Am. Bull.*, **102,** 900–914.

**Mutti, E.** (1977) Distinctive thin bedded turbidite facies and related depositional environments in the Eocene Hecho Group (south-central Pyrenees, Spain). *Sedimentology*, **24,** 107–131.

**Mutti, E.** and **Normark, W.R.** (1991) An integrated approach to the study of turbidite systems. In: *Seismic Facies and Sedimentary Processes of Submarine Fans and Turbidite Systems* (Eds P. Weimer and M. H. Link), pp. 75–106. Springer-Verlag, New York.

**Nakajima, T., Peakall, J., McCaffrey, W.D., Paton, D.A.** and **Thompson, P.J.** (2009) Outer-bank bars: a new intra-channel architectural element within sinuous submarine slope channels. *J. Sed. Res.*, **79,** 872–886.

**Nemec, W., Lønne, I.** and **Blikra, L.H.** (1999) The Kregnes moraine in Gauldalen, west-central Norway: anatomy of a Younger Dryas proglacial delta in a palaeofjord basin. *Boreas*, **28**, 454−476.

**O'Byrne, C.J., Barton, M.D., Steffens, G.S., Pirmez, C.** and **Buergisser, H.** (2007) Architecture of a laterally migrating channel complex: Channel 4, Isaac Formation, Windermere

Supergroup, Castle Creek North, British Columbia, Canada. In: *Atlas of Deepwater Outcrops* (Eds T.H. Nilsen, R.D. Shew, G.S. Steffens and J.R.J. Studlick), *AAPG Stud. Geol.*, **56,** 115–118.

**Peakall, J., Amos, K.J., Keevil, G.M., Bradbury, P.W.** and **Gupta, S.** (2007) Flow processes and sedimentation in submarine channel bends. *Mar. Petrol. Geol.*, **24,** 470–486.

**Phillips, S.** (1987) Dipmeter interpretation of turbidite-channel reservoir sandstones, Indian Draw field, New Mexico. In: *Reservoir Sedimentology* (Eds R.W. Tillman and K.J. Weber), *Soc. Econ. Paleontol. Mineral. Spec. Publ.*, **40,** 113–128.

**Pirmez, C., Beaubouef, R.T., Friedmann, S.J.** and **Mohrig, D.C.** (2000) Equilibrium profile and base-level in submarine channels: examples from Late Pleistocene systems and implications for the architecture of deepwater reservoirs. In: *Deep-water Reservoirs of the World* (Eds P. Weimer, R.M. Slatt, A.H. Bouma and D.T. Lawrence), pp. 782–805. Proceedings of the Gulf Coast Section SEPM Foundation 20th Annual Research Conference, Houston.

**Posamentier, H.W.** (2003) Depositional elements associated with a basinfloor channel–levee system: case study from the Gulf of Mexico. *Mar. Petrol. Geol.*, **20,** 667–690.

**Posamentier, H.W.** and **Kolla, V.** (2003) Seismic geomorphology and stratigraphy of depositional elements in deep-water settings. *J. Sed. Res.*,**73,** 367–388.

**Pyles, D.R., Jennette, D.C, Tomasso, M., Beaubouef, R.T.** and **Rossen, C.** (2010) Concepts learned from a 3D outcrop of a sinuous slope channel complex: Beacon Channel Complex, Brushy Canyon Formation, West Texas, U.S.A. *J. Sed. Res.*, **80,** 67–96.

**Rozovskiĭ, I.L.** (1961) *Flow of Water in Bends of Open Channels.* Israel Program for Scientific Translations, Jerusalem, 233 pp.

**Slatt, R.M., Minken, J., Van Dyke, S.K., Pyles, D.R., Witten, A.J.** and **Young, R.A.** (2007) Scales of heterogeneity of a leveed-channel system, Cretaceous Dad Sandstone Member, Lewis Shale, Wyoming, U.S.A. In: *Atlas of Deepwater Outcrops* (Eds T.H. Nilsen, R.D. Shew, G.S. Steffens and J.R.J. Studlick), *AAPG Stud. Geol.*, **56,** 490–496.

**Smith, R.D.A.** (1995) Complex bedding geometries in proximal deposits of the Castelnuovo Member, Rocchetta Formation, Tertiary Piedmont Basin, NW Italy. In: *An Atlas of Deep-water Environments: Architectural Style in Turbidite Systems* (Eds K.T. Pickering, R.N. Hiscott, N.H. Kenyon, F. Ricci Lucchi and R.D.A. Smith), pp. 244–249. Chapman & Hall, London.

**Straub, K.M., Mohrig, D., McElroy, B.** and **Buttles, J.** (2008) Interactions between turbidity currents and topography in aggrading sinuous submarine channels: a laboratory study. *Geol. Soc. Am. Bull.*, **120,** 368–385.

**Straub, K.M., Mohrig, D., Buttles, J., McElroy, B.** and **Pirmez, C.** (2011) Quantifying the influence of channel sinuosity on the depositional mechanics of channelized turbidity currents: a laboratory study, *Mar. Petrol. Geol.*, **28,** 744–760.

**Sullivan, M.D., Jensen, G.N., Goulding, F.J., Jennette, D.C., Foreman, J.L.** and **Stern, D.** (2000) Architectural analysis of deep-water outcrops: implications for exploration and development of the Diana sub-basin, western Gulf of Mexico. In: *Deep-water Reservoirs of the World* (Eds P. Weimer, R. M. Slatt, A. H. Bouma and D. T. Lawrence), pp. 1010–1032. Proceedings of the Gulf Coast Section SEPM Foundation 20th Annual Research Conference, Houston.

**Timbrell, G.** (1993) Sandstone architecture of the Balder Formation depositional system, UK quadrant 9 and adjacent areas. In: *Petroleum Geology of Northwest Europe: Proceedings of the 4th Conference* (Ed. J.R. Parker), pp. 107–121. Geological Society, London.

**Vrolijk, P.J.** and **Southard, J.B.** (1997) Experiments on rapid deposition of sand from high-velocity flows. *Geosci. Canada*, **24**, 45–54.

**Willis, B.J.** (1993) Interpretation of bedding geometry within ancient point-bar deposits. In: *Alluvial Sedimentation* (Eds M. Marzo and C. Puigdefábregas), *Int. Assoc. Sedimentol. Spec. Publ.*, **17**, 101–114.

**Wynn, R.B., Cronin, B.T.** and **Peakall, J.** (2007) Sinuous deep-water channels: genesis, geometry and architecture. *Mar. Petrol. Geol.*, **24**, 341−387.

## APPENDIX

### The transport of sediment particles on point-bar flank

The transport of sediment at a meander bend is considered here, on the basis of Lerner (1997) and Beiser (2004), in terms of the mechanical issue of a body moving in curved line along a counter-banked turn. The body is considered to be a sediment particle, such as a gravel clast, and the counter-banked turn to be meander bend with a curvature approximated by an osculating circle (Fig. A-1A). According to the Newton

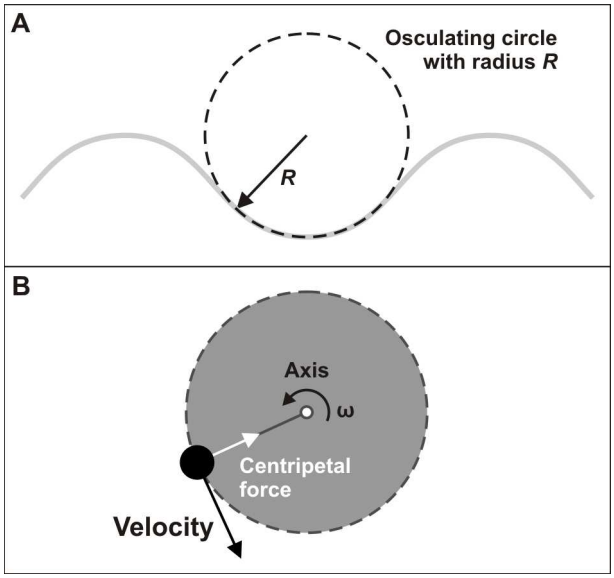


**Fig. A-1.** Definition diagrams: (A**)** An osculating circle is the tangent circle that adequately approximates particular segment of a given curve. (B) A body moving in a curved line is subject to a force causing the centripetal acceleration required for circular motion; $\omega$ is the angular velocity.

second law, a body moving in a curved path is subject to a force causing centripetal acceleration that corresponds to the body's semicircular motion (Fig. A-1B). For a particle to move in a horizontal curved path (Fig. A-2A), the gravity force acting on the particle must be counterbalanced by the normal force (Fig. A-2B).

The sediment particle is considered to be moving with a velocity imposed by the drag force of the transporting flow (Middleton & Southard, 1984):

$$F_D = c_D(\rho \cdot v^2 / 2)A \qquad [1]$$

where $c_D$ is the drag coefficient; $\rho$ and $v$ are the flow density and velocity; and $A$ is the particle cross-sectional area, scaling with the square of the particle diameter $D^2$. The $c_D$ value for a given particle is roughly constant for a wide range of flow conditions and depends mainly on the particle shape; the value varies from ~0.1 for streamlined elongate particles to ~1.0 for platy particles normal to the flow, with an average ~0.5 for subspherical particles.

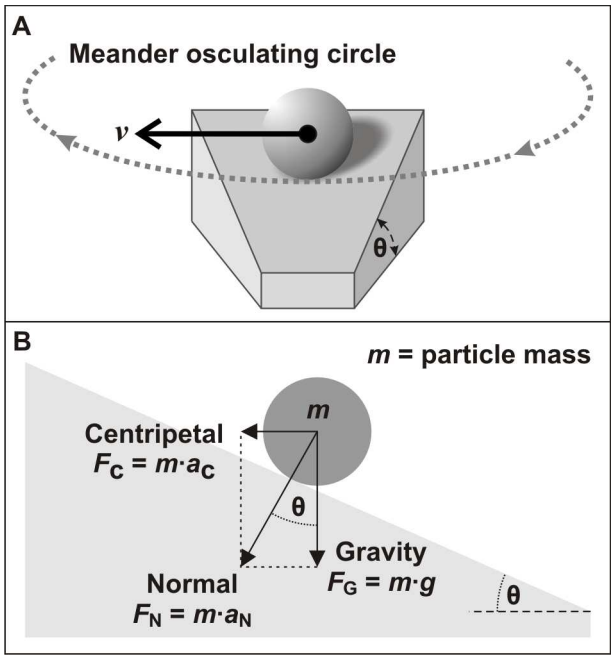


**Fig. A-2.** (A) Particle moving with a linear velocity $v$ on the inclined surface of a point bar in a curved line defined by the meander bend's osculating circle. (B) The 2D stress field of forces acting on the particle in a radial cross-section (symbols as in the text). For the particle to move along a horizontal path, the 'pinning' normal force $F_N$ must counterbalance the gravity force $F_G$, which requires normal acceleration to be $a_n = g/\cos\theta$, where $g$ is the gravitational acceleration (9.81 m/s$^2$).

Apart from any acceleration or deceleration that may occur in the direction of the particle path, the particle stress field (Fig. A-2B) involves only two other forces:

- The force of gravity acting vertically downwards through the centre of mass of the particle, $F_G = m \cdot g$, where $m$ is the particle mass and $g$ is the gravitational acceleration.
- The normal force acting perpendicularly to the substrate surface, $F_N = m \cdot a_N$, where $a_N$ is the corresponding acceleration.

The resultant centripetal force $F_C = m \cdot a_C$ (Fig. A-2B) is not a third force applied to the particle, but the horizontal net force on the particle resulting from the tensor addition of the normal force and gravity force. This net force can be regarded simply as the horizontal component of the normal force:

$$F_h = m \cdot a_N \cdot \sin\theta \qquad [2]$$

whereas the vertical component of the normal force for a horizontal particle path will equal the gravity force:

$$F_v = m \cdot a_N \cdot \cos\theta = m \cdot g \qquad [3]$$

which implies $a_N = g/\cos\theta$. Substituting into the above formula for $F_N$ gives the horizontal force to be:

$$F_h = m \cdot g \frac{\sin\theta}{\cos\theta} = m \cdot g \cdot \tan\theta \qquad [4]$$

For the particle to travel at velocity $v$ on a curved horizontal path of radius $R$, the required radial centripetal (inward) force is:

$$F_C = m \cdot a_C = \frac{m \cdot v^2}{R} \qquad [5]$$

Consequently, the particle will be in a stable horizontal path if the particle velocity satisfies the following condition:

$$\frac{m \cdot v^2}{R} = m \cdot g \cdot \tan\theta \qquad [6]$$

or

$$v^2 = g \cdot R \cdot \tan\theta \qquad [7]$$

Since $g$ is a constant, the latter formula can be simplified further as:

$$v^2 \approx R \cdot \tan\theta \quad \text{or} \quad v \approx \sqrt{R \cdot \tan\theta} \qquad [8]$$

This means that, for a particle with a given velocity, a lower turning angle and/or lower counter-bank inclination will favour an upward drift of the particle (Fig. A-3). A sharper meander bend and/or a less inclined point-bar flank will thus enhance the updip drift of sediment particles on the bar surface (Fig. A-4). The smaller sediment particles, by entering the point bar at higher level, will have a smaller turn angle and hence a

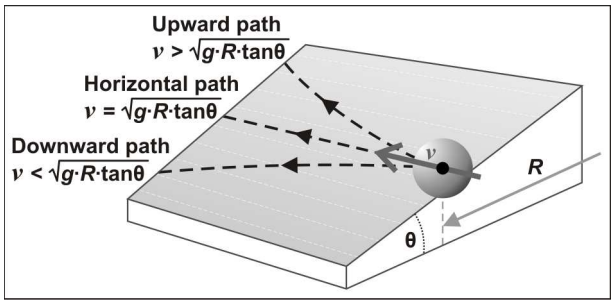


**Fig. A-3.** The particle on a counter-banked turn will move along a horizontal path if the velocity of the particle, $v$, meets the criterion $v = \sqrt{g \cdot R \cdot \tan\theta}$. Otherwise, the trajectory of particle motion will be either rising or falling along the particle path. $R$ is the entrance rotation radius of the particle, corresponding to the meander-bend curvature, and $\theta$ is the inclination angle of the point-bar surface.

greater potential to be drifted updip, while the up-drift will reduce further the particle's turn angle.

We have thus far assumed for simplicity that the particle will travel along the channel bend at a constant linear velocity. However, the turning flow with its particles will be subject to an angular acceleration (Fig. A-5A) proportional to the channel-bend radius:

$$a \approx R\left(\omega^2 + \frac{d\omega}{dt}\right) \qquad [9]$$

For a uniform motion ($v$ = const.), the total acceleration of the particle in a semicircular path is equal to the particle's radial acceleration, $a = a_{rad}$. For a non-uniform motion, this relationship will no longer hold, because of the presence of a tangential acceleration.

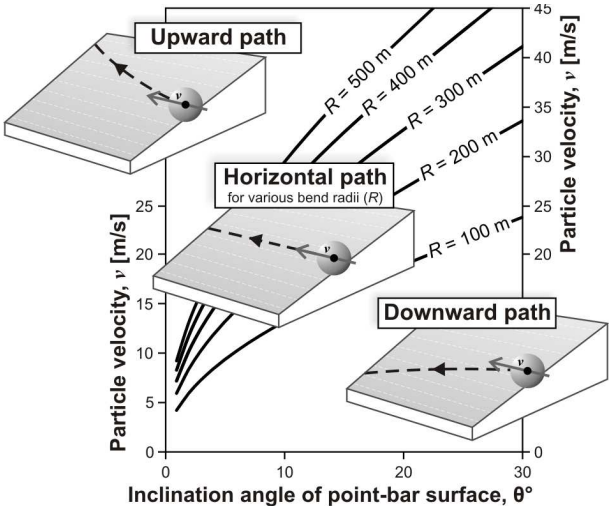


**Fig. A-4.** The transport trajectory of a sediment particle arriving on a point bar depends upon the particle velocity, the point-bar surface inclination and the radius of the particle rotation (corresponding to the meander-bend curvature and the particle's relative height of arrival). In this limiting frictionless case, the particle is assumed to be carried by flow in suspension.

The tangential component of the angular acceleration is:

$$a_{\tan} \approx R \cdot \omega^2 \approx \frac{v^2}{R} \qquad [10]$$

and it changes the velocity of the particle movement, whereas the radial component is:

$$a_{rad} \approx R\frac{d\omega}{dt} \approx \frac{dv}{dt} \qquad [11]$$

and it changes the direction of the particle movement. The equilibrium radius of turn at which $a_{tan} = a_{rad}$ is:

$$R_E = v^2 \frac{dt}{dv} \qquad [12]$$

which can be regarded as defining the semicircular boundary between the thalweg proper and the point-bar proper of the meander bend (Fig. A-5B). Particles arriving at a velocity greater than required by the latter equation will be swept up over the point-bar surface, whereas those arriving at a smaller velocity will travel along the channel thalweg.

In our reasoning, we have so far assumed that the particle will move with a velocity imposed by the flow and exceeding the particle's settling velocity. This limiting frictionless case may hold for particles carried by the flow in suspension, but not for those transported in bedload traction, where bottom friction plays its role. If the coefficient of dynamic friction ($f$) is taken into account, a generalized equation for the velocity allowing the particle to move along a stable horizontal path of radius $R$ is:

$$v^2 = \frac{g \cdot R(\sin\theta + f \cdot \cos\theta)}{\cos\theta - f \cdot \sin\theta} \quad \text{, or}$$

$$v = \sqrt{\frac{g \cdot R(\sin\theta + f \cdot \cos\theta)}{\cos\theta - f \cdot \sin\theta}} \qquad [13]$$

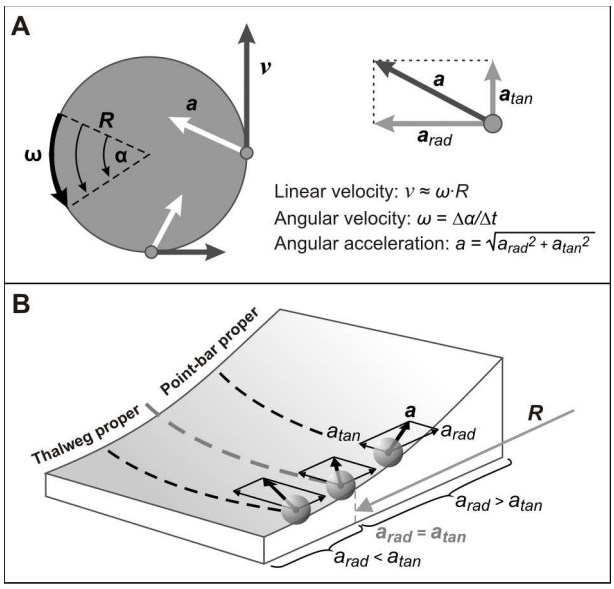


**Fig. A-5.** (A) A particle with velocity $v$ subject to an angular acceleration at the channel bend will have two acceleration components: a radial acceleration $a_{rad}$ and a tangential acceleration $a_{tan}$. (B) For a given particle accelerating at the channel bend, the equilibrium line $a_{rad} = a_{tan}$ can be regarded as the boundary between the channel's thalweg proper (where $a_{rad} < a_{tan}$) and the point-bar proper (where $a_{rad} > a_{tan}$).

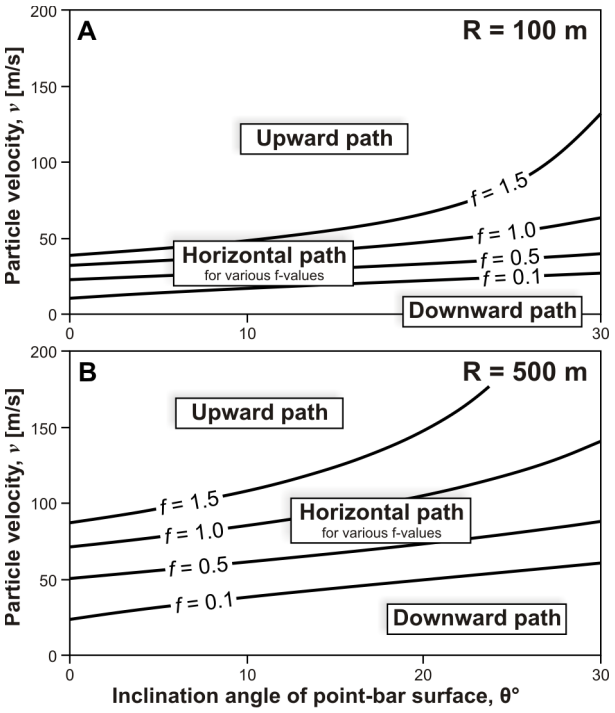


**Fig. A-6.** The transport trajectory of a sediment particle arriving on a point bar in bedload traction depends upon the particle velocity and the inclination and roughness of the point-bar surface, as shown here for the particle rotation radius of 100 m (A) and 500 m (B). The radius reflects different meander-bend curvature and/or different relative height of particle arrival.

The corresponding boundary between the thalweg proper and the accretional point-bar proper of the channel bend will then be at the equilibrium radius:

$$R_E = \frac{v^2(\cos\theta - f \cdot \sin\theta)}{g(\sin\theta + f \cdot \cos\theta)} \qquad [14]$$

For a given $R_E$, all the bedload particles arriving at the channel bend with a velocity greater than specified by Equation 13 will be drifted updip on the point-bar flank, although the required critical velocity will also depend on the inclination and roughness of the point-bar surface and the meander-bend radius (Fig. A-6). As the particle drifts upslope, its turn radius decreases and it arrives on a less rough substrate, which enhances the upward drift.